New ways of valorizing biochar in bio-based materials with controlled properties : characterization and technical-economic study

Guillermina Feliz Florian

Normandie Université

INSA INSTITUT NATIONAL DES SCIENCES APPLIQUÉES ROUEN NORMANDIE

THÈSE

Pour obtenir le diplôme de doctorat

Spécialité **GENIE DES PROCEDES**

Préparée au sein de l'**INSA Rouen Normandie**

Nouvelles voies de Valorisation du biochar en Matériaux Biosourcés à propriétés contrôlées : Caractérisation et étude technico-économique

Présentée et soutenue par

FELIZ FLORIAN GUILLERMINA

Thèse soutenue le 20/02/2026

devant le jury composé de :

M. ABDELOUAHED LOKMANE	MAÎTRE DE CONFÉRENCES HDR - INSA Rouen Normandie	Directeur de thèse
MME DUQUESNE SOPHIE	PROFESSEUR DES UNIVERSITÉS - Centrale Lille Institut - VILLENEUVE-D'ASCQ	Président du jury
MME LEBLANC NATHALIE	MAÎTRE DE CONFÉRENCES HDR - UniLaSalle	Co-directeur de thèse
M. RAGOUBI MOHAMED	MAÎTRE DE CONFÉRENCES HDR - UniLaSalle	Co-encadrant de thèse
MME CHETIBI LOUBNA	PROFESSEUR - Ecole Nationale Polytechnique de Constantine	Membre
M. KOUBAA AHMED	PROFESSEUR - Université du Québec en Abitibi-Témiscamingue, Canada	Rapporteur

Thèse dirigée par **ABDELOUAHED LOKMANE** (LABORATOIRE DE SECURITE DES PROCEDES CHIMIQUES) et **LEBLANC NATHALIE** (TRANSFORMATIONS ET AGRO-RESSOURCES)

ED 591 PSIME

LSPC Laboratoire de sécurité des procédés chimiques

Acknowledgements

The preparation of this doctoral thesis is the outcome of a long and demanding journey of academic and personal development, which would not have been possible without the support and contributions of many individuals and institutions. I would therefore like to express my sincere gratitude to all those who accompanied me and made the completion of this work possible.

First and foremost, I give thanks to God, who inspired in me the desire to pursue research, sustained me throughout this journey during which I grew in many dimensions, and whose faithfulness never failed.

I would like to express my deepest appreciation to my thesis supervisors, Lokmane Abdelouahed, Nathalie Leblanc, and Mohamed Ragoubi, for their expert guidance, scientific rigor, and constant support throughout this research. Their advice, encouragement, and confidence in my work were decisive in ensuring the quality of this thesis. I also thank the members of the jury—Loubna Chetibi, Ahmed Koubaa, and Sophie Duquesne—for the time they devoted to reviewing my work and for their valuable comments, which greatly contributed to improving and enriching the final manuscript.

I am grateful to INSA Rouen, UniLaSalle, LSPC, and the ECLORE research unit for providing the resources and research environment necessary to carry out this work. I also extend my sincere thanks to the Ministry of Higher Education, Science and Technology (MESCyT) of the Dominican Republic, which funded this research through the CALIOPE program; without this support, this project would not have been possible.

My heartfelt gratitude goes to my family, my fiancé Moisés Heredia, and my extended family for their unwavering support, understanding, and patience throughout these years. Thank you for enduring the challenges with me, for continually reminding me—through your actions—why I began this journey and why I was capable of completing it. You each played an essential role in the realization of this thesis.

I also wish to thank the friends and colleagues with whom I shared this period of doctoral training. I am especially grateful to the Dominican members of the CALIOPE group, who became my family in France. To my office mates—José, Jesús, Zhu, Gabriel, Lwhathanish, Flora, Khalid, and others—thank you for the invaluable moments we shared, far beyond lunch breaks. I extend special thanks to Corine Lacour, who from the very beginning created opportunities that supported my development—my “French angel.” I am also thankful to the Carnavaleros group, the Dominican community in France, and Nota Musical for allowing me to share my culture through dance and other activities.

Finally, I thank all those who, directly or indirectly, contributed to the completion of this thesis, including Bruno, Clément, Samantha, Jean-Baptiste, Morgan, Désiré, and others, whose experience and assistance with the experimental setup, equipment usage, and training were essential to the progress of this project. To everyone who may not have been explicitly mentioned, I also extend my sincere appreciation.

Agradecimientos

La elaboración de la presente tesis doctoral es el resultado de un proceso de formación académica y personal largo y exigente, que no habría sido posible sin el apoyo y la contribución de numerosas personas e instituciones. Por ello, me gustaría expresar mi agradecimiento a quienes han acompañado y hecho posible la culminación de este trabajo.

En primer lugar, doy gracias a Dios, quien puso en mí el deseo de investigar, me sostuvo en el proceso en el que crecí en muchos ámbitos y es fiel todo el tiempo.

Doy mi sincero agradecimiento a la dirección y supervisión de tesis Lokmane ABDELOUAHED, Nathalie LEBLANC y Mohamed RAGOUBI por su orientación experta, su rigor científico y su acompañamiento durante este proceso de investigación. Su apoyo, sus sugerencias y su confianza en el desarrollo de este trabajo han sido determinantes para la calidad de la investigación. Agradezco igualmente a los miembros del jurado Loubna CHETIBI, Ahmed KOUBAA y Sophie DUQUESNE por el tiempo dedicado a su lectura y por las observaciones realizadas, que han contribuido a enriquecer y mejorar el resultado final.

Deseo agradecer al INSA de ROUEN, UniLaSalle, el LSPC y la unidad de investigación ECLORE por proporcionar los medios necesarios para la realización de este trabajo. Asimismo, expreso mi reconocimiento al MESCyT de República Dominicana, quien ha financiado esta investigación por medio del programa CALIOPE y sin cuyo respaldo este proyecto no habría sido posible.

Agradezco a mi familia, prometido Moisés Heredia, familia de otra sangre, por su apoyo constante, su comprensión y su paciencia a lo largo de estos años. Por soportar las crisis conmigo y recordarme constantemente con evidencias por qué comencé y por qué puedo terminar. Porque tuvieron varios papeles en esta tesis. Muchas gracias.

Mi agradecimiento se extiende a los amigos, amigas y colegas con quienes he compartido este período de formación doctoral. Los dominicanos del grupo CALIOPE (en especial CALIOPE V), quienes fueron como mi familia en Francia. La mejor oficina (José, Jesús, Zhu, Gabriel, Lwhathanish, Flora, Khalid, ...), simplemente por todo ese tiempo de calidad, y no me refiero solo a los almuerzos. A Corine LACOUR porque desde el principio ha estado creando condiciones para mi desarrollo (mi ángel francés). Al grupo Carnavaleros, Dominicanos en Francia y Nota Musical. Por permitirme compartir mi cultura a través del baile y otras actividades.

Finalmente, a todas aquellas personas que, de forma directa o indirecta, han contribuido a la realización de esta tesis: Bruno, Clement, Samantha, Jean Baptiste, Morgan, Desire, ... cuya experiencia y ayuda con el montaje experimental, utilización y formación en los equipos fueron esenciales para el desarrollo de este proyecto. Y a todos los que no han sido mencionados explícitamente, les expreso igualmente mi más sincero agradecimiento.

ABSTRACT

Biochar, a carbon-rich material produced through the thermal conversion of biomass, represents a promising and versatile filler for the development of sustainable, high-performance polymer composites. This thesis explores the valorization of biochar into biobased materials with tailored properties. Biochar was produced from three biomass feedstocks—*Laminaria digitata* algae, beech wood, and flax shives—via slow pyrolysis at 600 °C, followed by physical activation with CO_2 at 900 °C.

The activation process significantly enhanced the specific surface area, with an increase of up to 774 % observed for algae-derived biochar, while slightly decreasing the carbon content. This modification improved interfacial compatibility with polylactic acid (PLA). The biochars were incorporated into PLA at loadings of 10, 40, and 70 wt.%, and the resulting biocomposites were characterized using FTIR, XRD, DSC, TGA, DMA, BDS, and tensile testing.

At low filler content (~10 wt.%), biochar improved composite stiffness (increased storage modulus, E′) and promoted nucleated crystallization of PLA without affecting the glass transition temperature (Tg). Higher biochar loadings significantly enhanced electrical conductivity, reaching 1.24×10^{-2} $S \cdot cm^{-1}$ at 70 wt.% activated beech biochar, and imparted antistatic and electromagnetic shielding properties. However, excessive biochar content led to particle agglomeration, resulting in reduced tensile strength and diminished processability.

A techno-economic assessment of an integrated production facility processing 1 t day^{-1} of beech wood waste biomass indicated a moderate capital expenditure (~€ 5 M), with production costs of € 1.55 kg^{-1} for biochar and €3.95 kg^{-1} for composite pellets. Scenario analysis demonstrated strong economic viability when all biochar was valorized in composite formulations, with a high net present value, a payback period of 3 years, and an internal rate of return of approximately an internal rate of return of about 48 %.

Overall, the findings emphasize the critical roles of feedstock selection, pyrolysis and activation conditions, and filler loading in designing biochar-PLA biocomposites with optimized mechanical, thermal, and functional properties, offering a viable pathway toward circular and biobased material systems.

Keywords: Biochar, Pyrolysis, PLA, Aspen Plus, Biocomposite, Physical activation, biomass, technical economic.

RÉSUMÉ

Le biochar, un matériau riche en carbone produit par la conversion thermique de la biomasse, représente une charge prometteuse et polyvalente pour le développement de composites polymères durables et hautement performants. Cette thèse explore la valorisation du biochar en matériaux biosourcés aux propriétés contrôlées. Le biochar a été produit à partir de trois matières premières issues de la biomasse (algues Laminaria digitata, bois de hêtre et copeaux de lin) par pyrolyse lente à 600 °C, suivie d'une activation physique avec du CO_2 à 900 °C.

Le processus d'activation a considérablement amélioré la surface spécifique, avec une augmentation pouvant atteindre 774 % pour le biochar dérivé d'algues, tout en réduisant légèrement la teneur en carbone. Cette modification a amélioré la compatibilité interfaciale avec l'acide polylactique (PLA). Les biochars ont été incorporés dans le PLA à des teneurs de 10, 40 et 70 % en masse, et les biocomposites obtenus ont été caractérisés par FTIR, XRD, DSC, TGA, DMA, BDS et essais de traction.

À faible teneur en charge (~ 10 % en masse), le biochar a amélioré la rigidité du composite (augmentation du module de stockage, E′) et favorisé la cristallisation nucléée du PLA sans affecter la température de transition vitreuse (Tg). Des charges plus élevées de biochar ont considérablement amélioré la conductivité électrique, atteignant $1{,}24 \times 10^{-2}$ S·cm^{-1} à 70 % en masse de biochar de hêtre activé, et ont conféré des propriétés antistatiques et de blindage électromagnétique. Cependant, une teneur excessive en biochar a entraîné une agglomération des particules, ce qui a réduit la résistance à la traction et diminué l'aptitude au traitement.

Une évaluation technico-économique de la simulation d'une installation de production intégrée traitant 1 t·jour^{-1} de biomasse issue de déchets de bois de hêtre a indiqué des dépenses d'investissement modérées (~5 millions d'euros), avec des coûts de production de 1,55 € kg^{-1} pour le biochar et de 3,95 € kg^{-1} pour les granulés composites. L'analyse de scénarios a démontré une forte viabilité économique lorsque tout le biochar est valorisé dans des formulations composites, avec une valeur actuelle nette élevée, un délai de récupération de 3 ans et un taux de rendement interne d'environ 48 %.

Dans l'ensemble, les résultats soulignent le rôle essentiel du choix des matières premières, des conditions de pyrolyse et d'activation du biochar, ainsi que le taux de charge dans la conception de biocomposites biochar-PLA aux propriétés mécaniques, thermiques et fonctionnelles optimisées, offrant ainsi une autre voie de valorisation en matériaux biosourcés.

Mots-clés : Biochar, Pyrolyse, PLA, Aspen Plus, Biocomposite, Activation physique, biomasse, Économie technique.

Table of Contents

List of figures

List of tables

Glossary of abbreviations and symbols

ALD	Laminaria digitate algae
ATR	Attenuated Total Reflection
BC	Biochar – carbon-rich solid produced by thermal treatment of biomass
BCALD	Biochar derived from Laminaria digitata
BCALDA	Activated biochar derived from Laminaria digitata
BCBW	Biochar derived from beech wood
BCBWA	Activated biochar derived from beech wood
BCFS	Biochar derived from flax shives
BCFSA	Activated biochar derived from flax shives
BDS	Broadband dielectric spectroscopy – determines dielectric constant, loss and AC conductivity
BET	Brunauer-Emmett-Teller theory used for surface area determination
BW	Beech Wood
Ca	Calcium
CAPEX	Capital expenditure – long-term investment costs
CF	Carbonized Fibers
CHP	Combined Heat and Power
Ci	Crystallinity indices – DRX measurements
Cl	Chlorine
cm	Centimeter
CO	Carbon monoxide – product of biomass devolatilization
CO_2	Carbon dioxide – used for physical activation of biochar
Cp	Electrical capacitance – BDS measurements
DMA	Dynamic mechanical analysis

DSC	Differential scanning calorimetry – measures heat flow and thermal transitions
E′	Storage modulus (elastic response) from DMA
E″	Loss modulus (viscous response) from DMA
EBITDA	Earnings Before Interest, Taxes, Depreciation, and Amortization.
EC	Electrical conductivity
EDS	Energy dispersive Xray spectroscopy (often coupled with SEM)
ep	Distance between electrodes – BDS measurements
FS	Flax Shives
FTIR	Fourier Transform InfraRed spectroscopy – identifies functional groups
g	Grams
g/cm³	Grams per cubic centimeter – density
H	Hydrogen
H_2O	Water
H_{cc}	Cold crystallisation enthalpy
HDT	Heat Deflection Temperature
H_m	Melting enthalpies
Hz	Hertz – frequency unit in dielectric measurements
IRR	Internal rate of return
k	Potassium
k€	Thousands of Euros
kJ kg^{-1}	Kilojoules per kilogram – specific energy
kW	Kilowatt – unit of power
kWh	Kilowatt-hour
LOI	Limiting Oxygen Index

m	Meter
MAPP	Maleic anhydride-grafted polypropylene – coupling agent
mm	Millimeter – used for specimen dimensions
MPa	Megapascal – pressure unit
Mw	Microwave
N	Nitrogen
N_2	Nitrogen – inert carrier gas during pyrolysis
Na	Sodium
NCPSD	Non-conventional solid particle size distribution
NPV	Net present value
O	Oxygen
O_2	Molecular oxygen – present in combustion/oxidation steps
OPEX	Operating expenditure – recurring operational costs
PA	Polyamide
Pa·s	Pascal second – viscosity unit
PBAT	Poly(butylene adipate co-terephthalate)
PBS	Poly(butylene succinate)
PCI	Lower calorific value
pH	Potential of hydrogen
PHBV	Poly(3-hydroxybutyrate-co-3-hydroxyvalerate)
PLA	Poly(lactic acid) – biodegradable polymer matrix of this thesis.
PP	Polypropylene
PVA	Poly(vinyl alcohol)
PYRO-REA	Name assigned to the pyrolysis reactor block

RHE	Reference hydrogen electrode (used in electrochemical measurements)
ROI	Return on investment
RSTOIC / RGIBBS	Specific reactor models in Aspen Plus (Stoichiometric and Gibbs free energy)
S	Cross-sectional area
S·cm^{-1}	Siemens per centimetre – unit of electrical conductivity
SBET	Specific surface area measured by the Brunauer-Emmett-Teller method
S_c	Surface area of the crystalline domain – DRX measurements
SEM	Scanning electron microscopy
SEP / SPLITTER	Separation and flow division units
S_t	Surface area of the total domain – DRX measurements
Syngas	Synthesis gas
T	Temperature
T_c	Crystallisation temperature
T_{cc}	Cold crystallisation temperature (on heating)
T_g	Glass transition temperature of the polymer
TGA	Thermogravimetric analysis – measures mass change vs. temperature
TM	Tensile modulus
T_m	Melting temperature
T_{pyro}	Pyrolysis (or carbonisation) temperature
TS	Tensile strength
UHMWPE	Ultra-high molecular weight polyethylene
VP	Pore volume
wt %	Weight percent – composition of filler or matrix

Xc	Degree of crystallinity (percentage)
XRD	Xray diffraction – assesses crystalline/amorphous structure
Δ	Change (used in thermodynamic equations, e.g., ΔT, ΔH)
ε'	Dielectric constant
ε0	Permittivity of vacuum
σ	Electrical conductivity ($S \cdot cm^{-1}$)
ω	Angular frequency
f	Electrical frequency (Hz)
°C	Degrees Celsius – temperature unit
°C min^{-1}	Temperature ramp rate in DSC/TGA (degrees per minute)
µm	Micrometer – particle size unit

GENERAL INTRODUCTION

General introduction

One of the major challenges facing science, industry, and society in the 21st century is the transition to more sustainable production and consumption systems. Currently, the materials sector remains heavily dependent on fossil resources, both for the synthesis of polymer matrices and, for example, the manufacture of fillers or functional additives. This heavy dependence on fossil resources contributes to a high carbon footprint, a major impact on non-renewable resources, and the generation of persistent plastic waste in the environment.

As shown in Figure 1, global plastic production has increased exponentially in recent decades, reaching a historic high of 410 million tons in 2023 [1]. This demonstrates not only the global economy's structural dependence on fossil-based polymers, but also the urgent need to embark on a path toward more sustainable and circular production and consumption systems.

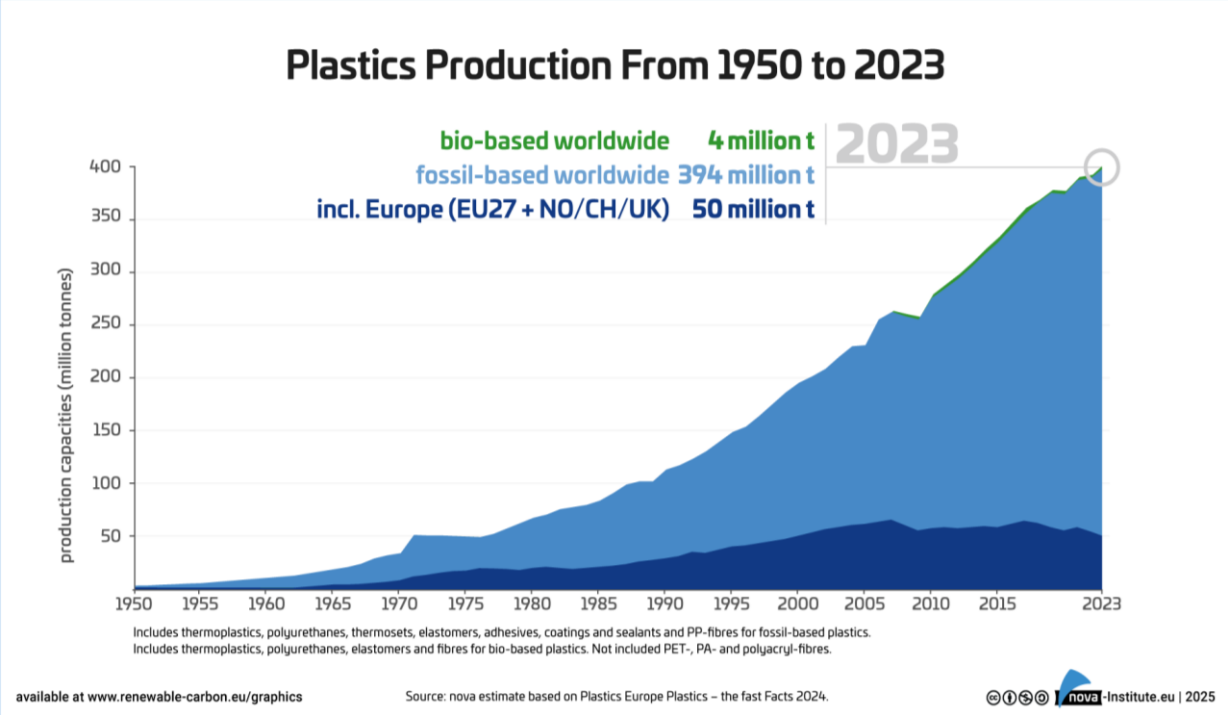

Figure 1: Global evolution of plastics production (1950–2023). Source: nova-Institute (2025). Reproduced under CC BY-NC-SA 4.0 license.

Even though the bioplastics and biopolymers sector is beginning to gain relevance, its market share remains marginal compared to conventional production. This disparity has driven the search for biocomposites that combine biodegradable matrices with sustainable reinforcements, representing one of the most promising solutions for high value-added sectors such as automotive, biomedical, and technical packaging.

In this context, biochar—a porous, carbon-rich material produced from biomass through pyrolysis—emerges as an effective alternative for use as a functional reinforcement. Biochar is characterized by its highly porous structure, large specific surface area, thermal stability, electrical conductivity, and environmentally friendly nature, combined with relatively low production costs. Although its applications have traditionally been confined to agriculture and

environmental remediation, its physicochemical properties make it particularly attractive as a reinforcing agent in biobased composite materials.

One of biochar's major competitive advantages lies in its versatility. Its properties can be tailored through the selection of biomass feedstock, precise control of pyrolysis conditions, and the application of post-treatment activation processes. This tunability enables biochar to be adapted for a wide range of material applications.

Despite its considerable potential and the growing body of research on biochar-based biocomposites, significant scientific gaps remain. In particular, the relationship between the intrinsic properties of biochar and the overall performance of the resulting biocomposites has not yet been fully elucidated. Critical challenges—including particle dispersion, interfacial interactions with biobased polymer matrices such as polylactic acid (PLA), and the real impact of activation treatments on final material functionality—require further in-depth investigation. Moreover, the technical and economic aspects related to biochar production and its industrial-scale integration have been only partially addressed, limiting effective technology transfer.

Within this framework, there is a clear need for research that simultaneously addresses material optimization at the physicochemical level and its feasibility in engineering applications. To bridge these scientific and technological gaps, this thesis, entitled *"**New ways of biochar valorization in biobased materials with controlled properties: characterization and techno-economic study**,"* is proposed.

The main objective of this research work is to study new ways of valorizing biochar in biobased materials with controlled properties. To achieve this goal, the present research program is structured around the following specific objectives:

1. Analyze the influence of biomass type and pyrolysis conditions on the structural, thermal, and surface properties of biochar.
2. Study the effect of physical activation on the porosity, surface chemistry, and functionality of the resulting biochar.
3. Establish relationships between the intrinsic properties of biochar and the mechanical, thermal, and functional behavior of reinforced PLA biocomposites.
4. Analyze the technical and economic feasibility of producing biochar and PLA-biochar biocomposites.

The main research question guiding this work is decrypted as follows: what are the specific physicochemical properties of biochar necessary to obtain biobased materials with efficient technical performance and economic viability?

To answer this question, a methodological approach is considered that combines the production of biochar from three different types of biomasses, the optimization of properties through activation, and exhaustive characterization. The biochar produced is then used as a reinforcement structure in the manufacture of PLA biochar biocomposites. These biocomposites are evaluated in terms of mechanical, thermal, and functional properties, with a deep focus on the effect of biochar. Finally, a technical-economic analysis is developed using process simulation to evaluate the production cost and feasibility of manufacturing biochar and biocomposites. This research falls within the framework of the circular economy and climate

change mitigation, providing information that facilitates the replacement of fossil-based reinforcements with high-performance biobased alternatives.

This document is organized around four closely interconnected sections:

- Chapter 1: The state of the art provides a comprehensive review of the scientific literature on the production, properties, and activation strategies of biochar. Also, it analyzes the current limitations in the development of biocomposites and their applications and identifies opportunities for innovation in the use of biobased carbonaceous fillers.
- Chapter 2: Materials and methods section, where the raw materials and experimental protocols used for the synthesis of biochar by slow pyrolysis are detailed, as well as the activation method used. The manufacturing procedures for polylactic acid (PLA) and biochar biocomposites are also described, in addition to the physicochemical characterization techniques applied to the different products.
- Chapter 3: Results and discussion section, this chapter is divided into two main parts. The first part concerns the properties of biochar. It presents an analysis of the results obtained after the pyrolysis of different biomasses and the activation of biochar. It discusses how the treatment temperature and activation processes modulate the porosity, specific surface area, surface chemistry, and structure of biochar. The second part deals with PLA biochar based biocomposites, evaluating the integration of biochar into PLA matrices and analyzing the influence of reinforcement load and type of reinforcement on chemical, mechanical, thermal, and electrical properties.
- Chapter 4: Technical-Economic Analysis. Based on process simulations (Aspen Plus), this chapter evaluates the economic viability of industrial scaling of biochar production from waste and the subsequent production of biochar PLA biocomposites.

At the end of this document, the most relevant contributions of the thesis are summarized in general conclusion and future lines of research are proposed to continue advancing in the recovery of waste through high-performance materials.

CHAPTER 1
State of the art

1 State of the art

Introduction

Biochar, an organic, porous, and carbon-rich material originating from biomass via pyrolysis, showcases compelling attributes and intrinsic performances. Its appeal as a reinforcement material for biocomposites and its auspicious electrical properties retains more attention and make biochar a versatile candidate for applications ranging from energy storage to catalytic devices.

This state of art undertakes a comprehensive exploration of biochar, spanning production methodologies, physicochemical intricacies, and critical process parameters. The focus extends to optimization strategies for biochar properties tailored to specific applications, with a dedicated inquiry into diverse production methods and activation strategies. The review's second phase delves into a meticulous analysis of key properties within biochar-based composites, emphasizing limitations and unique performance characteristics crucial for diverse applications. By synthesizing a substantial body of research, this review aims to catalyze future investigations by pinpointing areas demanding attention in upcoming experiments, ultimately emphasizing the profound potential of biochar-based materials across technical and scientific domains.

1.1 Biochar: production and properties

1.1.1 Sources of biomass for biochar production

Biomass is defined as any material that is derived from a biological source that can be plant-based and animal-based. Biomass are classified as lignocellulosic and non- lignocellulosic.

Lignocellulosic Biomass represents the most abundant feedstock on Earth to produce biofuels. It primarily consists of two carbohydrate-based polymers, cellulose and hemicellulose along with lignin, a complex aromatic polymer. Naturally occurring biomass is generally categorized into two major types: woody and herbaceous. Woody biomass is typically derived as a by-product of wood processing industries, from forest residues, or cultivated specifically through energy crops. In contrast, herbaceous biomass originates from plants with non-woody stems and is characterized by shorter growth cycles, making it a rapidly renewable resource compared to woody species [2].

Non-lignocellulosic biomass is composed of a variety of components, including proteins, lipids, saccharides, inorganics, and a small fraction of lignin and cellulose [3]. Categories include sewage sludge [4], a by-product of wastewater treatment, which is frequently utilized in agricultural applications and land reclamation, offering potential as a bioresource despite variability in its composition. Manure [5], produced by both humans and animals, is rich in nutrients and commonly applied as a natural fertilizer in farming systems. Aquatic plants, including seaweeds, aquatic seed plants, and microalgae from freshwater and marine environments, represent a promising feedstock, especially in the field of bioplastic and biochar production [6]. Additionally, other organic residues such as animal hair, bones, and meat by-

products are increasingly explored for their utility in biochar synthesis, given their high carbon and mineral content.

1.1.2 Biochar production

Biochar is a carbon-rich solid derived from the thermal stabilization of biomass or any other organic material [7]. In addition to carbon (C), it includes ash, hydrogen (H), oxygen (O), nitrogen (N), and sulfur (S) [8]. Its richness, along with the abundance of functional groups such as phenolics, alcohols, hydroxyls aromatics [9], contributes to its diverse characteristics, including alkaline pH, large specific surface areas, well-structured pores, tunable microstructure, good electrical conductivity, high thermal and chemical stability, make biochar attractive and useful in many fields [10], [11]. Table 1 presents the properties of various biochar produced by pyrolysis at temperatures ranging from 400 °C to 900 °C.

Table 1: Properties of several raw biochar.

Raw biochar material	T_{pyro} (°C)	S_{BET} ($m^2 \cdot g^{-1}$)	V_p ($cm^3 \cdot g^{-1}$)	pH	EC ($S \cdot cm^{-1}$)	C (%)	O (%)	H (%)	N (%)	Ref.
Wheat Straw	500	----	----	10.4	6.53×10^{-3}	67.4	7.3	1.0	1.4	[12]
Canola	600	< 2	0.001	9.4	1.12×10^{-3}	77.5	12.3	2.3	7.6	[13]
Conocarp waste	600	----	----	12.2	9.03×10^{-3}	82.9	6.5	1.3	0.7	[14]
Alkaline lignin	900	27.0	----	----	2.00×10^{-3}	64.0	21.3	0.7	0.8	[15]
Lignin-rich residue	700	14.3	0.029	----	5.00×10^{-2}	70.2	28.2	1.0	0.6	[16]
Walnut shells	700	296.2	0.154	----	1.00×10^{-2}	87.4	10.5	2.1	0.1	[16]
Sewage sludge	700	10.2	0.041	----	2.00×10^{-2}	80.1	10.4	1.0	8 .5	[16]
Bamboo	600	181.0	0.150	----	----	82.9	5.0	2.2	0.5	[17]
Bamboo	600	307.1	0.180	10.1	----	88.4	8.6	2.7	0.3	[10]
Bio solid	400	7.6	0.048	7.5	167×10^{-4}	21.4	20.4	0.9	3.3	[18]
Bio solid	600	32.0	0.058	11.3	406×10^{-4}	14.2	18.5	0.2	2.0	[18]

Caption: T_{pyro} - Pyrolysis or carbonization temperature; S_{BET} – Bruner-Emmett-Teller, surface area; V_P - Pore volume; EC - Electrical conductivity; C - carbone; O - oxygen; H - hydrogen; N - nitrogen, wt.%.

These physico-chemical properties are affected by biochar production conditions, in particular temperature [19]. Studies in the literature show that due to dehydration and decarboxylation reactions, the carbon content in char decreases with increasing temperature. Indeed, under the effect of temperature, light organic compounds essentially volatilize into CO, CO_2, H_2O and light hydrocarbons [20]. Also, unlike biochar produced from lignocellulosic biomass, in which constituents such as lignin are degraded, forming carbon-rich product (T > 500 °C) [21]. It has been shown that the heating rate during pyrolysis has no influence on pH, whereas temperature does. Indeed, the evolution of pH is proportional to the increase in temperature [12]. With increasing temperature, specific surface area and pore volume increase [22], in relation to the

gradual development of porous structure of biochar [18]. However, deformation of the pore structure has been observed at high temperatures greater than 500 °C [23]. Another property positively affected by pyrolysis temperature is electrical conductivity [18]. Some authors link this behavior with the decrease in oxygen rate [15]. While others attribute it to the increase in the content of soluble salts and the decrease in acidic functional group amount in biochar as temperature increases [24].

Due to its multiple and adaptable properties, biochar is increasingly being studied and tested for a wide range of applications such as soil remediation [25], CO_2 capture [26], and the removal of organic [27], inorganic [28], and gaseous [29] pollutants. Moreover, biochar finds application in the production of capacitors [30], batteries [31], composites [32], and the reinforcement of bioplastics [33], among other uses [34], [35].

1.1.2.1 Biochar production techniques

There are various thermochemical routes such as (I) torrefaction, (II) hydrothermal carbonization, (III) gasification, and (IV) pyrolysis to produce biochar [34].

- Biomass torrefaction, also known as light pyrolysis, is a low-temperature (200 - 300 °C) heat treatment used as a pre-treatment of biomass to increase its calorific value and hydrophobicity [36]. During this process, hemicellulose and a portion of the cellulose undergo thermal decomposition, reducing the availability of hydroxyl groups. This prevents the formation of hydrogen bonds that would otherwise capture water molecules, making torrefied biomass more hydrophobic in nature [37]. The process is conducted within a controlled environment under atmospheric pressure, with oxygen content below 21 %, and residence times of biomass ranging from 5 to 120 minutes [38]. Torrefaction is further sub-classified based on temperature range and the medium used, and each sub-classification results in a product with distinct characteristics [39].

- Hydrothermal carbonization is a thermal depolymerization process that is used to convert wet biomass into crude oil, gas, and hydrochar [34]. This process is environmentally friendly and uses moderate temperatures between 180 and 250 °C [40] under a saturated pressure of 2 to 20 MPa [41].

- Gasification is a thermochemical process in which the carbon content of biomass is converted onto a gaseous fuel in the presence of a gaseous medium such as oxygen, carbon dioxide, steam or a mixture of these gases. This process takes place at a high temperature between 700 °C and 900 °C [42]. When air or oxygen is used, gasification is considered a partial combustion process [43]. Gasification is also considered an efficient method of converting waste into energy. Comprising various stages such as drying, combustion, pyrolysis, and the reduction zone also known as the gasification zone [44]. The yield of biochar obtained by gasification is lower than that of pyrolysis [8], but the structural morphology of the biochar produced by the two processes is similar [45].

- Pyrolysis is a high-temperature (300 - 1300 °C) heat treatment that breaks down biopolymer macromolecules into lower molecular weight compounds under an inert atmosphere [7], [10]. It is considered the most extensively studied thermochemical technique

[3]. During pyrolysis, moisture and volatile compounds are released from biomass due to reactions such as dehydration, decarboxylation, volatilization, and polymerization. This process produces syngas, bio-oil, and biochar [46].

1.1.2.2 Types of pyrolysis

Depending on operating conditions, pyrolysis can be classified into different sub-classes. Each pyrolysis class has its own advantages and limitations [47]. The various subclasses include fast, slow, flash, and intermediate pyrolysis, depending on temperature ranges, pressure range, heating rates, biomass, and steam residence time [10], [47]. Other types of pyrolysis, such as vacuum pyrolysis and microwave pyrolysis, have also been reported in the literature [7], [46].

- Slow pyrolysis (also known as conventional pyrolysis): this is the oldest method of charcoal production. It is characterized by a slow heating rate and a long residence time [47]. These conditions of temperature and slowness of the process favor cracking and secondary reactions, which in turn lead to higher yields of biochar [8], [48]. During this pyrolysis, a high production of quinone groups produced by the aromatic radicals of lignin is observed, which can be correlated with complete carbonization of the material [49].

- Fast pyrolysis: this method is characterized by a high heating rate (10-200 $°C \cdot s^{-1}$) and a short residence time for vapor (0.5-10 s). The high heating rate involved in fast pyrolysis transforms the input biomass into a liquid product with a low exposure time in order to avoid cracking reactions that favor biochar formation [50]. The main product of fast pyrolysis is a liquid called bio-oil, which can find application as a liquid biofuel or from which valuable chemicals can be extracted [51]. The biochar produced by this type of pyrolysis has a higher porosity than that obtained by slow pyrolysis, which may be linked to a higher production of bio-oil [49].

- Flash pyrolysis: is a variant of fast pyrolysis, with higher heating rates and temperature (> 900°C) and shorter exposure time (< 1 s) [47]. The combination of these two features results in high yield of bio-oil and low yield of biochar [52]. Some of the disadvantages of this process are illustrated by the thermal instability of the bio-oil composition and its low pH, which make it corrosive. Also, fine particles can be entrained and find their way into the bio-oil [53].

- Intermediate pyrolysis: this type of pyrolysis is generally used to achieve a balance between liquid and solid products, i.e. between slow pyrolysis that gives the high biochar yields, but relatively low liquid products [10], and fast pyrolysis [43], [47].

- Vacuum pyrolysis: is the thermal degradation of biomass under low pressure (0.001-0.02 MPa), in the absence of oxygen and without the need for a carrier gas to maintain the inert atmosphere [54]. This methodology is considered a promising technology for recovering energy from biomass and has proved to be an alternative means of obtaining oils enriched with valuable fatty acids [55].

- Microwave-assisted pyrolysis: use microwave radiation as a heat source during pyrolysis, providing non-contact, rapid, selective, and energy-efficient heating. Also has a shorter processing time than conventional technologies using electrical energy as the heating source [46], [56]. This type of pyrolysis has many advantages, but its industrialization is a

challenge due to the complexity of reactor design, process control, and safety. Furthermore, most studies have been carried out on a laboratory scale, which contracts with the growing need for large-scale systems [57]. The design of the microwave oven will depend on the final product [7], [46]. For heating, microwaves penetrate the material forming a temperature gradient from the inside to the outside [58]. This type of pyrolysis promotes the development of porosity [7], [56]. The operating conditions for the above-mentioned pyrolysis process are shown in Table 2.

Table 2: Operating conditions for pyrolysis thermal conversion.

Conditions	**Pyrolysis type**					
	Slow	**Fast**	**Flash**	**Intermediate**	**Microwave - assisted**	**Vacuum**
Temperature (°C)	300 - 700	500 - 1000	800 - 1300	500 - 650	300 - 700	300 - 600
Heating rate (°C/s)	0.01 - 1	10 - 300	> 1000	1.0 - 10	0.5 - 2	0.1 - 1.0
Vapor residence time (s)	Minutes to hours	0.5 - 10	< 0.5	0.5 - 20	< 30	0.001 - 1.0
Particle size (mm)	5 - 50	< 1	< 0.2	1 - 5	----	----
Pressure (MPa)	0.1	0.1	0.1	0.1	5-20	0.01 - 0.02
References	[30], [43], [47], [52], [59], [60], [61]	[30], [43], [47], [52], [57], [59], [62]	[43], [47], [52], [59], [60], [61]	[43], [47], [60], [61], [63]	[46], [52], [60]	[54], [57], [61]

Even though fast pyrolysis and flash pyrolysis are unfavorable for biochar production [52], biochar obtained has a higher specific surface area than the derived from slow pyrolysis. Due to the shrinkage of the solid matrix at higher temperature, the average pore diameter of biochar decreases, leading to the increase in specific surface area and availability of diffusion /reaction sites [64].

The effect of temperature, heating rate, and pyrolysis residence time has been studied by several authors in the literature [12]. In general, they have observed that biochar yield decreases with increasing pyrolysis temperature [65]. The amount of fixe carbon, pH, surface area and pore diameter rise with temperature due to thermal degradation of organic biomass [10]. The dominant functional groups of biochar, C-O and C-H, also decrease with higher heating temperatures due to more favorable dehydration [12]. At high temperatures, there are few hydrophilic functional groups available to establish a hydrogen bond with water [49]. Consequently, biochar produced at high temperatures has little affinity for water [66].

Another factor that has a significant effect on biochar properties is the way it is heated. The relatively high porosity of low-temperature biochar in microwave pyrolysis may be attributed

to the heat and mass transfer mechanisms during microwave heating. Because this heating is volumetric with a slow-temperature front, volatile substances formed inside the particles can escape freely, leading to pore formation, resulting in a great advantage [7].

1.1.2.3 Biochar activation

Even with precise control of pyrolysis parameters, the desired biochar properties may not be attained, necessitating activation. Among the most crucial properties of biochar are its porosity and surface area, which can be significantly altered through physical and/or chemical treatments [67], as illustrated in Figure 2. These treatments are also valuable for modifying the functional groups within the biochar. This adaptability renders biochar a versatile product suitable for various applications, as its properties can be tailored to enhance its performance [68]. Additionally, electrical properties may be potentially influenced after activation [69].

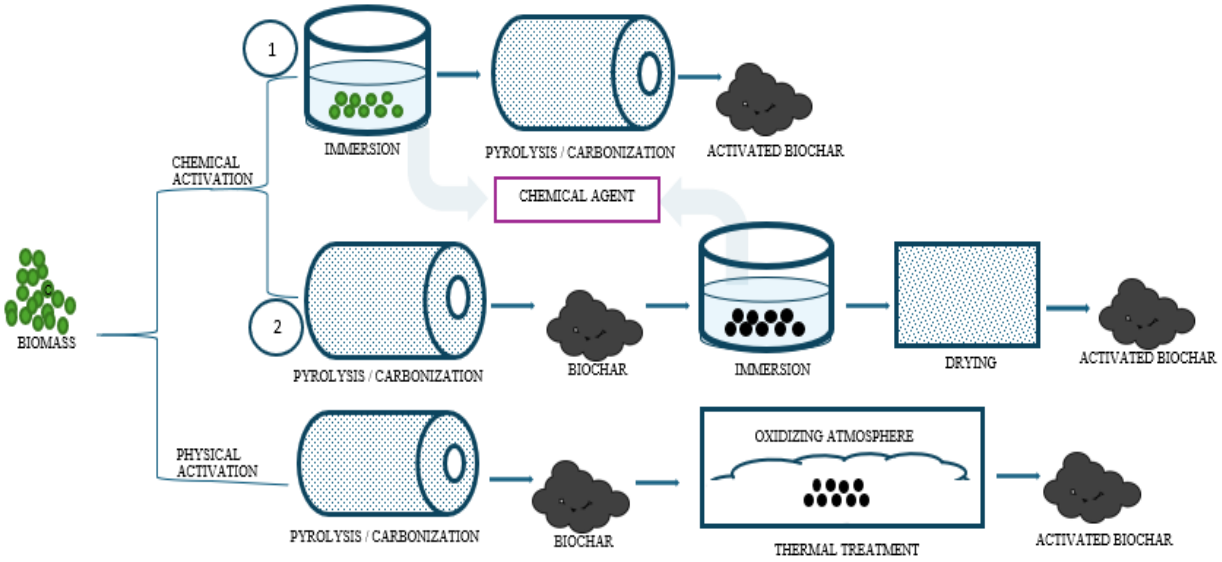

Figure 2: Physical and chemical activation process.

Chemical activation of biochar can be achieved through two processes: (i) impregnating the raw biomass with a chemical agent and then subjecting it to heat treatment. During this process, the chemical agent dehydrates the sample and inhibits tar formation and evolution of volatile compounds. This increases the efficiency of the carbonization process [70]. In this case, porosity and elemental composition depend on the distribution of chemical agents in the biomass and on the activation parameters [71]. In the second process (ii) the biochar is immersed in a solution of a chemical agent (acid, base, salt, etc.) at room temperature up to 120 °C for a set period of time [72], and then a secondary heat treatment is used to obtain the desired modified biochar [72], [73].

Physical activation takes place in two stages. First, carbonization, often carried out by pyrolysis in an inert atmosphere between 600 °C and 900 °C. Secondly, activation of biochar by thermal treatment in an oxidizing medium such as water vapor, carbon dioxide, ozone, limited air or moisture. The active oxygen in the activating agent is responsible for the combustion of the

most reactive parts of the carbon structure and the tar retained in the porous structure [68]. The most common activating agent is steam [74]. The increase in porosity is more significant at higher temperatures [68]. Furthermore, high-temperature steam activation significantly mitigates the adverse impact of low-temperature pyrolysis on the surface and porosity of biochar [75].

Compared to physical treatment, chemical activation produces higher activity with greater total surface area and pore volume [76]. This activation can be carried out at relatively low temperatures. However, the improved biochar activity and process efficiency is achieved with chemicals that are expensive, difficult to recover and responsible for corrosion of equipment leading to various environmental problems [70].

1.2 Biochar composites

Biochar composites and biocomposites retain more attention in recent years and exhibit excellent properties such as mechanical [77], thermal [78], and remarkable electrical conductivity [16]. The formulation of biochar composites is made by using synthetic polymers (PP, PVA, PC, etc.) or biopolymers (PLA, PBS, PHBV, etc.) as illustrated by Figure 3**.**

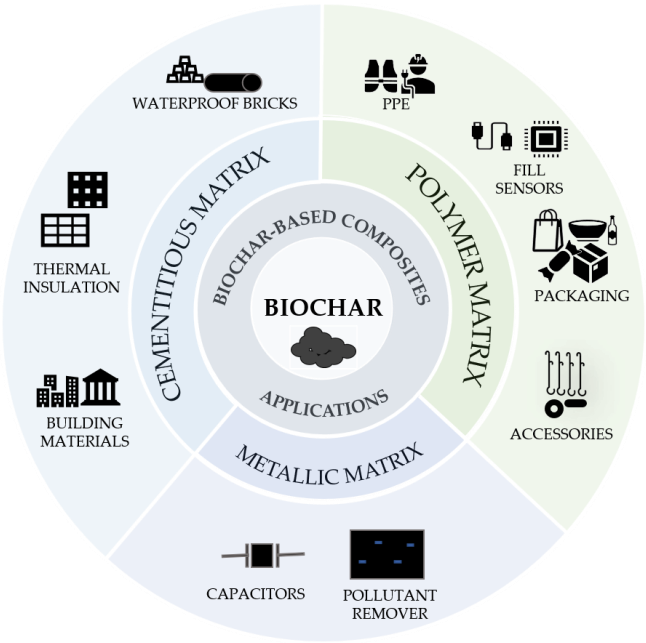

Figure 3: Composite reinforced with biochar.

Moreover, biochar biocomposites demonstrate good degradability and compostability [79] as well as high performance shielding against electromagnetic interference [80]. In addition, due to biochar's high CO_2 adsorption and retention capacity, it is also used to enhance the CO_2 sequestration capacity of certain composites [81]. Furthermore, the low density of biochar allows for the inclusion of a larger quantity of fillers in synthetic polymers, while significantly limiting the increase in the weight of the overall product. To illustrate, the final product weight of a composite containing 50 % biochar (with a density of approximately 1,3 -1,4 $g \cdot cm^{-3}$) in PP matrix (~ 0,91 $g \cdot cm^{-3}$) is much lower than that of a composite containing talc (~ 2,7 - 2,8 $g \cdot cm^{-3}$) and carbon black (1,8 - 2,1 $g \cdot cm^{-3}$) with the same filler content [82]. The utilization of biochar

as reinforcement in biocomposites is highly versatile and diverse. Biochar can be used as a standalone reinforcement [82] or can be effectively combined with various materials, including wood fibers [83], cellulose [84], glass fibers [85], and more. Its applications extend across a wide spectrum of matrix groups, as illustrated in Figure 3. It is also employed in composites with cementing matrices [86], and with polymer matrices such as PE [87], PLA [88], PP [89], nylon [90], rigid polyurethane foams [91], PC [92], Epoxy Resin [93], etc. The latter being the most widely studied and used matrix in the world [34].

1.2.1 Metal and cementitious matrix-based biochar composites

Industrialization and rapid technological progress have led to chemical contamination of water, affecting the environment and the health of living organisms. As some pollutants do not degrade and accumulate within living organisms, new alternatives have been sought. One alternative is the use of biochar-based composites to ensure the product's biodegradability. As shown in the study by Jinchuan Yan *et al.* [94], biochar-supported nanoscale zerovalent iron composite was employed for trichloroethylene removal. Also, Zhang *et al.* [95] used chitosan-modified magnetic biochar to enhance Cr (VI) removal from aqueous solution. The maximum adsorption capacity increased from 75.8 $mg \cdot g^{-1}$ for the magnetic biochar to 127 $mg \cdot g^{-1}$ for the modified magnetic biochar. Other examples are highlighted by L. Liang *et al.* [96] where they reported different methods of producing magnetic biochar composites to remove inorganic contaminants such as acid orange 7(AO_7), Ni(II), Cr(VI), Pb(II), Cu(II), Cd(II),Zn, etc., and organic pollutants such as dyes, phenol, pesticides, and antibiotics.

Silva *et al.* [97] show the potential application of waste-based magnetic biochar/titanium dioxide (BC/TiO_2) composite materials in the photocatalytic removal of antibiotics from aquaculture effluents. In their study, the authors evaluated the photodegradation of two widely used aquaculture antibiotics, sulfadiazine (SDZ) and oxolinic acid (OXA). The observed removal rates were 87 % for SDZ and 98 % for OXA when using 100 $mg \cdot L^{-1}$ of the $BCMag\_TiO_2$ composite.

1.2.1.1 Cementitious composites

The properties of biochar-based composites extend beyond water decontamination; they are also finding applications in building materials using clay as a matrix [98], concrete [99] and cement [100], as depicted in Figure 3. The use of biochar is seen as a potential solution for improving the properties of cementitious composites. The addition of mixed wood feedstock biochar significantly improves the mortar's waterproof, compressive strength, and flexural strength. In addition, it promotes waste recycling and carbon sequestration [89]. Gupta & Kashani [101] found that adding 3 % of pyrolyzed peanut shell biochar at 500 °C to cement matrix reduces its workability; however, it increases the setting speed of cement by 30 %, increases hydration by 23 %, improves compressive strength by 20 % and can reduce CO_2 equivalent emissions due to net carbon sequestration of the biochar. Similar results were obtained by K. Tan *et al.* [102] by studying the effect on certain properties when replacing some portions (0 %, 1 %, 3 %, 5 %, et 10 %) of cement with pyrolyzed wood biochar obtained at different temperatures (between 400 - 700 °C). They also found that the albedo (the fraction of

light that is reflected by an object) and thermal conductivity of the mortars decreased linearly with the biochar content.

This trend in physical properties and environmental benefits was also presented by Roychand *et al.* [103], when studying the recycling of bio-solids as cement composites. They compared the properties of three composites: I) composites with cement and biosolids in raw form; II) composites cement and biochar from bio-solids pyrolyzed under nitrogen at 600 °C for 1 hour; III) finally, composite cement and ash produced from bio-solids calcined at 550 °C for 15 hours. They observed that adding 10 % biosolids to the cement compound increased its total porosity by more than 21 times and decreased its compressive strength by 80 % at 28 days of curing. On the other hand, adding the same percentage of biochar enhanced its mechanical resistance of ~ 278 % and reduced its total porosity of ~ 87 % compared to that of cement compounds mixed with biosolids. Finally, replacing 10 % cement with bioash showed a ~ 66 % reduction in total porosity and 11 % reduction in compression strength at 28 days compared to cement specimens mixed with biochar. In contrast, Laili *et al.* [104] showed that using oil palm empty fruit bunch biochar as cement reinforcement has no effect on compressive strength but positively affects water resistance. Cement specimens reinforced with more than 8 wt.% biochar, were found to be water resistant. In contrast, samples containing 5 wt.% biochar failed the water immersion test, cracking and crumbling after four weeks.

1.2.1.2 Influence of particle size in cementitious biochar composites

It should be noted, however, that the particle size of the biochar used plays an important role. According to Restuccia & proFerro [105], the toughness of cementitious composites is significantly influenced by the particle size of materials and their effective dispersion within the cement paste. Lieu *et al.* [106] indicate that dispersion is a critical factor influencing the capacity of particles to enhance composites. Consequently, inadequate dispersion of particles results in various defects within the composites and diminishes the reinforcing impact of particles.

Gupta and Kua conducted a study investigating the effect of particle size and biochar dosage on the fresh and hardened properties of cement mortar [107]. The findings revealed that both coarse biochar (2 - 100 μm) and fine biochar (0.10 - 2 μm) expedite cement hydration, leading to higher early strength development compared to control samples. Additionally, the authors noted a significant reduction in early age (One day) water permeability by approximately 50 % with the addition of 0.50 wt.% coarse and 1 wt.% fine biochar. This reduction was attributed to the pore refining and densification effects of biochar in the cementitious paste. However, it is important to note that the rugged texture of biochar adversely affects the workability and rheology of cementitious mixes, while the fine particles of biochar enhance water tightness in cementitious materials through pore compaction and blocking [108].

1.2.2 Polymeric biochar-based composites

Biocomposites and biodegradable polymers offer an alternative to the ecological crisis and plastic pollution. They are already used in a wide range of applications, including biomedical [109], automotive [110], aviation [111], packaging [112], textile fibers [113] and others [114].

However, these biocomposites have certain weaknesses in terms of mechanical, electrical, and thermal properties. Consequently, biochar has been used to improve their physical behavior and increase their biodegradability. Table 3 illustrates the mechanical and thermal properties of biochar-based composites.

Table 3: Mechanical and thermal properties of some biochar-based composites.

Polymer or biopolymer	**Raw Biochar**	**Biochar Temperature (T_{pyro}) (°C)**	**Biochar load (wt. %)**	**T_C (◦C)**	**T_m (◦C)**	**T_S (MPa)**	**T_M (GPa)**	**Ref.**
PP	Date palm	900	0.0	120.9	165.7	35.0	1.1	[115]
			5.0	123.2↗	165.2↘	34.5↘	1.1↗	
			15.0	123.1↗	166.6↗	34.0↘	1.4↗	
PLA	Coffee powder waste	700	0.0	129.3	153.4	52.5	2.5	[116]
			5.0	128.3↘	152.8↘	51.0↘	2.7↗	
			7.5	126.6↘	150.2↘	50.1↘	2.8↗	
PLA	Bamboo	-	0.0	129.1	159.8	34.0	2.8	[117]
			7.5	135.1↗	156.6↘	40.7↗	3.7↗	
PLA	Cotton fibers	1 000	50.0	-	151.0↘	47.6↗	-	[118]
PA 4,10	Corn cob	500	10.0	247.3	225.9	68.0	3.1	[119]
			20.0	248.4↗	224.9↘	66.0↘	3.4↗	
PP	Starch	1 100	0.0	113.2	159.7	21.7	0.4	[120]
			0.50	113.5↗	160.2↗	36.6↗	0.6↗	
			1.0	121.3↗	162.9↗	36.9↗	0.7↗	
PLA/PBAT 75/20 70/20	Coconut shell	800	5.0	99.0	176.7	28.2	2.5	[32]
			10.0	98.0↘	176.8↗	24.6↘	2.5↗	
UHMWPE	Bamboo	1 000	60.0	134.3	121.7	94.5	1.4	[121]
			70.0	133.9↘	122.4↗	128.9↗	2.0↗	
			80.0	132.8↘	122.8↗	95.0↗	2.1↗	
PBS	Miscanthus	~ 500	0.0	91.2	115.7	41.5	0.8	[122]
			10.0	89.4↘	115.2↘	42.5↗	1.1↗	
			15.0	89.8↘	115.8↗	42.5↗	1.2↗	
			20.0	88.4↘	115.5↘	43.0↗	1.3↗	
			25.0	87.9	115.6↘	44.0↗	1.3↗	
Nylon	Miscanthus	650	20.0	196.4	222.3	81.0	2.5	[90]
PHBV	Miscanthus	650	0.0	124.0	174.0	38.3	3.5	[123]
			10.0	121.0↘	175.0↗	32.2↘	3.7↗	
			20.0	122.0↘	174.0≡	33.1↘	4.7↗	
			30.0	124.0≡	174.0≡	32.8↘	5.2↗	

Caption: - No data; T_{pyro} - Pyrolysis or carbonization temperature; T_C - Crystallization temperature; T_m - Melting Temperature; T_S - Tensile Strength; T_M - Tensile Modulus; PLA - polylactic acid; PP - polypropylene; PA - polyamide; PBAT - polybutylene adipate-co-terephthalate; UHMWPE - Ultra high modular weight polyethylene; PBS - Poly(butylene

succinate); PHBV - poly(3-hydroxybutyrate-co-3-hydroxyvalerate); ↘ - diminution; ↗ - Increase; ≡ - no or very little variation from reference.

Several studies have shown that the addition of biochar to PLA promotes crystallization and increases its biodegradability. This addition can also result in a composite material which is recyclable, compostable, and can be used to manufacture agricultural accessories, such as branch separators or tomato supports [124]. This is due to the fact that modified PLA presents good mechanical properties and thermal stability compared to PLA alone [125]. A similar trend toward improving these properties is evident in biocomposites with other polymers matrix, such as bio-sourced polyamide [119]. Papadopoulou *et al.*[79] studied biocomposites of butylene succinate with varying biochar content (1 %, 2.5 %, and 5 % by weight). They found that the inclusion of 2.5 wt.% miscanthus straw biochar, compared to butylene succinate alone, resulted in notable enhancements: around 19 % in tensile strength, 19 % in Young's modulus, and 39 % in impact resistance. Moreover, they observed an increase in crystallization, diffusivity, and thermal conductivity. As well, Cooper *et al.* [122] added miscanthus biochar to a bio-sourced poly(butylene succinate) matrix to improve the thermomechanical properties of the bioplastic. They observed that biocomposites filled with 25 % biochar showed improvements of 57 %, 13 % and 32 % in tensile modulus, thermal deflection temperature, and thermal expansion, respectively.

The addition of biochar to some polymers has beneficial effects with respect to the heat release rate. The high thermal stability of the biochar contributes to reducing it. Das *et al.* [126] show that adding 35 wt.% pine wood biochar to Polypropylene reduces around 54 % peak heat release rate (PHRR). The biochar is also useful to improve the mechanical properties of other biocomposites. Das *et al.* [127] exposed that adding 24 wt.% of biochar to a wood-polypropylene bio-composite increases its tensile modulus from 3.1 to 3.5 GPa, and flexural modulus from 2.3 to 3.4 GPa approximately.

In some cases, it is possible to obtain biocomposites reinforced with biochar derived from the same material. For instance, in the research conducted by Das *et al.* [128] three different charcoals 6 wt.% (gluten char, pine bark char and carbon black) to make a composite with wheat gluten plastic. They found that the addition of biochars to gluten significantly enhanced its properties. However, among all the composites, the one with gluten char was found to have the best mechanical and water-resistant properties, with a substantial reduction in water uptake by 38% and increase in indenter-modulus by 1 525 %.

The manufacturing capability of biochar-based composites is diverse and highly applicable, for example: PLA reinforced with biochar from wheat stalks pyrolyzed at 800 °C used for 3D printing, as shown in Figure 4A [129] or composite of thermoplastic polyurethane (TPU) and digitalis purpurea biochar, produced at 450 °C for 3D printed film [130]. Other examples include BIOPLAST GS2189 reinforced with 2.5 % and 5 % wood biochar pyrolyzed at 550 °C for the manufacture of agricultural accessories such as biodegradable supports to avoid breaking tomato stalks (Figure 4 C) [78]. As well as a 50/50 blend of starch and polycaprolactone reinforced with various fillers (10 %, 20 % and 30 %) of biochar pyrolyzed at 800 °C from coffee grounds to produce thermoformed containers (Figure 4 B) [131]. Other research has

highlighted the appeal of biochar-based biocomposites for lightweight automotive parts due to their low weight and environmental impact.[132].

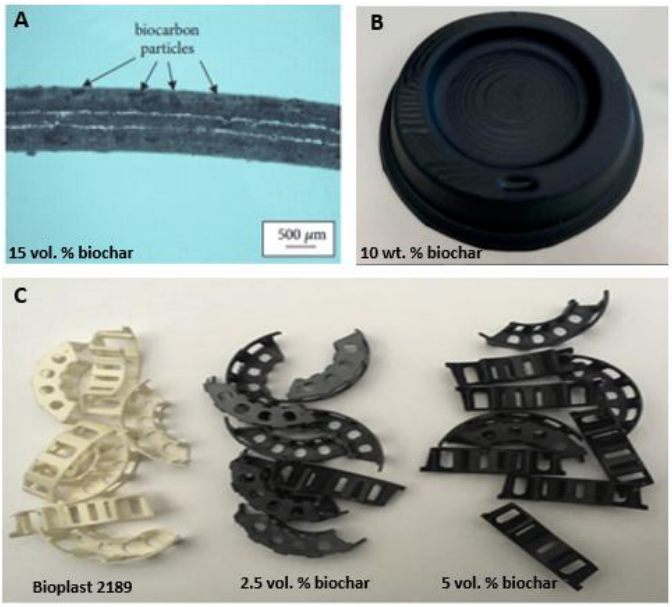

Figure 4: Images of different biochar-based biocomposites taken from the literature presented above: A) filaments PLA with 5 vol.% biocarbon. B) thermoformed coffee lid made with 10 wt.% biochar from spent coffee grounds. C) biodegradable support, Bioplast 2189 and Bioplast 2189-biochar composites.

1.2.3 Factors affecting the properties of biochar-based biocomposites

The properties of biochar-based composites are influenced by several factors, including the textural and structural characteristics, and dispersion of biochar added [125]. Additionally, the use of coupling agents plays an important role. The proper dispersion of biochar particles has been shown to improve the mechanical properties and rheology of biocomposites [133]. In some cases, the addition of biochar severely increased the zero-shear viscosity from approximately 160 Pa·s to over 5000 Pa·s. However, reducing the particle size significantly reduced it to approximately 260 Pa·s [134]. To achieve this, various techniques are used, such as ball milling, which reduces the size of biochar particles. However, this reduction can sometimes lead to a decrease in functional properties like electrical conductivity [135]. Richard *et al.* [136] studied the effect of loading and particle size on the tribological properties of polymer composites reinforced with biochar particles. They found that increasing the content rate with biochar particles reduces the coefficient of friction and wear rate of the composite compared to the neat polymer.

Zhang *et al.* [87] emphasized the significance of a well-structured porous surface. They revealed that increasing the pyrolysis temperature reduces the number of functional polar groups in biochar, increasing the affinity between biochar and non-polar groups of the polymer. However, it's important to note that the porous structure of the biochar, which facilitates strong physical and mechanical bonding within the bio-composite, has a more pronounced impact on mechanical properties than this affinity. The authors highlight that better mechanical properties of biocomposite were reached with biochar pyrolyzed at 500 °C and 600 °C, which exhibited

the best pore structure. Nizamuddin *et al.* [137] observed this phenomenon in which high porosity favors polymer infiltration into its pores, resulting in better properties.

In some cases, coupling agents such as maleic anhydride grafted polypropylene (MAPP) have been used to improve the interfacial bonding of components in composites. The use of MAAP can potentially improve the mechanical and water absorption properties as well as the dimensional stability of the composites [138]. By adding 9 wt.% MAPP to the bamboo-polypropylene composite, the flexural, tensile and impact strengths increased by 22.9, 29.6 and 1.92 %, respectively, compared to the base composite [139]. Other studies have shown that the use of MAPP in biochar-wood-polymer composite improves the materials due to the reaction of the MAAP carbonyl group with the hydroxyl group of the wood or natural fiber [140]. However, due to the porous structure of biochar that facilitates polymer infiltration and creates mechanical interlocking or physical bond, certain properties such as the flexural strength in the biochar-polymer composite is increased by 12 % compared to the polymer alone, without any needs of coupling agents [141]. Therefore, for biochar-polymer biocomposites, it is preferable not to use MAAP due to the absence of functional groups on the biochar surface, which would not contribute to the adhesion of the composite elements [126].

1.2.4 Biocomposites based on activated biochar

The surface of biochar can be readily modified to improve its compatibility with polymers and thus obtain composites with better properties. For this purpose, some authors have chosen to use plasma-retreated biochar or activated carbon to ensure a better interface between filler and polymer [120].

A study conducted by Zhang *et al.* [84] showed that the incorporation of active biochar into MCC/PLA composites had the effect of stimulating an early exothermic crystallization, increasing the glass transition temperature and melting temperature and retarding composite degradation. With the addition of biochar, certain mechanical properties were improved, notably (i) tensile strength, (ii) flexural strength, and (iii) impact strength. The stiffness, elastic, creep resistance, and anti-stress relaxation capacity of the composite were also improved.

Another study, conducted by Lan *et al.* [142] showed that using chemically modified tree bark biochar to prepare polydimethylsiloxane composite membranes improved the overall performance of the membranes. The modified particles were well dispersed in the polymer matrix, resulting in enhanced mechanical properties. However, it should be noted that while activation of biochar can improve many mechanical properties, the activation method used can have an impact on the electrical properties of composites. Some studies show that KOH activation tends to attack the structural domains of the carbon matrix, resulting in a highly porous and disordered structure, with poor electrical conductivity [143].

Ho *et al.* [117] observed that the tensile and flexural strengths and also the ductility index of PLA/bamboo biochar composites increased with the percentage of biochar. The latter reached maximum values when the bamboo biochar charge was at its optimum at around 7.5 %. This improvement was attributed to a good dispersion of biochar particles in the polymer matrix. Similarly, Pudełko *et al.* [78], who used biochar derived from wood and sewage sludge (10 - 20 %) as reinforcement in polylactic acid (PLA) and BIOPLAST GS2189, found a decrease in

the mechanical properties of the composites due to the agglomeration of the biochar particles. This observation underlines the importance of good dispersion to improve the mechanicals properties of biochar-based composites.

In summary, as explained by Das *et al.* [141], the use of activated carbon in composites has several advantages. First, it promotes sustainable and cleaner production by using waste. Second, higher surface area, carbon content, hardness and stiffness of the active biochar improve the performance of biocomposites. In addition, adding active biochar to the bio-composite could reduce manufacturing costs, as less MAPP can be used to maintain comparable mechanical and flammability properties.

1.2.5 Fire-resistant biocomposites

Although biochar is used as a fuel, it is also useful to improve the fire resistance of biocomposites. Choi *et al.* [144] reported that the presence of biochar improves the thermal stability of composite blocks of corn cob powder, achieving a 27.6 % improvement in composites containing 10 % biochar (Figure 5 part A). In a recent study, Shah *et al.* [145] evaluated the fire-retardant properties of rice husk biochar reinforced recycled high-density polyethylene. Using different loads of biochar from 10 to 40 wt.%, authors observed that the flammable properties were improved with biochar rate and affirm that at high content (40 wt.%), the rice husk biochar reinforced recycled PE exhibited the best thermal stability (Figure 5 part B), the lowest burning rate, the highest limited oxygen index (LOI), and displayed the best fire-retardant properties.

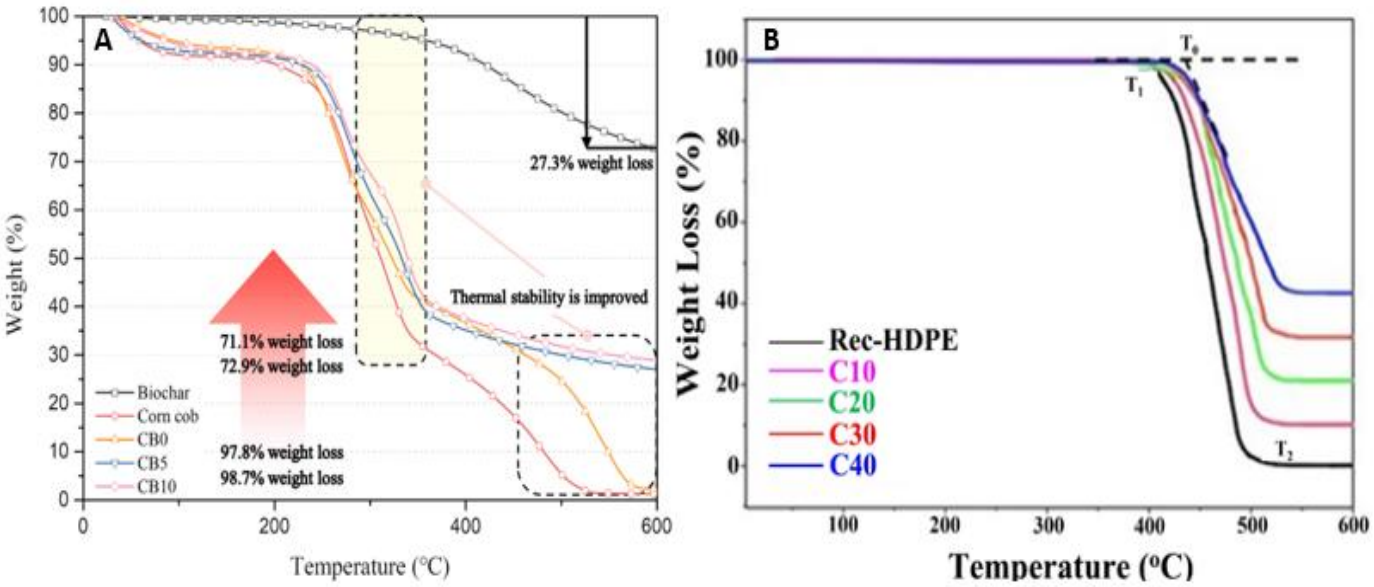

Figure 5: A) TG curves of corn cob, corn cob biochar and their composites from Choi et al. [144]. B) TG curves of the recycled HDPE and HDPE rice husk biochar composites from Shah et al. [145].

The trend of reduced flammability in composites due to the presence of biochar has been observed by Das *et al.* [146] who also observed that in biochar-based wood/polypropylene

composites, a higher proportion of biochar and less wood is beneficial in reducing flammability. The stability of biochar contributes to the formation of effective carbon to limit the transfer of oxygen gas to polymers as seen in Figure 6. This also compromises tensile and flexural strength, as when biochar pores are filled with flame-retardant substances, polymer infiltration into the biochar becomes ineffective and thus limits physical adhesion.

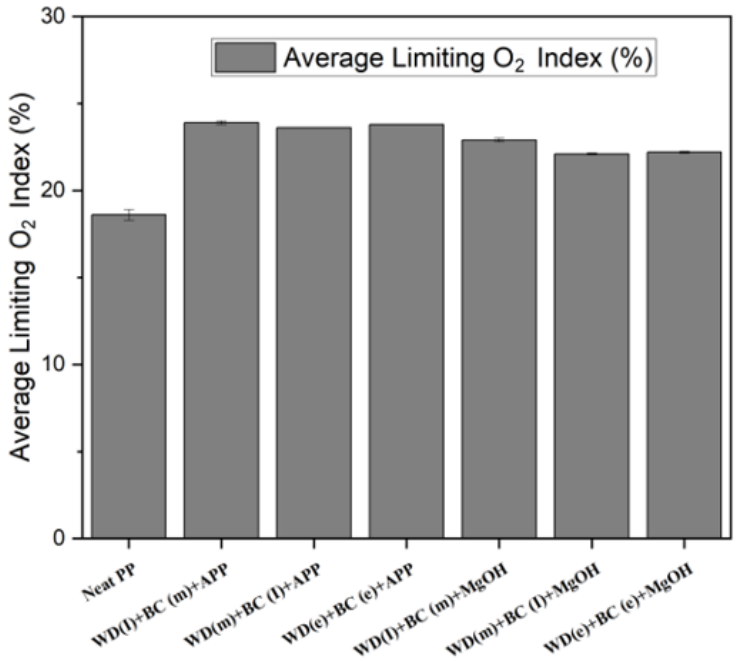

Figure 6: Graph of the average limiting oxygen index in different biocomposites, created from data provided by Das et al. [146].

In other studies, biochar is used to host a naturally flame-resistant material, such as lanosol. Perroud *et al.* [33] Studied the effects of lanosol-doped biochar on the mechanical and fire resistance properties of bioplastics. To manufacture the composite, 4 wt.% of lanosol was initially doped into 6 wt.% of biochar using various techniques: mechanical (dry mixing), chemical, and thermal doping. Subsequently, this biocarbon, doped with lanosol, was blended with 65 wt.% wheat gluten and 25 wt.% glycerol. The study revealed that all bioplastics incorporating the doped biocarbon exhibited enhanced flame retardancy compared to the bioplastic alone. Notably, the composites utilizing lanosol thermally doped in biochar demonstrated superior mechanical resistance compared to the other two composite variations.

1.2.6 Electrical characteristics of biochar-based biocomposites and their practical applications

Owing to their fundamental molecular arrangement, naturally-occuring polymeric compounds generally demonstrates insulating behaviour, due to covalent bonds, and absence of readily available charge transporters, consequently impeding electron movement across the material structure [147]. Such a characteristic, useful where dielectric steadfastness matters, in practice restricts their deployment where electrical conductance is critical, like in sensors, antistatic layers, and flexible electrical components.

Nevertheless, incorporating biochar, a carbon enriched substance, represents a hopeful tactic for getting past this barrier. Properly designed to boast appropriate properties, *e.g.* large area, right porosity, and graphitic carbon regions [148], biochar can greatly improve pathways for transporting electrical charges within the material. The approach not just improves electrical conductance, of resultant biocomposites, but additionally, works in tandem with values of both eco-friendliness, alongside affordability. Derived from agricultural or waste products, biochar emerges as a renewable and relatively economical additive. Therefore, biocomposite-polymers strengthened with biochar, signify an ecologically sound solution when it comes to advanced functional material generation, and these are useful for electronic systems, sensing elements, protection against electromagnetic radiation, as well as "smart" packaging.

Ahmed *et al.* [149] indicated that 5 wt.% biochar is the minimum required amount to make an electrically conductive sugarcane bagasse biochar / polyvinyl alcohol biocomposite films. Unterweger *et al.* [150] analyzed the properties of poly(3-hydroxybutyrate-co-3-hydroxyvalerate) and biochar derived from carbonized wood dust and cellulose fibers at temperatures ranging from 900 to 2 300 °C. They observed a significant improvement in mechanical performance and electrical conductivity. The latter improved by increasing the biochar charge, reaching 1.7 $S \cdot cm^{-1}$ when the biochar load was 15 to 20 % by volume. As presented in Figure 7.

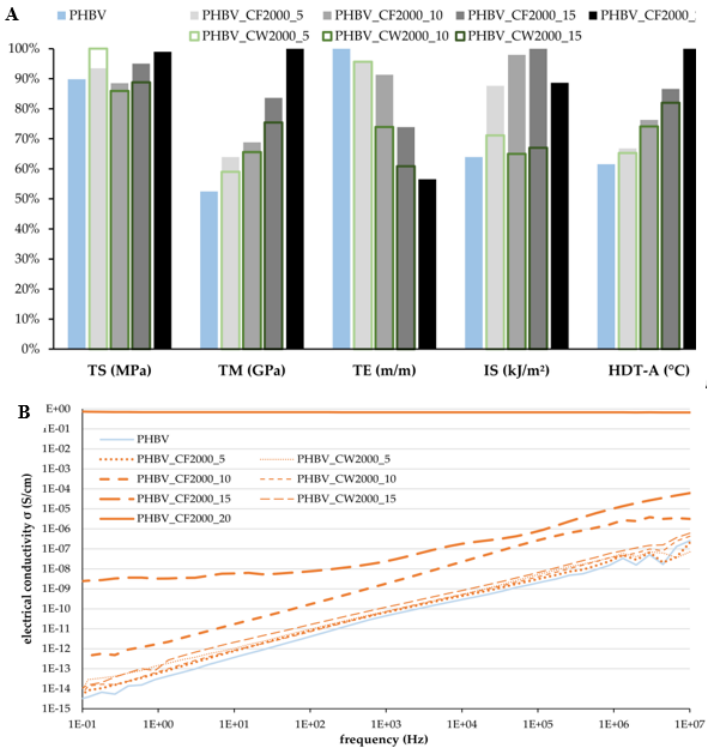

Figure 7: Graphs of mechanical and electrical properties of biocomposites extracted from Unterweger et al. [150]. A) Relative mechanical performance in dependence of filler type and fill content. Tensile. Tensile strength (TS), modulus (TM) and elongation at break (TE), impact strength (IS), and heat deflection temperature (HDT-A). B) Electrical conductivity of PHBV composites in the measured frequency range. Impact of filler content (5 - 20 vol.%) and filler type (carbonized cellulose fibers (CF) or wood dust (CW)).

Figure 7 part A, shows that biochar loading has a pronounced effect on the mechanical properties of the composite. In particular, the tensile modulus and tensile strength improved significantly with increasing biochar fraction, suggesting an increase of stiffness and strength in the polymer base. In contrast, the elongation at break decreased with a general increase in the matrix stiffness that resulted in decreased ductility. Conversely, both impact strength and heat deflection temperature improved significantly, suggesting that the thermo-mechanical stability of the reinforced composites is enhanced.

The changes to electrical conductivity (σ) with frequency are presented in Figure 7 part B. The control (PHBV) had a very low conductivity value, which is expected as it is insulating polymer. However, the addition of the biochar, CF2000 in particular, demonstrates that the conductivity increased exponentially with biochar content, even exceeding several orders of magnitude of the neat polymer. This effect arises from conductive networks forming in the matrix that assists the charge transport process. Importantly, the findings demonstrate that biochar will enhance the stiffness, thermal stability of PHBV and electrical conductivity of the material, providing more direction for novel applications within functional biocomposites.

This behavior of conductivity as a function of biochar loading has also been demonstrated by Umerah *et al.* [151] who showed that the conductivity of biochar composites from coconut shell waste and PLA increases with the increment of biochar load. Their results suggest that it is possible to create polymer nanocomposites with high mechanical, thermal, and electrical properties, suitable for use in 3D printing, biomedical, and food packaging applications. These applications have also been highlighted by George *et al.* [32]. On other hand, Jasim *et al.* [152] found that due to the electrical and hydrophilic properties of biochar, PLA/Thymol/biochar composites can be used in antistatic packaging to dissipate static charges.

The electrical conductivity of biochar is influenced by the composition of biomass. Indeed, high lignin content gives a biochar with better conductivity in comparison with low lignin biomasses [15]. However, the electrical conductivity of biochar is mainly influenced by the pyrolysis temperature, as indicated by Bartoli *et al.* and shown in Figure 8 [16]. High pyrolysis temperatures increase the biochar aromatization [153], enhance the specific surface area and carbon content, with a notable impact on the quantity of sp2 hybridized carbon. This specific type of carbon significantly contributes to the electrical conductivity exhibited by the produced biochar [32], [154].

Graphitization has been observed at temperatures between 600 °C and 800 °C [155]. Al-Wabel *et al.* [14] show that in the biochar produced from conocarpus residues and pyrolyzed at temperature ranging from 200 °C to 800 °C, the conductivity varies from 0.76 ± 0.004 to 10.26 ± 0.04 $dS \cdot m^{-1}$, which may be due to the presence of salts and high carbonization. Conductivity is strongly dependent on the degree of carbonization, with high carbon content resulting in high electrical conductivity. Gabhi *et al.* [156] found that bulk conductivity increased from $2.5.10^{-4}$ to 399.7 $S \cdot m^{-1}$ when carbon content rise from 86.8 to 93.7 wt.% This information coincides with the idea that the electrical properties of biochar composites are enhanced by the presence of highly purified carbon, low functional group content and small particle size [32].

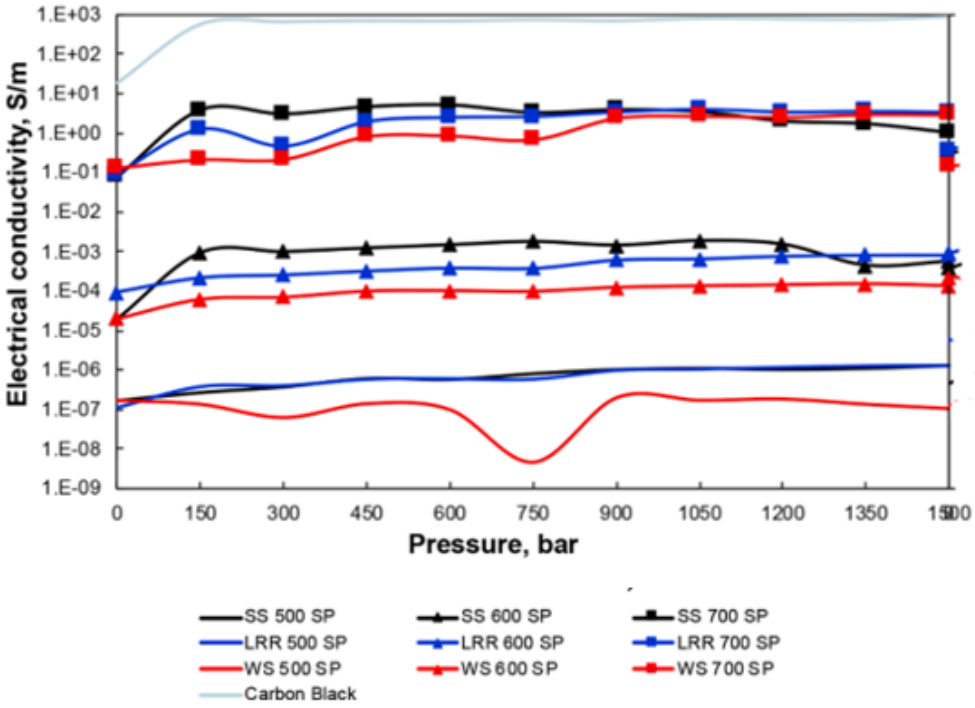

Figure 8: Electrical conductivity of biochar and commercial carbon black (VULCAN® 9 N115) as a function of pressure. Figure taken from Bartoli et al. 2022 [16].

Furthermore, the electrical conductivity of biochar is also affected by compression, which is described by the phenomenon of elastic electrical conductivity behavior. According to this phenomenon, the conductivity of biochar increases with compression load and decreases to the previous compression level when the load is released [156]. This phenomenon was also observed by Giorcelli *et al.* [148] who explained that it is due to the compaction process of biochar powders. As pressure increases, air is expelled from the pores and the void between particles decreases. As a result, the structure of biochar particles becomes deformed, increasing the effective contact between the biochar particles and thus conductivity. Biochar-polymer composites possess properties that enable them to be used as three-point bedding strain sensors with high sensitivity of electrical conductivity towards the applied strain [157].

To adapt biochar for specific applications that require enhanced conductivity, it often undergoes pre- or post-treatments. In the case of electromechanical detection, biochar is often impregnated with conductive materials, such as Cu^{2+}/Cu^{+} which has been used in conjunction with biochar to manufacture an ultra-sensitive enzyme-free electrochemical glucose sensor [158] and the ultra-sensitive electrochemical detector of nitrite in water [159].

For use in the materials production Giorcelli *et al.* [160] annealed (thermally activation) olive biochar at 1 500 °C to achieve a good degree of graphitization. This yielded an electrical conductivity of 103 S/m, enabling them to produce a fully reversible silicon-rubber piezoresistive material. In the case of Sobhan *et al.* [69], steam-activated biochar used at 800 °C for fabricating a biosensor from 85 wt.%. Activated biochar (ABC)/PLA-based composite. This biosensor exhibited good electrical conductivity, compared to PLA alone, high NH_3 sensitivity, and was suitable for smart food packaging.

As mentioned above, it is possible to create supercapacitors based on biochar with excellent electrochemical performance, promising specific capacitance and high energy [161]. Thomas *et al.* [162] produced a banana stem biochar pyrolyzed at 500 °C composite with polyaniline. They made several mixtures (polyaniline 3-6 mmol and biochar 0.2-1 g) and observed that the compound of 0.6 g biochar and 4 mmol of polyaniline had the best electrical conductivity of 4.1 $S \cdot cm^{-1}$. This composite exhibits a capacitance of 57.5 $F \cdot g^{-1}$ which means better electrochemical performance compared to various biochar-based electrode materials reported in the literature such as BC-NiO nanocomposite [163] and modified tea waste biochar [164].

Table 4 illustrates the electrical conductivity properties of composites based on biochar as an effective filler to enhance functional properties. Some possible applications are also indicated.

Table 4: Electrical conductivity of certain composites and their possible applications.

Polymer or biopolymer	**Raw Biomass**	**Biochar temperature (T_{pyro}) (°C)**	**Biochar load (%)**	**Electrical propriety**	**Possible applications**	**Ref.**
UHMWPE	Apple	900	70	8.2×10^{-2} $S \cdot cm^{-1}$	antistatic materials, electronic circuit	[165]
UHMWPE	Bamboo	1000	80	5.3×10^{-1} $S \cdot cm^{-1}$	antistatic materials, shielding against electromagnetic interference	[121]
UHMWPE	Bamboo	1 100	70	3.9×10^{-1} $S \cdot cm^{-1}$	antistatic materials, electronic circuit	[165]
PVA	Leaf mixture	-	6	2.4×10^{-7} $S \cdot cm^{-1}$	electronic devices, anti-static materials	[166]
			10	1.83×10^{-6} $S \cdot cm^{-1}$		
PVA	Cotton	1 000	10	1 m $S \cdot m^{-1}$	piezoresistive sensors, impact detectors	[167]
			20	2.90 $S \cdot m^{-1}$		
			30	7.5 $S \cdot m^{-1}$		
PVA	Sugar cane bagasse	800	12	2.38×10^{-2} S	electronic devices	[149]
PVA	Sugar cane bagasse	1 000	5	1.91×10^{-2} S	resistive piezo materials	[149]
Epoxide Resin	Coffee	1 000	15	35.96 $S \cdot m^{-1}$	electronic devices	[168]
Epoxide resin	Miscanthus	650	20	0.20 $S \cdot m^{-1}$	sensors	[148]
		700		1.88 $S \cdot m^{-1}$		
		750		2.75 $S \cdot m^{-1}$		

Caption: PLA - polylactic acid; PBAT - polybutylene adipate-co-terephthalate; UHMWPE - ultra high molecular polyethylene; PVA - Poly(vinyl alcohol; Electrical propriety may be resistance, conductance or electrical conductivity.

1.3 Conclusion

The literature review highlights the extensive opportunities for utilizing biochar as a filler in biobased materials, which allows for environmental and economic benefits. There is a well-documented need for enhanced waste valorization methods, and the production of sustainable materials. Biochar is typically understood as a very versatile bioproduct of thermochemical processes that have a carbon rich nature, tunable physicochemical properties, and wide functional versatility.

Biochar's intrinsic properties of high specific surface area, high porosity, thermal stability, and electrical conductivity make it an outstanding option for biopolymer reinforcement. Its intrinsic properties also afford a wide range of applications from energy storage systems and electromagnetic shielding to catalysis, sensors and advanced composites. Unfortunately, agglomeration and poor dispersion complications in matrices continue to be problematic and negatively impact the mechanical and electrical properties of the biocomposites. Figure 9 presents a summary of the properties of biochar, how they work, and the effects they have on the composite.

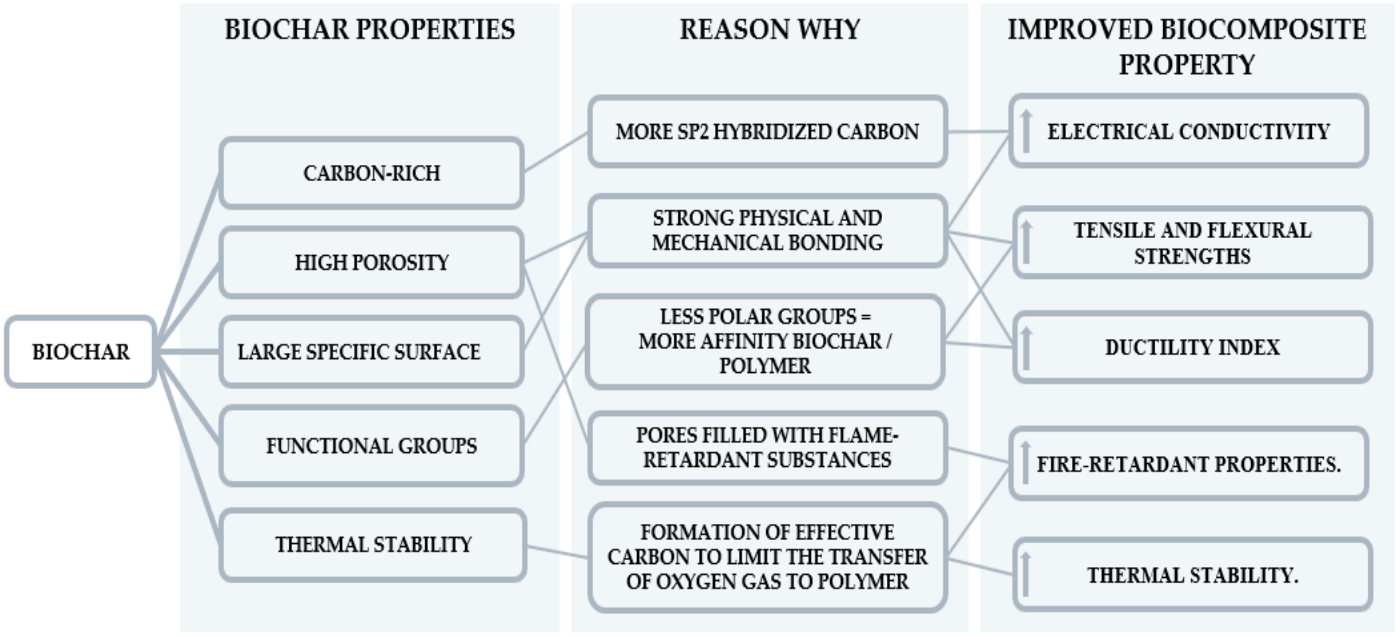

Figure 9: Summarizes of the causal effect between biochar properties and final properties of biocomposite performances.

The assessment of biochar's different production methods, activation methods, and process factors presented in this review contribute to the understanding of how synthesis conditions influence a material's structural and functional performance. The methods have been used to conduct comparative studies towards demonstrating the importance of refinements to factors to optimize biochar properties to applications while providing improved homogeneity of composites and performance.

In additionally, research into biochar-based composites are promising as they show mechanical, thermal, and chemical properties that are often superior to their natural fiber analogs. The

components of biochar such as hydrophobicity and thermal stability provide benefits in the stability of biopolymers, while the potential of modifying the electric manifestations of composting with biochar creates many opportunities for applied area such as electronic devices, smart packaging, and protective materials.

Also, in closure, the evidence provided by the studies reviewed show biochar provides a unique material in the quest to develop sustainable, high-performance biocomposites. Future studies should focus on improving biochar dispersion and compatibility with biopolymer matrices, test new forms of composites, and further studies on the electrical functionality in biochar-based composites systems. Studies need to be conducted on the long-term durability of biochar based biocomposites for the performance of these materials to contribute to a circular and sustainable biobased society.

Chapter 1 outlined the urgency of replacing fossil-based polymers with sustainable alternatives and introduced biochar as a versatile, carbon-rich filler capable of enhancing the mechanical, thermal, and functional properties of biopolymers. Having established the research gaps, this work now turns to the experimental procedures to produce biochar from three diferent biomasses and their integration into poly(lactic acid) matrices to make biocomposite, followed by the characterization methods.

CHAPTER 2
Materials and methods

2 Materials and methods

Introduction

This chapter describes the materials and methods used to produce biochar and PLA - biochar biocomposites. The chapter provides details on the biochar activation process, which aimed to improve its physicochemical properties, along with the experimental background and system configuration used for biomass pyrolysis. The formulation, mixing, and moulding processes used for the biocomposites are presented. Finally, a series of characterization methods are reviewed to evaluate the structure, thermal, mechanical, and morphological properties of biochar and biocomposites.

2.1 Biochar synthesis

2.1.1 Materials

The beech wood is the second most widespread hardwood in France [169]. It is moderately heavy and solid, with good mechanical properties and a high combustion value, as well as a low ash percentage, which makes it versatile in its use. This versatility has led to extensive study, making it a valuable reference for comparisons. Flax shives are the main waste product produced during fiber extraction, and they represent the lignified part of the flax stem [170]. Normandy accounts for 63 % of France's production of fiber flax [171]. Laminaria digitate seaweed is a large brown alga used in Europe as a food supply for algivores in the mariculture of abalone and sea urchins. It has been investigated for methane gas production through bioconversion trials in France and the US [172]. In addition, Laminaria digitate is being used for alginate extraction [173]. Biomasses were selected for their abundance in France.

The beech wood (BW) used in this study was provided by Pini Pellets Company, and its average particle size was 6 mm. Flax shives (FS), provided by "La Coopérative Terre de Lin", were ground and sieved at our laboratory. The average particle size ranges between 600 µm and 1 mm. Laminaria Digitata Algae Flakes (ALD) are provided by La Place des algues marketplace, and their particle size is 1mm. The table 5 below shows summarizes the characteristics, evaluated during this study, of the used biomasses.

Table 5: Elemental analysis and characteristics of biomass.

Biomass	Elemental analysis (wt.%)				Characteristics			Composition*		
	C	H	N	O	Density ($g \cdot cm^{-1}$)	pH	PCI ($cal \cdot g^{-1}$)	Hemicellulose %	Cellulose %	Lignins and cutins %
Beech wood (BW)	46.86	5.62	0.07	47.45	1.59	4.17	4 446.74	25	49	12
Flax shives (FS)	47.59	5.71	0.21	46.49	1.51	6.55	3 167.40	19	47	26

Laminaria digitata algae (ALD)	33.42	5.61	0.75	60.22	1.57	6.55	3 167.40	-

Caption: - No data C - Carbon; H - Hydrogen; N - Nitrogen; O - Oxygen ; *The remaining percentage represents the amount of soluble compounds.

2.1.2 Pyrolysis experimental setup

For the biochar production, the slow pyrolysis cycles were carried out in a semi-continuous experimental setup. It consisted of stainless steel (Ø = 90 mm, L = 970 mm) placed horizontally in a tubular furnace. A flow meter at one of the reactor inlets regulated nitrogen flow and was used as a carrier gas. At the outlet, it was connected to a condenser and a cold bath to recover the bio-oils formed from the condensation of the vapors. The furnace used was from Carbolite and had a maximum temperature of 1 200 °C and a maximum power of 2 340 W. The cold bath and the coolant were kept at a constant temperature of 0 °C.

Pyrolysis experiments were performed at 600 °C for each feedstock used. In the manipulations, about 500 g of feedstocks were introduced into the reactor and the reactor was fed with a flow rate of 500 mL·min^{-1} of nitrogen to create an inert atmosphere. The furnace was adjusted to the required temperature with a heating rate of 10 °C·min^{-1}. The feedstock was pyrolyzed for 2 hours. The heat was then turned off, and the facility was allowed to cool to temperatures below 70 °C to allow the solid carbon to accumulate without burning in contact with air. Once cooled, the biochar was weighed and collected in plastic bags for further analysis. Figure 10 illustrates the layout of the reactor used. With this process, a biochar yield between 25-27 % was obtained for each biomass.

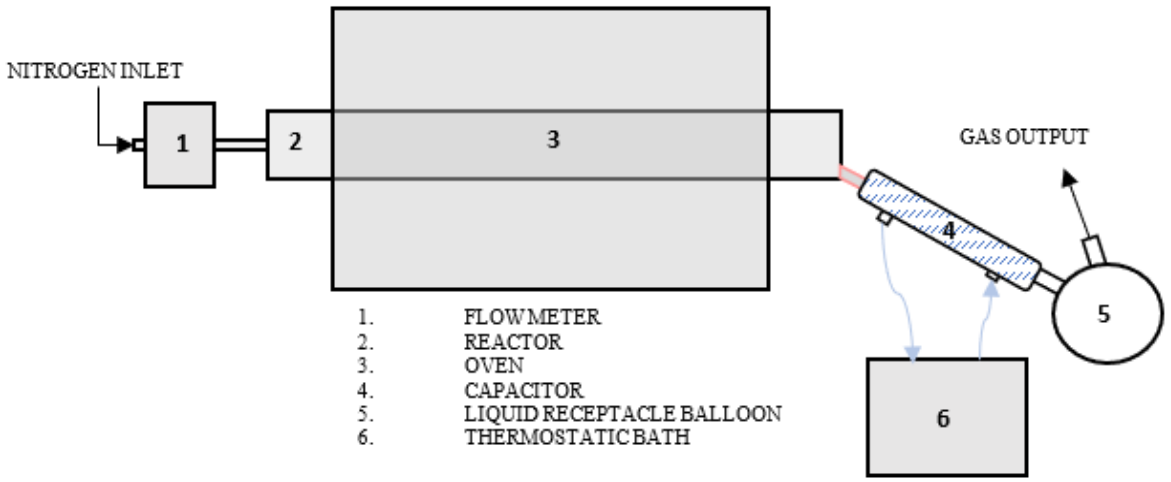

Figure 10: Layout of tubular reactor.

2.1.3 Activation experimental setup

As activation improves porosity and surface area [174], [175], some of the coals produced at 600 °C were physically activated in a CO_2 atmosphere. Before activation, each biochar

specimen was reduced to particles measuring less than 1 mm. The activation cycles were carried out in the same semi-continuous experimental setup used to perform pyrolysis. Only one spoon was added to hold the sample, and it was adapted to contain two inlets to which two flowmeters were connected to control the input of carbon dioxide and nitrogen, respectively.

For the activation, we use N_2/CO_2 with a cooling method at 900 °C [176]. Approximately 300 g of biochar were introduced into the reactor, and the reactor was fed with a flow rate of 500 $mL \cdot min^{-1}$of nitrogen to establish an inert atmosphere. The furnace was adjusted to the required temperature with a heating rate of 500 $°C \cdot min^{-1}$. The biochar was then subjected to an activation process for a duration of 2 hours in the presence of 300 $mL \cdot min^{-1}$ of carbon dioxide. Subsequent to this, the activated biochar was allowed to cool in a nitrogen atmosphere to room temperature. Once cooled, the biochar was weighed and collected in plastic bags for further analysis.

Table 6 shows a summary of the types of biochar produced, the pyrolysis temperature, and the activation temperature.

Table 6:Summary of the types of biochar produced

Biochar	**$T_{pyrolyse}$**	**Activation conditions**
Beech wood biochar **BCBW**	600°C	900°C CO_2
Activated beech wood biochar **BCBWA**		
Flax shives biochar **BCFS**		
Activated flax shives biochar **BCFS**		
Laminaria digitate algae biochar **BCALD**		
Activated laminaria digitate algae biochar **BCALDA**		

2.2 Biocomposites manufacture

For the preparation of the biocomposites, the biochar produced in the previous section were used. Beech wood, flax shives, and laminaria digitata algae biochar with particle size of less than 1 mm. The biopolymers used was PLA 2003D with a melt flow index of 1 g/10 min (210 °C / 2.16 kg) provided by NatureWorks LLC product (Annex 1).

2.2.1 Biocomposites processing

Biocomposites with different biochar loading rates of 10 %, 40 %, and 70 % were fabricated using beechwood biochar, with the remaining biochar variants comprising a 10 % loading. The composites were created by mixing biochar with a moisture content of less than 5% mass, as measured on a thermal balance (Sartorius MA160), and a particle size of less than 1 mm, with PLA20003D of size 4 mm for 1 minute in a mixer. The mixture is subsequently passed through a single-screw extruder (Standard extruder, Scamex**),** with zone temperatures ranging from 145

to 155 °C and a rotation speed of 30 revolutions per minute. This process results in the formation of composite yarn, which is subsequently cut into granules. These granules are then thermopressed (Scamex Press 200 T 500 x 500) in the form of plates (20 cm x 25 cm), with a thickness of approximately 2 mm, at a temperature of 155 °C and a pressure of 150 bar. The thermopressed plates are then cut using a laser cutter at 80 % power (Mllaser). Figure 11 summarizes the steps in the biocomposite production process.

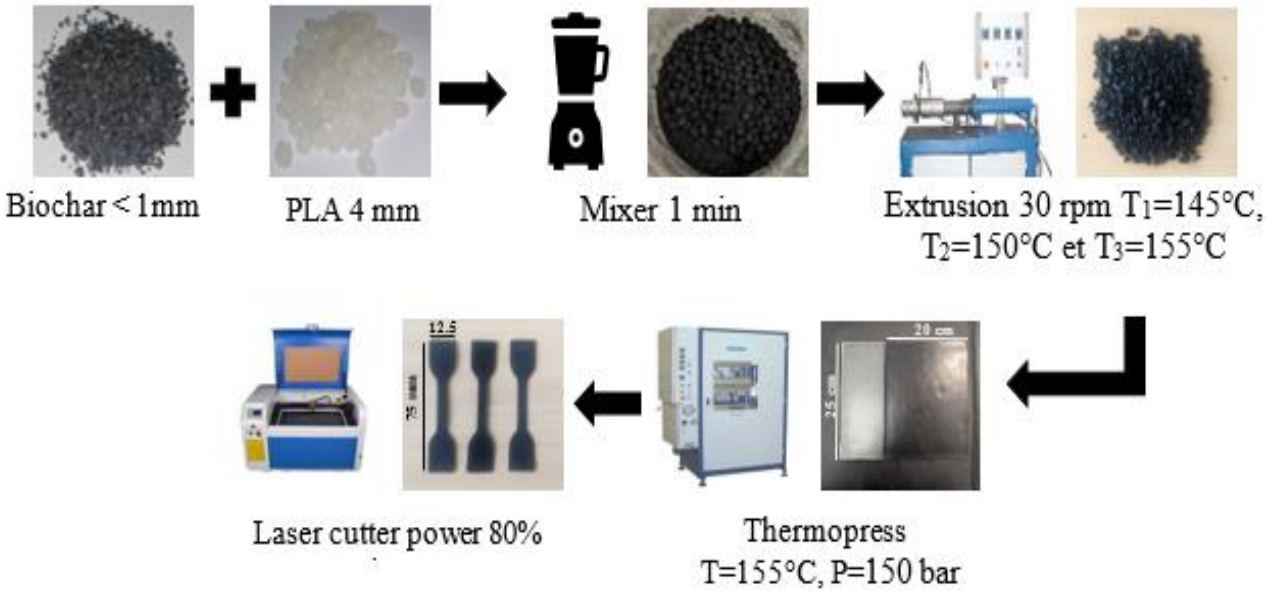

Figure 11: Illustration of the biocomposite production process.

2.3 Characterization

2.3.1 Physical-chemical testing

2.3.1.1 Skeletal density

True (skeletal) density is the intrinsic, porosity-free density of a material, governed by its chemical composition and crystal structure [177]. It is measured with a gas pycnometer, which calculates the sample volume from the pressure change of an ideal gas (PV = nRT) in two chambers, a reference chamber and a sample chamber that holds the specimen [178], [179], [180]. Helium is the preferred gas because it does not adsorb on particle surfaces and easily penetrates pores due to its small molecular size [181]. While the technique does not modify the material, it requires the specimen to fit the instrument; solid samples often need to be ground into powder, a step that can disrupt the original pore structure

In this study, biochar skeletal density was measured by helium pycnometer (Ultrapyc 5000 fitted with a 1.8 cm chamber) see in Figure 12. The instrument measures the density of solids and semi-solids, by detecting the change in pressure due to the volume of helium that is displaced by the sample within the sealed and pressure-equilibrated chamber. It is assumed that helium atoms can penetrate all open pores within the biochar particle. Each biochar sample was measured ten times, and the mean of three measurements was reported.

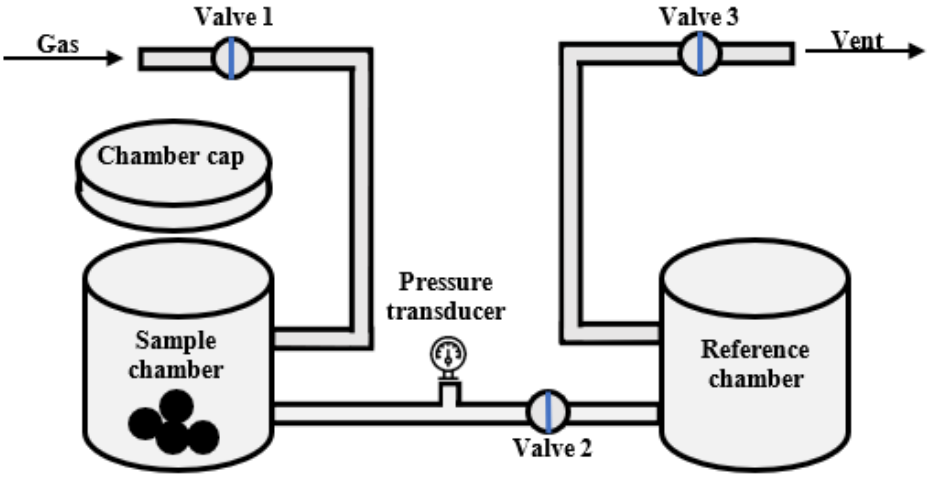

Figure 12: Simplified diagram of a gas pycnometer setup. Image recreated from the Ultrapyc 5000 Anton Paar scheme.

2.3.1.2 Specific surface area and porosity measure

The gas adsorption method is a common to measure the specific surface area and pore size distribution of materials. The Brunauer–Emmett–Teller (BET) theory is the most widely utilized model in determining the specific surface area of materials. Typically, BET analysis is performed using nitrogen gas (N_2) as the adsorbate due to its high affinity for solid surfaces. The gas is introduced at low pressures, and molecules begin to adsorb onto the surface. As the gas pressure increases, a monolayer is formed, followed by multilayer adsorption. The amount adsorbed is determined to calculate the surface area using the BET equation for two stages involved in the application of the BET method. First, it is necessary to transform a physisorption isotherm into the 'BET plot' and from it derive a value of the BET monolayer capacity, n_m . In the second stage, the BET-area, noted a(BET), is calculated from nm by adopting an appropriate value of the molecular cross-sectional area [182].

It is customary to apply the BET equation in the linear form:

$$\frac{p/p^o}{n(1-p/p^o)} = \frac{1}{Cn_m} + \frac{C-1}{Cn_m}(p/p^o) \qquad \textit{Equation 1}$$

where n is the specific amount adsorbed at the relative pressure p/p° and n_m is the specific monolayer capacity. According to the BET theory, parameter C is exponentially related to the monolayer adsorption energy, thereby serving as an indicator of the shape of the isotherm within the BET range.

The adsorption isotherms are qualitative evaluated using the six types groups of physisorption isotherms recommended by the IUPAC1985 [183]. However, over the past years, various new characteristic types of isotherms have been identified and shown to be closely related to

particular pore structures. The proposed updated classification of physisorption isotherms is presented in Figure 13[182].

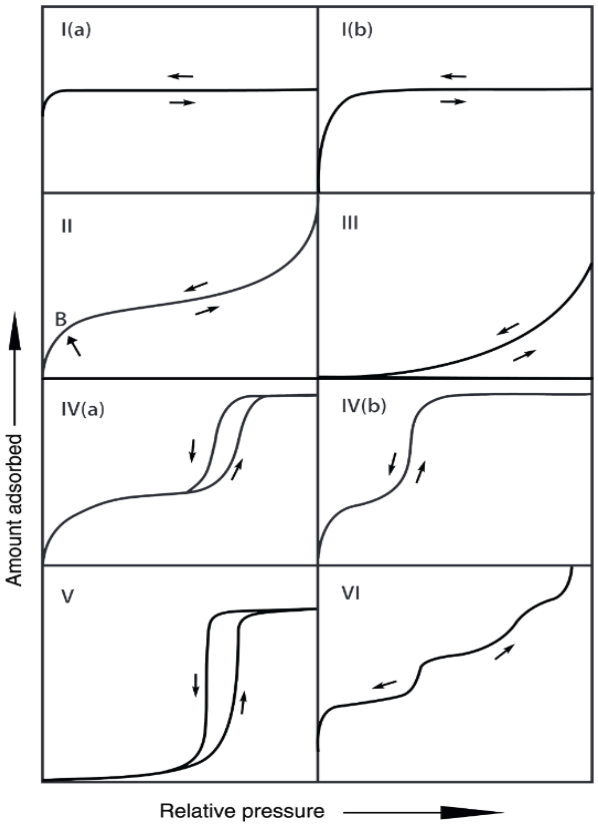

Figure 13: Classification of physisorption isotherms, from Thommes M. et al. [182]

Type I (a) isotherms are given by microporous solids having relatively small external surfaces, represents materials with narrow micropores (< 1 nm), showing rapid adsorption at low relative pressures, while I(b) isotherms are found with materials having pore size distributions over a broader range including wider micropores and possibly narrow mesopores (< ~2.5 nm).

Type II is typical of nonporous or macroporous solids (> 50 nm), with clear monolayer-multilayer adsorption, and Type III reflects weak adsorbate–adsorbent interactions, usually seen in nonporous surfaces, therefore no identifiable monolayer formation.

Type IV(a) isotherm, capillary condensation is accompanied by hysteresis. This occurs when the pore width exceeds a certain critical width, which is dependent on the adsorption system and temperature and IV(b) as IV(a) indicate mesoporous structures (2 - 50 nm), with hysteresis loops due to capillary condensation, the latter showing more complex pore connectivity, these types are given by conical and cylindrical mesopores that are closed at the tapered end.

Type V isotherms are observed for water adsorption on hydrophobic microporous and mesoporous adsorbents. Finally, Type VI isotherm is representative of layer-by-layer adsorption on a highly uniform nonporous surface. The step-height now represents the capacity for each adsorbed layer, while the sharpness of the step is dependent on the system and the temperature.

In this study, surface area, total pore volume and mean pore diameter of biochar were estimated with adsorption of nitrogen at 77 °K using BET surface area and pore size distribution analyzer (Make: BEL Microtrac BEL Corp. Model: Belsorp max II). Biochar samples were first dried at 105 °C for 24 hours and then vacuum degassed (Vacuum Degasser Belprep-VAC III) at 400 °C for 6 h before BET analysis [184].

2.3.1.3 Scanning electron microscopy (SEM)

Scanning electron microscopy (SEM) delivers high resolution surface imaging by rastering a focused electron beam across the specimen, achieving spatial resolution from subnanometer to a few nanometers that is far superior to optical microscopy [185]. Electron sample interactions generate signals that reveal both topography and composition. The most common detectors are the secondary electron detector (SED) for detailed surface morphology and the backscattered electron detector (BSD) for compositional contrast [186]. When coupled with energy dispersive Xray spectroscopy (EDS), SEM also provides elemental analysis by detecting characteristic Xray photons emitted during -electron atom interactions- [187].

To visualize the surface of composites, a JSM-IT100LA (Jeol) scanning electron microscope was used. A low accelerating voltage of 5 kV-10 kV was used for secondary electron SEM. A wide range of solid materials can be analyzed directly by SEM. Biological materials and insulating samples often require special imaging, such as low vacuum or low kV imaging, to reduce surface loading and beam damage. Insulating samples can be coated with a thin layer of gold or platinum to minimize loading [185]. In our case, biocomposites were previously metallized with two gold microlayers in a DII-29030SCTR Smart coater.

For the study of biochar and biomass, the analyses are being carried out on a JCM 7000 (Jeol), SEM-EDS was used for biochar surface morphology and surface composition. The tests were performed at an electron accelerating voltage between 5 and 10 kV and on surfaces of 100, 20 and 5 micrometers.

2.3.1.4 Fourier transform infrared spectroscopy

FTIR measures the absorption of infrared radiation by molecular bonds, allowing identification of functional groups in a material because each group exhibits characteristic vibrational frequencies in the mid-infrared region (≈ 400–4000 cm^{-1}) [188] [189]. The technique employs an interferometer to collect the entire spectrum simultaneously, and a Fourier transform converts the interferogram into a conventional absorbance spectrum [190]. Spectra can be recorded in transmission, attenuated total reflection (ATR) or reflection modes. ATR is a non-destructive, label- free method that requires no sample preparation; the sample is placed on a high- refractive- index crystal (e.g., Ge, ZnSe, Si, or diamond), and an evanescent wave penetrates a few micrometres into the material, providing surface- sensitive- information independent of thickness [191]. This makes ATR especially suitable for solid, liquid or polymer samples where traditional transmission is difficult [192]. The resulting spectra enable rapid qualitative and quantitative assessment of chemical composition and changes induced by processing or functionalisation.

FTIR-ATR equipment was used to analyze the chemical properties of raw biomass, composite samples, and pure biochar. An Invenio FTIR spectrometer in ATR mode was used, with 32 scans for each sample. The wavelength range studied was from 400 to 4000 cm^{-1} with a resolution of 4 cm^{-1}. FTIR spectra were processed using OPUS - Spectroscopy software and a smoothing filter of 25. To ensure the effectiveness of the measurement, in one biocomposite, which could well be heterogeneous, square samples of 1.5 cm x 1.5 cm (Figure 14) were cut and the analysis was performed at three points of the square and three samples per biocomposite.

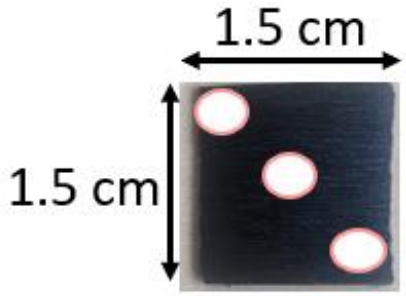

Figure 14: Square samples of biocomposites for ATR measurement.

2.3.1.5 Thermogravimetric analysis (TGA)

Thermogravimetric analysis (TGA) is a method of thermal analysis in which changes in the physical and chemical properties of materials are measured as a function of increasing temperature (with constant heating rate) or as a function of time (with constant temperature and/or constant mass loss). This analytical technique affords insights into a myriad of physical phenomena, including phase transitions, the occurrence of absorption and desorption, and chemical phenomena such as thermal decomposition and solid-gas reactions. In this method in which the mass of a sample is measured over time as the temperature changes, a negative mass variation signifies desorption or thermal degradation. Conversely, a positive mass variation is indicative of adsorption phenomena. TGA is a common technique for analyzing the thermal characteristics of composites and biomass [193], [194].

In this study, TGA was carried out using a NETZSCH TG 209 F1 thermal analyzer. The sample, placed in an alumina (AL2O3) crucible, was heated at a constant rate of 10 °C·min^{-1} from 25 to 800 °C, under an inert 20 ml·min^{-1} argon atmosphere.

2.3.1.6 Differential scanning calorimetry (DSC)

Calorimetry is a fundamental technique used to assess the thermal behavior of materials, linking temperature changes to specific physical properties. Calorimeters are specialized instruments used to investigate the thermodynamic properties of biomolecules and nanoscale materials. Among the various types, Differential Scanning Calorimetry (DSC) is one of the most widely utilized. DSC analyzes thermal transitions by measuring heat flow and temperature variations over time. As the temperature changes, the DSC detects the excess heat absorbed or released by a sample by comparing it to a reference, providing insights into phase transitions, crystallization, melting, and other thermal events [195], [196].

For this study DSC was performed using a NETZSCH DSC 214 thermal analyser. The sample (8-12 g) was placed in a closed concaves crucible. All experiments were repeated two times. The samples were subjected to the following heat-cool-heat cycles under an inert atmosphere (Argon (Ar)):

• First heating from 20 to 200 °C at 10 °C·min^{-1}, Ar. 40 mL·min^{-1}.

• Cooling from 200 to 20 °C at 10 °C·min^{-1}, Ar. 60 mL·min^{-1}.

• Second heating from 20 to 200 °C at 10 °C·min^{-1}. Ar. 40 mL·min^{-1}.

The thermal parameters, i.e., glass transition temperature (Tg), cold crystallization temperature (Tcc), melting temperature (Tm), crystallization temperature (Tc), and enthalpies, were determined.

The degrees of crystallinity of pure and reinforced PLA were calculated using the following equation [197]:

$$x_c = \frac{\Delta H_m - \Delta H_{cc}}{\Delta H_m^0} x \frac{100}{\omega} \qquad \textit{Equation 2}$$

Where x_c is the degree of crystallinity in %, Hcc and H_m are representatives of the cold crystallization and the melting enthalpies in J·g^{-1}, respectively, and H^0_m is the melting enthalpy of 100 % crystalline PLA, which is equal to 93.7 J·g^{-1}, according to H. Jung and S. Kimb, 2014 [198].

2.3.1.7 X-RAY Diffraction analysis (XRD)

XRD is a non-contact technique that is used to determine the crystalline structure and phase composition of materials. The crystalline substances in question produce a unique pattern, akin to a fingerprint [199], [200]. The process entails the direction of a monochromatic X-ray onto the specimen under investigation, followed by the meticulous analysis of the resulting diffraction pattern. The process under consideration provides insights into a variety of structural characteristics of crystalline materials, including the crystal structure, degree of crystallinity, crystallite size, atomic spacing, crystalline phase, transition, and their quantitative proportion. Additionally, it facilitates the determination of microstructure, quantitative resolution of chemical species, isomorphous substitutions, unknown crystalline materials, and solids [201].

The biochar was analyzed by powder diffraction on a Siemens D5000 XRD, in a 2-theta scan range of 30-90 °, with a step size of 0.02 for the biocomposites. In the case of PLA and biocomposites, they were analyzed in the form of 20 mm diameter discs with a scanning range of 2-70 ° for PLA and 2-90 ° for biocomposites. The samples were dried overnight at 105 °C before being placed on the sample holder.

The values of the crystallinity indices for samples were calculated by using the deconvolution method with the following equation:

$$C_i = \frac{S_c}{S_t} x\ 100$$ *Equation 3*

where Sc represents the area of the crystalline domain and St represents the area of the total domain.

2.3.2 Dynamic testing

2.3.2.1 Dynamic mechanical analysis (DMA)

DMA can be described as the application of an oscillatory force to a sample under various conditions of temperature or frequency, followed by analysis of the response of the material to that force. From this response, properties such as the tendency to flow (also known as viscosity) are calculated from the phase lag and the stiffness (modulus) from the sample recovery. These properties are typically characterized in terms of the material's capacity to dissipate energy in the form of heat (damping) and its ability to regain its original shape after deformation (elasticity). This approach enables the description of the relaxation process of the polymer chains [202]. The force in question generates stress, which in turn causes deformation. The relationship between these two factors provides information about the stiffness of the sample, also known as modulus. This indicates the performance of the material in a specific application in the real world; however, the DMA modulus is not exactly the same as the Young's modulus of the classic stress–strain [203]. Depending on the test setup, it is possible to make statements about several different material properties such as physical properties as glass transition temperature T_g [204], and mechanical properties [205].

For this study DMA was performed on 60 × 10 × 2 mm samples (Figure 15) with an Artemis DMA 242 E (Netschz, Selb, Germany). Double cantilever method with a ramp between 20 °C and 145 ◦C at 5◦C-min^{-1} at a frequency of 1 Hz, with a dynamic amplitude of up to 30 µm and a force range between 4 ± 4 N.

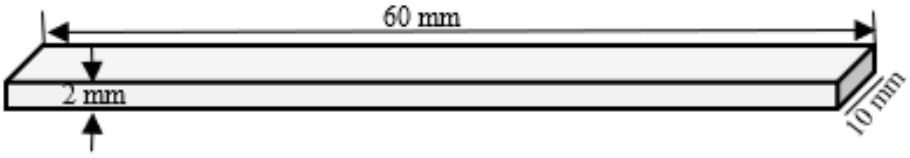

Figure 15: Dimensions (mm) of DMA specimen.

2.3.2.2 Broadband dielectric spectroscopy (BDS)

Broadband dielectric spectroscopy (BDS) is the process of measuring the interaction of an electromagnetic wave of a certain frequency with a sample. The response of the sample to this excitation is a time-dependent polarization, due to fluctuations in charge density, which can be expressed as a time-dependent current density according to the Maxwell-Ampère equation [206]. The primary function of BDS is to ascertain the dielectric properties of a material in relation to the applied electrical frequency. This technique yields a wealth of information, including the dielectric constant, dielectric loss, and electrical conductivity.

For this study, a Keysight E4980A Precision LCR Meter (Agilent Technologies, Santa Clara, CA, USA) was used. The sample dimensions were cut with an ML-W1290 (Mllaser, Pont-à-Mousson, FRA) into disks of 25 mm in diameter and ~ 2 mm in thickness. BDS tests were conducted at 20 °C. The frequency range was between 100 and 1 MHz. The E4980A gave the capacitance (Cp) and the loss tangent (tan δ). So, the dielectric constant (ε'), dielectric loss (ε") and electrical conductivities (σAC) were determined according to the following equations [207], [208].

$$\varepsilon' = \frac{C_p * ep}{\varepsilon_0 * S} \qquad \textit{Equation 3}$$

$$\varepsilon'' = \tan\delta * \varepsilon' \qquad \textit{Equation 4}$$

$$\sigma_{ac} = \omega * \varepsilon'' * \varepsilon_0 = 2\pi f * \varepsilon'' * \varepsilon_0 \qquad \textit{Equation 5}$$

where Cp is the electrical capacitance given in Farad, S is the cross-sectional area of the sample (in m^2), ep is the distance between electrodes (in m), and ε0 is the permittivity of vacuum (given as $8.541878*10^{-12}$ $F \cdot m^{-1}$). σ_{ac} is expressed in $S \cdot m^{-1}$, ω is the angular frequency and f is the applied electrical frequency (in Hz).

2.3.3 Static mechanical testing

The objective of conducting traction tests on specimens is to ascertain the mechanical characteristics of the specimen material [123], [209]. The mechanical properties of the produced composites were evaluated using tensile strength testing according to ISO 527-2 type 5a over a 50 mm gauge length (shown in Figure 16). Loading was applied at a rate of 5 $mm \cdot m^{-1}$ crosshead movement using an AGS-X 50 KN universal test machine Shimadzu. Eight repetitions from each formulation were tested. The tensile strength, tensile modulus of elasticity, and strain at failure were determined using the TRAPEZIUM LITE X data processing.

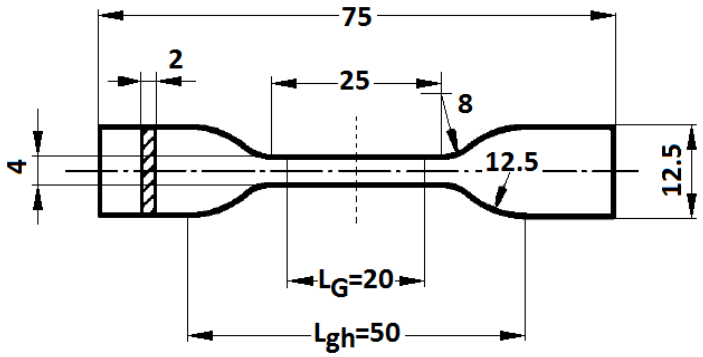

Figure 16: Dimensions (mm) of the ISO 527/2-5A specimen figure taken from E. Romero et al.2021 [210]

2.3.4 Process simulation framework

To evaluate the scalability of the biochar production process, a computer simulation was developed using Aspen Plus®, a commercial process simulation platform widely used for the steady state design and analysis of chemical engineering systems. The environment provides a library of unit operations (reactors, separators, heat exchangers, compressors, dryers, crushers, etc.) that can be linked together to construct a flowsheet representing the entire production chain, from raw material handling to product recovery. This software was used to perform mass and energy balances for the slow pyrolysis and mixing stages. The simulation results provide the basis for the technical-economic analysis (TEA). The specific details of which, including thermodynamic property methods, block specifications, and cost estimation parameters, are described extensively in Chapter 4.

Chapter 2 detailed the materials, the slow-pyrolysis at 600 °C, the CO_2 activation at 900 °C, the extrusion-injection protocol used to fabricate PLA-biochar composites at 10, 40, and 70 wt.% loadings, and the different methods of characterization. With these protocols in place, Chapter 3 presents the comprehensive physicochemical, thermal, electrical and mechanical characterization that reveals how feedstock, pyrolysis, and activation dictate composite performance.

CHAPTER 3
Results and discussion

3 Results and discussion

Introduction

Chapter 3 provides a detailed examination of the experimental results generated in this study, with a focus on the physico-chemical characterization of the biochar-based biocomposites. The first part, entitled "Analysis of biochar properties: effect of biomass and pyrolysis temperature" presents a systematic assessment of the three selected biomass feedstocks (*Laminaria digitata* algae, beech wood, and flax shives) following slow pyrolysis at 600 °C and subsequent CO_2 activation at 900 °C. The physico-chemical analysis includes skeletal density, specific surface area, pore volume, elemental composition, and surface functional groups (FTIR). Particular attention is given to elucidating the influence of biomass type and thermal treatment on crystalline structure (XRD) and porosity development (BET), and to establishing correlations with the micro- and nanoscale features observed by SEM–EDS.

In the second part, entitled "Biochar-based biocomposites: Influence of biochar type and content", the chapter evaluates the impact of these biochar properties on the performance of polylactic acid (PLA) matrices incorporating biochar at loadings of 10 wt.%, 40 wt.%, and 70 wt.%. Comprehensive data are presented on thermal transitions (DSC), thermal stability (TGA), crystallinity (XRD), viscoelastic behaviour (DMA), dielectric response (BDS), and tensile performance. The discussion highlights the role of CO_2 activation in enhancing interfacial adhesion, promoting PLA crystallite nucleation, and improving electrical conductivity within the composites.

This chapter highlights the findings to identify the most promising biochar–PLA combinations, while recognizing the trade-offs associated with stiffness, conductivity, and mechanical strength. This synthesis provides a rigorous foundation for the techno-economic analysis developed in Chapter 4.

3.1 Analysis of biochar properties: effect of biomass and pyrolysis temperature

3.1.1 Assessment of structural properties

3.1.1.1 Skeletal density

Figure 17 shows the evolution of the skeletal density of the three biomasses, laminaria digitata algae (ALD), beech wood (BW), and flax shives (FS) undergo a pyrolysis process (600 °C) followed by an activation process (CO_2, 900 °C). It can be observed that, although the initial real density of the three biomasses is similar, the variation of the density magnitude after pyrolysis and subsequent activation differs among them, likely indicating differences in their intrinsic structural features. However, a consistent trend emerges across all cases: the biochar derived from each biomass exhibits a higher density than the original biomass, and the activated biochar demonstrates a higher real density compared to the non-activated biochar. Considering that both pyrolysis and physical activation are thermally driven processes involving elevated temperatures, the observed behavior of the densities is consistent with the conclusions drawn by Brewer *et al.* [211] in *New Approaches to Measuring Biochar Density and Porosity* where it was stated that density increases with temperature.

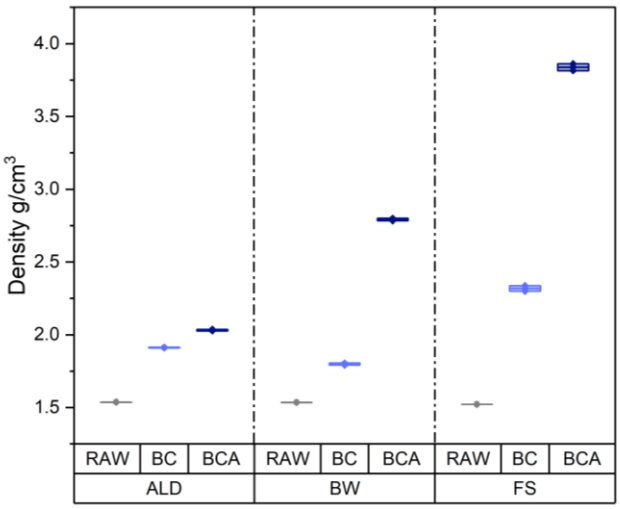

Figure 17: Skeletal density of the three biomasses, biochar produced at 600 °C and activated biochar.

A comparison of the biomasses reveals that following pyrolysis and activation, the change in density was most evident in flax shives in both cases, both in the biochar and the activated biochar. However, in the case of beech wood biochar, the density increase after pyrolysis was the smallest among the three biochar, but after activation, it surpassed the density of the activated algae biochar.

3.1.1.2 Specific surface area and porosity

This section presents the analysis of specific surface area and porosity using gas adsorption. Figure 18 shows the isotherms of different types of pyrolyzed carbon (noted BC) from laminaria digitata algae (BCALD), beech wood (BCBW), and flax shives (BCFS) at 600 °C, as well as their activated versions (noted A) under CO_2 at 900 °C, BCALDA, BCBWA, and BCFSA, respectively.

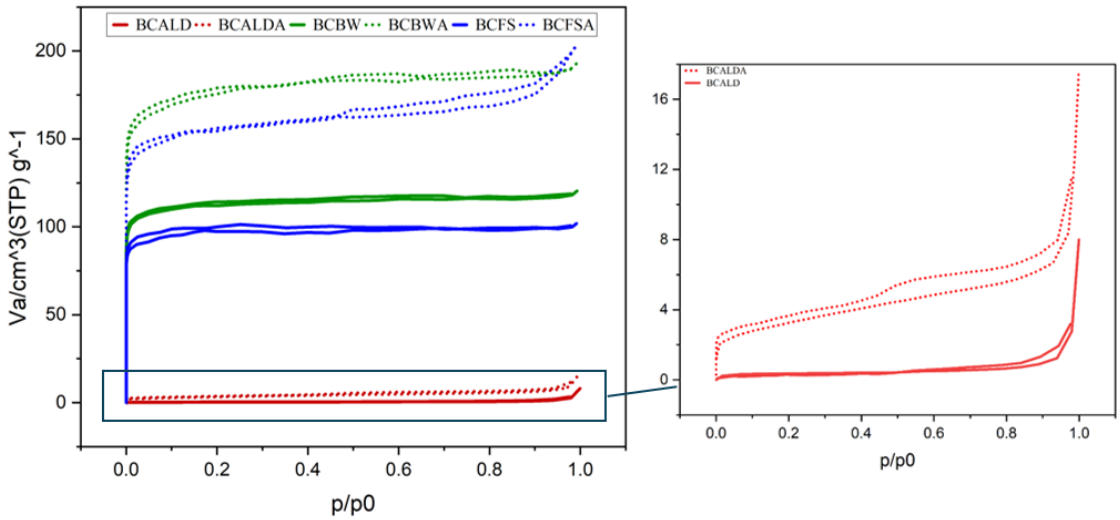

Figure 18: Comparison of N_2 adsorption isotherms at 77 K for the three-biochar samples BCALD, BCBW, BCFS and their activated version, BCALDA, BCBWA, BCFSA. The inset enlarges the low adsorption.

The isotherms of biochar in this figure are classified into six different types according to the IUPAC. Wood biochar and flax shives biochar have curves similar to those of type one, which are those that have micropores and mesopores on their surface, while the curves of algae biochar are more similar to those of type two, which is the category of materials that have macropores on their surface.

The curves for flax shives and wood biochar show rapid adsorption at very low relative pressures. This behavior is characteristic of materials in which adsorption mainly occurs by filling micropores. In contrast, the slow increase in higher pressures suggests a smaller contribution from mesopores or adsorption on the external surface. However, high adsorption volumes of over 100 cm^3 (STP) per gram are also observed, which is related to a larger surface area and greater pore volume. By contrast, algae biochar has low adsorption volumes, indicating that it is less porous. When activated, the three carbons show greater adsorption, synonymous with an increase in surface area and the development of porosity.

This observation is further substantiated by the results presented in Figure 19 where the impact of activation on the surface area is most evident.

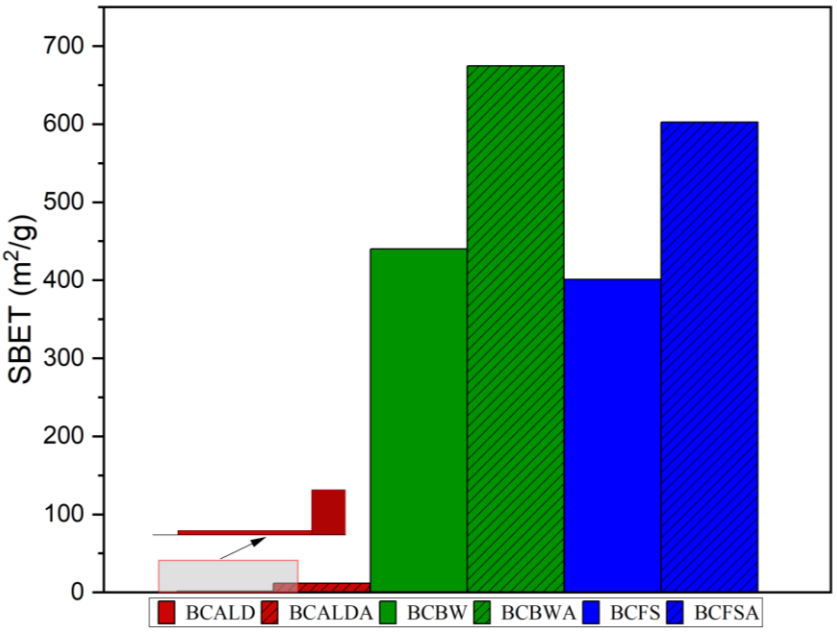

Figure 19: Effect of activation on the surface area (S_{BET}) of the three-biochar produced.

This increment is primarily attributed to the decomposition of organic matter, which leads to the formation of micropores. Additionally, higher temperatures cause the breakdown of aliphatic alkyls and ester groups, exposing the aromatic lignin core. This exposure further contributes to the observed increase in biochar surface area [212]. Furthermore, beech wood and flax shives biochar have a larger specific surface area than algae biochar, approximately 50 times larger because the surface is dependent on feedstock type [213]. Table 7 shows the specific surface, total pore volume, and mean pore diameter.

Table 7: Specific surface using Brunauer–Emmett–Teller method, total pore volume and mean pore diameter of different types of biochar.

Sample	S_{BET} ($m^2 \cdot g^{-1}$)	Total pore volume ($cm^3 \cdot g^{-1}$)	Mean pore diameter (nm)
BCALD	1.33 ± 0.01	0.01 ± 0.00	24.33 ± 1.92
BCALDA	11.63 ± 1.08	0.02 ± 0.00	6.68 ± 0.35
BCBW	440.15 ± 3.78	0.19 ± 0.01	1.72 ± 0.06
BCBWA	674.77 ± 1.42	0.81 ± 0.72	4.78 ± 4.27
BCFS	401.05 ± 4.16	0.16 ± 0.01	1.63 ± 0.07
BCFSA	602.56 ± 0.43	0.31 ± 0.00	1.89 ± 0.30

From this table, we can see that the activation process significantly increases the S_{BET}, representing an increase of around 774 % for algae biochar, 53 % for beech wood biochar, and 50 % for flax shives biochar. Knowing that high specific surface area biochar has high porosity, and that high porosity improves the physical bonds between the matrix and the reinforcement, from Figure 19 and Table 1 it can be deduced that the composites created using BCBW and BCFS will exhibit superior mechanical properties.

3.1.2 Assessment of morphological and elemental properties (SEM-EDS)

Figure 20 presents the surface morphology of the raw biomasses, their corresponding biochar pyrolyzed at 600 °C under N_2 and the biochar activated at 900 °C under CO_2, with images captured at a maximum scale of 20 micrometers.

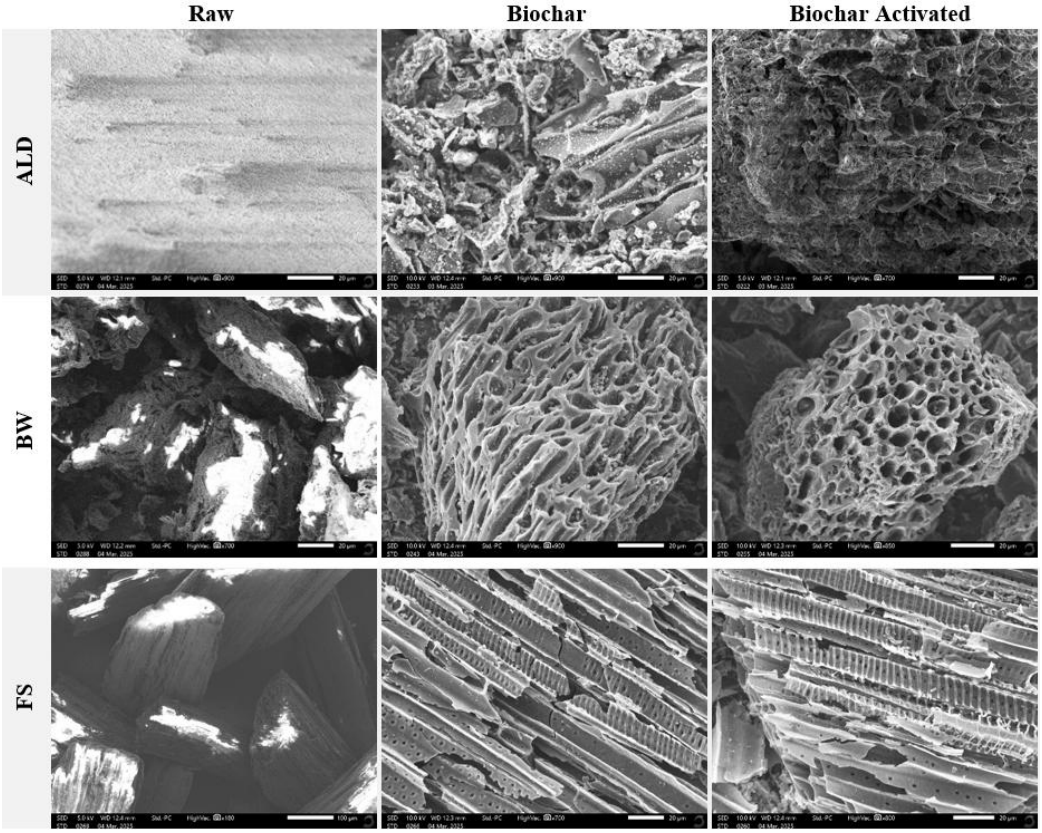

Figure 20: Surface morphology of the three biomasses, biochar derivatives and activated biochar. The scale bar of 20 micrometer.

The first column shows the untreated biomasses (ALD, BW and FS). For the algae (ALD), we see a homogeneous surface with no visible pores. This type of compact surface is common in algae, whose cell walls can be rich in polysaccharides or lipids [214]. This is consistent with the algae Laminaria digitata, which has a high content of polysaccharides such as alginates in ranges from roughly 44 % to 52 % of the dry algal material. [173]. For the cases of flax shives (FS) and beech wood (BW), image overexposure hinders clear visualization of surface features.

The second column displays the biochar (BCALD, BCBW, BCFS). Structural details begin to emerge at this stage. BCALD exhibits some visible channels, though without apparent pores. This indicates a slight thermal decomposition of cellular components, releasing gases that generate some internal porosity [215]. BCBW shows an increased porosity and more organized pattern. Pores with an alveolar structure similar to vascular bundles or tracheid are observed, while BCFS presents the most regular morphology, with remarkable structural development. Straight and well-defined canals are observed, with a highly organized and directional structure, typical of the vascular tissue of herbaceous plants, coinciding with the observations of Downie *et al.* in 2009 [215] on herbaceous biochar that preserves tubular xylem morphologies.

In the third column, the activated biochar (BCALDA, BCBWA, BCFSA). BCALDA reveals further surface development. The emergence of concavities likely macropores is observed in accordance with the effect that the activation significantly increases the specific surface area and porosity [216]. BCBWA exhibits a well-defined pore network, with great variability in size. A larger internal surface area is inferred, which is consistent with efficient activation. In literature, it has been reported that activated wood biochar present excellent adsorption properties [217], [218] and improve the mechanical properties of biocomposites. Similarly, BCFSA retains its linear structure, although it has a greater number of visible pores. In addition, it is characterized by its high regularity and order in pore arrangement, which is beneficial for adsorption and catalysis applications [219].

Both the BET analysis and the microscope images show that activation significantly promotes the development of pores in biochar. Biochar of terrestrial origin (BCBW and BCFS) have a much more porous structure than biochar of marine origin (BCALD). This could be related to the fact that minerals do not break down as quickly as carbon compounds.

Figure 21 shows the elemental distribution of the different biomasses, their biochar when pyrolyzed at 600 °C, and the version of biochar activated at 900 °C, determined by energy dispersive spectroscopy (EDS).

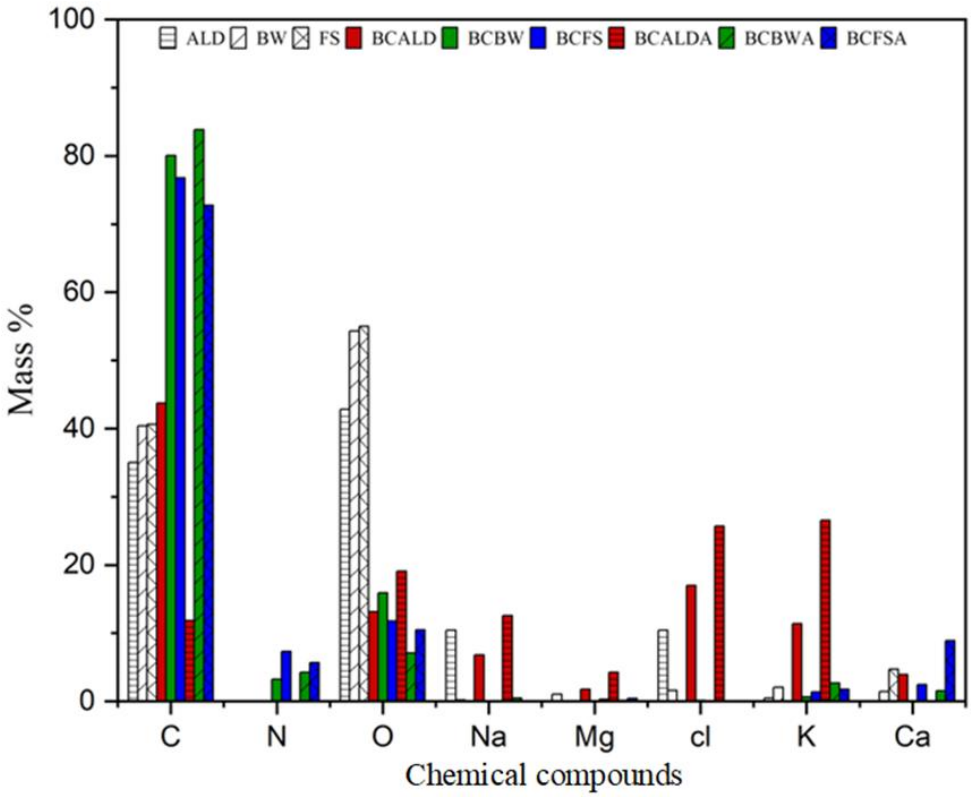

Figure 21: Elemental distribution in different biochar and biomass, data extracted by EDS.

The carbon content of biomass is relatively uniform among terrestrial feedstocks, typically around 40 %, and is slightly lower in marine biomass. Following pyrolysis, a substantial increase in carbon content is observed in all biochar samples compared to their original biomasses, with particularly pronounced enrichment in beech wood and flax shives-derived biochars, reaching values above 80 % in BCBW and BCFS. This carbon enrichment is a well-known characteristic of the pyrolysis process, which eliminates volatile and oxygen-rich compounds and leads to the formation of a more stable carbonaceous matrix [220], [221]. However, this trend is not consistently maintained after activation. While in some cases, such as BCBWA, the carbon content increases slightly relative to the non-activated biochar; this increment is modest compared to that induced by pyrolysis. In contrast, for BCFSA and BCALDA, activation results in a reduction of carbon content, in some cases to levels comparable to or even lower than those of the original biomass. This indicates that carbon is partially consumed or released during the activation process, which is consistent with pore development and surface gasification.

With respect to oxygen content, the opposite trend is initially observed, as oxygen decreases markedly after pyrolysis. This reduction is attributed to the progressive loss of oxygen-containing functional groups with increasing temperature [222], [223], reflecting a higher degree of carbonization and aromatization. Upon activation, the oxygen content continues to decrease in BCBWA and BCFSA, in agreement with the thermal effects described above. In contrast, an increase in oxygen content is observed for algae-derived biochar, which may result

from partial oxidation and the incorporation of oxygen-containing surface functionalities during CO_2 activation [176].

Furthermore, biochars derived from lignocellulosic residues (BCBW and BCFS) exhibit lower concentrations of potassium (K) and calcium (Ca) compared to algae-based biochars, reflecting the lower abundance of these elements in the original feedstocks. After pyrolysis and activation, a notable increase in the relative concentration of these inorganic elements is observed, likely due to their limited volatilization under the slow pyrolysis and activation conditions employed. Similar behavior has been reported in previous studies, where temperature and heating rate were shown to strongly influence the retention of inorganic nutrients [18], [224].

Although nitrogen (N) is not visible in the biomass samples in the figure, small amounts are detected in BCBW, BCFS, and their activated counterparts, possibly due to nitrogen retention on the biochar surface during pyrolysis and activation. Other elements, such as sodium (Na), magnesium (Mg), and chlorine (Cl), are present only in trace amounts in most samples, but occur at higher levels in BCALDA, which may be related to inorganic impurities or soluble salts present in the raw algal material.

Overall, these results demonstrate that the elemental composition of biochar is governed not only by the type of biomass precursor but also by the specific pyrolysis and activation conditions. These parameters must therefore be carefully considered when selecting biochar for targeted applications such as soil amendment, adsorption processes, or environmental remediation systems [215], [225].

3.1.3 Assessment of chemical properties FTIR-ATR

Figure 22Figure 22 shows the ATR spectra of biochars produced at 600 °C (BCALD, BCBW, and BCFS) and their activated forms (BCALDA, BCBWA, and BCFSA). The observed changes in peak positions and intensities reflect the presence and evolution of multiple functional groups. Overall, the ATR spectra exhibit numerous similarities, indicating the presence of shared functional groups among the samples. This similarity is particularly evident for flax shives- and beech wood-derived biochars, which is consistent with their common lignocellulosic origin. An important observation is that activation leads to a general decrease in peak intensities, suggesting a modification or reduction of surface functional groups. In addition, the BCALD spectrum shows distinct peaks at 1 177 cm^{-1} and 617 cm^{-1} that are absent in the activated algal biochar spectra.

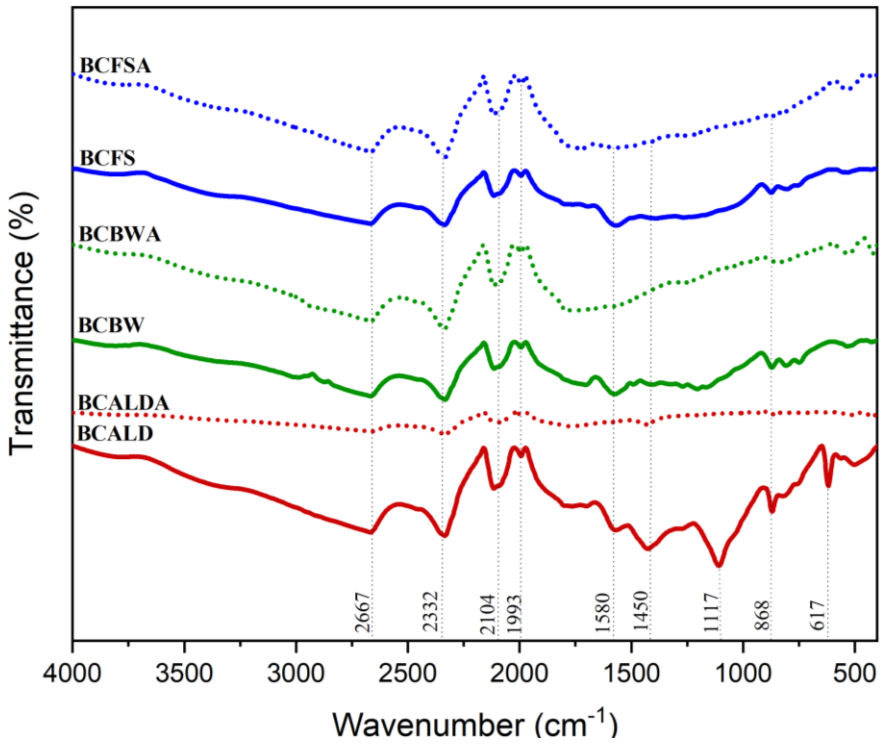

Figure 22: Comparison of infrared spectra of the three types of biochar (BCALD, BCBW, BCFS) and their activated version (BCALDA, BCBWA, BCFSA).

Table 7 summarizes the observed vibrational bands identified in the different biochar samples and their respective functional groups are detailed, allowing the surface chemical composition of the material to be identified.

Table 8: Functional groups present in different biochars.

Wavenumber (cm^{-1})	**Assigned functional group**	**Scientific reference**
~ 3400 – 3200	O–H stretching (hydroxyls, bound water, alcohols, phenols)	[226]
2667	O–H Vibration Carboxylic Acid (Carboxylic Acids)	[226]
2332	C≡C stretch or adsorbed CO_2 (trapped CO_2 resonance)	[227]
2104	C≡C (terminal alkyne) stretching or CO_2 combinations	[226]
1993	Transition metal carbonyl, Aromatic combination bands	[226], [228]
1580	Aromatic C=C stretching, or asymmetrical COO^- vibration (carboxylates)	[229]
1450	C–H strain in CH_2/CH_3, aromatic vibration	[221]
1177	C–O stretching (alcohols, ethers, esters, phenols)	[226]
868	Vibration outside the aromatic C–H plane (substituted benzene rings)	[227]
617	Vibration of aromatic rings (C–H out of plane) or inorganic compounds (silicates)	[226]

When comparing the curves of the different samples in Figure 6, we can see that flax shives biochar shows greater intensity in the region 3 400 – 3 200 cm^{-1} and carboxylic bands (2 607 cm^{-1}), which suggests a higher content of polar oxygenated groups (–OH, –COOH). In the case of wood biochar, they have a lower intensity of oxygenated bands, indicating a lower amount of surface oxygen. The aromatic bands (1 580 and 868 cm^{-1}) are relatively lighter, reflecting a certain aromaticity. While algae biochar exhibits the most intense bands in aromatic regions (1 580, 868, 617 cm^{-1}) and lower definition of polar bands (–OH, –COOH).

3.1.4 Effect of biomass and activation on the crystal structure of biochar

Figure 23 shows the X-ray diffractograms obtained for biochar derived from beech wood (BCBW), flax shives (BCFS) and Laminaria digitata algae (BCALD), pyrolyzed at 600 °C and their respective versions activated by CO_2 heat treatment at 900 °C (BCBWA, BCFSA, and BCALDA**).**

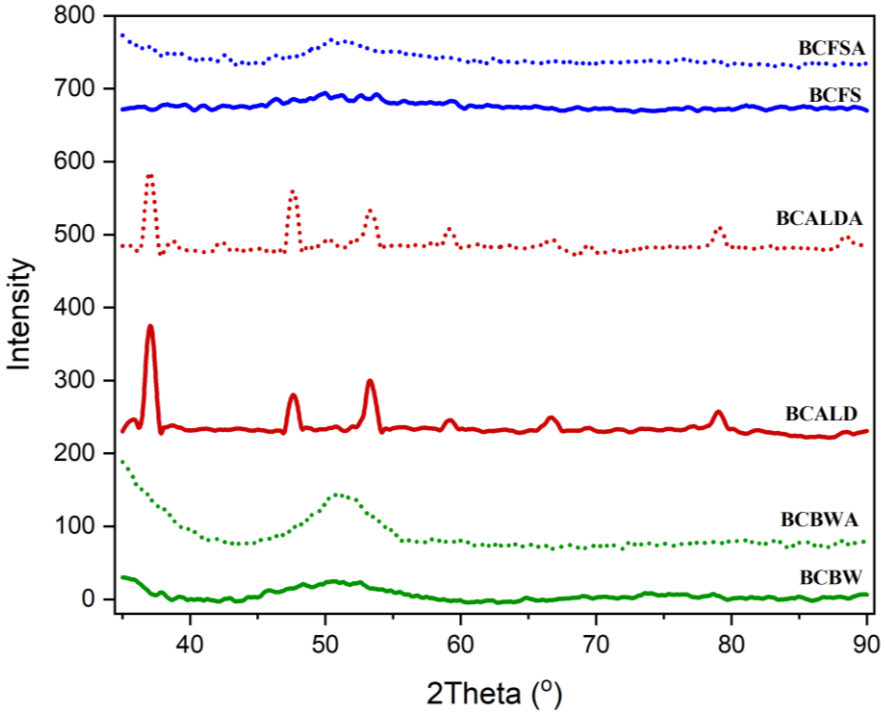

Figure 23: Comparison of the diffractograms of the three types of biochar (BCALD, BCBW, BCFS) and their activated version (BCALDA, BCBWA, BCFSA).

The X-ray diffraction (XRD) pattern of BCBW exhibits broad and diffuse peaks, indicating a predominantly amorphous structure. This behavior is characteristic of carbonaceous materials in which graphitic ordering has not yet been fully developed. The low intensity and large peak width suggest that graphitization remains limited under pyrolysis conditions at 600 °C [230]. Analysis of the activated sample shows a very similar diffraction profile to that of BCBW, with only a slight narrowing of the (100) peak in the 45–60° (2θ) range. This observation suggests that CO_2 activation at 900 °C induces only a minor increase in structural ordering. These results support the widely accepted view that activation primarily promotes pore development rather than the formation of crystalline carbon structures.

In contrast, the BCALD and BCALDA diffractograms display sharper and more intense peaks, which are indicative of the presence of crystalline mineral phases within this type of biochar. Following activation, a similar pattern is observed, albeit with changes in peak intensities. The amorphous background is markedly reduced, and mineral-related peaks become more pronounced, likely due to carbon loss during activation and the relative enrichment of inorganic

$$C_i = \frac{S_c}{S_t} x\ 100 \qquad \textit{Equation 3}$$

constituents, such as silica- and potassium-containing compounds, present in the ash of this agricultural residue. A minor peak at 42.3 ° is also detected and may be attributed to the presence of KCl [231] which is consistent with the EDS results showing potassium and chlorine in the algal biochar.

Finally, the BCFS and BCFSA diffractograms are dominated by amorphous features, characterized by broad undulations and the absence of well-defined crystalline peaks. A wide, low-intensity peak in the 45–60 ° (2θ) range is observed, similar to that seen in BCBW. This similarity indicates that, despite differences in biomass origin, biochars produced at the same pyrolysis temperature (600 °C) tend to exhibit largely amorphous structures. The broad diffuse peak between 45 ° and 60 ° is a hallmark of amorphous or turbostratic carbon, commonly found in biochars generated at moderate temperatures [232]. This feature is associated with reflections from the (100) and (101) planes of disordered graphitic domains [233].

Table 9 summarizes the crystallinity indices of the biochars, calculated using the deconvolution method described by Equation 3 in Chapter 2.

where Sc represents the area of the crystalline domain and St represents the area of the total domain.

Table 9: Crystallinity index of different biochars and their activated versions.

Biochar	Total area of the crystalline peaks (a.u.·2θ)	Total area of the crystalline and amorphous peaks (a.u.·2θ)	Crystallinity index (%)
BCALD	123.16	731.26	54.86
BCALDA	448.66	875.27	51.26
BCBW	203.40	743.54	27.36
BCBWA	444.35	1255.98	35.38
BCFS	161.95	579.16	27.96
BCFSA	54.50	789.08	28.46

According to the values in Table 9, the effects of seaweed biochar activation on the crystallinity index are small but show a downward trend. In contrast, for beech wood biochar, activation had a greater effect on the crystallinity index, and the trend is upward. In the case of flax shives biochar, there was no significant change in the crystallinity index with activation, as the change was less than 1 %. The general trend in the crystallinity index is, in descending order, algae biochar, activated algae biochar, then activated wood biochar, activated flax shives biochar,

then flax shives biochar, and the lowest is wood biochar. Consider that the latter three have a difference of less than 1 %, which could be considered negligible.

3.1.5 Preliminary conclusions on biochar properties

The physicochemical behaviour of the biochars is primarily governed by both the nature of the feedstock (Laminaria digitata algae, beech wood, and flax shives) and the applied thermal treatments (pyrolysis at 600 °C and CO_2 activation at 900 °C). Depending on the biomass type and processing conditions, several key trends were identified.

Activation consistently leads to an increase in specific surface area (S_{BET}) and total pore volume. In certain cases, particularly for algae-derived biochar, the specific surface area increases by more than an order of magnitude. In addition, activation increases the apparent bulk density and promotes the development of interconnected microporous and mesoporous networks, while macroporosity remains dominant in algae-based biochars.

Elemental analysis shows a clear enrichment in carbon content following pyrolysis. However, CO_2 activation generally results in a reduction of the surface carbon fraction, likely due to partial carbon gasification, which simultaneously contributes to the formation of new pores. FTIR spectroscopy indicates a relative loss of oxygen-containing functional groups during pyrolysis, with the type and abundance of surface functionalities varying according to the biomass source.

XRD analysis reveals predominantly amorphous, turbostratic carbon structures in beech wood- and flax shives-derived biochars, whereas algae derived biochars exhibit distinct crystalline mineral phases, likely associated with potassium- and chlorine-containing compounds.

The trends in biochar characteristics are summarized in the biochar physicochemical map. The data presented in Figure 24 represent the average values obtained from at least two independent measurements per sample.

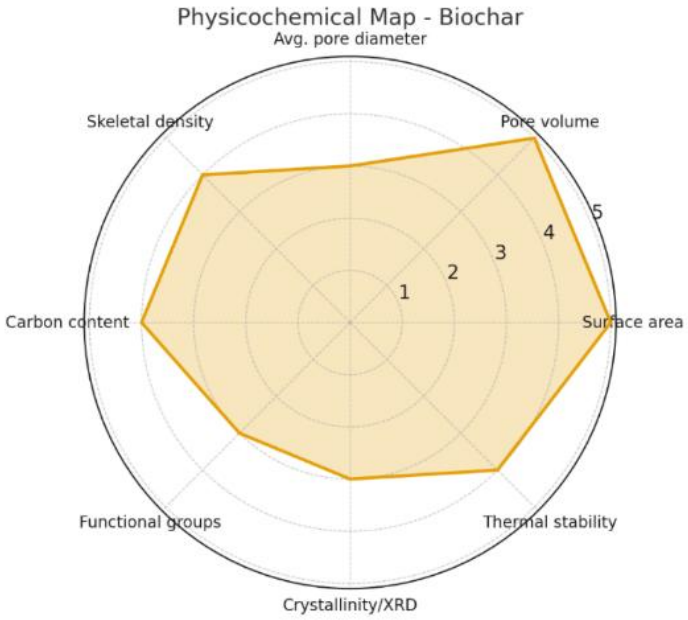

Figure 24: Physicochemical map of biochar properties.

Overall, the results are internally consistent and demonstrate that CO_2 activation effectively enhances surface area and porosity, thereby improving adsorption capacity and interfacial properties.

3.2 Biochar-based biocomposites: Influence of biochar type and content

This section describes the characteristics of different composites made with PLA and different types of biochar as fillers, as well as different load percentages. The polylactic acid (PLA) is used as the matrix, because it is one of the most widely used and studied biodegradable matrix in biocomposite research. It is commercially available and has well-characterized properties. This makes it a suitable reference for evaluating the specific effect of biochar on the properties of the material and reducing the uncertainty associated with the polymer matrix. In addition, there are studies that show its affinity with certain carbon reinforcements, which is what biochar is replacing. Finally, PLA is a widely used material in industry, which could facilitate the transfer of the new biochar PLA composite to industry. Figure 25 shows a diagram with the composition of the different composites studied in this section.

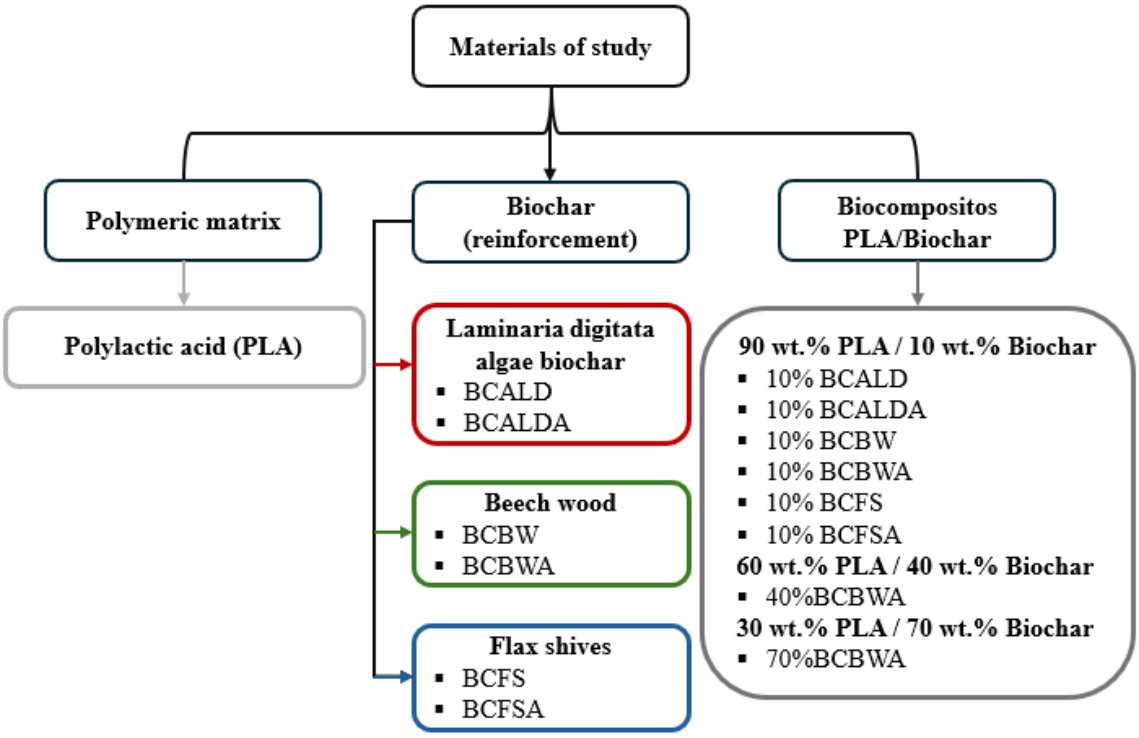

Figure 25: Diagram of the different types of biochar and biocomposites.

3.2.1 Assessment of morphological properties

Figure 26 shows the SEM micrographs corresponding to the surfaces of the different materials and treatments: PLA, PLA with biochar, and PLA with activated biochar.

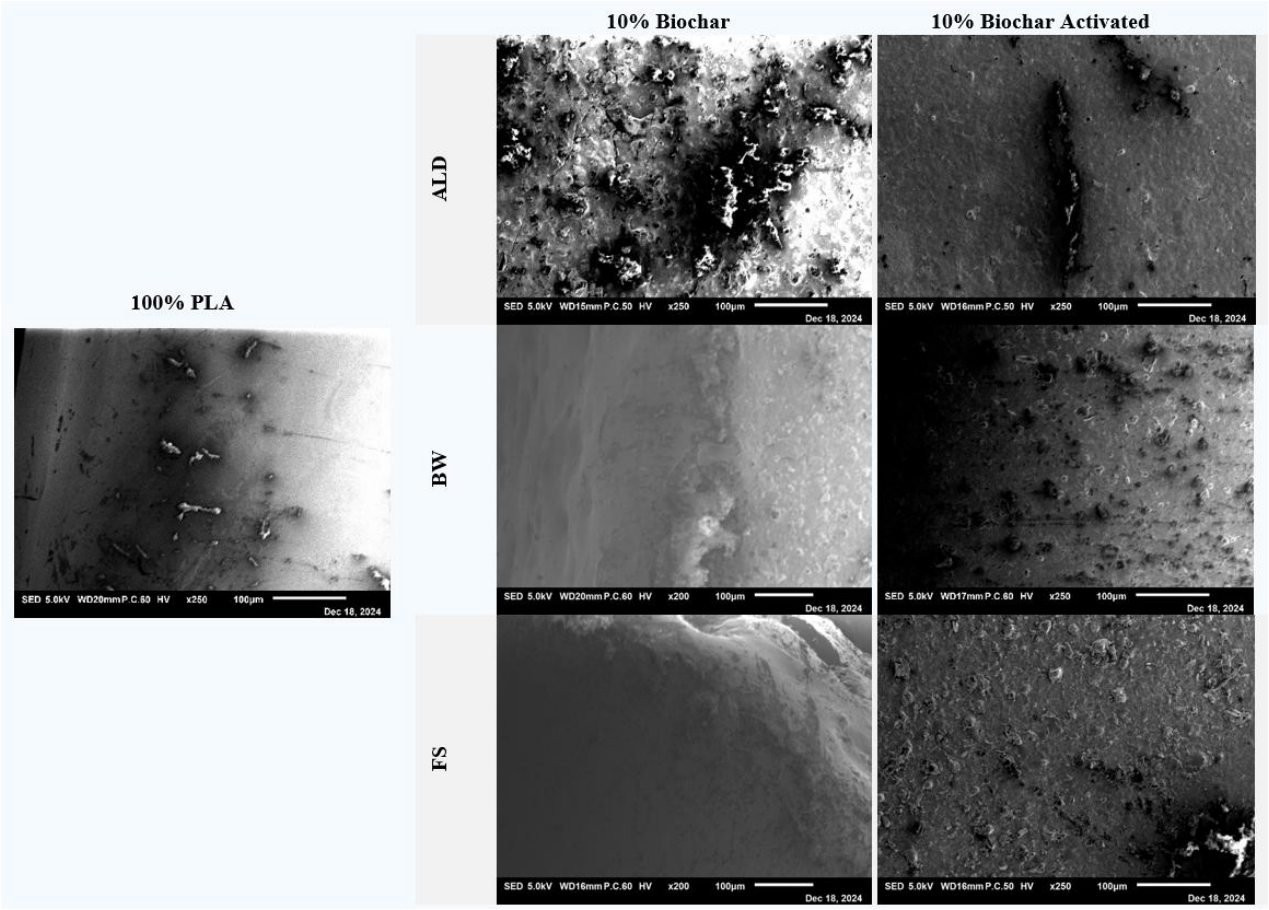

Figure 26: SEM images of the surface of various composites.

In the image of pure PLA, relatively smooth and homogeneous surfaces are observed, with the presence of superficial microcracks. These cracks could be associated with internal stresses generated during the manufacturing process or drying. No embedded particles or significant irregularities are visible, confirming the absence of additional phases.

In column 2, the different biocomposites with 10 wt.% biochar are observed. In the case of 10% BCALD, the surface shows a clear heterogeneity, with the presence of dark aggregates distributed irregularly. Particles embedded in the polymeric matrix are observed, although in some cases there seems to be a lack of interfacial compatibility, which generates cavities and voids. For 10% BCBW, the surface has a more compact area, but the rough morphology associated with the presence of biochar is still distinguished. Regions with partial detachment of the reinforcement are identified. However, for the 10% BCFS, the observed area presents low particle definition, probably due to detachment during the process, which suggests a lower interaction between the biochar and the matrix in this condition. These results coincide with what was reported by Zouari *et al.,* 2022 [125] where the addition of biochar increases roughness and generates areas of poor interfacial adhesion due to chemical incompatibility.

Column 3 presents the biocomposites with 10 wt.% activated biochar. For 10% BCALDA, a more homogeneous surface is observed compared to an inactivated biochar. The particle distribution appears finer and better integrated with the matrix. The activation of biochar generates an increase in porosity and specific surface, which favors adhesion at the interface

[234]. In the case of 10% BCBWA, it presents an intermediate pattern: there is roughness, but with more dispersed particles and better anchored in the matrix. The reduction of cavities and voids suggests greater compatibility. Finally, for 10% BCFSA, a rough but continuous surface is distinguished, with particles embedded in a more uniform way. This shows that activation improves dispersion and interfacial adhesion, reducing structural defects.

3.2.1.1 Influence of biochar activation on the biocomposite surface

Neat PLA exhibits smooth surfaces with only minor irregularities, although microcracks are present. Incorporating 10 wt.% non-activated biochar into the matrix increases surface roughness and leads to the formation of cavities, voids, and particle detachment, indicating limited interfacial compatibility. In contrast, composites containing activated biochar show markedly improved integration between the matrix and the reinforcement. The biochar particles are more uniformly distributed, and interfacial defects are reduced, suggesting enhanced adhesion and stability of the composite material.

These observations align with literature reports indicating that biochar activation increases the number of surface functional groups [235], which can enhance interactions with polymeric matrices. As a result, composites reinforced with activated biochar are expected to exhibit superior mechanical and thermal properties compared to those containing untreated biochar.

3.2.2 Assessment of microstructural properties

3.2.2.1 Evaluation of the PLA- biochar chemical interaction using FTIR

Figure 27 shows Infrared Fourier Transform (FTIR) spectra for four different samples: pure PLA and three PLA compounds with biochar additions (10% BCALD, 10% BCBW and 10% BCFS). It has been revealed that the addition of 10% biochar produces small changes to the chemical characteristics of PLA.

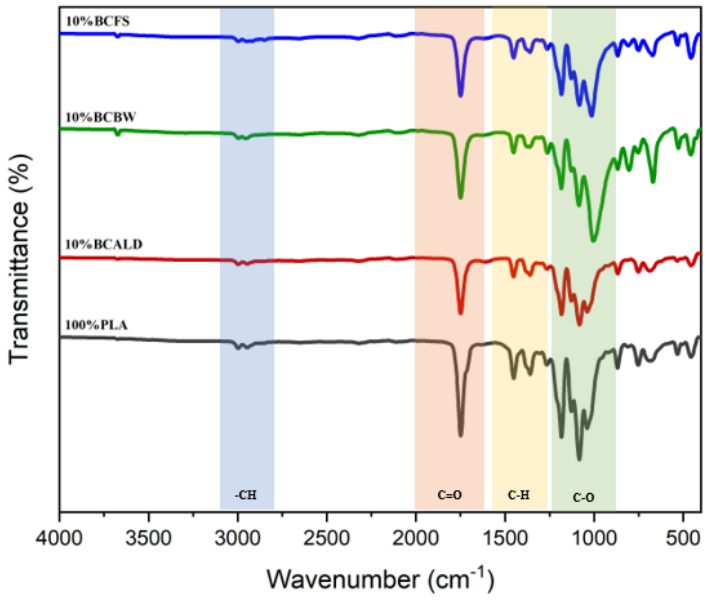

Figure 27: FTIR spectra of 100% PLA and biocomposites: 10% BCALD, 10% BCBW and 10% BCFS.

The 100% PLA spectrum exhibits the typical peaks of polyester, including C=O stretch near 1750 cm^{-1} and C–O bands between 1200 and 1100 cm^{-1} [226]. In mixtures containing 10 wt.% biochar (BCBW, BCFS and BCALD), changes in the intensity and shape of these bands are observed, indicating interactions between the functional groups of PLA and the oxygen-rich surfaces of biochar. This same behavior was observed in composites with activated biochar. This same behavior was observed in composites with activated biochar.

However, the change is most noticeable in Figure 28 which shows the characteristic transmittance of PLA samples with different charges of beech wood activated biochar (BCBWA). In this sense, it is observed that as the amount of biochar in the matrix increases, the absorption bands that correspond to the functional groups of the PLA decrease in intensity. In particular, the one of greatest interest, in the region of 1 750 cm^{-1} corresponds to the C=O stretch; and that of the region of 1 080–1 180 cm^{-1} is associated with C–O–C bonds. While at the same time the signals attributed to oxygenated groups that are present in the biochar (aromatic −OH, C=O and C=C) appear and increase in regions around 3 400 cm^{-1}, 1 600 cm^{-1} and 1 100 cm^{-1}, respectively. This suggests that the introduction of biochar not only dissipates the polymer signal but also introduces new surface functionalities that can cause interactions (hydrogen bonds or dipole interactions) at the interface.

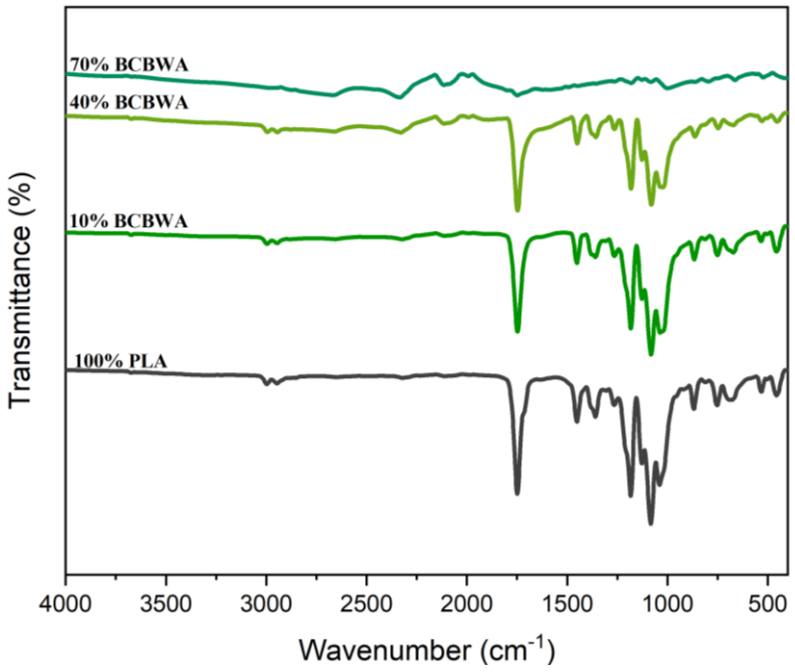

Figure 28: FTIR-ATR spectra of pure PLA and PLA–BCBWA composites with different loads of beech wood biochar (10, 40, and 70 wt.%)

However, at high concentrations (≥ 40 %), the intensity of the bands whose intensities were related to PLA are even more attenuated, which can be related to lower chemical compatibility and the possible existence of areas where interfacial adhesion can be very weak.

Despite the decrease in the intensity of the bands, the characteristic bands of PLA remain unchanged in position, suggesting that the addition of biochar does not fundamentally alter the

chemical structure of the polymer, and interactions are mainly physical in nature or through weak hydrogen bonds, with no formation of significant new covalent bonds.

3.2.3 Assessment of thermal stability (TGA)

The thermogravimetric curves presented in Figure 29 show the impact of the nature of biochar on the thermal stability of the different PLA formulations at 10 wt.% biochar. Initially, all samples, including pure PLA, show excellent thermal stability up to approximately 250 °C, where the mass remains constant, indicating the absence of degradation or loss of volatile compounds. This behavior is typical of polymers that do not contain low molecular mass additives.

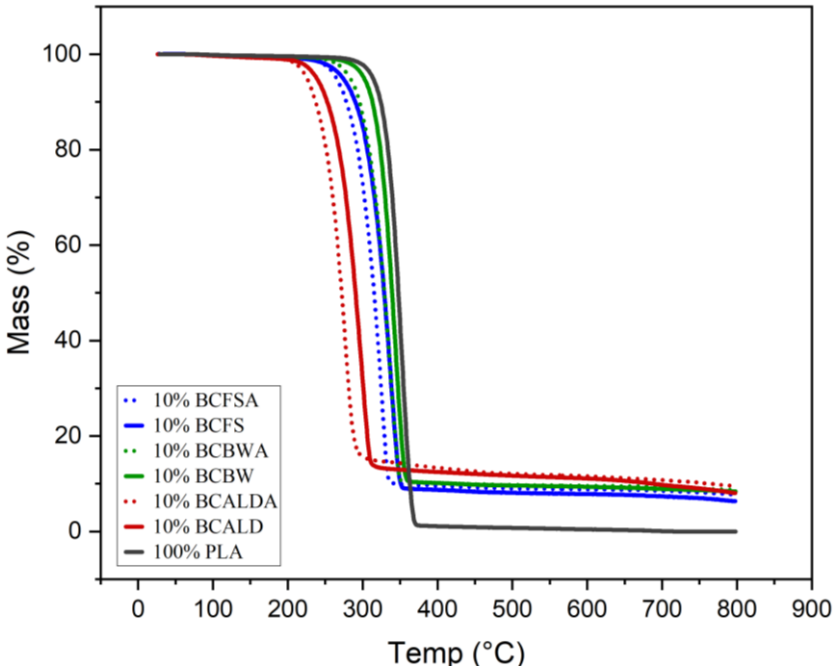

Figure 29: Mass degradation curves with respect to the temperature of PLA and PLA-biochar compounds (10 wt.%). Heated at a constant rate of 10 °C·min-1 from 25 to 800 °C, under an inert 20 ml·min-1 argon atmosphere.

The pure PLA curve features an abrupt decrease in mass that begins around 300 °C and completes around 375 °C. The loss of mass is almost total, leaving a negligible residue. In contrast, charged compounds in which degradation begins at slightly lower temperatures, suggesting that the presence of biochar could have altered the polymer's degradation mechanism and where residue remains between 10% and 15% of initial mass. The addition of biochar decreased thermal stability, which could be due to the presence of K in the biochar, causing it to act as a catalyst in degradation[236].

Comparing the maximum degradation temperature of biochars to that of their activated versions, it can be seen that in all cases, the temperature of the activated version is slightly lower. If, on the other hand, we make the comparison according to the type of biochar, it is obvious that those with the lowest degradation temperature are BCALDs, followed by BCFS and finally BCBWs. This is consistent with the elemental analysis presented above, which

shows that BCALD has the highest amount of K, followed by BCFS and finally BCBW, with 0.61%, 1.37%, and 11.37% potassium, respectively.

A comparison of the degradation curves for the biomasses, biochars, and biocomposites used can be found in annex 2, which shows that the biochar samples are the most stable. The maximum degradation temperatures for the biomasses and the 10% biochar-PLA biocomposites range from 280 °C to 350 °C. The degradation of biomass involves more stages than biocomposites and others, and if comparing with Figure 29, the curves for the biocomposites are more similar to the degradation curves of PLA than to the others, which is consistent with the fact that they are 90% PLA.

3.2.3.1 Effect of biochar beech wood loading on thermal stability of PLA-biochar biocomposite

Figure 30 shows the thermogravimetric analysis of biocomposites formulated with different proportions of activated biochar (BCBWA) in a PLA matrix to analyze the effect of loading on thermal stability.

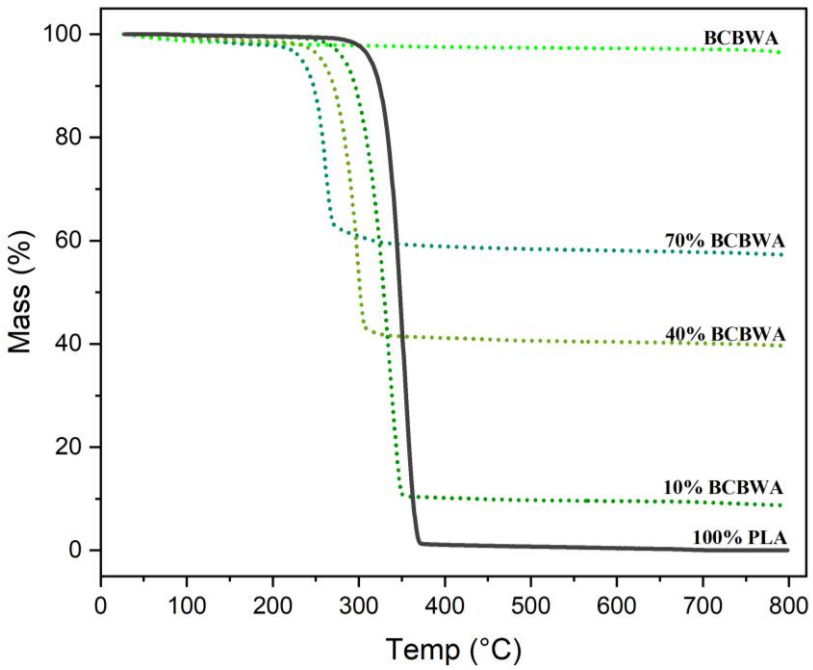

Figure 30: Mass degradation curves of PLA and PLA-BCBWA composites with different beech wood biochar contents (10, 40, and 70 wt.%). heated at a constant rate of 10 °C·min-1 from 25 to 800 °C, under an inert 20 ml·min-1 argon atmosphere.

The progressive incorporation of biochar has a significant effect on the thermal stability of the composite material. The 100 % PLA begins its main degradation at around 320 °C and reaches its maximum mass loss at around 370 °C. However, as the biochar loading increases, the thermal profile changes significantly: biocomposites with 10 wt.%, 40 wt.%, and 70 wt.% BCBWA show a reduction in the maximum degradation temperature, suggesting that in this temperature range, biochar acts as a catalyst for the thermal degradation of the matrix. Moreover, the final residue at 800 °C increases directly with biochar concentration, which aligns with a large part of the biochar being composed of carbon and its thermal stability.

In summary, the addition of the BCBWA filler and the increase in its concentration significantly reduce the thermal stability of the compound a, which is reflected in the reduction of the maximum degradation temperature.

3.2.4 Assessment of thermal transitions (DSC)

Figure 31 displays the DSC thermograms from biocomposites made with 10 wt.% of various biochars and a PLA matrix, along with pure PLA control. Showing the effect of the nature of biochar and its activation on the matrix. The thermal transitions have taken place at the following locations: glass transition temperature (Tg) at approximately 55 – 60 °C; cold crystallization (Tcc) temperatures at approximately between 100 – 130 °C; and melting point (Tm) between about 145–160 °C. Pure PLA presented a clear thermal signal and little crystallinity; the data indicated that biochar alters these thermal responses.

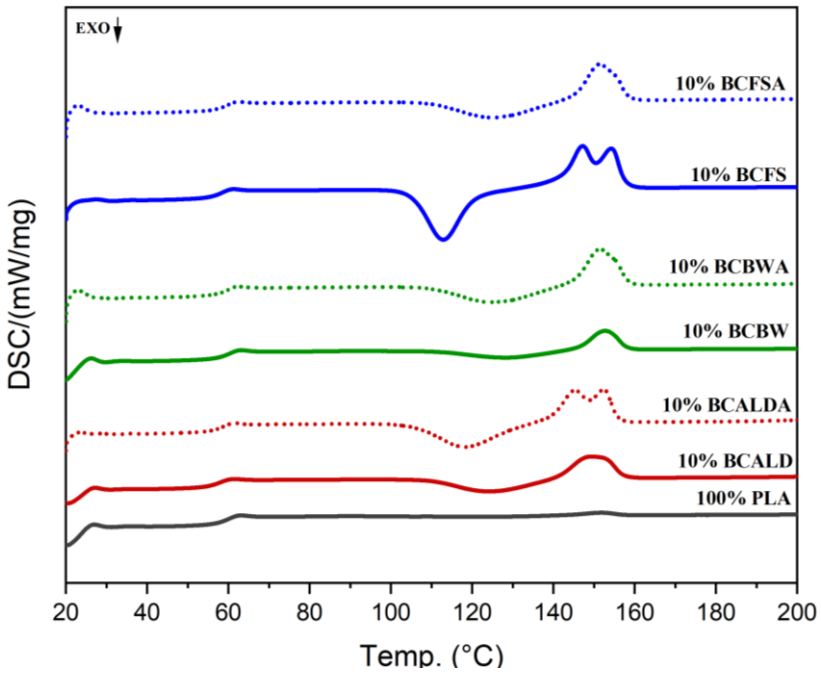

Figure 31: DSC thermograms from biocomposites made with 10 wt.% of the three biochar in PLA. First heating from 20 to 200 °C at 10 °C·min^{-1}, Ar. 40 mL·min^{-1}. Cooling from 200 to 20 °C at 10 °C·min^{-1}, Ar. 60 mL·min^{-1}. Second heating from 20 to 200 °C at 10 °C·min^{-1}. Ar. 40 mL·min^{-1}.

It was noted that the biocomposite 10% BCFS had a double exotherm in the cold crystallization region, which could indicate that biochar is affecting nucleation mechanisms or induction of heterogeneous crystalline phases. In addition, it was noted that the melting peak intensity and location were different for each of the biocomposites. Specifically, there was generally an increase in the intensity of Tcc for composites like 10% BCALDA and 10% BCFSA which would indicate a nucleating effect of biochar which promotes PLA crystallization [237], [238]. The 10% BCBWA biocomposite exhibited less definition of thermal events which could indicate poor dispersion or limited interfacial interaction between the biochar and the polymer matrix.

In broad terms, these findings indicate that the type of biochar (biomass, activation method) has a direct effect on the thermal properties of the biocomposite, particularly crystallization of the biocomposite will affect the mechanical properties and dimensional stability of the final biocomposite.

3.2.4.1 Effect of biochar beech wood loading on thermal transition of PLA biocomposite

Figure 32 displays the DSC thermograms for pure PLA and for biocomposites with 10 wt.%, 40 wt.%, and 70 wt.% of the beech wood activated biochar (BCBWA). For pure PLA, one notices a glass transition at around 62.6 °C, cold crystallization at 126.7 °C, and a melting point (Tm) of 151.9 °C, which is indicative of PLA with low initial crystallinity.

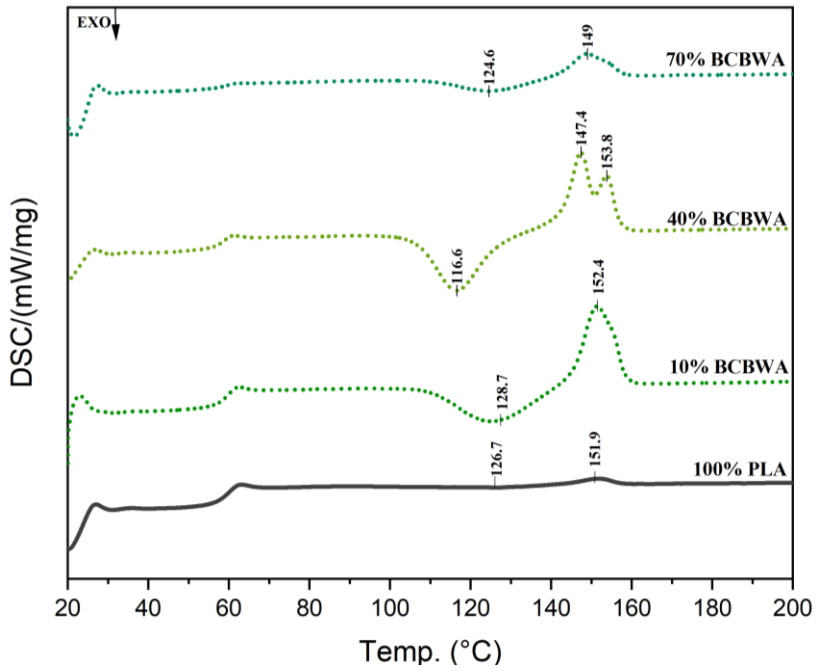

Figure 32: DSC thermograms of PLA and biocomposites made with different charges of beech wood biochar (10, 40, and 70 wt.%). First heating from 20 to 200 °C at 10 °C·min-1, Ar. 40 mL·min-1. Cooling from 200 to 20 °C at 10 °C·min-1, Ar. 60 mL·min-1. Second heating from 20 to 200 °C at 10 °C·min-1. Ar. 40 mL·min-1.

Upon introduction of biochar, we can see severe alteration of the thermal transitions. The biocomposite containing 10 % BCBWA presents decreased Tcc (123.7 °C) and decreased Tm (152.4 °C), indicating that biochar has begun nucleating PLA. At 40 % BCBWA there is even earlier cold crystallization (116.6 °C) and clear double melting (Tm) at 147.4 °C and 153.8 °C showing there is crystal or secondary recrystallized crystals forming during heating. For the case of 70 % BCBWA, the Tcc lowered even more (114.6 °C), and Tm appears lower (149 °C) indicating a stronger nucleating effect, which, however, compromises the perfection of the crystalline structure formed. Table 10 shows a summary of the characteristics highlighted in the DSC analysis.

Table 10: summary of characteristic data obtained from ATG and DSC analysis.

ATG/ DSC	T_{dmax} °C	Tg °C	Tcc °C	Tm °C	△Hc J/g	△Hf J/g	x_c
100% PLA	353.9	58.60	126.70	151.90	1.92	1.63	0
10% BCALD	299.7	56.90	124.00	149.30	15.51	14.68	0
10% BCALDA	279.0	57.60	118.20	145.3/152.4	24.79	25.52	0.87
10% BCBW	345.2	58.80	127.90	152.70	8.92	9.51	0.70
10% BCBWA	337.9	58.70	128.70	152.40	10.65	11.25	0.71
40% BCBWA	299.6	57.50	116.60	147.4/153.8	22.38	22.81	0.76
70% BCBWA	261.4	57.80	124.60	148.90	6.89	6.99	0.38
10% BCFS	338.3	57.20	112.90	147.2/154.2	31.58	34.89	3.93
10% BCFSA	325.5	58.60	125.50	151.40	19.49	20.25	0.90

Caption: T_{dmax} - maximal degradation temperature; T_g – Glass transition temperature T_{cc} – Cold crystallization temperature; T_m - Melting Temperature; ΔH_c – Crystallization enthalpy; ΔH_m – Melting enthalpy; x_c – Crystallinity index by DSC.

These findings confirm that the content of biochar has a significant effect on the crystallization abilities of PLA, acting as a nucleation source and advancing the crystallization time. The nucleating effects of biochar are most evident in composites derived from shives biochar (10% BCFS, 10% BCFSA) and algae activated biochar (10% BCALDA). However, the multiple melting peaks along with the lower T_m at high loadings may be due to heterogeneity in the crystalline morphology or restrictions on the mobility of the polymer chain because of the high loading amount.

3.2.5 Assessment of structural properties (XRD)

Figure 33 shown is an X-ray diffractogram (XRD) of different PLA compounds with 10 wt.% of various biochar, in addition to pure PLA as a reference.

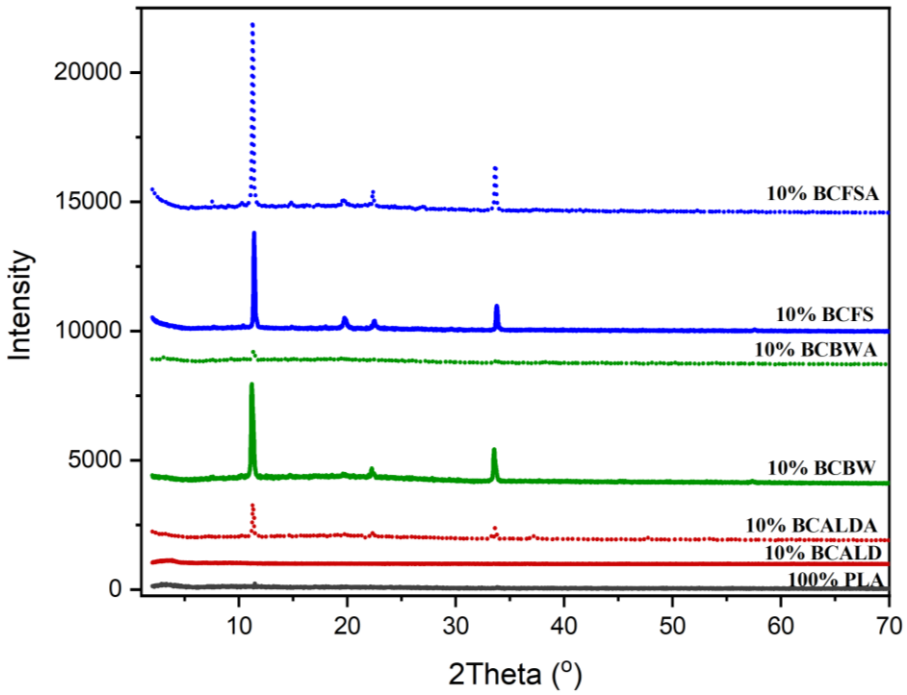

Figure 33: XRD curves of PLA and 10 % PLA-biochar biocomposites with the three types of biochar and their activated versions.

The diffractograms of PLA show a mostly amorphous tendency. For the 10% BCALD compound, an increase in the amorphous halo is observed with the loss of the only peak visible at this scale. However, changes in the curve of the compound with the BCALDA in which several defined peaks are evident, alluding to an increase in the crystallinity of the biocomposite. When passing through the beechwood biochar, we observe a similar phenomenon in which the bioparticles have more defined peaks.

In this case, the activated version presented an inverse behavior to the previous one, with the active version being more amorphous than the non-active version. This spectrum is very similar to that of PLA alone. So, this suggests that they do not promote crystallization at all. Finally, the BCFS curves in which the appearance of crystalline peaks is evident. The appearance of these sharp peaks on the amorphous halo of PLA is evidence that flax shives biochar induced PLA crystallization. The intensification of the crystalline peaks in the compound with activated biochar (BCFSA) could indicate that activation with CO_2 at 900 °C enhanced the nucleating properties of flax shives biochar, probably due to an increase in surface area and the creation of active sites.

When comparing biomass types, flax shives biochar behaves as an effective nucleating agent for PLA, while beech wood biochar and some are less so. A material's ability to induce crystallization depends on its surface properties (such as area and chemistry), which provide sites for the formation of crystalline cores.

3.2.5.1 Effect of activated biochar beech wood loading on the structure of PLA biocomposite

Figure 34A shows the curve of pyrolyzed beech wood biochar at 600 °C, PLA and the 10 wt.% beech wood biocomposite. The biochar is an amorphous line, which does not have any obvious peak on this scale. Continuing with the PLA, which, although it is also mostly amorphous, is possible to distinguish peaks at 11.4 ° and 33.8 °. Finally, the biocomposite, which not only has more defined crystalline peaks, but also others are more evident at 22.3 ° and 57.3 °.

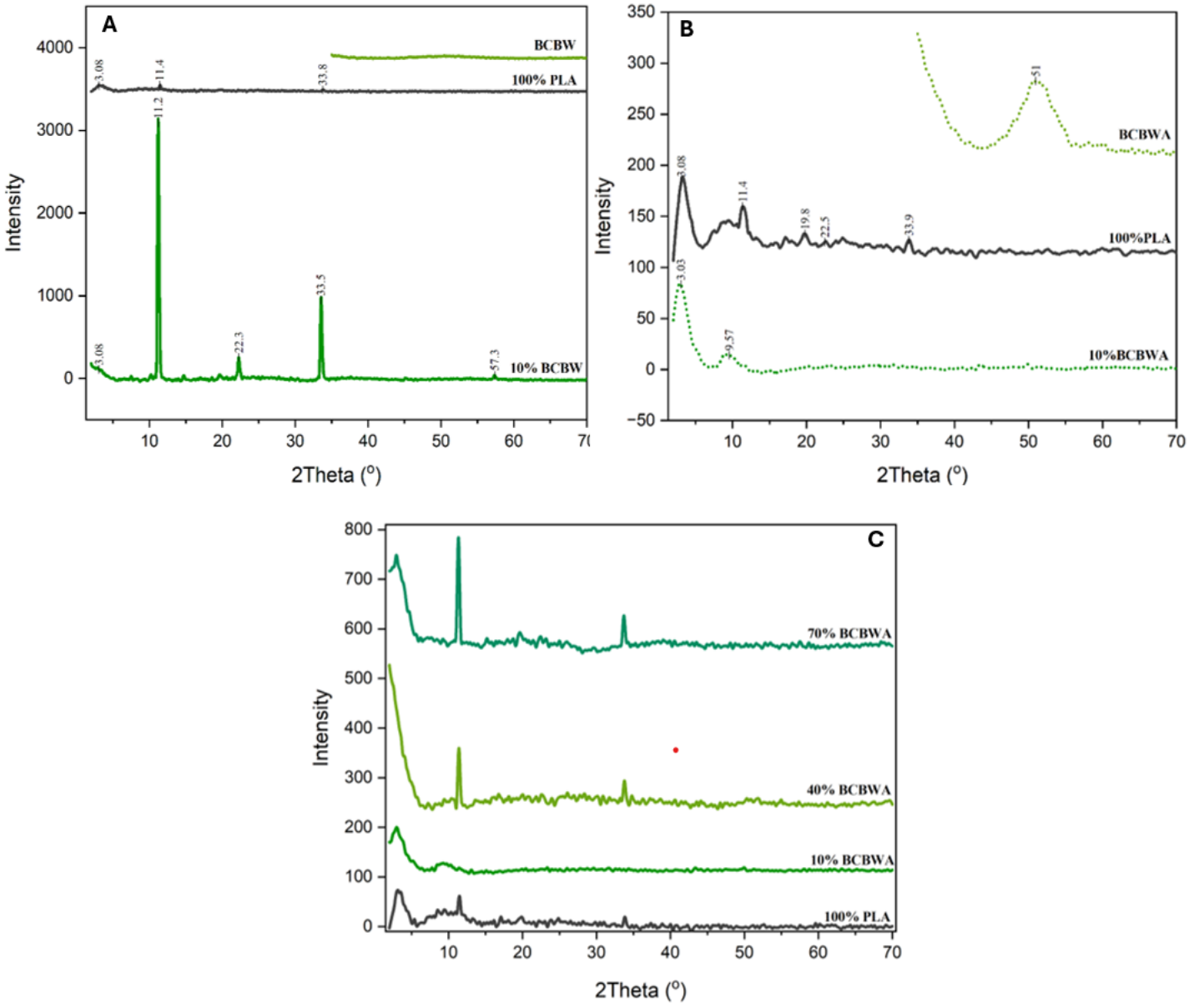

Figure 34: XRD curves: A) comparison between beech wood biochar (BCBW), PLA, and BCBW-PLA biocomposite (10% BCBW), B) comparison between activated beech wood biochar (BCBWA), PLA and BCBWA-PLA biocomposite (10% BCBWA). C) effect of the activated biochar loading on the structure of PLA.

Figure 34B shows the X-ray diffractograms obtained for activated beech wood biochar, PLA and composite from the mixture of these two. For start focus on the curve of activated biochar, which presents a wide and amorphous beak, characteristic of pyrolyzed products 600 °C. At this scale for the PLA, it is more evident to see the wide beaks, however they continue to be in the amorphous halo. In the case of biocomposite it is also maintained in the amorphous halo, and if the curve becomes more stable, other than that, there is no significant effect on the addition of biochar to PLA.

Figure 35C shows us the effect of biochar loading on the crystallinity of biocomposites. The PLA has a pronounced amorphous background, and with some wide and not very intense peaks. By adding 10 wt.% activated biochar, it becomes even more amorphous. However, that changes as the percentage of biochar exceeds 10 wt.%. At 40 and 70 wt.% we can observe how the peaks become more crystalline and increase in intensity, which could denote that the biochar acts as a nucleating agent, increasing the crystallinity of the biocomposites.

3.2.5.2 Effect of BCALD and BCALDA on the structure of PLA

Following the same sequence of comparative analyses of biochar, versus PLA and its compounds, Figure 35A shows the curves of activated biochar, pure PLA and of the compounds 10% activated algal biochar. It appears that although the algal biochar has defined crystalline peaks, which could be due to the minerals present in the seaweed, at the time of creating the polymer, the crystalline peaks that are most defined are the characteristic peaks of the biopolymer. It is interesting how biochar works as a nucleating agent for the polymer, highlighting peaks. It is also observed that some characteristic peaks of biochar are not visible at this scale in biocomposites. This is because the proportion of semblances with respect to the polymeric matrix is not so important. In spite of them, some of them are appreciable.

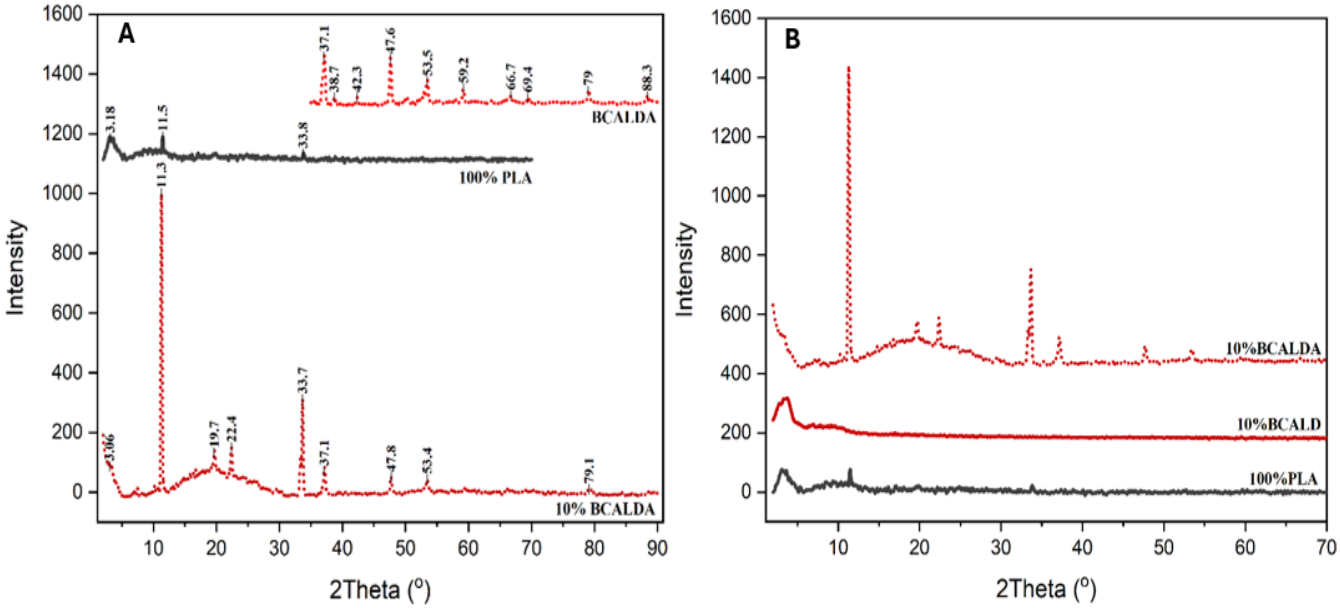

Figure 35: A) XRD curves of PLA, activated laminaria digitata algae biochar (BCALDA) and the 10 % BCALDA-PLA biocomposite (10% BCALDA). B) comparative curves of PLA, 10 % BCALD and 10 % BCALDA biocomposites.

Figure 35B presents the comparison of biocomposites 10 % algal biochar and 10 % activated algal biochar. Interestingly, the biocomposite of 10 % algal biochar without activation is amorphous, even more so than PLA itself, even though inactivated algal biochar exhibits crystalline peaks. Something similar happens with activated beech wood biochar that does not promote crystallinity but rather reduces it.

3.2.5.3 Effect of non-activated (BCFS) and activated (BCSFA) flax shives biochar on the structure of PLA

Figure 36 illustrates the different diffractograms of flax shives biochar and flax shives biochar-PLA composites. The diffractogram of flax shives biochar is compared in Figure 37 A to the ones of 100% PLA and 10% BCFSA biocomposite, and here it is evident how an amorphous biochar, being mixed with PLA can highly promote crystallinity in the polymer. It is perhaps due to the chemistry of the surface in the biochar. In the case of activated biochar, it also promotes crystallinity in the polymer and makes it much more powerful, even doubling the intensity of some peaks such as the one present at 11.4 ° theta.

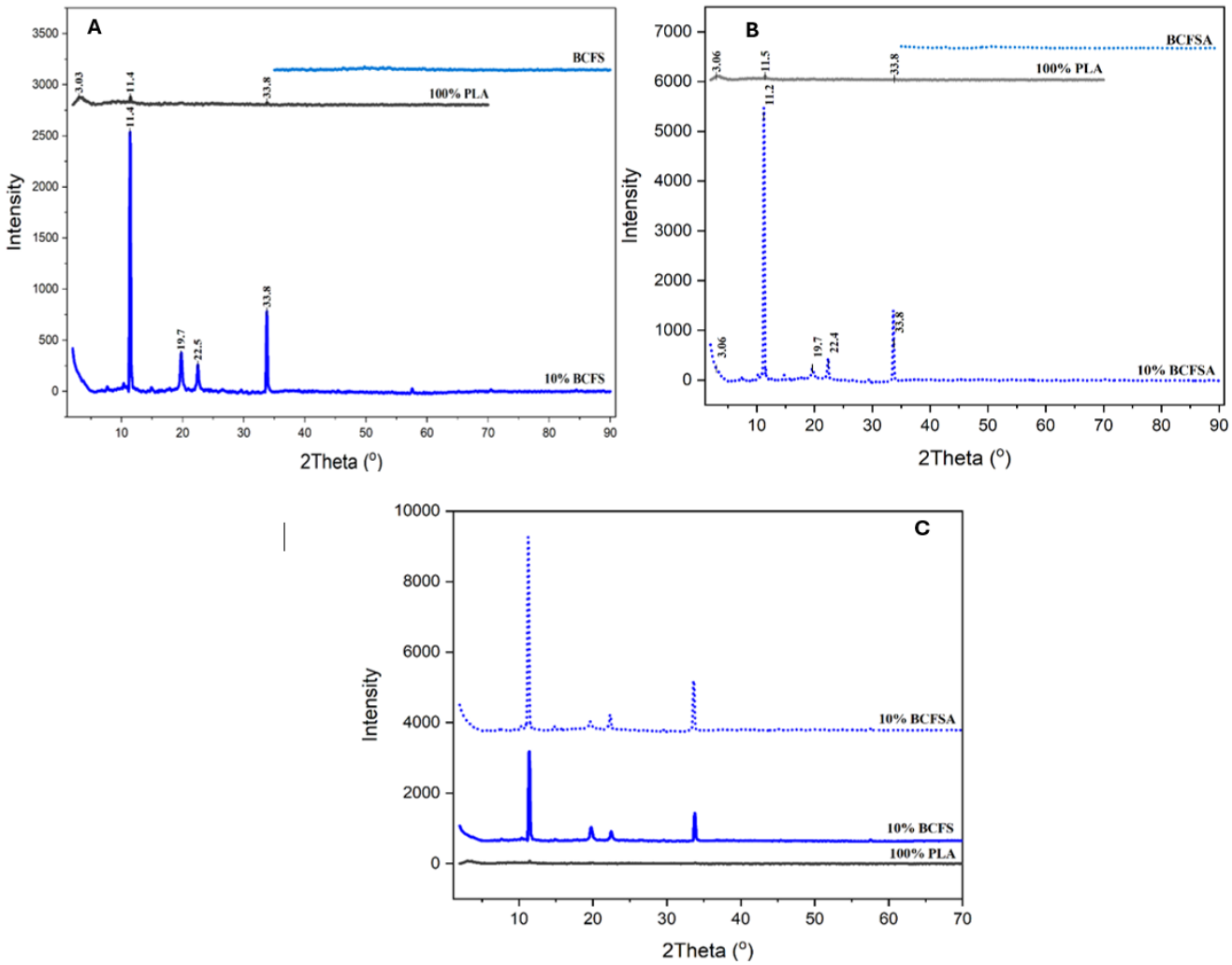

Figure 36: A) XRD curves of PLA, flax shives biochar (BCFS) and 10% flax shives biochar-PLA composite (10% BCFS). B) activated flax shives biochar (BCFSA), PLA and its biocomposite (10% BCFSA) C) comparative curves of 100% PLA with flax shives biochar-PLA composites (10% BCFS and 10%BCFSA).

Figure 36B shows the curves for BCFSA, PLA, and the 10% BCFSA composite. In this case, we observe that although the activated biochar is generally amorphous, as is the PLA, the composite exhibits crystalline peaks. The peaks corresponding to the PLA increase when mixed with this biochar filler, suggesting a nucleating effect. In both cases, adding BCFS or BCFSA increases crystallinity. However, when comparing the 10% BCFS and 10% BCFSA biocomposites, as shown in Figure 36C, it can be observed that the peak intensity for some cases of the activated version is almost double that of the non-activated version. This would suggest that the 10% BCFSA composite is more crystalline, but when calculating the crystallinity, it can be seen that the value is very similar, and this is because not only did the crystalline area increase, but the entire area increased, so the ratio remains the same.

Table 11 shows a summary of the values of the crystallinity indices for biochar, PLA and its biocomposites calculated by using the deconvolution method equation 3 presented in chapter 2 and remembered in the biochar section 3.1.4 (page 49).

Table 11: DRX analysis summary table

Material	Type	Crystallinity index (%)	Comments
Beech wood biochar (BCBW)	non-activated	27.36	amorphous structure: diffuse peaks
	activated*	35.38	amorphous structure: narrowing and minimal peak definition, slight increase in crystalline index
Flax shive biochar (BCFS)	non-activated	27.96	amorphous structure: no defined peaks
	activated*	28.46	amorphous structure: activation has no significant effects
Laminaria digitata biochar (BCALD)	non-activated	54.86	Presence of crystalline structure: defined peaks, possible presence of minerals
	activated*	51.26	Presence of crystalline structure: slight reduction in peak intensity with activation
PLA	100%		Mostly amorphous: small peaks can be distinguished
PLA + BCBW	10% BCBW non-activated	44.59	Presence of crystalline structure: increase in the intensity of PLA peaks and in the crystallinity index
	10% BCBW activated*	25.62	Amorphous structure: reduction in PLA peaks, does not significantly affect the crystallinity index
	40% BCBW activated*	37.66	Presence of crystalline structure: increase in the intensity of PLA peaks and in the crystallinity index
	70% BCBW activated*	37.75	Presence of crystalline structure: increase in the intensity of PLA peaks and in the crystallinity index.

			Peak intensity greater than 40% but no significant changes in the crystallinity index
PLA + BCFS	10% BCFS non-activated	48.26	Presence of crystalline structure: increase in the intensity of PLA peaks and in the crystallinity index
	10% BCFS activated*	47.07	Presence of crystalline structure: increase in the intensity of PLA peaks and in the crystallinity index Activation increases the intensity of the peaks, without significantly affecting the crystallinity index
PLA + BCALD	10% BCALD non-activated	33.20	Amorphous structure: reduction in PLA peaks, slight increase in the crystallinity index
	10% BCALD activated*	49.25	Presence of crystalline structure: increase in the intensity of PLA peaks and in the crystallinity index

** Activation under CO_2 at 900 °C*

The calculation is based on the relationship of the crystalline area and the total area of the X-ray diffractograms. Presented that PLA with a crystallinity index of 26.00 % increased considerably with the addition of certain additives, such as 10% BCALDA (49.25 %) and 10% BCFS (48.26 %), indicating greater molecular organization induced by the presence of these components. However, not all additives had this effect: the 10% BCBWA material showed a crystallinity of 25.62 %, even lower than that of pure PLA, suggesting possible interference in the crystallization process, possibly due to the chemical nature or morphology of the biofiller used. On the other hand, when the BCBWA concentration was increased to 40 % and 70%, an increase in the absolute crystalline area was observed, although the crystallinity index remained relatively constant (~37.7 %), indicating that, although more crystalline regions were formed, the ratio between crystalline and amorphous phases did not vary significantly. These results are interesting, as the crystallinity of PLA directly influences properties such as stiffness, thermal resistance, and biodegradation rate, which are critical aspects in the design of functional biopolymers.

In general, the crystal structure is affected by many factors, and clear trends are not always apparent. In the case of biochar, activation only caused a slight decrease in peak intensity for BCALD, while for BCBW it caused a slight broadening of the peaks. Overall, it did not cause a drastic change in crystallinity.

On the other hand, in biocomposites, BCFS biochar, which presented more amorphousness in their structure, contributed more to the increase in PLA peaks, perhaps due to the chemistry on the surface. Those whose crystallinity was evident, such as BCALD, did not always favor this increase; perhaps a high mineral content can cause the opposite effect.

3.2.6 Assessment of rheological behavior (DMA)

Figure 37 shows the dynamic mechanical analysis (DMA) curves of 7 samples: pure PLA (100% PLA), three mixtures with 10% of different biochar (BCBW, BCFS, BCALD) and three other mixtures with 10% of activated biochar (BCBWA, BCFSA, BCALDA).The curves show

how the storage module and the loss module change with temperature. With this analysis, it is possible to see how the material behaves with heat and force. It is also possible to calculate its glass transition temperature (Tg), among other important factors [239]. The pure PLA sample (gray line) shows that when the temperature increases, E' falls, especially near 65 °C, indicating the change in the vitreous state of the polymer. This sudden drop comes with a marked peak in the loss modulus E (around 170 MPa), which shows a greater loss of mechanical energy and confirms the T_g that exists. This behavior is typical of an amorphous PLA, whose T_g is normally between 55 and 65 °C [240], [241].

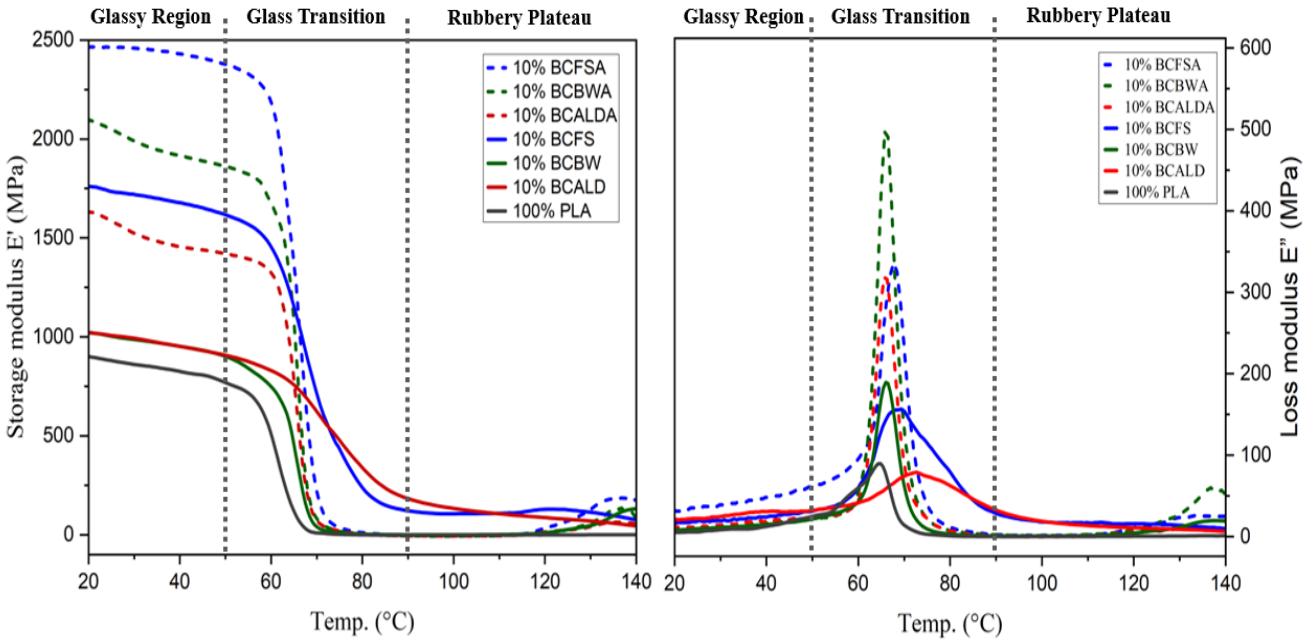

Figure 37: Curves of DMA for PLA pure and PLA-biochar composites: 10% BCBW, 10% BCFS 10% BCALD and 10% BCBWA, 10% BCFSA 10% BCALDA. Double cantilever method with a ramp between 20 °C and 145 ◦C at 5◦C-min-1 at a frequency of 1 Hz, with a dynamic amplitude of up to 30 µm and a force range between 4 ± 4 N.

3.2.6.1 Effect of the biochar type on viscoelastic properties

The effect of biochar type on viscoelastic properties is visible in Figure 37, when mixing PLA with 10 wt.% BCALD (red line), changes the way PLA behaves mechanically. The E' curve gradually decreases with temperature, which means that it gradually loses stiffness. The peak of E" is lower and wider compared to the other mixtures (10% BCBW and 10% BCFS), indicating a more dispersed Tg and perhaps a more heterogeneous system. This can happen because biochar is not evenly distributed or because it does not bind well to the polymer matrix [125]. The fact that there are pores within the sample could also play a role.

However, for 10% BCBW biocomposite (green line) although at first the E' value increases slightly compared to pure PLA, the stiffness is lost more gently. The peak of E" is slightly higher in temperature (around 68 °C), which could indicate there's more energy dissipation. This may be because biochar restricts the movement of the chains somewhat. This could say that adding inactivated BCBW doesn't improve stiffness much, but it does increase damping

capacity. In addition, E' recovers a little above 110 °C, perhaps because heat causes it to recrystallize [242].

On the other hand, incorporating 10 wt.% BCFS (blue line) increases the stiffness quite a bit, with a higher initial E' (around 1700 MPa). This may be that the reinforcement is better distributed or that it gets along better with the matrix. The estimated Tg is also around 69 °C, with a sharper, narrower peak of E', which could suggest that the structure is more rigid, but can still release energy well in that transition.

In general, the comparison of PLA with 10 wt.% biochar blends, shows that the addition of biochar usually improves the material's stiffness at room temperature (higher E'), which is consistent with other studies on PLA and biochar compounds [243] But, the type and origin of the biochar has a big influence on how the system behaves with heat and mechanically, especially on Tg, how it releases energy, and how stable it is at high temperatures. According to this data, the mixture with 10% BCFS is the one that best increases the storage module without affecting the Tg, which makes it interesting for things that need more mechanical strength without losing flexibility.

3.2.6.2 Effect of activated biochar to the properties of PLA viscoelastic properties

Figure 37 also presented the effect of the addition of activated biochar. The storage module and the loss module of 10% BCBWA biocomposite (green line) double compared to 10% BCBW (green dotted line) one. The peak of Tg is clearer, but it is still around 66 °C. This means that activation did not change much the temperature at which the biocomposite goes into the glassy state. This makes sense because activating biochar improves the ratio of PLA to backfill, causing PLA to move less and increase both stiffness and dissipation.

On the other hand, BCFSA makes PLA more rigid, with a higher initial E' (close to 2500 MPa). Perhaps this is because the reinforcement material is better distributed or because it interacts better with the PLA. It also has a loss modulus of about 350 MPa. The T_g is also calculated at 68°C, with a sharper and narrower peak of E", suggesting that the structure is harder, but can still release energy well in that transition. As in 10% BCBWA, in the activated case of flax shives biochar-PLA biocomposites, the ambient temperature values of the modulus of loss are twice those of biocomposites. The E" peak is more pointed and intense than in 10% BCFS, indicating a very marked glass transition with high energy dissipation. But such a high E" could also indicate more friction within the material, which may have to do with areas that are not equal.

Finally, we also saw this increase in E' and E" in the 10% BCALDA compounds. But E′ has lower values than 10% BCBWA and 10% BCFSA, more similar to the original PLA, although somewhat better. The peak of E″ is at Tg, above 66 °C, but it is not as intense as in the other two compounds. This indicates that the improvement in the bond between PLA and biochar is not very good, probably because they do not get along very well. There are studies that say that chemistry and how biochar is activated influence how it binds with polymers.

In short, PLA becomes stiffer and its thermal response changes when activated biochar is added. This agrees with previous studies reporting that biochar can reinforce biopolymers, improving

their mechanical properties and thermal stability. Among the fillers, BCBWA achieves a good balance between stiffness and energy dissipation, showing strong reinforcement together with a pronounced Tg. BCFSA provides the highest reinforcement, increasing stiffness significantly, although its energy dissipation is lower than that of BCBWA. BCALDA also improves the properties of PLA, but to a lesser extent compared to BCBWA and BCFSA.

3.2.6.3 Effect of beech wood biochar loading in PLA-biochar composites viscoelastic properties

Figure 38 shows the dynamic mechanical analysis (DMA) curves of 3 samples: pure PLA (100 % PLA), two mixtures of PLA with 10 wt.% biochar (10% BCBWA), and 40 wt.% biochar (40% BCBWA). The curves show how the storage module and the loss module change with temperature. With this analysis, the glass transition temperature is estimated.

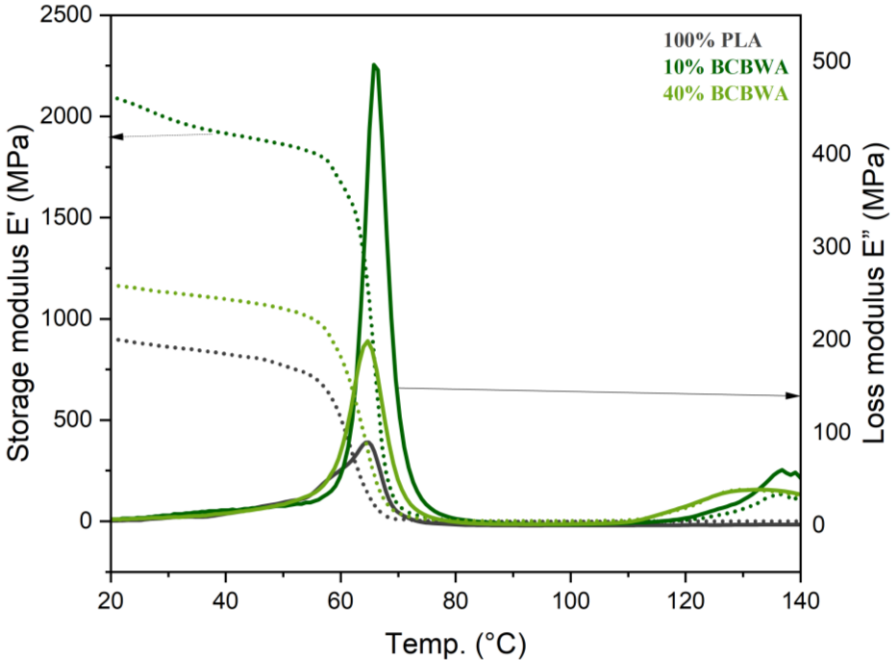

Figure 38: Effect of charging on DMA curves of beech wood activated biochar PLA biocomposites. Double cantilever method with a ramp between 20 °C and 145 ◦C at 5◦C-min-1 at a frequency of 1 Hz, with a dynamic amplitude of up to 30 µm and a force range between 4 ± 4 N.

The storage module (E′) of pure PLA starts at around 900 MPa at room temperature. As the temperature rises, it gradually drops until it drops suddenly to around 60-70 °C. This matches the typical glass transition temperature (T_g) of PLA. The modulus of loss (E″) is at its highest point around 65 °C, which confirms the T_g. This is normal in a semi-crystalline polymer such as PLA, where the stiffness decreases greatly when Tg is exceeded.

For 10% BCBWA biocomposite, the storage module (E′) goes up quite a bit compared to PLA. At room temperature, E′ is almost twice as high (~2 000 MPa). The peak of E″ becomes larger and centered near 66 °C, with more area below the curve, indicating that the activated biochar better strengthens the matrix. Activating biochar surely improves the way it binds with PLA, making the compound stiffer and better able to withstand heat.

Finally, for 40% BCBWA biocomposite, although E′ is higher than in pure PLA, it does not reach the levels of 10% BCBWA. Here, the peak of E″ stays close to the T_g of the PLA, but the curve gets weird at higher temperatures (above 100 °C). This indicates that the particles are coming together and that the matrix may not be entirely homogeneous. This shows that if there is a lot of biochar, the interactions are not as good and can act as faults that reduce the transfer of forces.

In summary, PLA has a T_g close to 65 °C, which is consistent with what has been seen in other studies. If you add 10 wt.% activated biochar (BCBWA), the storage module improves a lot. This means that activated biochar strengthens the material because it binds better, so activation is key for the matrix and reinforcement to come together well. However, if a lot of biochar (40% BCBWA) is used, irregular areas and possible failures are created, which makes the reinforcement not as good and affects thermal stability.

3.2.7 Assessment of dielectric behavior (BDS)

Figure 39 shows the variation in electrical conductivity (in $S \cdot cm^{-1}$) of PLA biocomposites with 10 % by weight of different biochar: BCALD, BCFSA, and BCBW, compared to pure PLA, in a frequency range of 100 Hz to 1 MHz.

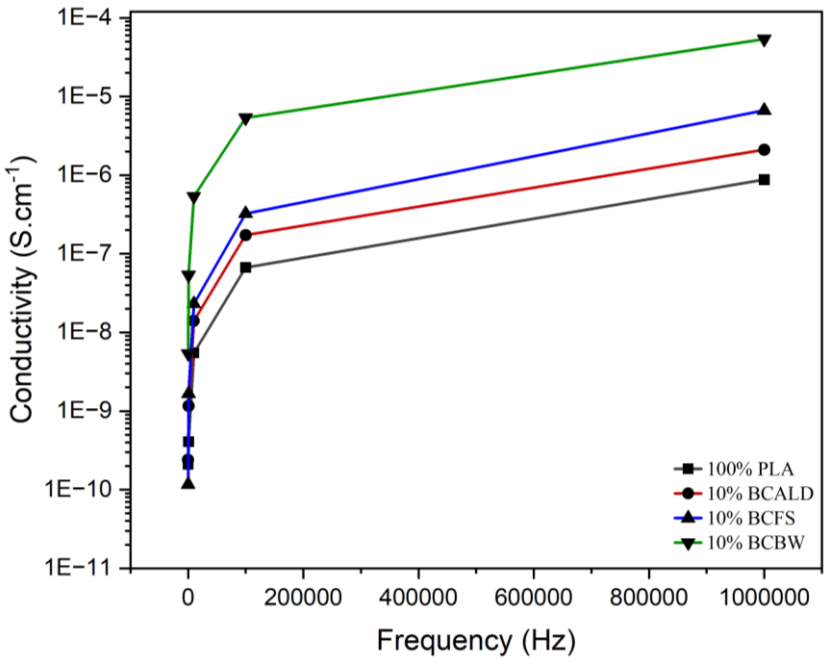

Figure 39: Effect of frequency on the conductivity of PLA and respective biocomposites loading 10% of different biochar.

Pure PLA is found to exhibit extremely low electrical conductivity, in the order of 6.68 $x10^{-11}$ to 1.20x 10^{-6} $S \cdot cm^{-1}$, which is consistent with its insulating nature. The incorporation of biochar generates a notable increase in conductivity, especially at frequencies above 10^4 Hz. Among the different biocomposites, 10% BCBW shows the highest conductivity, reaching values close to 10^{-4} $S \cdot cm^{-1}$ at 1 MHz. This suggests greater effectiveness in forming continuous conductive paths, possibly due to the presence of mineral residues or more continuous carbonaceous

structures that facilitate electronic transport. It is followed by 10% BCFSA and 10% BCALD, with conductivities in the order of 10^{-5} and 10^{-6} S·cm^{-1} respectively, indicating that the treatment or origin of the biochar has a considerable influence on its electrical performance.

These results suggest that, even at low concentrations (10 wt.%), the type of biochar has a significant impact on the electrical property of biocomposites, which could be exploited in applications such as antistatic materials, sensors or electromagnetic interference (EMI) barriers.

3.2.7.1 Effect of beech wood biochar loading on the conductivity of PLA-biochar biocomposite

Table 12 shows the electrical conductivity (S·cm^{-1}) values obtained for PLA biocomposites with different biochar contents (0, 10, 40 and 70 wt.%) in a frequency range from 100 Hz to 1 MHz. A clear trend of significant increase in conductivity is observed with the increase in the amount of biochar incorporated.

Table 12: Effect of biochar loading on electrical conductivity (S·cm^{-1}), measured at different frequencies (Hz) of the PLA and BCBWA biocomposite.

Frequency (HZ)		**10^2**	**10^3**	**10^4**	**10^5**	**10^6**
Conductivity (S·cm^{-1})	**100% PLA**	6.68x10^{-11}	4.15x10^{-10}	5.80x10^{-09}	7.76x10^{-08}	1.20x10^{-06}
	10% BCBWA	7.94x10^{-11}	3.68 x10^{-10}	5.07x10^{-09}	6.48x10^{-08}	8.83x10^{-07}
	40% BCBWA	5.84x10^{-05}	6.33 x10^{-05}	6.32x10^{-05}	7.22x10-^{05}	9.46x10^{-05}
	70% BCBWA	1.02x10^{-02}	1.21 x10^{-02}	1.24x10^{-02}	1.24x10^{-02}	1.20x10^{-02}

As in the previous graph, we observe that pure PLA has highly insulating behavior. This low conductivity remains at 10 wt.% in the compounds, but slightly higher than that of pure PLA. However, by incorporating 40 wt.% BCBWA, there is a considerable jump in conductivity, reaching values in the order of 10^{-5} S·cm^{-1}, with a relatively stable response throughout the frequency range. Finally, with 70% BCBWA, a drastic increase is observed, with values of up to 10^{-2} S·cm^{-1}, which indicates a clear formation of continuous conductive networks within the polymer matrix.

In conclusion, the addition of biochar increased conductivity. Beech wood biochar has the best impact on conductivity. The higher the percentage of biochar, the greater the conductivity, reaching 2.21x10^{-2} S·cm^{-1} for composites containing 70 wt.% biochar. These results confirm that biochar not only acts as a structural load, but also as a functional component, improving the electrical response of the material, making it potentially useful for applications in sensors, antistatic coatings or EMI (electromagnetic interference) materials.

3.2.8 Assessment of mechanical behavior (tensile test)

Figure 40A and Figure 40B compare the effect of biochar type on Young's modulus and the tensile strength of mixtures with PLA. It is observed that the addition of biochar maintains, or

even slightly improves, the Young's modulus in most cases, indicating a strengthening of stiffness due to the dispersion of carbonaceous particles in the polymer matrix. However, the tensile strength decreases noticeably compared to pure PLA, especially in formulations with a high biochar content, reflecting a loss of ductility attributed to the brittle nature of the biochar and the lesser interfacial cohesion with the matrix. This behavior is consistent with what is reported in the literature, where biochar acts as a rigid phase that increases stiffness but sacrifices resistance to plastic deformation [88].

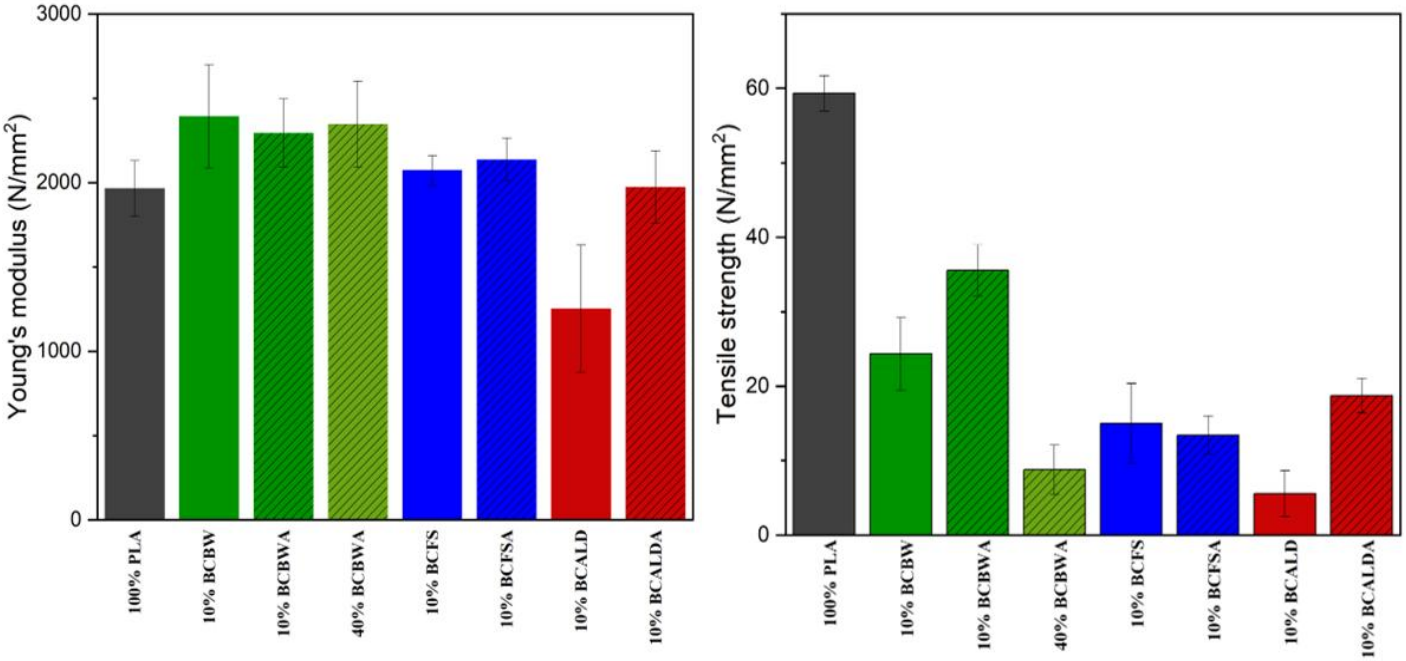

Figure 40: A) Young's modulus of PLA and composites. B) Tensile strength.

These graphs of the mechanical properties allow us to confirm several elements mentioned throughout these results. Biochar influences the mechanical properties of biocomposites. Compounds containing a high proportion of biochar discourage dispersion. When the biochar content reaches 70%, the material breaks even before the mechanical test is performed, which is why no results appear in the graph. In addition, it is confirmed that composites based on terrestrial biochar have better mechanical properties than those based on algae biochar.

3.2.9 Preliminary conclusions on biochar-PLA biocomposites.

The data suggest that the addition of biochar changes the properties of PLA in multiple directions:

- At low contents (10 wt.%), stiffness (E′, Young's modulus) would either increase or stay the same, while tensile strength would, due to embrittlement and poor interfacial cohesion, continue to decrease.
- Biochar activation enhances dispersion and interfacial bonding (SEM) and enhances stiffness and dissipation (DMA), but at some very high loads (≥ 40 – 70 wt.%), heterogeneities and structure failure occurs.
- In TGA/DSC, biochar behaves as a nucleating agent (especially BCFS), advancing Tcc and changing Tm (double melting in medium/high loads).

- Electrical conductivity increased with contents and was greater in wood biochar (BCBW) than others.
- FTIR implied that there were no covalent reactions, but physical interactions (H-bonding/dipoles) were instead implied

3.3 Conclusion on Chapter 3:

Chapter 3 shows that the activated beech wood biochar (BCBWA) delivers the most balanced performance for PLA-biochar biocomposites. After CO_2 activation its BET surface area rose by ~53 % and the carbon content remained high (> 80 %), producing a dense, porous filler that, when mixed at 10–40 wt.%, increased the storage modulus by up to 2 × that of neat PLA and generated an electrical conductivity of $\approx 10^{-4}$ S cm^{-1} at 40 wt.% and $\approx 10^{-2}$ S cm^{-1} at 70 wt.%. The same activation markedly improved interfacial adhesion, as SEM revealed finer, more uniformly dispersed particles and fewer voids compared with untreated biochar, while FTIR showed a reduction of PLA characteristic bands and the appearance of oxygenated groups, indicating mainly physical (hydrogen bond/dipole) interactions.

Flax shives-activated biochar (BCFSA) produced the strongest nucleating effect, increasing PLA crystallinity from 26% to ~48% and shifting cold crystallization to lower temperatures (Fig. 33 34), which improved thermal stability. Algae-derived activated biochar (BCALDA) achieved the largest increase in BET (≈774%) compared to its non-activated version, but due to its lower porosity, lower carbon content, and mineral residues, it contributed less to mechanical reinforcement.

Overall, both the selection of biomass, the processes of production and activation of biochar, and the processes of production of biocomposites controls filler morphology, surface chemistry and particle dispersion, which in turn dictate composite stiffness, crystallinity, electrical pathways and tensile strength. Consequently, activated beechwood biochar is the most suitable filler for multifunctional, high performance biobased materials, while activated flax shive biochar is preferred when maximal crystallinity and thermal stability are required.

At the end, we could highlight the following correlations:

- **Activation increases the surface area, which in turn improves dispersion, resulting in a higher DMA storage modulus (E′) and Young's modulus**: the activated samples (BCALDA, BCBWA, BCFSA) show more porous surfaces (SEM), which directly translates into the higher E′ values observed in DMA for the activated composites (especially BCBWA).
- **Carbon content and crystallinity of filler increase electrical conductivity**: wood biochar (high C, moderate crystallinity) delivers the highest conductivity at low loadings (10 % BCBW).
- **Filler content (≥ 40% by weight) increases the percolation threshold, which causes an increase in conductivity and, in turn, greater mechanical fragility:** conductivity jumps from 10^{-5} S cm^{-1} (40 % BCBWA) to 10^{-2} S cm^{-1} (70 % BCBWA), coinciding with the observed loss of tensile strength and the appearance of cracks in SEM at high loadings.

- **Nucleating effect (high crystallinity filler) causes a change in the T_{cc} of the DSC, which in turn alters the thermal transitions**: activated flax shives biochar (BCFSA) raises PLA crystallinity to ≈ 48 %, causing the cold crystallization temperature to fall from 126.7 °C to ≈ 115 °C (DSC), which also leads to a more pronounced double melting behavior (indicative of heterogeneous crystals).

CHAPTER 4

Techno-economic evaluation of biochar transformations

4 Techno-economic evaluation of biochar transformations

Introduction

As announced in chapter 1 of this thesis, the transition to eco-friendly materials, renewable energy systems, has sparked interest in biochar, a porous, versatile, and carbon-laden material produced by thermochemical processing of biomass.

To assess the reliability and viability of biochar transformations, this chapter presents a theoretical technical-economic assessment of biochar production by pyrolysis of beech wood waste and the subsequent manufacture of PLA-biochar biocomposites. Several scenarios (S1, S2, S3, S4) are presented in which the biocomposite is marketed as a pellet and as clips for cultivation, used in agriculture. The analysis presents results of the simulation of the process in ASPEN Plus, mass and energy balances, capital expenditure (CAPEX), operational expenditure (OPEX) and financial indicators such as net present value (NPV), internal rate of return (IRR), payback period, and return on investment (ROI). This study aims to evaluate the profitability of a biochar and biocomposite production plant at an industrial level. Figure 42 presents a summary of the topics covered in the chapter, shows the production process for biochar and PLA-biochar biocomposites, the scope of the ASPEN plus simulation, the four scenarios production studied under the two sales hypotheses (100 % and 80 %), and the economic indicators evaluated.

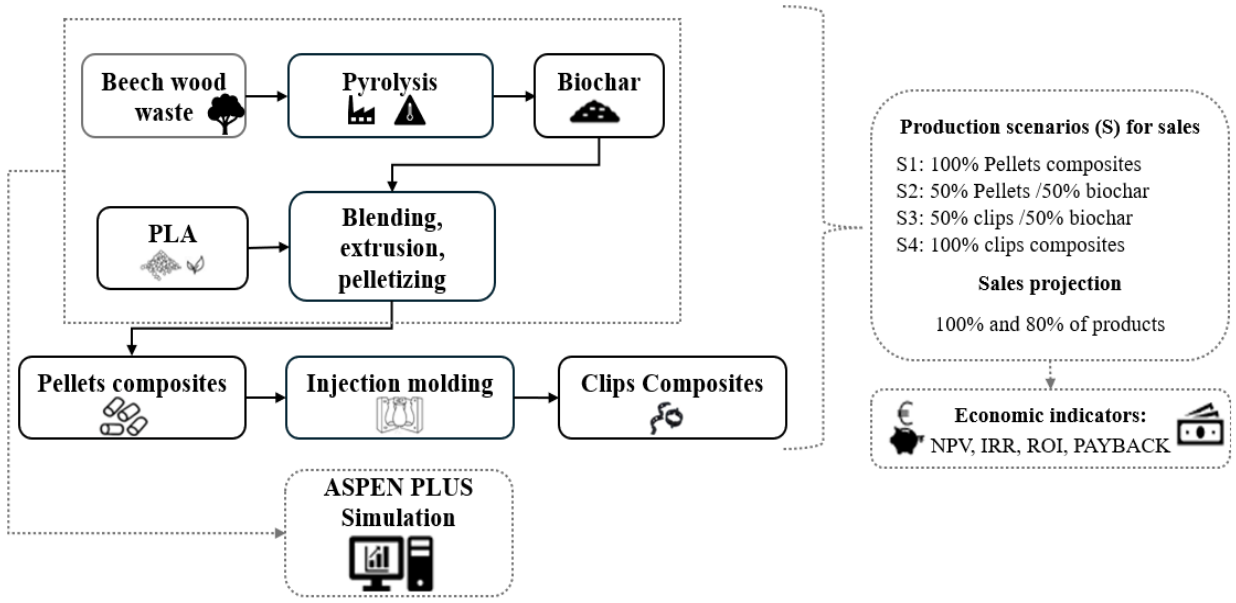

Figure 41: Graphic summary of chapter 4.

The economic viability of biochar depends mainly on the type of biomass, the technological scale, local logistics, and the valorization of co-products, e.g. the integration of energy recovery and co-product used significantly improves profitability by diversifying revenue streams [244]. To enable standardized comparison, all monetary data presented in this section have been converted to euros (€). Annex .

Table 13 shows the cost of biochar production at different technological scales.

Table 13: Cost of biochar production at different scales.

Category	Feedstock / Technology	Cost / Price Value	Ref.
Traditional Small-Scale	Agricultural residues / Earth-block kilns	€ 0.03 to 0.07 kg^{-1} ($ 0.03–0.08 kg^{-1})	[245]
Small-Scale / Batch	Agricultural waste	€ 0.03 kg^{-1} to € 1.87 kg^{-1} ($ 0.03-2.06 kg^{-1})	[246]
Mobile Systems	Agricultural waste / Prototype mobile kilns	€ 0.79 kg^{-1} and € 1.87 kg^{-1} ($ 0.87–2.06 kg^{-1})	[246]
Industrial Scale	General production	€ 0.04 kg^{-1} to € 0.13 kg^{-1} ($ 50-150 ton^{-1})	[247]

Feedstock cost is an important factor, usually representing between 15 % and 30 % of total production cost [248], although it can reach up to 60 % when acquisition and processing are included [249]. Consequently, local waste availability and public policy support (such as carbon removal subsidies) are decisive for system profitability [250]. For example, a industrial-scale projet in Spain, achieves an internal rate of return of 22.35 % due to CO_2 removal revenues [251], also in Poland, biochar applied to agriculture is viable when supported by subsidies of of approximately € 21.88 ($ 30) per ton of CO_2 sequestered [252], and fixed facilities in the United States (e.g., Michigan) are profitable due to abundant biomass [253].

A significant challenge for this research is the scarcity of specific techno-economic data regarding biochar production and biochar-PLA biocomposites within the French context. To address this limitation, this study utilizes references from European Union members (such as Spain and Poland) and outside EU (such as United States).

PLA is one of the most commercially important biodegradable polymers, however, it has limitations in hardness, thermal resistance, and cost [110]. The integration of biochar as a reinforcement opens a path to improve yield, reduce cost and, in turn, increase sustainability. Current studies offer fragmented analyses, some on biochar production [254], [255], [256], and on PLA production [257]. But few carry out the economic study to manufacture biochar and biocomposites, integrating a complete simulation of Aspen Plus. This work aims to bridge this gap, providing a techno-economical study for a market expected to reach €410.84 million by 2030 [258].

4.1 Production Cost Analysis (raw materials, processing processes, and necessary equipment)

The cost analysis was carried out by evaluating two integrated blocks:

(i) the production of biochar from beech wood waste, slow pyrolyzed at 600 °C.

(ii) And the manufacture of PLA-biochar biocomposites in granular form, which contains an average of 10 wt.% of biochar as filler and 90 wt.% of PLA as matrix. An estimated bulk density of 1.28 $g \cdot cm^{-3}$ and a processing temperature of 180 – 200 °C. The process is aimed at the production of technical pellets for applications in the sustainable sectors. The scenario in which these pellets are processed and sold as clips for crops is also evaluated. Table 12 shows a summary of the assumptions on which the calculations in this technical economic analysis were based.

Table 14: Key techno-economic assumptions and operational parameters for the biochar-PLA biocomposite plant in Rouen.

Basic Assumptions of Operation	
Location	Rouen, Normandie
Feedstock (Beech wood waste)	330 $ton \cdot year^{-1}$
Biochar Yield	26 wt.%
PLA-biochar biocomposites	536 $ton \cdot year^{-1}$
Days of operation	330 days
Weight of biocomposites clips	2 g
Bank loan financing (5 years**)**	€ 5,500,000.00
Interest annual	5 %
Tax	25% [259]
Plant's lifespan	10 years

The limits of the system include: the acquisition of biomass, the crushing and drying of the biomass, transport, and pyrolysis. Also, the acquisition of biopolymers and the manufacturing process of biocomposites is important. Figure 42 shows the simplified flow of the process.

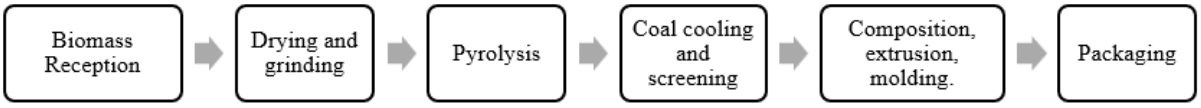

Figure 42: Simplified process flow.

In this study, the calculations are made considering several scenarios:

- S1) All biochar produced is processed into biocomposite that will later be sold in the form of pellets, with a loss during the process of 3 %.
- S2) 50 % of the biochar produced will be marketed and the other 50 % will be processed into biocomposites to be sold in pellet forms with a loss of 3% during the process.
- S3) 50 % of the biochar produced will be marketed and the other 50 % will be processed into biocomposites to be sold in the form of crop clips with a 5 % loss during processing.

- S4) All biochar produced is processed into biocomposite that will be sold in the form of agriculture clips, with a loss during processing of 5 %.

4.2 ASPEN Plus Simulation Methodology

This section provides a comprehensive and technically rigorous description of the Aspen Plus model developed to simulate the integrated thermochemical conversion of biomass as seen in Figure 43, combined with the co-processing of PLA. The model represents the full processing chain, including biomass preparation, drying, pyrolysis, partial combustion, char separation, and the final PLA-char blending step. This section explains the structure of the flowsheet, the underlying assumptions, and the role of each unit of operation in the process.

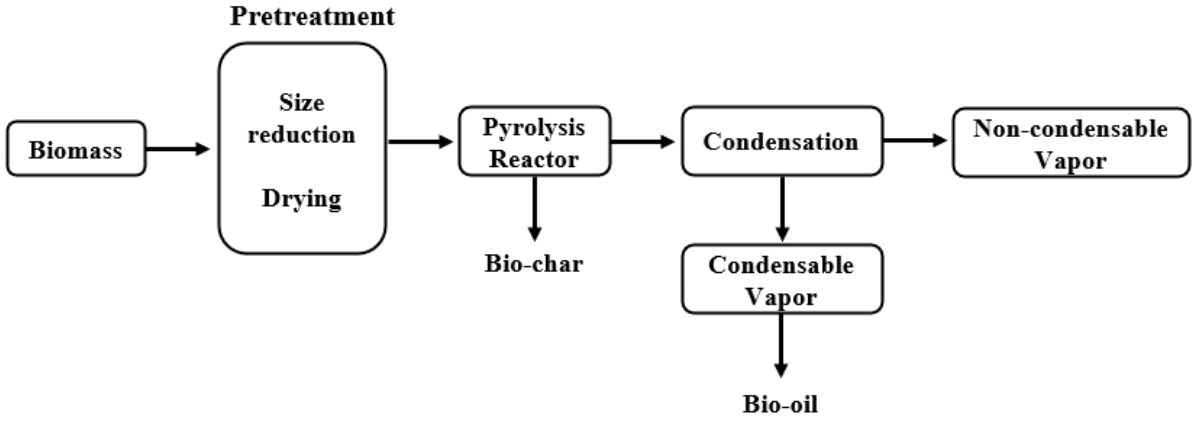

Figure 43: Simplified process flow diagram of biomass pyrolysis and product recovery.

4.2.1 Biomass Description

The used biomass data into the Aspen Plus model is defined as a non-conventional component (NCPSD) to accurately capture its physicochemical characteristics and particle size distribution. Its ultimate analysis specifies a composition dominated by carbon (46.7 %), hydrogen (5.57 %), and oxygen (47.72 %), with negligible nitrogen and sulfur contents. These elemental values enable reliable estimation of the heating value and predict the decomposition pathways occurring during drying and pyrolysis.

The biomass is represented as a homogeneous WOOD-type material with a mass fraction equal to unity. A particle size distribution (PSD) is integrated into the model, a critical element for representing heat and mass transfer, drying kinetics, and char formation. The PSD follows the Rosin-Rammler-Sperling-Bennett (RRSB) function with a characteristic diameter D_{63} = 0.03 m and a dispersion coefficient of 1, providing a realistic distribution across particle size classes. Illustration of biomass configuration in Figure 44.

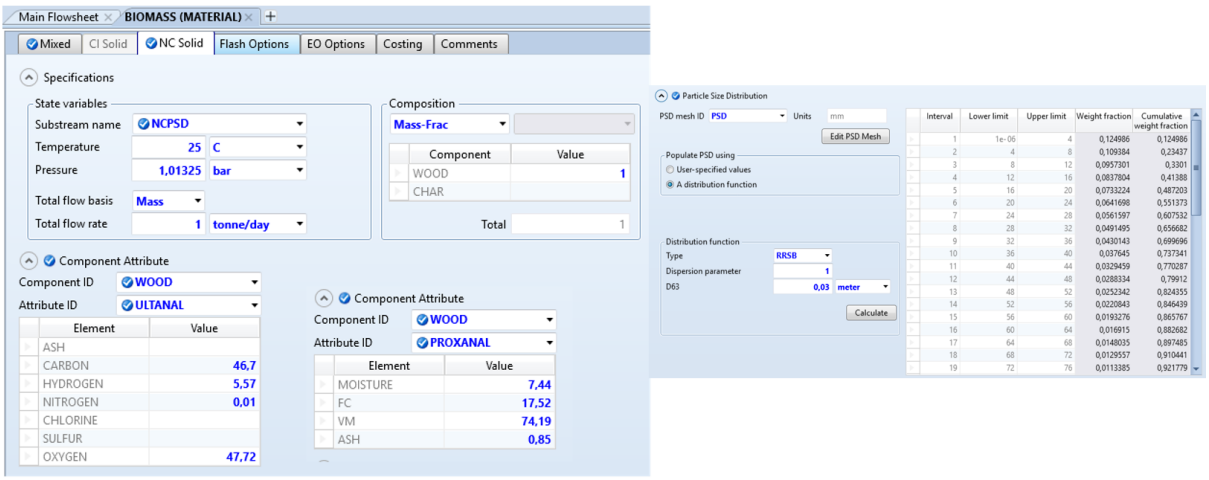

Figure 44: Biomass composition and PSD definition (ULTANAL, PROXANAL, NCPSD).

4.2.2 Biomass Preparation - CRUSHER

The CRUSHER unit models the initial particle size reduction of raw biomass. This mechanical operation ensures homogenization of particle size distribution, which improves drying efficiency and enhances reactivity during pyrolysis. Although no chemical changes occur, the physical transformation significantly influences heat transfer rates and fluidization behavior in downstream units. The crushed biomass stream (C-BIOM) exits the unit with identical mass flow but modified granulometry. Illustration of crusher configuration in Figure 45.

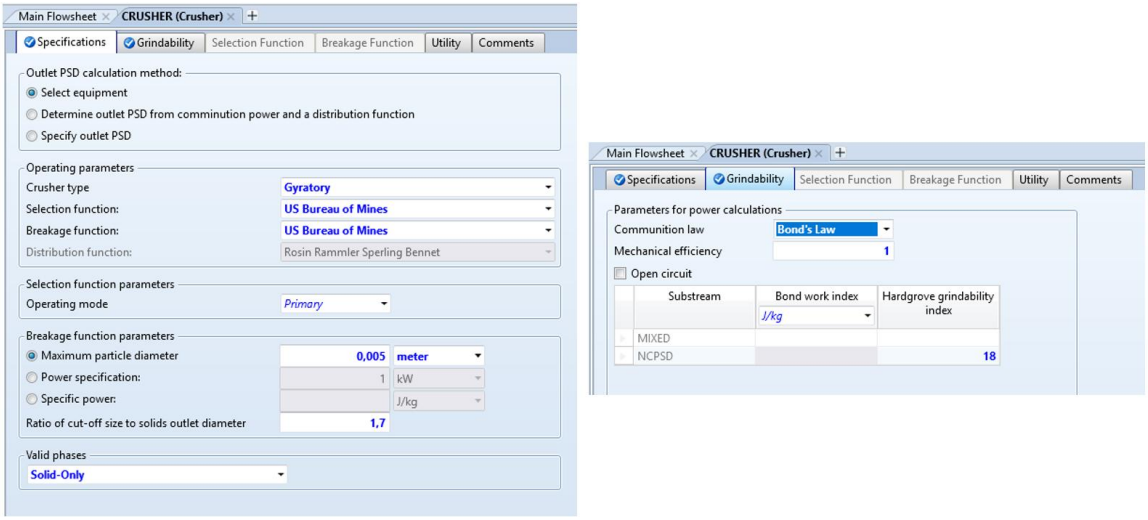

Figure 45: Aspen Plus configuration of the CRUSHER unit for biomass size reduction.

4.2.3 Biomass Drying - DRYER

The DRYER block, implemented with a **DRYER** model, simulates moisture evaporation from the biomass according to its proximate analysis. Heated air drives moisture removal while maintaining the chemical integrity of the solid fraction. The thermal duty assigned to the unit quantifies the energy required to vaporize internal moisture. This step ensures that the biomass entering the pyrolysis reactor has an appropriate residual water content, reducing energy demand, and minimizing tar production. Illustration of dryer configuration in Figure 46.

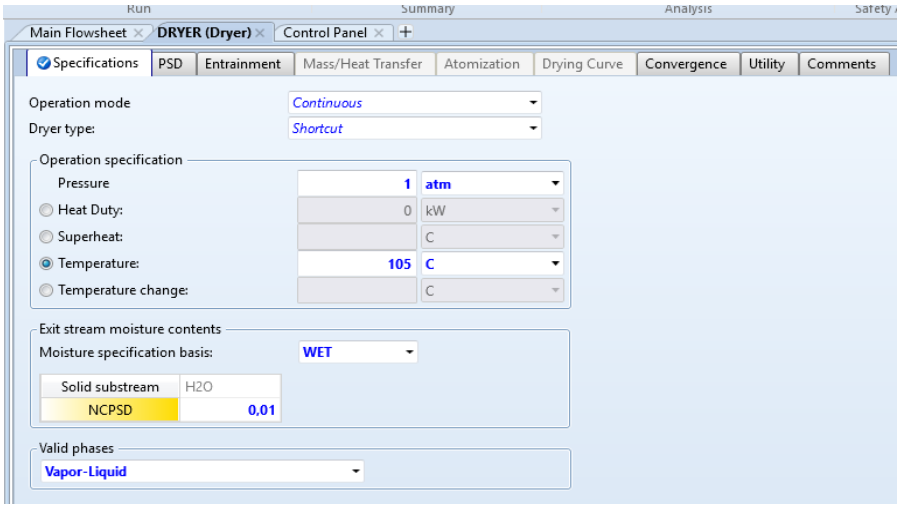

Figure 46: Aspen Plus representation of the DRYER (RYIELD) unit and moisture evaporation process.

4.2.4 Pyrolysis Reactor - PYRO-REA

The PYRO-REA reactor models the thermochemical decomposition of dried biomass into gases, condensable vapors, and char. The reaction is represented using an RYIELD block, where the conversion fractions toward each phase are imposed based on proximate analysis and literature correlations. The reactor operates at elevated temperatures, typically between 500 and 600 °C, and requires significant thermal input to maintain these conditions. The products form a multiphase mixture that is subsequently separated into the cyclone.

Table 15 summarizes the main chemical families, the representative components of each family present in wood pyrolysis products, and the identification number of each of these components. Figure 47 shows the configuration of the pyrolysis reactor described above, as well as the mass distribution of each of the elements involved in the process.

Table 15: Chemical Families and Representative Compounds Identified in Pyrolysis-Derived Products.

Chemical family	Representative / major molecule	CAS Number
Acids	Acetic acid	64-19-7
Alkanes	Dodecane	112-40-3
Alkenes	1-Hexene	592-41-6
Alcohols	Methanol	67-56-1
Aldehydes	Furfural	98-01-1
Amides	Acetamide	60-35-5
Ketones	Hydroxyacetone (1-hydroxy-2-propanone)	116-09-6
Esters	Methyl acetate	79-20-9

Chemical family	Representative / major molecule	CAS Number
Furans	Methylfurfural	620-02-0
Guaiacols	Guaiacol (2-methoxyphenol)	90-05-1
Phenols	Phenol	108-95-2
Sugars (anhydrosugars)	Levoglucosan	498-07-7

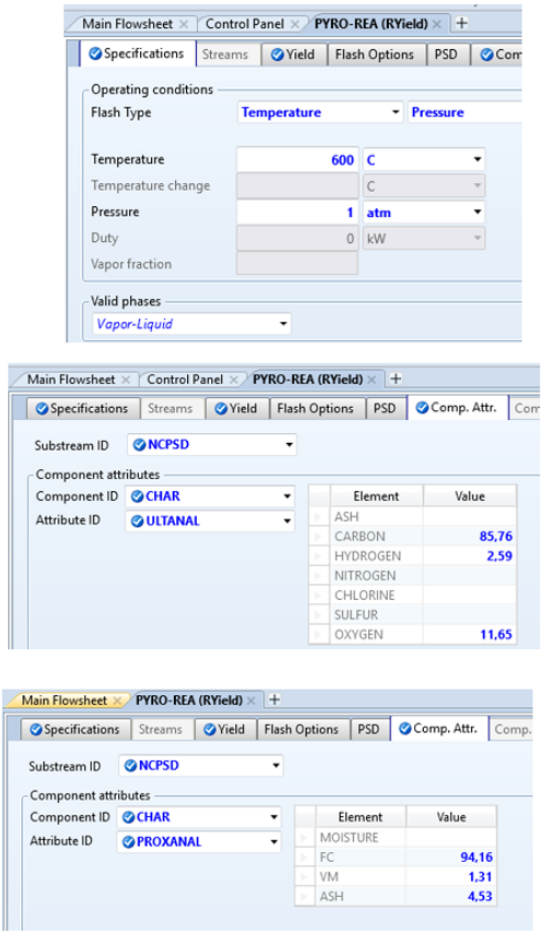

Component	Basis	Basis Yield
H2	Mass	0.0002674
CO	Mass	0.1611
CH4	Mass	0.0892
C2H6	Mass	0.012
CO2	Mass	0.06227
N2	Mass	0
O2	Mass	0
H2O	Mass	0.08
C	Mass	0
PLA	Mass	0
WOOD	Mass	0
CHAR	Mass	0.26
ACE-ACID	Mass	0.119193
DODECANE	Mass	0.001206
HEXENE	Mass	0.0007705
METHANOL	Mass	0.0243545
FURFURAL	Mass	0.0135675
ACETAMID	Mass	0.0072025
HYXACETO	Mass	0.0523605
MTYACETA	Mass	0.0333995
MTYFURAL	Mass	0.005628
GUAIACOL	Mass	0
PHENOL	Mass	0.0218085
LEVOGLUG	Mass	0.055476

Figure 47: Aspen Plus configuration of the PYRO-REA reactor used for biomass pyrolysis.

4.2.5 Cyclone - CYCLON

The cyclone performs mechanical separation of solids (char) from the pyrolysis gas stream. Using centrifugal force, it removes entrained particles to prevent their accumulation in downstream equipment. No chemical reactions occur in this unit; its function is purely physical, ensuring the quality of the gas entering the combustion unit and the recovery of sufficiently pure char for further valorization.

4.2.6 Combustor - COMBUST

The combustor simulates the complete or partial oxidation of pyrolysis gases in the presence of air or oxygen. The model uses an RSTOIC or RGIBBS block to calculate equilibrium products such as CO_2, H_2O, and CO depending on the oxidation level. This step generates significant thermal energy, which is redistributed to heat the pyrolysis reactor or dryer through an internal energy loop. The resulting flue gases may also be pre-cooled or directly reused depending on process requirements. Illustration of combustor configuration in Figure 48.

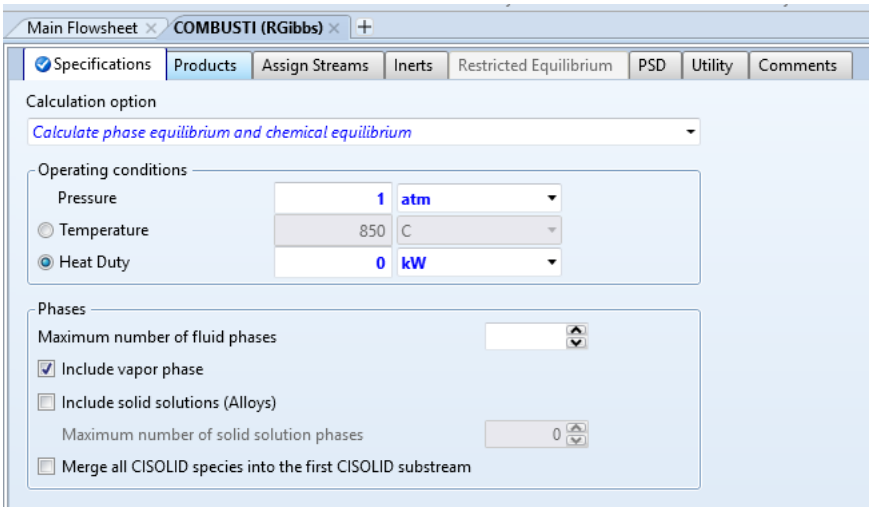

Figure 48: Combustor (COMBUST) unit showing oxidation reactions of pyrolysis gases.

4.2.7 Heat Exchanger - COOL-FG

The COOL-FG heat exchanger cools the hot flue gases emerging from the combustor to reach a temperature suitable for discharge or reuse. This cooling step recovers part of the thermal energy as useful heat for the process. No compositional changes occur within this unit; it performs strictly thermal conditioning of the gas stream.

4.2.8 Condenser–Separator for Condensable Vapors – SEP

The flowsheet, a SEP unit has been added downstream of the cyclone to perform a partial condensation of the vapors leaving the pyrolysis reactor. This unit operates as a condenser, enabling the separation of the liquid phase (bio-oil) from the non-condensable gas phase (syngas).

The condensable vapors are directed to the BIO-OIL outlet stream, while the non-condensable fraction forms a cleaner syngas stream, which is more suitable for combustion or additional valorization routes.

The integration of this separation unit provides several advantages:

- Recovery of a liquid fraction rich in organic compounds, suitable for further applications (chemical synthesis, extraction of platform molecules, fuel precursors, etc.).
- Reduction of condensable loads in the gas sent to the combustor, improving combustion stability and reducing fouling.

- Enhanced flexibility in adjusting the composition of the syngas supplied to downstream units.

This new separation step thus increases the valorization potential of the liquid products and improves overall process operability.

4.2.9 Syngas Stream Division – SPLITTER (SYN-GAS)

The flowsheet also includes a splitter used to divide the non-condensable gas fraction (syngas) into two separate streams:

1. A portion of the syngas is redirected to the combustion reactor (COMBUST). This internal recycling provides the heat required for: the pyrolysis reactor (PYRO-REA) via the internal heat loop and for the dryer (DRYER) to ensure moisture evaporation. This closed energy loop increases the overall energy efficiency of the process and reduces the need for external utilities.
2. The remaining fraction is sent to the process outlet (SYN-GAS2). This part of the syngas may be used for energy production, upgraded chemically, or analyzed for alternative valorization pathways.

By adjusting the split ratio, different operational scenarios can be evaluated in Aspen Plus, such as energy self-sufficiency of the process (higher fraction sent to COMBUST), maximization of syngas available for valorization, or combined optimization of pyrolysis and drying performance. This modification enhances the realism of the simulation by more accurately representing internal thermal interactions and energy recycling loops. In this simulation, the amount of energy required for our plant to be self-sufficient in the biochar production process is obtained by recycling the gases produced during pyrolysis.

4.2.10 Extruder: PLA and Char Mixing

The Extruder mixer combines the recovered char with PLA, defined as a pseudo-component. This unit simulates the preparation of a composite or catalytic material obtained by blending carbonaceous solid with molten polymer. The thermodynamic properties assigned to PLA (melting point, molecular weight limit, density) provide a simplified representation of its behavior in the process. No chemical reactions occur; the unit produces a homogeneous mixture of the two solids.

4.2.11 Energy Loops

The entire model is structured around energy loops connecting combustion, pyrolysis, and drying units. Heat generated from combustion is redistributed to satisfy the thermal requirements of the other steps, thereby reducing external energy input. Duty values indicate the heat demand of each unit, particularly for water evaporation in the dryer and temperature maintenance in the pyrolysis reactor. This integrated thermal structure models an optimized and energy-efficient process.

4.2.12 Overall Model Consistency

All units are interconnected to reproduce the complete thermochemical conversion chain of biomass and PLA. The model satisfies mass and energy balances and incorporates ultimate and proximate analyses for defining non-conventional solids. The chosen Aspen blocks (RYIELD, RSTOIC, separators, and heat exchangers) provide a flexible and reliable structure for analyzing the process, testing operating scenarios, and evaluating material and energy performance. Table 16 shows the different Aspen units we will use in this simulation and a brief description.

Table 16: Description of Aspen Plus Units and Their Roles in the Integrated Biomass Pyrolysis and Valorisation Process.

No.	Aspen Unit	Main Function	Block Type	Transformation Type
1	CRUSHER	Biomass size reduction	CRUSH/MILL	Physical (granulometry)
2	DRYER	Moisture removal	RYIELD	Fictitious reaction (water decomposition)
3	Air-Biomass Mixer	Flow homogenization	MIXER	Physical (mixing)
4	PYRO-REA	Biomass pyrolysis	RYIELD	Thermochemical decomposition
5	CYCLON	Solid-gas separation	SEP	Mechanical separation
6	COMBUST	Gas oxidation	RSTOIC / RGIBBS	Oxidation reactions
7	COOL-FG	Flue gas cooling	HEATX	Thermal exchange
8	B3 (Char + PLA)	Composite preparation	MIXER	Physical mixing
9	Heat Loops	Energy redistribution	Heat Streams	No composition change

Figure 49 shows a simplified schematic diagram of the complete flow diagram of the Aspen Plus simulation, providing information on the operating units and the mass and energy flows involved.

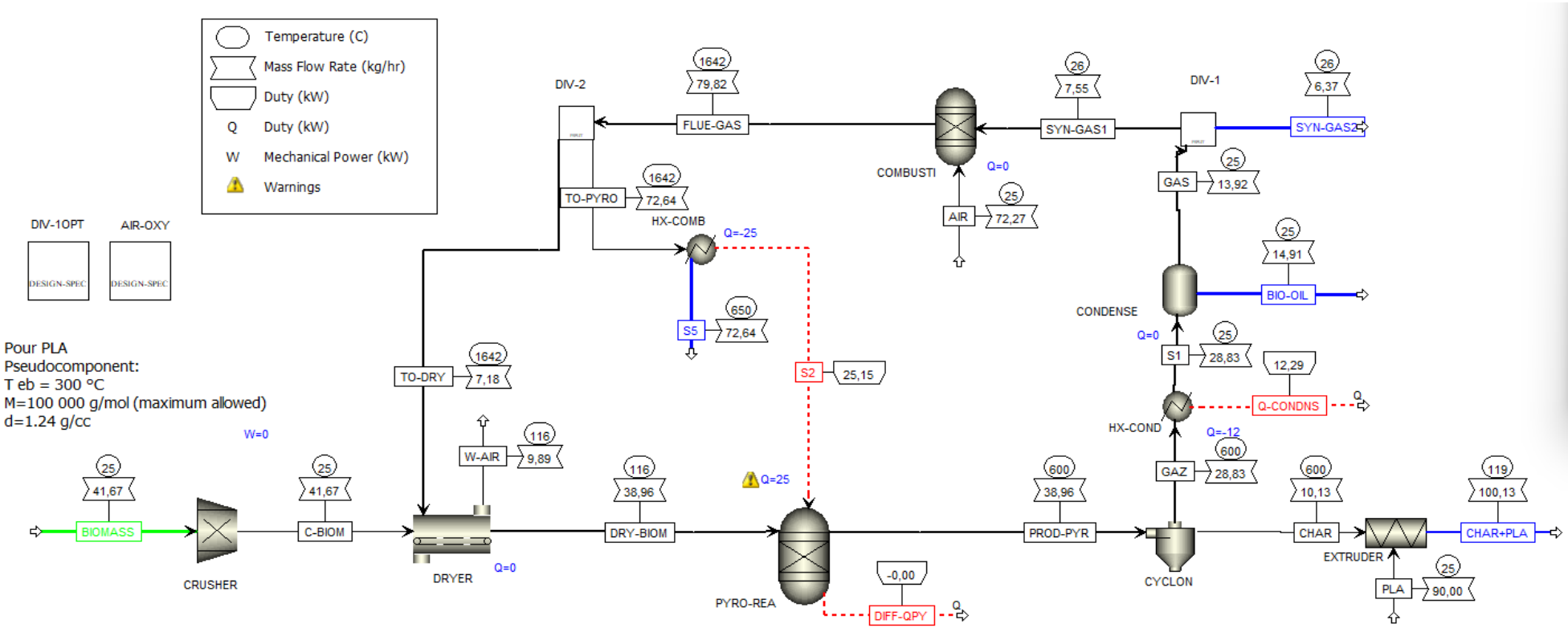

Figure 49: Summary schematic diagram of the complete Aspen Plus simulation flowsheet.

4.2.13 Modeling Assumptions

- Steady-state operation; no dynamic behavior considered.
- Perfect mixing at each unit inlet and outlet.
- No heat or pressure loss to the environment unless specified.
- Biomass modeled as a non-conventional solid using ultimate/proximate analyses and PSD.
- PLA modeled as a single pseudo-component with fixed properties.
- Thermodynamic properties are calculated with a single EOS/property method for all streams.
- Crusher performs only mechanical size reduction, no reactions.
- Dryer modeled with a fictitious decomposition of water; only moisture is removed.
- Pyrolysis simulated with fixed yield fractions (RYIELD); no detailed reaction kinetics.
- Pyrolyser assumed isothermal/isobaric with no intra-particle gradients.
- Char treated as inert; no secondary char reactions modeled.
- Cyclone assumed to achieve ideal gas–solid separation.
- Condenser/SEP performs ideal vapor–liquid separation at given T and P.
- No entrainment between liquid and gas phases in the separator.
- Syngas splitter divides flow based solely on a fixed split ratio.
- Combustor modeled with stoichiometric or equilibrium combustion; no pollutant formation modeled.
- Cooler modeled as a simple heat exchanger with no pressure drop.
- Extruder modeled as a physical mixer; no PLA degradation reactions are considered.
- Heat exchanged between units via ideal heat streams with no losses.
- Pressure drops across units and piping are neglected unless specified.
- All phases assumed in thermal equilibrium at unit outlets.
- Physical property data from Aspen databases assumed valid across all operating conditions.

4.3 Material and energy balance

4.3.1 Biochar Recovery and Integration into PLA-Based Composites

During the pyrolysis process, the solid fraction of the biomass is converted into a biochar and separated from the gas–vapor stream using a cyclone. Based on the process simulation, the mass flow rate of dry biomass fed to the pyrolysis reactor is 38.96 $kg \cdot h^{-1}$, while the biochar recovered at the cyclone outlet reaches 10.13 $kg \cdot h^{-1}$, corresponding to approximately 26 wt.% of the dry biomass. This biochar stream is fully recovered and directly valorized without disposal. It is sent to an extrusion unit where it is blended with 90.0 $kg \cdot h^{-1}$ of PLA, producing 100 $kg \cdot h^{-1}$ of a CHAR–PLA composite. The final composite contains around 10 wt.% biochar and 90 wt.% PLA, demonstrating a closed-loop valorization strategy for the solid by-product of pyrolysis through the production of high-added-value biobased materials. Figure 50 shows the mass flow of the process.

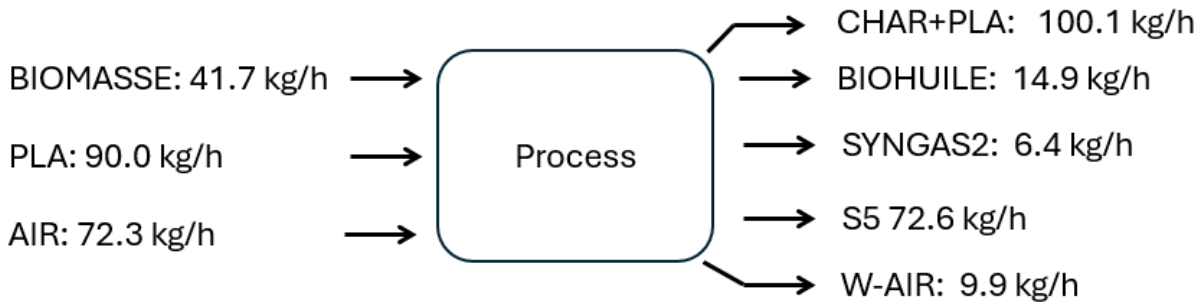

Figure 50: Mass flow balance of the process.

4.3.2 Pyrolysis Gas Management, Combustion, and Energy Integration

The non-condensable fraction leaving the pyrolysis reactor, after solid separation, corresponds to a total gas flow rate of 13.92 $kg \cdot h^{-1}$, representing approximately 35.7 wt.% of the dry biomass feed. This pyrolysis gas stream is subsequently divided into two distinct fractions. A first fraction of 7.55 $kg \cdot h^{-1}$, accounting for about 54% of the total gas produced, is directed toward a combustion unit. The combustion of this gas provides the thermal energy required to sustain the endothermic pyrolysis reaction via a heat exchanger and to supply hot gases for biomass drying. This internal energy recovery significantly reduces external energy demand and contributes to the energetic autonomy of the process. The remaining fraction, 6.37 $kg \cdot h^{-1}$, corresponding to approximately 46 % of the pyrolysis gas, is recovered as a synthesis gas stream. This syngas can be further valorized for energy production (e.g., CHP) or advanced thermochemical applications, such as hydrogen production or catalytic conversion, thereby enhancing the overall efficiency and flexibility of the integrated biorefinery system. Figure 51 presents the energy balance of the process.

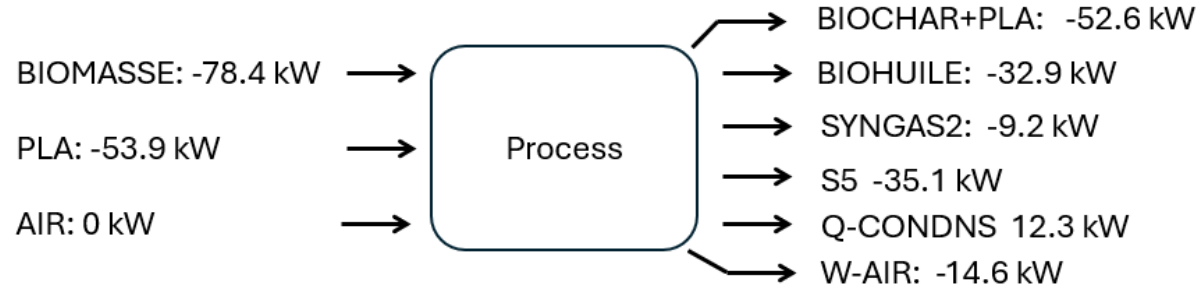

Figure 51: Energy balance of the process.

Looking at the flow sheet and evaluating it with the energy balance figure, it is noticeable that, in addition to supplying the heat for drying and the 25 kW required for pyrolysis, we have at least 70 kW in the different outputs of bio-oil, syngas, and S5 that can be valorized in other areas.

4.4 Technical and economic analysis

4.4.1 Capital expenditure - CAPEX

Capital expenditure, or CAPEX, refers to investments in long-term assets, such as buildings, land, machinery, or equipment. These expenses are often large and are used to build, improve,

or expand the company's infrastructure. CAPEX expenses are typically recorded as assets on the company's balance sheet and amortized over several years because they are expected to provide benefits over a longer period. Table 17 shows the breakdown of CAPEX for the nominal plant with a feed of 1000 kg·day^{-1}.

Table 17: Nominal plant CAPEX for 1 000 kg·day^{-1} biomass.

Item	Scenario 1 (k€)	Scenario 2 (k€)	Scenario 3 (k€)	Scenario 4 (k€)	Ref.
Industrial Warehouse	180.00	180.00	180.00	180.00	Estimated
Biochar Section	1 645.00	1 645.00	1 645.00	1 645.00	Estimated
Composites Pellets Section	1 150.00	1 150.00	1 150.00	1 150.00	Estimated
Tomatoes Clips Section	0.00	0.00	500.00	500.00	Estimated
Auxiliary infrastructure	200.00	200.00	200.00	200.00	Estimated
Laboratory and quality control	150.00	150.00	150.00	150.00	Estimated
Working Capital	1 535.59	1 011.90	1 110.49	1 650.26	6 months of OPEX
Total CAPEX	**4 860.59**	**4 336.90**	**4 935.49**	**5 475.26**	

The estimated data were based on averages of costs found online, and consider a percentage dedicated to installation and/or adaptation. In the case of the biochar section, the cost was based on the budget provided by ETIA (Annex 4) for the pyrolysis section plus approximately € 250 000 for biomass pretreatment machinery and biochar storage logistics. In addition, the working capital included six months of OPEX, of which one month was allocated to the payment of permits, licenses, engineering, and commissioning.

4.4.2 Operational expenditure - OPEX

All expenses that are not directly associated with the production or provision of goods and services can be classified as operating expenses (OPEX). In the context of our project, OPEX corresponds to the sum of the following elements: purchase of raw materials, consumables, labor and maintenance cost, energy consumption. These expenses are essential, as they establish the necessary basis for the operation of revenue generating activities. Table 18 shows an annual estimate of OPEX based on nominal operation (330day·year^{-1}).

Table 18: Indicative annual OPEX €/year.

Item	Scenario 1 (k€/year)	Scenario 2 (k€/year)	Scenario 3 (k€/year)	Scenario 4 (k€/year)
Wood waste	3.63	3.63	3.63	3.63
Virgin PLA	2 065.03	10 032.51	1 032.51	2 065.03
Energy	33.46	18.61	50.79	97.41
Labor	360.00	360.00	450.00	450.00
Maintenance	166.25	166.25	191.25	191.25
Consumables & Packaging	40.00	40.00	40.00	40.00
Overheads	332.50	332.50	382.50	382.50
Waste management	15.00	15.00	15.00	15.00
Logistics costs	50.00	50.00	50.00	50.00
Water consumption	5.30	5.30	5.30	5.30
Total OPEX anual	**3 071.17**	**2 023.81**	**2 220.98**	**3 300.52**

For the costs of wood, it was considered low, as it consists of wood waste and scrap available in areas near Rouen, Normandy. In the analysis, we observed that between the Lyon forest, the Eawy forest, and the Yvetot area, around 84 000 tons of waste are produced. Therefore, there is enough to supply the plant's annual needs, which are only 330 tons. Traveling between these locations and Rouen would involve traveling about 581 km per year. As for PLA, which is one of the critical points, a price of € 2.86 kg^{-1} was considered, which according to the global analysis by imarcgroup [260]. However, when averaging the prices of several suppliers online, the average cost of PLA is around € 6 kg^{-1}, so using this latter price, and maintaining the sale of the product at 1.8 times the cost of production, is profitable for all four scenarios, but the sales prices of composites would be much higher, at around € 12.90 kg^{-1} and € 13.96 kg^{-1} for composite pellets and composite clips, respectively. This remains competitive but is less attractive to buyers.

Using these OPEX values the calculated unit production cost for each of our products provided that for biocomposite pellets € 3.95 kg^{-1}, and € 4.95 kg^{-1} for biocomposite tomatoes clips. In the case of biochar, an OPEX was carried out considering only the production of biochar, in order to evaluate its unit cost resulting in € 1.55kg^{-1}.

For OPEX, the workforce was 8 employees divided into 2 shifts of 8 and 10 employees in two shifts for scenarios that include mold injection. Table 19 shows the positions, function and salaries.

Table 19: Job descriptions and salaries.

Job title	Main Fonction	Gross cost Total per year (k€)
Shift supervisor	Coordinates and supervises the entire shift. Documentation, basic quality control	51.00
Reactor operator	Operate and control the reactor. Support in mixing when not loading/cooking.	43.90
Biocomposites / mixing technician	Formulating and blending biocomposites In-reactor support	45.50
Maintenance operator	Maintain critical equipment. Lightweight operational support	42.90

For these salaries, the average salary of these positions in Normandy was considered, plus 30% considered as the burden for the company.

4.4.3 Sales

To set the sale price for each product, the unit production cost was calculated and set at 2 times the unit production cost, resulting in values of € 3.11 kg^{-1}, for biochar, € 7.89kg^{-1}, for biocomposite pellets, and € 8.66 kg^{-1}, for biocomposite clips. Selling biocomposites at prices below average market prices. The following Figure 52 shows the market price range for biochar, PLA, biocomposite pellets, and tomato clips. This data was collected online from different companies such as 3DJake/Spectrum, Nanovia, Eolasprints, Arianeplast, SmartMaterials3D, Alibaba (exporters), Rezomes/others, Agrifournitures, Frenc Alibaba, AUXINE, Adorla, Ecoforce, AUXINE, Triangle, Direct-filet, and Jardinet (Annex 5). In the case of biochar, in most cases, sales were directed at agriculture. In the case of pellet composites, only two were found products, PLA-carbon and PLA-wood composites. In the case of tomato clips, those that are biodegradable or made from biopolymers were in the range of € 33-49 kg^{-1}, but those made from polypropylene are cheaper, which is why we see in the graph that prices start at € 9 kg^{-1}.

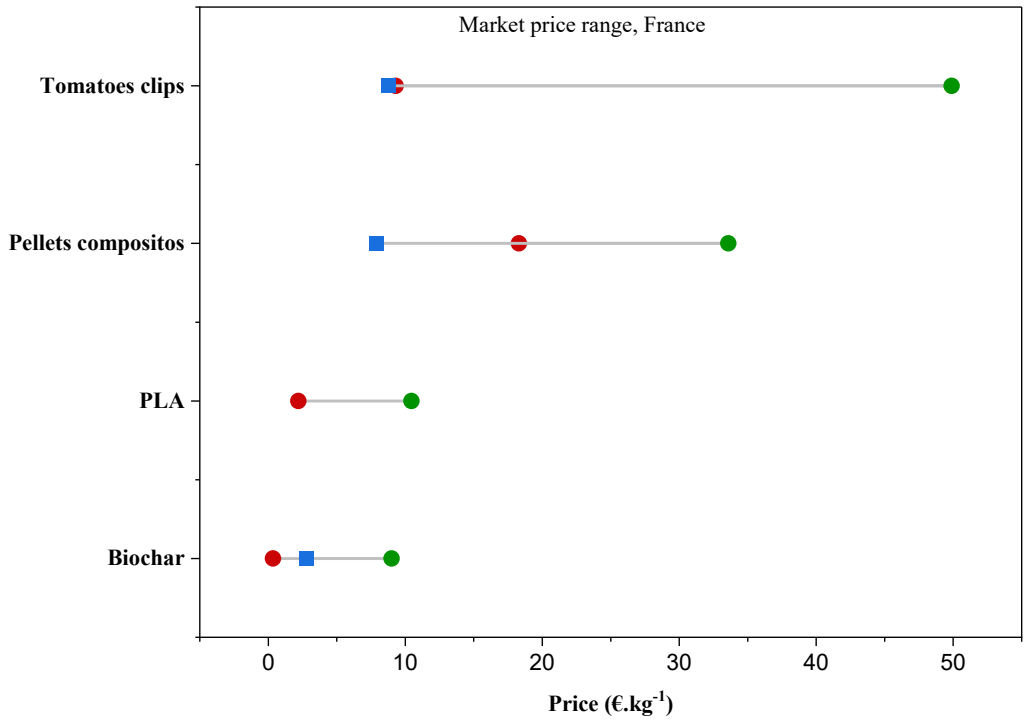

Figure 52: Market price range in France

In Figure 52, the green dots represent the maximum prices of those evaluated, the red dots represent the minimum prices, and the blue box represents the selling price considered in this study, which is equivalent to 1.8 times the production price. As can be seen in the graph, our composite products are cheaper than those of our competitors.

4.4.4 Cash flow

Once there is a clear idea of the infrastructure costs, expenses, and monthly income, it's time to work on the cash flow, which shows the movement of money in and out of the project. It serves to measure liquidity, that is, the actual ability to pay expenses, and is essential for making financial decisions, as cash flows are used to calculate the economic indicators in the next section 4.4.5. Table 20 shows the 10-year cash flow of Scenario 1. The cash flows for the other scenarios are presented in Annex 7.

Table 20: 10-year cash flow for scenario 1 considering the sale of 100% of the proceeds.

Year	CAPEX (k€)	Income (k€)	OPEX (k€)	EBITDA (k€)	Depreciation	Interests	Tax	Net profit (k€)	Free Cash Flow (k€)
0	4 860.59								-4 860.59
1		6 142.34	3 071.17	3 071.17	486.06	252.45	583.17	1,749.50	2 235.56
2		6 234.48	3 117.24	3 117.24	486.06	201.64	607.38	1 822.15	2 308.21

3		6 327.99	3 164.00	3 164.00	486.06	148.24	632.43	1 897.28	2 383.34
4		6 422.91	3 211.46	3 211.46	486.06	92.10	658.33	1 974.98	2 461.03
5		6 519.26	3 259.63	3 259.63	486.06	33.09	685.12	2 055.36	2 541.42
6		6 617.05	3 308.52	3 308.52	486.06	0.00	705.62	2 116.85	2 602.91
7		6 716.30	3 358.15	3 358.15	486.06	0.00	718.02	2 154.07	2 640.13
8		6 817.05	3 408.52	3 408.52	486.06	0.00	730.62	2 191.85	2 677.91
9		6 919.30	3 459.65	3 459.65	486.06	0.00	743.40	2 230.19	2 716.25
10		7 023.09	3 511.55	3 511.55	486.06	0.00	756.37	2 269.12	2 755.17

Several parameters are considered in cash flow: CAPEX (capital expenditure), OPEX (operating expenditure) and revenue, the latter of which refers only to sales and has already been defined above. EBITDA stands for earnings before interest, tax, depreciation, and amortization. It is a metric used to provide insights into a company's profitability. Depreciation is the reduction in the value of an asset over time due to wear and tear, among other factors. In this study, the useful life of all assets and equipment was assumed to be 10 years, which is the duration of the project. Therefore, although the asset value will decrease, it will not need to be replaced, as it will only be acquired once. Interest payable is also included. For the purposes of this study, it was assumed that start-up costs were covered by a € 5 500 k loan at 5 % interest over five years. The same loan was considered for all scenarios. The loan amortization table shows the gradual repayment of debt over a certain period (five year) through periodic payments consisting of the original loan amount and interest (Annex). Taxes are the money that the company must pay and are applied to net profits, i.e., if there are no profits, no taxes are paid. In France, the corporate tax rate is 25 % as mentioned in section 4.1. Net profits are the amount of money left over after deducting a company's total expenses from its total revenue for a given accounting period. Return on Investment is calculated based on net profits. Free cash flow is the amount of cash left over for a company after accounting for operating expenses and maintenance of fixed assets. Investors and analysts use it as a measure of a company's profitability, and Net Present Value and Internal Rate of Return are calculated based on free cash flow data.

To represent the evolution of money more realistically, in terms of both income and expenses, an annual inflation rate of 2 % has been assumed, starting in year 2, which is close to the inflation rate in France in 2025 [261]. In addition, a discount rate of 10 % was considered. This interest rate is used to calculate the present value of a series of future income payments.

To assess the economic viability of the project, a ten-year financial projection analysis was performed under two commercial performance assumptions: a base case scenario with 100 % sales and a conservative sensitivity scenario with 80 % sales. The results are broken down (Figure 53) in terms of net profit (parts A and C) and free cash flow (B and D).

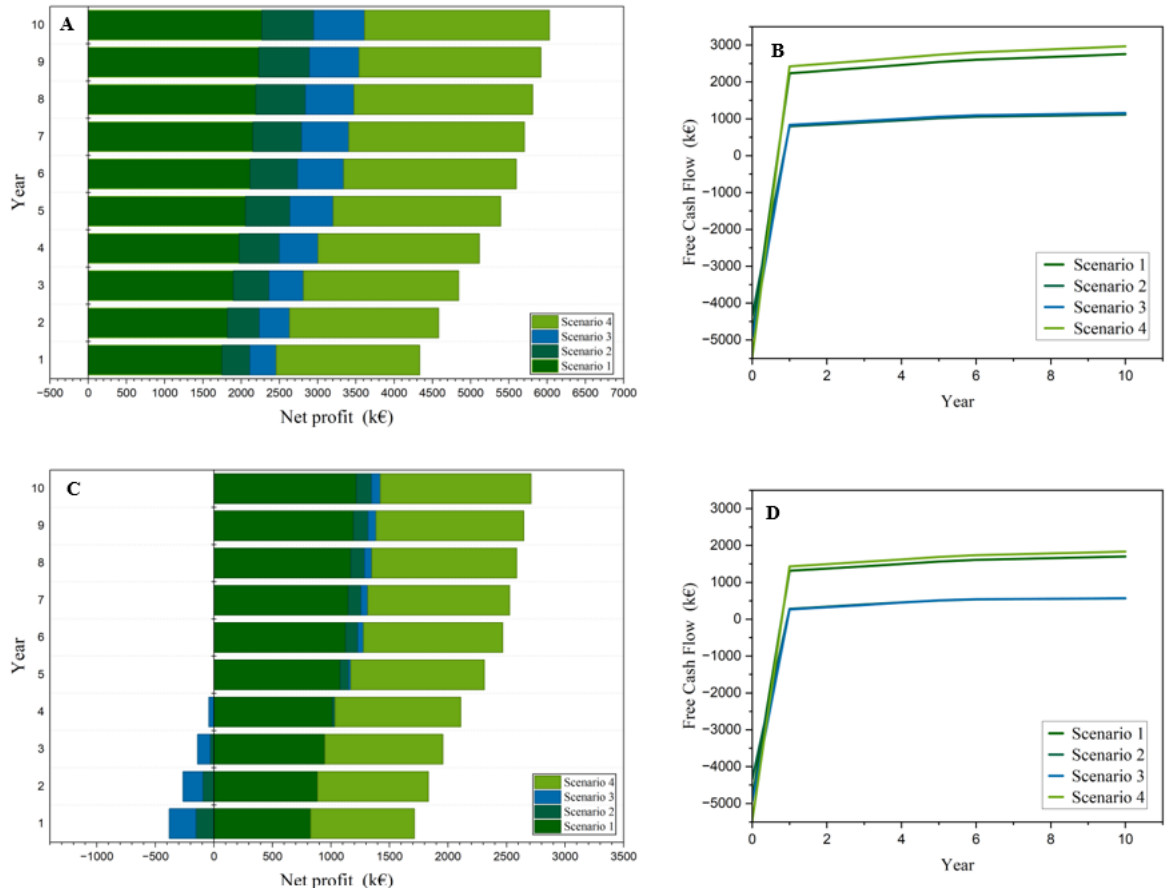

Figure 53: Comparison of financial projections under full sales (100 %) and reduced sales (80 %) scenarios. The graphs on the left (A, C) show the distribution of net profit by scenario, while those on the right (B, D) represent the evolution of free cash flow.

The net profit projections allow us to see how they evolve. A stacked bar chart was used to represent net profit (Figure 53 A and C) in order to facilitate direct comparison of the profitability generated by each independent scenario. With an optimal return of 100 % of sales, the project shows financial strength. Some scenarios, such as 1 and 4, show a positive profit close to € 1 700 k from the first year, exceeding € 2 200 k by the tenth year. In contrast, the scenarios 2 and 3 didn't even reach 700 k after 10 years. This suggests that all scenarios are viable, but the scenario 4 is the most robust in terms of net profit. in contrast by reducing sales volume to 80 %, a critical change in the profit structure can be observed. Scenarios 2 and 3 have constant operating losses (negative values), indicating that these components are highly dependent on sales volume to reach their break-even point. This is particularly true of scenario 3.

Figure 53 B and D illustrate the project's ability to generate liquidity after meeting investment and working capital requirements. In this context, we see that in the full sales scenario, free cash flow shows an accelerated recovery. Despite a significant initial investment (approx. € 5 500 k), the break-even point is reached early on. Scenarios 1 and 4 show stabilization above € 2 500 k per year. However, with a 20 % reduction in sales, although the project remains technically viable (positive free cash flows), the margin for manoeuvre is considerably reduced.

In the case of the lower-performance scenarios, they barely exceed € 500 k per year, suggesting a high risk in the event of possible increases in operating costs or unforeseen financial events.

4.4.5 Economic indicators: ROI (Return on Investment), NPV (Net Present Value), IRR (Internal Rate of Return), and Payback to assess the economic viability of the project.

Within the economic indicators we have ROI, which is a static and simple method to obtain a quick analysis of a short-term investment. It is calculated as the quotient between the profit generated before interest and taxes and the value of the investment.

$$ROI = \frac{Revenue - investment}{investment} \qquad \textit{Equation 6}$$

Another important indicator is NPV (net present value), or VC (equity value) is a measure that considers the different value of money over time. It updates the monetary units, that is, it gives us the present value of our future flows valued at a given discount rate. This method measures the overall profitability of an investment project. It is calculated with the equation:

$$NPV = \sum_{t=1}^{n} \frac{V_t}{(1+k)^t} - I_0 \qquad \textit{Equation 7}$$

Where NPV is the net current value, it represents the cash flows in each period of time. $V_t I_0$value of the initial investment, n is the number of periods considered, and k is the interest rate.

On the other hand, there is also the IRR (Internal Rate of Return) provides the return on investment in percentage terms and measures the profit of the asset with respect to the capital that remains invested at the beginning of each period and not on the one initially invested. It is calculated with the following equation.

$$TIR = \frac{Future\ value^{\frac{1}{n}}}{Present\ value} - 1 \qquad \textit{Equation 8}$$

The equations are presented for general information, but for the calculations we will rely on Excel, which already has the integrated equations.

Using the cash flow information and assumptions from the previous section, the different indicators for scenario 1 in which all the biochar produced was used for the production of biocomposites in pellet forms were calculated. The result shows a Roi total of 421 % which indicates that in for every € 4 invested, € 4.2 will be recovered, which would be an average annual ROI of 42 % over 10 years, indicating that, on average, each year the project returns a

net profit, after taxes and depreciation, equivalent to 42 % of the initial inversion. An NPV of € 9 469.51 k indicating that the project is expected to generate about 9 millions of euros in value beyond its costs. An IRR of 48 %, which indicates that it is much higher than the minimum accepted rate, which is about 10 %, indicates that this project is profitable. And finally, the payback period indicates the project will pay back its initial investment by the third year. Basically, it is profitable and attractive.

Table 21 shows the financial performance of the four investment scenarios under two sales assumptions: 100 % sales capacity and sales capacity reduced to 80 %. This provides a broader view of profitability, value creation, and risk exposure.

Table 21: summary table of economic indicators for all scenarios.

Sales 100%	**ROI (%)**	**NPV (k€)**	**IRR (%)**	**Payback (year)**
Scenario1	421	9 469.51	48	3rd
Scenario 2	129	1 454.90	17	5th
Scenario 3	110	1 136.93	15	6th
Scenario 4	399	10 013.11	46	3rd
Sales 80%				
Scenario1	218	4 024.56	27	4th
Scenario 2	9	1 433.13	1.5	9th
Scenario 3	-4	2 002.73	1	Non recovered
Scenario 4	205	3 592.18	26	4th

At full sales capacity, scenarios 1 and 4 stand out for their high profitability, with a high IRR and short payback periods. Scenarios 2 and 3 remain profitable but are less attractive due to a lower return on investment and slower payback. On the other hand, when considering that only 80 % is sold, there is a decrease in the IRR in scenario 1 from 48 % to 27 %. Even so, it remains solid and profitable. In contrast, when sales decline by 20 %, scenarios 2 and 3 become financially unsustainable, as they have a negative NPV. Finally, scenario 4 remains profitable despite the decline in sales.

In conclusion, the results show that the focus should be on scenarios 1 and 4, which ensure high profitability and resilience even in the face of declining sales. Scenarios 2 and 3 represent a high risk and should not be a priority in investment planning.

4.4.5.1 Scenario analysis and sensitivity assessment

To assess the sensitivity of the project to changes in certain factors such as CAPEX, OPEX, and sales, economic indicators were calculated, varying these by plus or minus 10 %, with the

exception of sales, which varied between minus 10 % and 20 %, as we cannot sell more than what is produced since no product reserve was considered. Figure 54 shows the influence of changes in CAPEX, OPEX, and sales on the net present value of the four scenarios.

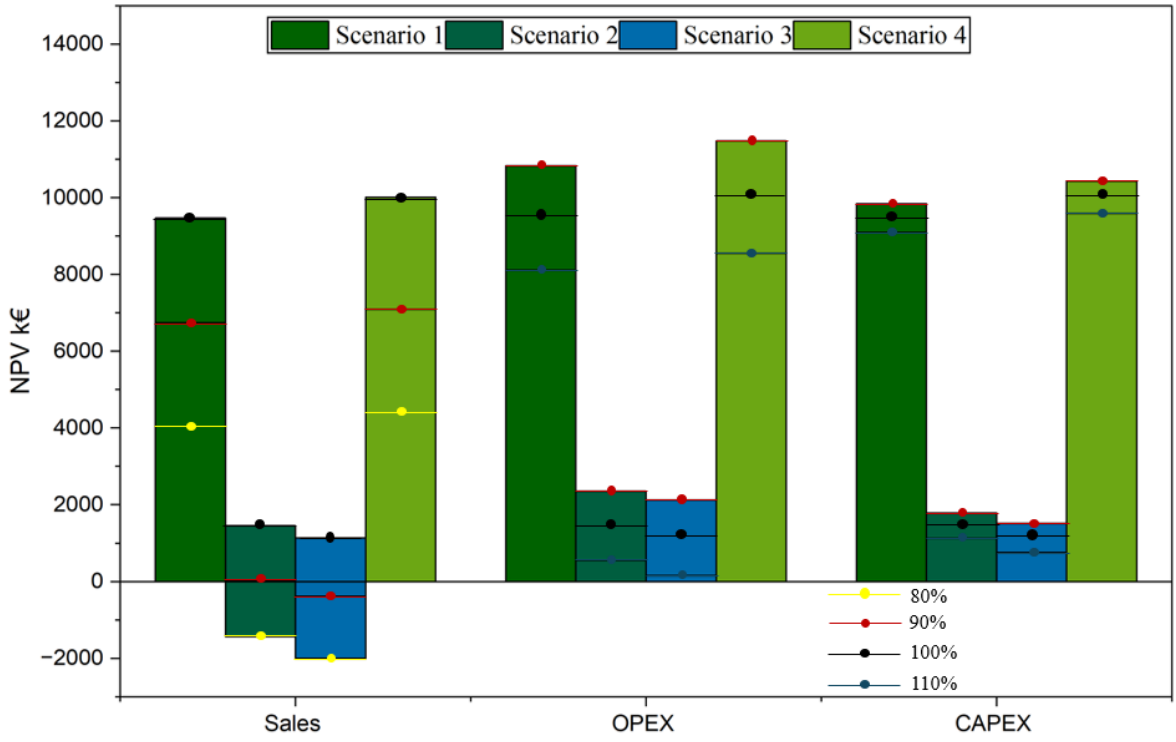

Figure 54: Effect of the variation in OPEX, CAPEX, and sales on the net present value of the project.

In Figure 54, the yellow dots refer to the factor at 80 %, the red dots at 90 %, the black dots at 100 %, and the blue dots at 110%. In other words, in the case of sales, the yellow dot indicates that only 80 % of what was produced was sold, and the blue dot indicates that 110 % of the actual CAPEX considered in the base calculations was considered CAPEX. Once this is understood, it seemed that sales have the greatest impact on the project's NPV, followed by OPEX and finally CAPEX. Therefore, in order to improve the profitability of scenarios 2 and 3, the ideal solution is to vary the sales price of the different products and also draw up a sales plan that ensures the highest possible sales.

At least a 15 % increase in the sale price of the products is needed for scenarios 2 and 3 to become profitable, assuming 80 % of sales. This would result in a NPV of € 548.34 k and an IRR of 13 % for scenario 2, and a NPV of € 165.31 k and an IRR of 11 % for scenario 3. Therefore, with sales prices of € 9.23 kg^{-1} for biocomposite pellets, € 10.13 kg^{-1} for clips, and € 3.64 kg^{-1} for biochar, scenarios 2 and 3 would become profitable, maintaining competitive prices for biocomposites and acceptable prices for biochar.

Conclusion

The technical-economic assessment demonstrates that integrating biochar production with PLA-based biocomposite manufacturing can be commercially viable. Capital expenditure for a 1 t·day^{-1} plant is modest and the main cost drivers are the biochar section and auxiliary infrastructure. Operating costs are dominated by energy consumption and raw material purchase, leading to a unit production cost of € 1.55 kg^{-1} for biochar and € 3.90 kg^{-1} for composite pellets (Scenario 1).

Four scenarios were evaluated. When all biochar is valorized as composite pellets (Scenario 1), the project achieves an ROI of 421 %, an NPV of € 9 470 k, an IRR of 48 % and a payback within three years, confirming strong profitability. A similar performance is obtained in Scenario 4 (biochar-PLA biocomposites clip products) with ROI ≈ 399 % and IRR ≈ 46 %. Scenarios 2 and 3, which split the biochar between sale and composite production, generate lower returns and become unprofitable when sales drop to 80 % of capacity. Sensitivity analysis shows that sales price has the greatest impact on NPV, followed by OPEX and CAPEX, indicating that market positioning and demand assurance are critical for the less favourable scenarios. Figure 55 shows a comparison of the different economic indicators for the four scenarios outlined in Chapter 4 and the assumptions of 100 % and 80 % sales. Where it is shown that scenario 4 (S4) is resilient as well as being the most balanced and cost-efficient (CAPEX/OPEX), scenario 1 offers the best returns (ROI/IRR), and a 20 % drop in sales significantly reduces the profitability of all scenarios.

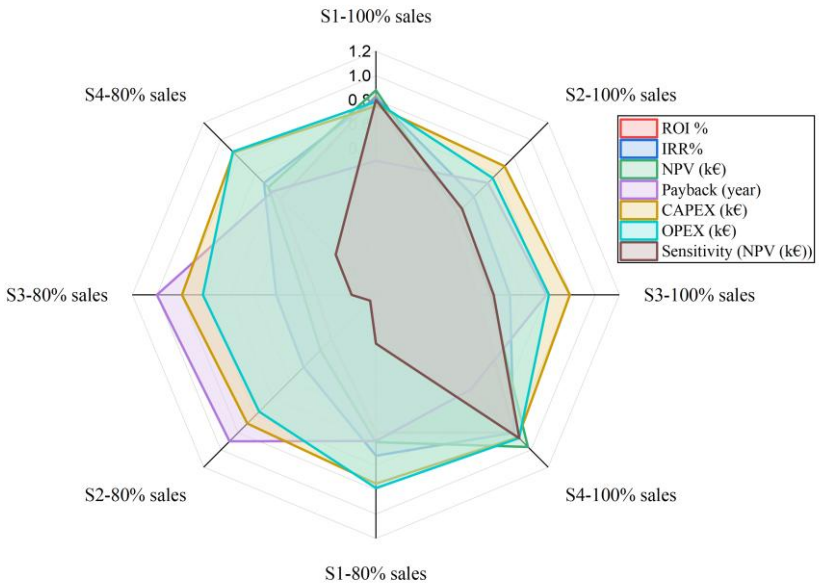

Figure 55: Financial sensitivity analysis of different scenarios.

Overall, the model confirms that a fully integrated biochar to biocomposite plant can achieve economic sustainability while delivering high value, multifunctional materials. The analysis also highlights the importance of optimizing product mix, maintaining high sales volumes, and controlling energy and raw material costs to preserve the attractive financial indicators identified for the most promising scenarios.

GENERAL CONCLUSION

General conclusion

This thesis presents comprehensive research into the utilisation of biochar in biobased materials with controlled properties, addressing critical gaps in our understanding of biochar-biocomposite systems. Through a systematic analysis of biochar production, activation and application in polylactic acid (PLA) matrices, the research has demonstrated the versatility and promise of biochar as a reinforcement material for developing sustainable and economically viable biocomposites.

The study was organized around three biomass (Laminaria digitata algae, beech wood and flax) all subjected to a slow pyrolysis process at 600 °C followed by physical activation with CO_2 at 900 °C. This double-treatment approach was highly effective, as activation significantly increased the specific surface area (up to 774 % for Laminaria digitata algae) and pore volume, which improves interfacial adhesion to the PLA matrix, raises the storage modulus of biocomposites ($E' \approx 2{,}000$ MPa for 10% BCBWA) and allows the formation of conductive networks (electrical conductivity reaching $\approx 10^{-2}$ S·cm^{-1} a 70 % beech wood infill by weight). These results demonstrate that the intrinsic properties of biochar can be designed and adapted through careful selection of feedstock type and thermal processing parameters to meet specific application requirements.

The research identified an optimal biochar loading of 10 % by weight strikes a critical balance between improving mechanical properties, especially Young's modulus, while maintaining processability and avoiding embrittlement. At this loading, the biochar acts as a nucleating agent, enhancing the crystallinity of the PLA matrix without negatively affecting the glass transition temperature. It was also identified that wood-derived biochar offers the best balance between stiffness, conductivity and thermal stability, while flax shives-derived biochar stands out as a nucleating agent, increasing the crystallinity of PLA and displacing cold crystallization at lower temperatures. In addition, terrestrial biochars (beech wood, flax shives) outperform algae biochar in mechanical reinforcement and conductivity.

Higher biochar loads (> 40 % by weight) demonstrated improved electrical conductivity, with values reaching 1.24×10^{-2} S·cm^{-1} at 70 % beech activated biochar, making these compounds suitable for electromagnetic and antistatic shielding applications. This functional improvement opens news ways for biocomposites in electronic devices and advanced packaging applications, moving beyond purely mechanical reinforcement to multifunctional materials. However, high filler loads (> 40 % by weight) cause agglomeration, reducing tensile strength and processability, highlighting the need to optimize dispersion or employ coupling agents.

It reveals the limitation that there is an inverse relationship between technical functionality and structural stability: while biochar enhances the rigidity and electrical capacity of the biocomposite, excess biochar compromises its deformation capacity (ductility) and energy absorption (toughness). This defines a critical threshold for the material's mechanical integrity.

Our findings provide critical evidence of the commercial viability of integrated biochar and biocomposite production systems. The techno-economic assessment indicates that an integrated facility (1 t·day^{-1}) for the conversion of beech wood waste into biochar, followed by the production of PLA–biochar pellets, is technically feasible and economically attractive.

With a modest capital expenditure (~ € 5.5 M), the unit costs of production are € 1.57 kg^{-1} for biochar and € 3.95 kg^{-1} for composite pellets, the project achieves an NPV ≈ € 9 million and a payback period of three years, when all biochar produced is valued as composite material. The sensitivity analysis shows that the selling price is the dominant economic lever, underlining the importance of the market position. This study shows several scenarios and shows that scenarios in which 50 % of the biochar is sold as a finished product and the other 50 % is valued in biocomposites, are riskier and only viable at full sales capacity.

Together (physico-chemical and financial analysis), this work provides a comprehensive design framework that links the surface, porosity, carbon content, and crystallinity of biochar to the mechanical, thermal, and functional performance of PLA-based biocomposites. It further demonstrates that this valorization pathway offers both technical advantages and strong economic returns, while aligning with the broader objectives of the circular economy and climate change mitigation by enabling the replacement of fossil-based boosters with sustainable alternatives derived from waste biomass. Several scientific and technological gaps persist that deserve attention in future research:

1. The compression and development of surface functionalization strategies or coupling agents to improve the dispersion of biochar in PLA and strengthen interfacial adhesion, especially at higher fill levels.
2. Conduct ageing, biodegradation, and fatigue studies to assess the shelf life of biobased compounds under realistic service conditions.
3. Leverage pronounced electrical conductivity for exploration of additional high-value applications such as antistatic coatings, EMI shielding, and sensor platforms.
4. Integration with renewable energy systems, optimization of pyrolysis gas titration and co-product exploration (bio-oil, syngas) could significantly improve overall system profitability and energy efficiency.
5. Refine the product portfolio (pellets, agricultural clips, special fillers) and evaluate alternative market niches to mitigate the sales price sensitivity identified in the techno-economic analysis.

Scientific production:

Peer reviewed scientific paper:

Guillermina Feliz Florian, Mohamed Ragoubi, Nathalie Leblanc, Bechara Taouk and Lokmane Abdelouahed. *Production and Its Potential Application for Biocomposite Materials: A Comprehensive Review*. J. Compos. Sci. 2024, 8, 220. https://doi.org/ 10.3390/jcs8060220

Scientific papers in progress:

- Paper 1 - Comparative study of different biocomposite mixtures. *Under correction.*
- Paper 2 - Production cost evaluation of biocarbon and PLA-biocarbon composites: Economic viability and industrial applications. *Under correction.*

International conference (oral or poster communication):

- Guillermina Feliz Florian, Mohamed Ragoubi, Nathalie Leblanc, and Lokmane Abdelouahed. *Biosourced biochar as a conductive filler in polymeric biocomposites: effect of biomass type and filler content*. Oral presentation at the IVth International Congress on Research, Development, and Innovation, Universidad Autónoma de Santo Domingo (UASD), November 2025, Dominican Republic.
- Guillermina Feliz Florian, Mohamed Ragoubi, Nathalie Leblanc, and Lokmane Abdelouahed. *Analysis of biochar derived from different biomasses used as filler in PLA biocomposites*. Oral presentation at the IIIrd International Congress on Research, Development, and Innovation, Universidad Autónoma de Santo Domingo (UASD), November 2024, Dominican Republic.

National communication (oral or poster communication):

- Guillermina Feliz Florian, Mohamed Ragoubi, Nathalie Leblanc, and Lokmane Abdelouahed. *Characterization of biocomposites made from biochar and polylactic acid (PLA)*. Poster at Société française de génie des procédés (SFGP) congress, October 2024, Deauville, France.
- Guillermina Feliz Florian, Mohamed Ragoubi, Nathalie Leblanc, Bechara Taouk and Lokmane Abdelouahed. *New ways of utilizing biochar in bio-based materials with controlled properties.* Oral presentation at Laboratoire de Sécurité des Procédés Chimiques (LSPC) doctoral students' day, 2023, Rouen, France.
- Guillermina Feliz Florian, Mohamed Ragoubi, Nathalie Leblanc, Bechara Taouk and Lokmane Abdelouahed. *New ways of utilizing biochar in bio-based materials with controlled properties*. Poster at UniLaSalle doctoral students' day, 2022, Mont-Saint-Aignan, France.
- Scientific speed dating / Science Festival 2024, Rouen.

References

[1] "Keep in touch," Renewable Carbon Publications. Accessed: Jan. 03, 2026. [Online]. Available: https://renewable-carbon.eu/publications/download-confirmation-page/

[2] L. Martes Hernández, "Catalytic cracking of tar model compounds using biochar as catalyst," INSA Rouen Normandie, 2025. [Online]. Available: https://theses.hal.science/tel-05031371/

[3] D.-C. Li and H. Jiang, "The thermochemical conversion of non-lignocellulosic biomass to form biochar: A review on characterizations and mechanism elucidation," *Bioresour. Technol.*, vol. 246, pp. 57–68, Dec. 2017, doi: 10.1016/j.biortech.2017.07.029.

[4] L. Zhao *et al.*, "Sewage sludge derived biochar for environmental improvement: Advances, challenges, and solutions," *Water Res. X*, vol. 18, p. 100167, Jan. 2023, doi: 10.1016/j.wroa.2023.100167.

[5] A. Rehman, S. Nawaz, H. A. Alghamdi, S. Alrumman, W. Yan, and M. Z. Nawaz, "Effects of manure-based biochar on uptake of nutrients and water holding capacity of different types of soils," *Case Stud. Chem. Environ. Eng.*, vol. 2, p. 100036, Sep. 2020, doi: 10.1016/j.cscee.2020.100036.

[6] P. Singh, M. Dhanorkar, and S. Sharma, "Valorization of aquatic plant biomass resource to fortified biochar and paper pulp: A strategic approach towards closed-loop technologies, circular economy, and sustainability," *Resour. Conserv. Recycl.*, vol. 202, p. 107385, Mar. 2024, doi: 10.1016/j.resconrec.2023.107385.

[7] O. Mašek *et al.*, "Microwave and slow pyrolysis biochar—Comparison of physical and functional properties," *J. Anal. Appl. Pyrolysis*, vol. 100, pp. 41–48, Mar. 2013, doi: 10.1016/j.jaap.2012.11.015.

[8] M. H. Duku, S. Gu, and E. B. Hagan, "Biochar production potential in Ghana—A review," *Renew. Sustain. Energy Rev.*, vol. 15, no. 8, pp. 3539–3551, Oct. 2011, doi: 10.1016/j.rser.2011.05.010.

[9] R. Janu *et al.*, "Biochar surface functional groups as affected by biomass feedstock, biochar composition and pyrolysis temperature," *Carbon Resour. Convers.*, vol. 4, pp. 36–46, Jan. 2021, doi: 10.1016/j.crcon.2021.01.003.

[10] S. S. Sahoo, V. K. Vijay, R. Chandra, and H. Kumar, "Production and characterization of biochar produced from slow pyrolysis of pigeon pea stalk and bamboo," *Clean. Eng. Technol.*, vol. 3, p. 100101, Jul. 2021, doi: 10.1016/j.clet.2021.100101.

[11] K. Weber and P. Quicker, "Properties of biochar," *Fuel*, vol. 217, pp. 240–261, Apr. 2018, doi: 10.1016/j.fuel.2017.12.054.

[12] X. Zhang, P. Zhang, X. Yuan, Y. Li, and L. Han, "Effect of pyrolysis temperature and correlation analysis on the yield and physicochemical properties of crop residue biochar," *Bioresour. Technol.*, vol. 296, p. 122318, Jan. 2020, doi: 10.1016/j.biortech.2019.122318.

[13] R. Azargohar, S. Nanda, B. V. S. K. Rao, and A. K. Dalai, "Slow Pyrolysis of Deoiled Canola Meal: Product Yields and Characterization," *Energy Fuels*, vol. 27, no. 9, pp. 5268–5279, Sep. 2013, doi: 10.1021/ef400941a.

[14] M. I. Al-Wabel, A. Al-Omran, A. H. El-Naggar, M. Nadeem, and A. R. A. Usman, "Pyrolysis temperature induced changes in characteristics and chemical composition of biochar produced from conocarpus wastes," *Bioresour. Technol.*, vol. 131, pp. 374–379, Mar. 2013, doi: 10.1016/j.biortech.2012.12.165.

[15] S. Kane, R. Ulrich, A. Harrington, N. P. Stadie, and C. Ryan, "Physical and chemical mechanisms that influence the electrical conductivity of lignin-derived biochar," *Carbon Trends*, vol. 5, p. 100088, Oct. 2021, doi: 10.1016/j.cartre.2021.100088.

[16] M. Bartoli *et al.*, "Effect of heating rate and feedstock nature on electrical conductivity of biochar and biochar-based composites," *Appl. Energy Combust. Sci.*, vol. 12, p. 100089, Dec. 2022, doi: 10.1016/j.jaecs.2022.100089.

[17] H. Wang, X. Wang, Y. Cui, Z. Xue, and Y. Ba, "Slow pyrolysis polygeneration of bamboo (Phyllostachys pubescens): Product yield prediction and biochar formation mechanism," *Bioresour. Technol.*, vol. 263, pp. 444–449, Sep. 2018, doi: 10.1016/j.biortech.2018.05.040.

[18] S. Aktar *et al.*, "Effects of temperature and carrier gas on physico-chemical properties of biochar derived from biosolids," *J. Anal. Appl. Pyrolysis*, vol. 164, p. 105542, Jun. 2022, doi: 10.1016/j.jaap.2022.105542.

[19] D. Angın, "Effect of pyrolysis temperature and heating rate on biochar obtained from pyrolysis of safflower seed press cake," *Bioresour. Technol.*, vol. 128, pp. 593–597, Jan. 2013, doi: 10.1016/j.biortech.2012.10.150.

[20] S. Guo, X. Xiong, D. Che, H. Liu, and B. Sun, "Effects of sludge pyrolysis temperature and atmosphere on characteristics of biochar and gaseous products," *Korean J. Chem. Eng.*, vol. 38, no. 1, pp. 55–63, Jan. 2021, doi: 10.1007/s11814-020-0685-0.

[21] J. Du *et al.*, "Non-isothermal kinetics of biomass waste pyrolysis by TG-MS/DSC," *Carbon Capture Sci. Technol.*, vol. 6, p. 100097, Mar. 2023, doi: 10.1016/j.ccst.2023.100097.

[22] Z. Hong *et al.*, "Effects of temperature and particle size on the compositions, energy conversions and structural characteristics of pyrolysis products from different crop residues," *Energy*, vol. 190, p. 116413, Jan. 2020, doi: 10.1016/j.energy.2019.116413.

[23] P. Fu *et al.*, "Effects of Pyrolysis Temperature on Characteristics of Porosity in Biomass Chars," in *2009 International Conference on Energy and Environment Technology*, Guilin, China: IEEE, 2009, pp. 109–112. doi: 10.1109/ICEET.2009.33.

[24] R. Narzari *et al.*, "Fabrication of biochars obtained from valorization of biowaste and evaluation of its physicochemical properties," *Bioresour. Technol.*, vol. 242, pp. 324–328, Oct. 2017, doi: 10.1016/j.biortech.2017.04.050.

[25] S. Tan *et al.*, "Utilization of current pyrolysis technology to convert biomass and manure waste into biochar for soil remediation: A review," *Sci. Total Environ.*, vol. 864, p. 160990, Mar. 2023, doi: 10.1016/j.scitotenv.2022.160990.

[26] A. N. Shafawi, A. R. Mohamed, P. Lahijani, and M. Mohammadi, "Recent advances in developing engineered biochar for CO2 capture: An insight into the biochar modification approaches," *J. Environ. Chem. Eng.*, vol. 9, no. 6, p. 106869, Dec. 2021, doi: 10.1016/j.jece.2021.106869.

[27] B. Qiu, Q. Shao, J. Shi, C. Yang, and H. Chu, "Application of biochar for the adsorption of organic pollutants from wastewater: Modification strategies, mechanisms and challenges," *Sep. Purif. Technol.*, vol. 300, p. 121925, Nov. 2022, doi: 10.1016/j.seppur.2022.121925.

[28] T. G. Ambaye, M. Vaccari, E. D. Van Hullebusch, A. Amrane, and S. Rtimi, "Mechanisms and adsorption capacities of biochar for the removal of organic and inorganic pollutants from industrial wastewater," *Int. J. Environ. Sci. Technol.*, vol. 18, no. 10, pp. 3273–3294, Oct. 2021, doi: 10.1007/s13762-020-03060-w.

[29] S.-H. Cho *et al.*, "Applications of agricultural residue biochars to removal of toxic gases emitted from chemical plants: A review," *Sci. Total Environ.*, vol. 868, p. 161655, Apr. 2023, doi: 10.1016/j.scitotenv.2023.161655.

[30] Y. Xie *et al.*, "A critical review on production, modification and utilization of biochar," *J. Anal. Appl. Pyrolysis*, vol. 161, p. 105405, Jan. 2022, doi: 10.1016/j.jaap.2021.105405.

[31] S. Kane, A. Storer, W. Xu, C. Ryan, and N. P. Stadie, "Biochar as a Renewable Substitute for Carbon Black in Lithium-Ion Battery Electrodes," *ACS Sustain. Chem. Eng.*, vol. 10, no. 37, pp. 12226–12233, Sep. 2022, doi: 10.1021/acssuschemeng.2c02974.

[32] J. George, D. Jung, and D. Bhattacharyya, "Improvement of Electrical and Mechanical Properties of PLA/PBAT Composites Using Coconut Shell Biochar for Antistatic Applications," *Appl. Sci.*, vol. 13, no. 2, Art. no. 2, Jan. 2023, doi: 10.3390/app13020902.

[33] T. Perroud *et al.*, "Testing bioplastic containing functionalised biochar," *Polym. Test.*, vol. 113, p. 107657, Sep. 2022, doi: 10.1016/j.polymertesting.2022.107657.

[34] M. Bartoli, M. Giorcelli, P. Jagdale, M. Rovere, and A. Tagliaferro, "A Review of Non-Soil Biochar Applications," *Materials*, vol. 13, no. 2, p. 261, Jan. 2020, doi: 10.3390/ma13020261.

[35] M. He *et al.*, "Waste-derived biochar for water pollution control and sustainable development," *Nat. Rev. Earth Environ.*, vol. 3, no. 7, Art. no. 7, Jul. 2022, doi: 10.1038/s43017-022-00306-8.

[36] W.-H. Chen, J. Peng, and X. T. Bi, "A state-of-the-art review of biomass torrefaction, densification and applications," *Renew. Sustain. Energy Rev.*, vol. 44, pp. 847–866, Apr. 2015, doi: 10.1016/j.rser.2014.12.039.

[37] W.-H. Chen, B.-J. Lin, B. Colin, A. Pétrissans, and M. Pétrissans, "A study of hygroscopic property of biomass pretreated by torrefaction," *Energy Procedia*, vol. 158, pp. 32–36, Feb. 2019, doi: 10.1016/j.egypro.2019.01.030.

[38] A. Soria-Verdugo, E. Cano-Pleite, A. Panahi, and A. F. Ghoniem, “Kinetics mechanism of inert and oxidative torrefaction of biomass,” *Energy Convers. Manag.*, vol. 267, p. 115892, Sep. 2022, doi: 10.1016/j.enconman.2022.115892.

[39] K. B. Kota, S. Shenbagaraj, P. K. Sharma, A. K. Sharma, P. K. Ghodke, and W.-H. Chen, “Biomass torrefaction: An overview of process and technology assessment based on global readiness level,” *Fuel*, vol. 324, p. 124663, Sep. 2022, doi: 10.1016/j.fuel.2022.124663.

[40] C. Yang *et al.*, “Hydrothermal liquefaction and gasification of biomass and model compounds: a review,” *Green Chem.*, vol. 22, no. 23, pp. 8210–8232, 2020, doi: 10.1039/D0GC02802A.

[41] X. He, N. Zheng, R. Hu, Z. Hu, and J. C. Yu, “Hydrothermal and Pyrolytic Conversion of Biomasses into Catalysts for Advanced Oxidation Treatments,” *Adv. Funct. Mater.*, vol. 31, no. 7, p. 2006505, 2021, doi: 10.1002/adfm.202006505.

[42] Y. Zhang *et al.*, “Chapter 14 - Gasification Technologies and Their Energy Potentials,” in *Sustainable Resource Recovery and Zero Waste Approaches*, M. J. Taherzadeh, K. Bolton, J. Wong, and A. Pandey, Eds., Elsevier, 2019, pp. 193–206. doi: 10.1016/B978-0-444-64200-4.00014-1.

[43] L. Zhang, C. (Charles) Xu, and P. Champagne, “Overview of recent advances in thermo-chemical conversion of biomass,” *Energy Convers. Manag.*, vol. 51, no. 5, pp. 969–982, May 2010, doi: 10.1016/j.enconman.2009.11.038.

[44] Ö. Tezer, N. Karabağ, A. Öngen, C. Ö. Çolpan, and A. Ayol, “Biomass gasification for sustainable energy production: A review,” *Int. J. Hydrog. Energy*, vol. 47, no. 34, pp. 15419–15433, Apr. 2022, doi: 10.1016/j.ijhydene.2022.02.158.

[45] R. Muvhiiwa, A. Kuvarega, E. M. Llana, and A. Muleja, “Study of biochar from pyrolysis and gasification of wood pellets in a nitrogen plasma reactor for design of biomass processes,” *J. Environ. Chem. Eng.*, vol. 7, no. 5, p. 103391, Oct. 2019, doi: 10.1016/j.jece.2019.103391.

[46] C. Nzediegwu, M. A. Naeth, and S. X. Chang, “Biochar production from lignocellulosic and nonlignocellulosic biomass using conventional and microwave heating,” in *Biochar in Agriculture for Achieving Sustainable Development Goals*, Elsevier, 2022, pp. 85–95. doi: 10.1016/B978-0-323-85343-9.00022-7.

[47] M. Tripathi, J. N. Sahu, and P. Ganesan, “Effect of process parameters on production of biochar from biomass waste through pyrolysis: A review,” *Renew. Sustain. Energy Rev.*, vol. 55, pp. 467–481, Mar. 2016, doi: 10.1016/j.rser.2015.10.122.

[48] S. Sohi, E. Lopez-Capel, E. Krull, and R. Bol, “Biochar, climate change and soil:A review to guide future research”.

[49] T. Yuan, W. He, G. Yin, and S. Xu, “Comparison of bio-chars formation derived from fast and slow pyrolysis of walnut shell,” *Fuel*, vol. 261, p. 116450, Feb. 2020, doi: 10.1016/j.fuel.2019.116450.

[50] D. Mohan, C. U. Pittman, and P. H. Steele, “Pyrolysis of Wood/Biomass for Bio-oil: A Critical Review,” *Energy Fuels*, vol. 20, no. 3, pp. 848–889, May 2006, doi: 10.1021/ef0502397.

[51] S. Ghysels, A. E. Estrada Léon, M. Pala, K. A. Schoder, J. Van Acker, and F. Ronsse, “Fast pyrolysis of mannan-rich ivory nut (Phytelephas aequatorialis) to valuable biorefinery products,” *Chem. Eng. J.*, vol. 373, pp. 446–457, Oct. 2019, doi: 10.1016/j.cej.2019.05.042.

[52] Y. Li, R. Gupta, Q. Zhang, and S. You, “Review of biochar production via crop residue pyrolysis: Development and perspectives,” *Bioresour. Technol.*, vol. 369, p. 128423, Feb. 2023, doi: 10.1016/j.biortech.2022.128423.

[53] T. Cornelissen, J. Yperman, G. Reggers, S. Schreurs, and R. Carleer, “Flash co-pyrolysis of biomass with polylactic acid. Part 1: Influence on bio-oil yield and heating value,” *Fuel*, vol. 87, no. 7, pp. 1031–1041, Jun. 2008, doi: 10.1016/j.fuel.2007.07.019.

[54] S. Y. Foong *et al.*, “Valorization of biomass waste to engineered activated biochar by microwave pyrolysis: Progress, challenges, and future directions,” *Chem. Eng. J.*, vol. 389, p. 124401, Jun. 2020, doi: 10.1016/j.cej.2020.124401.

[55] D. Dusso, J. F. Téllez, V. C. Fuertes, J. M. De Paoli, and E. L. Moyano, “Vacuum pyrolysis of chia flour residues: An alternative way to obtain omega-3/omega-6 fatty acids and calcium-enriched biochars,” *J. Anal. Appl. Pyrolysis*, vol. 161, p. 105379, Jan. 2022, doi: 10.1016/j.jaap.2021.105379.

[56] S. S. Lam, P. N. Y. Yek, W. Y. Cheng, R. K. Liew, M. Tabatabaei, and M. Aghbashlo, “Production of biochar using sustainable microwave pyrolysis approach,” in *Biochar in Agriculture for Achieving Sustainable Development Goals*, Elsevier, 2022, pp. 323–332. doi: 10.1016/B978-0-323-85343-9.00015-X.

[57] H. Li *et al.*, “Food waste pyrolysis by traditional heating and microwave heating: A review,” *Fuel*, vol. 324, p. 124574, Sep. 2022, doi: 10.1016/j.fuel.2022.124574.

[58] Y. Zhang, S. Fan, T. Liu, M. M. Omar, and B. Li, “Perspectives into intensification for aviation oil production from microwave pyrolysis of organic wastes,” *Chem. Eng. Process. - Process Intensif.*, vol. 176, p. 108939, Jun. 2022, doi: 10.1016/j.cep.2022.108939.

[59] A. Demirbas and G. Arin, “An Overview of Biomass Pyrolysis,” *Energy Sources*, vol. 24, no. 5, pp. 471–482, May 2002, doi: 10.1080/00908310252889979.

[60] A. K. Vuppaladadiyam *et al.*, “Biomass pyrolysis: A review on recent advancements and green hydrogen production,” *Bioresour. Technol.*, vol. 364, p. 128087, Nov. 2022, doi: 10.1016/j.biortech.2022.128087.

[61] A. Zaker, Z. Chen, X. Wang, and Q. Zhang, “Microwave-assisted pyrolysis of sewage sludge: A review,” *Fuel Process. Technol.*, vol. 187, pp. 84–104, May 2019, doi: 10.1016/j.fuproc.2018.12.011.

[62] S. S. Lam, A. D. Russell, C. L. Lee, and H. A. Chase, “Microwave-heated pyrolysis of waste automotive engine oil: Influence of operation parameters on the yield, composition, and

fuel properties of pyrolysis oil," *Fuel*, vol. 92, no. 1, pp. 327–339, Feb. 2012, doi: 10.1016/j.fuel.2011.07.027.

[63] K. Kebelmann, A. Hornung, U. Karsten, and G. Griffiths, "Intermediate pyrolysis and product identification by TGA and Py-GC/MS of green microalgae and their extracted protein and lipid components," *Biomass Bioenergy*, vol. 49, pp. 38–48, Feb. 2013, doi: 10.1016/j.biombioe.2012.12.006.

[64] F. G. de Mendonça, I. T. da Cunha, R. R. Soares, J. C. Tristão, and R. M. Lago, "Tuning the surface properties of biochar by thermal treatment," *Bioresour. Technol.*, vol. 246, pp. 28–33, Dec. 2017, doi: 10.1016/j.biortech.2017.07.099.

[65] S. Arnold, A. Rodriguez-Uribe, M. Misra, and A. K. Mohanty, "Slow pyrolysis of bio-oil and studies on chemical and physical properties of the resulting new bio-carbon," *J. Clean. Prod.*, vol. 172, pp. 2748–2758, Jan. 2018, doi: 10.1016/j.jclepro.2017.11.137.

[66] O. Das and A. K. Sarmah, "The love–hate relationship of pyrolysis biochar and water: A perspective," *Sci. Total Environ.*, vol. 512–513, pp. 682–685, Apr. 2015, doi: 10.1016/j.scitotenv.2015.01.061.

[67] H. Kazemi Shariat Panahi *et al.*, "A comprehensive review of engineered biochar: Production, characteristics, and environmental applications," *J. Clean. Prod.*, vol. 270, p. 122462, Oct. 2020, doi: 10.1016/j.jclepro.2020.122462.

[68] B. Sajjadi, W.-Y. Chen, and N. O. Egiebor, "A comprehensive review on physical activation of biochar for energy and environmental applications," *Rev. Chem. Eng.*, vol. 35, no. 6, pp. 735–776, Jul. 2019, doi: 10.1515/revce-2017-0113.

[69] A. Sobhan, K. Muthukumarappan, L. Wei, Q. Qiao, M. T. Rahman, and N. Ghimire, "Development and characterization of a novel activated biochar-based polymer composite for biosensors," *Int. J. Polym. Anal. Charact.*, vol. 26, no. 6, pp. 544–560, Aug. 2021, doi: 10.1080/1023666X.2021.1921497.

[70] B. Sajjadi, T. Zubatiuk, D. Leszczynska, J. Leszczynski, and W. Y. Chen, "Chemical activation of biochar for energy and environmental applications: a comprehensive review," *Rev. Chem. Eng.*, vol. 35, no. 7, pp. 777–815, Oct. 2019, doi: 10.1515/revce-2018-0003.

[71] A.-N. A. El-Hendawy, "An insight into the KOH activation mechanism through the production of microporous activated carbon for the removal of Pb2+ cations," *Appl. Surf. Sci.*, vol. 255, no. 6, pp. 3723–3730, Jan. 2009, doi: 10.1016/j.apsusc.2008.10.034.

[72] S. Pizzanelli *et al.*, "The Effect of Activation on the Structure of Biochars Prepared from Wood and from Posidonia Oceanica: A Spectroscopic Study," *Physchem*, vol. 2, no. 3, pp. 286–304, Sep. 2022, doi: 10.3390/physchem2030021.

[73] I. Ahmed Hared, J.-L. Dirion, S. Salvador, M. Lacroix, and S. Rio, "Pyrolysis of wood impregnated with phosphoric acid for the production of activated carbon: Kinetics and porosity development studies," *J. Anal. Appl. Pyrolysis*, vol. 79, no. 1–2, pp. 101–105, May 2007, doi: 10.1016/j.jaap.2006.12.016.

[74] J. M. Rincón, S. Rincón, P. Guevara, D. Ballén, J. C. Morales, and N. Monroy, "Producción de carbón activado mediante métodos físicos a partir de carbón de El Cerrejón y su aplicación en el tratamiento de aguas residuales provenientes de tintorerías," *Rev. Acad. Colomb. Cienc. Exactas Físicas Nat.*, vol. 39, no. 51, p. 171, Jun. 2015, doi: 10.18257/raccefyn.138.

[75] M. Kołtowski, I. Hilber, T. D. Bucheli, and P. Oleszczuk, "Effect of steam activated biochar application to industrially contaminated soils on bioavailability of polycyclic aromatic hydrocarbons and ecotoxicity of soils," *Sci. Total Environ.*, vol. 566–567, pp. 1023–1031, Oct. 2016, doi: 10.1016/j.scitotenv.2016.05.114.

[76] C.-H. Hsiao, S. Gupta, C.-Y. Lee, and N.-H. Tai, "Effects of physical and chemical activations on the performance of biochar applied in supercapacitors," *Appl. Surf. Sci.*, vol. 610, p. 155560, Feb. 2023, doi: 10.1016/j.apsusc.2022.155560.

[77] M. Giorcelli, A. Khan, N. M. Pugno, C. Rosso, and A. Tagliaferro, "Biochar as a cheap and environmental friendly filler able to improve polymer mechanical properties," *Biomass Bioenergy*, vol. 120, pp. 219–223, Jan. 2019, doi: 10.1016/j.biombioe.2018.11.036.

[78] A. Pudełko, P. Postawa, T. Stachowiak, K. Malińska, and D. Dróżdż, "Waste derived biochar as an alternative filler in biocomposites - Mechanical, thermal and morphological properties of biochar added biocomposites," *J. Clean. Prod.*, vol. 278, p. 123850, Jan. 2021, doi: 10.1016/j.jclepro.2020.123850.

[79] K. Papadopoulou *et al.*, "Synthesis and Study of Fully Biodegradable Composites Based on Poly(butylene succinate) and Biochar," *Polymers*, vol. 15, no. 4, Art. no. 4, Jan. 2023, doi: 10.3390/polym15041049.

[80] J. Tolvanen, J. Hannu, M. Hietala, K. Kordas, and H. Jantunen, "Biodegradable multiphase poly(lactic acid)/biochar/graphite composites for electromagnetic interference shielding," *Compos. Sci. Technol.*, vol. 181, p. 107704, Sep. 2019, doi: 10.1016/j.compscitech.2019.107704.

[81] J. Liu, G. Liu, W. Zhang, Z. Li, F. Xing, and L. Tang, "Application potential analysis of biochar as a carbon capture material in cementitious composites: A review," *Constr. Build. Mater.*, vol. 350, p. 128715, Oct. 2022, doi: 10.1016/j.conbuildmat.2022.128715.

[82] M. Bartoli *et al.*, "Influence of pyrolytic thermal history on olive pruning biochar and related epoxy composites mechanical properties," *J. Compos. Mater.*, vol. 54, no. 14, pp. 1863–1873, Jun. 2020, doi: 10.1177/0021998319888734.

[83] X. Wang, F. Sotoudehniakarani, Z. Yu, J. J. Morrell, J. Cappellazzi, and A. G. McDonald, "Evaluation of corrugated cardboard biochar as reinforcing fiber on properties, biodegradability and weatherability of wood-plastic composites," *Polym. Degrad. Stab.*, vol. 168, p. 108955, Oct. 2019, doi: 10.1016/j.polymdegradstab.2019.108955.

[84] Q. Zhang *et al.*, "Improvement on the properties of microcrystalline cellulose/polylactic acid composites by using activated biochar," *J. Clean. Prod.*, vol. 252, p. 119898, Apr. 2020, doi: 10.1016/j.jclepro.2019.119898.

[85] R. K. Dahal, B. Acharya, G. Saha, R. Bissessur, A. Dutta, and A. Farooque, “Biochar as a filler in glassfiber reinforced composites: Experimental study of thermal and mechanical properties,” *Compos. Part B Eng.*, vol. 175, p. 107169, Oct. 2019, doi: 10.1016/j.compositesb.2019.107169.

[86] D. Ali *et al.*, “Thermo-physical properties and microstructural behaviour of biochar-incorporated cementitious material,” *J. Build. Eng.*, vol. 64, p. 105695, Apr. 2023, doi: 10.1016/j.jobe.2022.105695.

[87] Q. Zhang *et al.*, “Production of high-density polyethylene biocomposites from rice husk biochar: Effects of varying pyrolysis temperature,” *Sci. Total Environ.*, vol. 738, p. 139910, Oct. 2020, doi: 10.1016/j.scitotenv.2020.139910.

[88] K. Aup-Ngoen and M. Noipitak, “Effect of carbon-rich biochar on mechanical properties of PLA-biochar composites,” *Sustain. Chem. Pharm.*, vol. 15, p. 100204, Mar. 2020, doi: 10.1016/j.scp.2019.100204.

[89] S. Gupta, H. W. Kua, and S. Y. Tan Cynthia, “Use of biochar-coated polypropylene fibers for carbon sequestration and physical improvement of mortar,” *Cem. Concr. Compos.*, vol. 83, pp. 171–187, Oct. 2017, doi: 10.1016/j.cemconcomp.2017.07.012.

[90] E. O. Ogunsona, M. Misra, and A. K. Mohanty, “Accelerated hydrothermal aging of biocarbon reinforced nylon biocomposites,” *Polym. Degrad. Stab.*, vol. 139, pp. 76–88, May 2017, doi: 10.1016/j.polymdegradstab.2017.03.013.

[91] K. Uram, M. Kurańska, J. Andrzejewski, and A. Prociak, “Rigid Polyurethane Foams Modified with Biochar,” *Materials*, vol. 14, no. 19, Art. no. 19, Jan. 2021, doi: 10.3390/ma14195616.

[92] J. Andrzejewski, M. Misra, and A. K. Mohanty, “Polycarbonate biocomposites reinforced with a hybrid filler system of recycled carbon fiber and biocarbon: Preparation and thermomechanical characterization,” *J. Appl. Polym. Sci.*, vol. 135, no. 28, p. 46449, 2018, doi: 10.1002/app.46449.

[93] A. Alhelal, Z. Mohammed, S. Jeelani, and V. K. Rangari, “3D printing of spent coffee ground derived biochar reinforced epoxy composites,” *J. Compos. Mater.*, vol. 55, no. 25, pp. 3651–3660, Oct. 2021, doi: 10.1177/00219983211002237.

[94] J. Yan, L. Han, W. Gao, S. Xue, and M. Chen, “Biochar supported nanoscale zerovalent iron composite used as persulfate activator for removing trichloroethylene,” *Bioresour. Technol.*, vol. 175, pp. 269–274, Jan. 2015, doi: 10.1016/j.biortech.2014.10.103.

[95] H. Zhang, R. Xiao, R. Li, A. Ali, A. Chen, and Z. Zhang, “Enhanced aqueous Cr(VI) removal using chitosan-modified magnetic biochars derived from bamboo residues,” *Chemosphere*, vol. 261, p. 127694, Dec. 2020, doi: 10.1016/j.chemosphere.2020.127694.

[96] L. Liang, F. Xi, W. Tan, X. Meng, B. Hu, and X. Wang, “Review of organic and inorganic pollutants removal by biochar and biochar-based composites,” *Biochar*, vol. 3, no. 3, pp. 255–281, Sep. 2021, doi: 10.1007/s42773-021-00101-6.

[97] C. P. Silva *et al.*, “Biochar-TiO2 magnetic nanocomposites for photocatalytic solar-driven removal of antibiotics from aquaculture effluents,” *J. Environ. Manage.*, vol. 294, p. 112937, Sep. 2021, doi: 10.1016/j.jenvman.2021.112937.

[98] H. Lee, S. Yang, S. Wi, and S. Kim, “Thermal transfer behavior of biochar-natural inorganic clay composite for building envelope insulation,” *Constr. Build. Mater.*, vol. 223, pp. 668–678, Oct. 2019, doi: 10.1016/j.conbuildmat.2019.06.215.

[99] I. Oancea, C. Bujoreanu, M. Budescu, M. Benchea, and C. M. Grădinaru, “Considerations on sound absorption coefficient of sustainable concrete with different waste replacements,” *J. Clean. Prod.*, vol. 203, pp. 301–312, Dec. 2018, doi: 10.1016/j.jclepro.2018.08.273.

[100] L. Mo, J. Fang, B. Huang, A. Wang, and M. Deng, “Combined effects of biochar and MgO expansive additive on the autogenous shrinkage, internal relative humidity and compressive strength of cement pastes,” *Constr. Build. Mater.*, vol. 229, p. 116877, Dec. 2019, doi: 10.1016/j.conbuildmat.2019.116877.

[101] S. Gupta and A. Kashani, “Utilization of biochar from unwashed peanut shell in cementitious building materials – Effect on early age properties and environmental benefits,” *Fuel Process. Technol.*, vol. 218, p. 106841, Jul. 2021, doi: 10.1016/j.fuproc.2021.106841.

[102] K. Tan, X. Pang, Y. Qin, and J. Wang, “Properties of cement mortar containing pulverized biochar pyrolyzed at different temperatures,” *Constr. Build. Mater.*, vol. 263, p. 120616, Dec. 2020, doi: 10.1016/j.conbuildmat.2020.120616.

[103] R. Roychand *et al.*, “Recycling biosolids as cement composites in raw, pyrolyzed and ashed forms: A waste utilisation approach to support circular economy,” *J. Build. Eng.*, vol. 38, p. 102199, Jun. 2021, doi: 10.1016/j.jobe.2021.102199.

[104] Z. Laili, M. S. Yasir, M. A. Wahab, N. A. Mahmud, and N. Z. Abidin, “EVALUATION OF THE COMPRESSIVE STRENGTH OF CEMENT-SPENT RESINS MATRIX MIXED WITH BIOCHAR,” vol. 19, no. 3, 2015.

[105] L. Restuccia and G. A. proFerro, “Promising low cost carbon-based materials to improve strength and toughness in cement composites,” *Constr. Build. Mater.*, vol. 126, pp. 1034–1043, Nov. 2016, doi: 10.1016/j.conbuildmat.2016.09.101.

[106] J. Liu, Q. Li, and S. Xu, “Influence of nanoparticles on fluidity and mechanical properties of cement mortar,” *Constr. Build. Mater.*, vol. 101, pp. 892–901, Dec. 2015, doi: 10.1016/j.conbuildmat.2015.10.149.

[107] S. Gupta and H. W. Kua, “Carbonaceous micro-filler for cement: Effect of particle size and dosage of biochar on fresh and hardened properties of cement mortar,” *Sci. Total Environ.*, vol. 662, pp. 952–962, Apr. 2019, doi: 10.1016/j.scitotenv.2019.01.269.

[108] S. Gupta, H. W. Kua, and H. J. Koh, “Application of biochar from food and wood waste as green admixture for cement mortar,” *Sci. Total Environ.*, vol. 619–620, pp. 419–435, Apr. 2018, doi: 10.1016/j.scitotenv.2017.11.044.

[109] C. E. Tanase and I. Spiridon, “PLA/chitosan/keratin composites for biomedical applications,” *Mater. Sci. Eng. C*, vol. 40, pp. 242–247, Jul. 2014, doi: 10.1016/j.msec.2014.03.054.

[110] M. Murariu and P. Dubois, “PLA composites: From production to properties,” *Adv. Drug Deliv. Rev.*, vol. 107, pp. 17–46, Dec. 2016, doi: 10.1016/j.addr.2016.04.003.

[111] M. Z. Rahman, M. Rahman, T. Mahbub, M. Ashiquzzaman, S. Sagadevan, and M. E. Hoque, “Advanced biopolymers for automobile and aviation engineering applications,” *J. Polym. Res.*, vol. 30, no. 3, p. 106, Feb. 2023, doi: 10.1007/s10965-023-03440-z.

[112] E. L. Sánchez-Safont, A. Aldureid, J. M. Lagarón, J. Gámez-Pérez, and L. Cabedo, “Biocomposites of different lignocellulosic wastes for sustainable food packaging applications,” *Compos. Part B Eng.*, vol. 145, pp. 215–225, Jul. 2018, doi: 10.1016/j.compositesb.2018.03.037.

[113] M. Fernandes, A. P. Souto, F. Dourado, and M. Gama, “Application of Bacterial Cellulose in the Textile and Shoe Industry: Development of Biocomposites,” *Polysaccharides*, vol. 2, no. 3, Art. no. 3, Sep. 2021, doi: 10.3390/polysaccharides2030034.

[114] A. Partanen and M. Carus, “Biocomposites, find the real alternative to plastic – An examination of biocomposites in the market,” *Reinf. Plast.*, vol. 63, no. 6, pp. 317–321, Dec. 2019, doi: 10.1016/j.repl.2019.04.065.

[115] A. M. Poulose *et al.*, “Date palm biochar-polymer composites: An investigation of electrical, mechanical, thermal and rheological characteristics,” *Sci. Total Environ.*, vol. 619–620, pp. 311–318, Apr. 2018, doi: 10.1016/j.scitotenv.2017.11.076.

[116] R. Arrigo, M. Bartoli, and G. Malucelli, “Poly(lactic Acid)–Biochar Biocomposites: Effect of Processing and Filler Content on Rheological, Thermal, and Mechanical Properties,” *Polymers*, vol. 12, no. 4, Art. no. 4, Apr. 2020, doi: 10.3390/polym12040892.

[117] M. Ho, K. Lau, H. Wang, and D. Hui, “Improvement on the properties of polylactic acid (PLA) using bamboo charcoal particles,” *Compos. Part B Eng.*, vol. 81, pp. 14–25, Nov. 2015, doi: 10.1016/j.compositesb.2015.05.048.

[118] S. Lepak-Kuc *et al.*, “Innovative Biochar-Based Composite Fibres from Recycled Material,” *Materials*, vol. 14, no. 18, p. 5304, Sep. 2021, doi: 10.3390/ma14185304.

[119] E. Watt, M. A. Abdelwahab, A. K. Mohanty, and M. Misra, “Biocomposites from biobased polyamide 4,10 and waste corn cob based biocarbon,” *Compos. Part Appl. Sci. Manuf.*, vol. 145, p. 106340, Jun. 2021, doi: 10.1016/j.compositesa.2021.106340.

[120] Z. Mohammed, S. Jeelani, and V. K. Rangari, “Effect of Low-Temperature Plasma Treatment on Starch-Based Biochar and Its Reinforcement for Three-Dimensional Printed Polypropylene Biocomposites,” *ACS Omega*, vol. 7, no. 44, pp. 39636–39647, Nov. 2022, doi: 10.1021/acsomega.2c02372.

[121] S. Li, H. Wang, C. Chen, X. Li, Q. Deng, and D. Li, “Mechanical, electrical, and thermal properties of highly filled bamboo charcoal/ultra-high molecular weight polyethylene

composites," *Polym. Compos.*, vol. 39, no. S3, pp. E1858–E1866, 2018, doi: 10.1002/pc.24839.

[122] C. J. Cooper, M. A. Abdelwahab, A. K. Mohanty, and M. Misra, "Hybrid Green Bionanocomposites of Bio-based Poly(butylene succinate) Reinforced with Pyrolyzed Perennial Grass Microparticles and Graphene Nanoplatelets," *ACS Omega*, vol. 4, no. 24, pp. 20476–20485, Dec. 2019, doi: 10.1021/acsomega.9b01771.

[123] Z. Li, C. Reimer, T. Wang, A. K. Mohanty, and M. Misra, "Thermal and Mechanical Properties of the Biocomposites of Miscanthus Biocarbon and Poly(3-Hydroxybutyrate-co-3-Hydroxyvalerate) (PHBV)," *Polymers*, vol. 12, no. 6, Art. no. 6, Jun. 2020, doi: 10.3390/polym12061300.

[124] C.-C. Huang, C.-W. Chang, K. Jahan, T.-M. Wu, and Y.-F. Shih, "Effects of the Grapevine Biochar on the Properties of PLA Composites," *Materials*, vol. 16, no. 2, Art. no. 2, Jan. 2023, doi: 10.3390/ma16020816.

[125] M. Zouari, D. B. Devallance, and L. Marrot, "Effect of Biochar Addition on Mechanical Properties, Thermal Stability, and Water Resistance of Hemp-Polylactic Acid (PLA) Composites," *Materials*, vol. 15, no. 6, Art. no. 6, Jan. 2022, doi: 10.3390/ma15062271.

[126] O. Das, D. Bhattacharyya, D. Hui, and K.-T. Lau, "Mechanical and flammability characterisations of biochar/polypropylene biocomposites," *Compos. Part B Eng.*, vol. 106, pp. 120–128, Dec. 2016, doi: 10.1016/j.compositesb.2016.09.020.

[127] O. Das, A. K. Sarmah, and D. Bhattacharyya, "Nanoindentation assisted analysis of biochar added biocomposites," *Compos. Part B Eng.*, vol. 91, pp. 219–227, Apr. 2016, doi: 10.1016/j.compositesb.2016.01.057.

[128] O. Das *et al.*, "An all-gluten biocomposite: Comparisons with carbon black and pine char composites," *Compos. Part Appl. Sci. Manuf.*, vol. 120, pp. 42–48, May 2019, doi: 10.1016/j.compositesa.2019.02.015.

[129] E. G. Ertane, A. Dorner-Reisel, O. Baran, T. Welzel, V. Matner, and S. Svoboda, "Processing and Wear Behaviour of 3D Printed PLA Reinforced with Biogenic Carbon," *Adv. Tribol.*, vol. 2018, pp. 1–11, Aug. 2018, doi: 10.1155/2018/1763182.

[130] V. Mayakrishnan, J. K. Mohamed, N. Selvaraj, D. SenthilKumar, and S. Annadurai, "Effect of nano-biochar on mechanical, barrier and mulching properties of 3D printed thermoplastic polyurethane film," *Polym. Bull.*, vol. 80, no. 6, pp. 6725–6747, Jun. 2023, doi: 10.1007/s00289-022-04380-2.

[131] C. A. Diaz, R. K. Shah, T. Evans, T. A. Trabold, and K. Draper, "Thermoformed Containers Based on Starch and Starch/Coffee Waste Biochar Composites," *Energies*, vol. 13, no. 22, Art. no. 22, Jan. 2020, doi: 10.3390/en13226034.

[132] D. Tadele, P. Roy, F. Defersha, M. Misra, and A. K. Mohanty, "A comparative life-cycle assessment of talc- and biochar-reinforced composites for lightweight automotive parts," *Clean Technol. Environ. Policy*, vol. 22, no. 3, pp. 639–649, Apr. 2020, doi: 10.1007/s10098-019-01807-9.

[133] C. Das, S. Tamrakar, A. Kiziltas, and X. Xie, “Incorporation of Biochar to Improve Mechanical, Thermal and Electrical Properties of Polymer Composites,” *Polymers*, vol. 13, no. 16, p. 2663, Aug. 2021, doi: 10.3390/polym13162663.

[134] T. Huber, M. Misra, and A. K. Mohanty, “The effect of particle size on the rheological properties of polyamide 6/biochar composites,” presented at the PROCEEDINGS OF PPS-30: The 30th International Conference of the Polymer Processing Society – Conference Papers, Cleveland, Ohio, USA, 2015, p. 150004. doi: 10.1063/1.4918500.

[135] T. Wang, A. Rodriguez-Uribe, M. Misra, and A. K. Mohanty, “Sustainable Carbonaceous Biofiller from Miscanthus: Size Reduction, Characterization, and Potential Bio-composites Applications,” *BioResources*, vol. 13, no. 2, pp. 3720–3739, Apr. 2018, doi: 10.15376/biores.13.2.3720-3739.

[136] S. Richard, J. Selwin Rajadurai, and V. Manikandan, “Effects of Particle Loading and Particle Size on Tribological Properties of Biochar Particulate Reinforced Polymer Composites,” *J. Tribol.*, vol. 139, no. 1, p. 012202, Jan. 2017, doi: 10.1115/1.4033131.

[137] S. Nizamuddin *et al.*, “Synthesis and characterization of polylactide/rice husk hydrochar composite,” *Sci. Rep.*, vol. 9, no. 1, p. 5445, Apr. 2019, doi: 10.1038/s41598-019-41960-1.

[138] Md. M. Billah, M. S. Rabbi, and A. Hasan, “Injection molded discontinuous and continuous rattan fiber reinforced polypropylene composite: Development, experimental and analytical investigations,” *Results Mater.*, vol. 13, p. 100261, Mar. 2022, doi: 10.1016/j.rinma.2022.100261.

[139] X. Zhou, Y. Yu, Q. Lin, and L. Chen, “Effects of Maleic Anhydride-Grafted Polypropylene (MAPP) on the Physico-Mechanical Properties and Rheological Behavior of Bamboo Powder-Polypropylene Foamed Composites,” *BioResources*, vol. 8, no. 4, pp. 6263–6279, Oct. 2013, doi: 10.15376/biores.8.4.6263-6279.

[140] O. Das, A. K. Sarmah, and D. Bhattacharyya, “Biocomposites from waste derived biochars: Mechanical, thermal, chemical, and morphological properties,” *Waste Manag.*, vol. 49, pp. 560–570, Mar. 2016, doi: 10.1016/j.wasman.2015.12.007.

[141] O. Das, D. Bhattacharyya, and A. K. Sarmah, “Sustainable eco–composites obtained from waste derived biochar: a consideration in performance properties, production costs, and environmental impact,” *J. Clean. Prod.*, vol. 129, pp. 159–168, Aug. 2016, doi: 10.1016/j.jclepro.2016.04.088.

[142] Y. Lan, N. Yan, and W. Wang, “Application of PDMS pervaporation membranes filled with tree bark biochar for ethanol/water separation,” *RSC Adv.*, vol. 6, no. 53, pp. 47637–47645, 2016, doi: 10.1039/C6RA06794H.

[143] V. Subramanian, C. Luo, A. M. Stephan, K. S. Nahm, S. Thomas, and B. Wei, “Supercapacitors from Activated Carbon Derived from Banana Fibers,” *J. Phys. Chem. C*, vol. 111, no. 20, pp. 7527–7531, May 2007, doi: 10.1021/jp067009t.

[144] J. Y. Choi, Y. U. Kim, J. Nam, S. Kim, and S. Kim, “Enhancing the thermal stability and fire retardancy of bio-based building materials through pre-biochar system,” *Constr. Build. Mater.*, vol. 409, p. 134099, Dec. 2023, doi: 10.1016/j.conbuildmat.2023.134099.

[145] A. ur R. Shah, A. Imdad, A. Sadiq, R. A. Malik, H. Alrobei, and I. A. Badruddin, “Mechanical, Thermal, and Fire Retardant Properties of Rice Husk Biochar Reinforced Recycled High-Density Polyethylene Composite Material,” *Polymers*, vol. 15, no. 8, Art. no. 8, Jan. 2023, doi: 10.3390/polym15081827.

[146] O. Das, N. K. Kim, A. L. Kalamkarov, A. K. Sarmah, and D. Bhattacharyya, “Biochar to the rescue: Balancing the fire performance and mechanical properties of polypropylene composites,” *Polym. Degrad. Stab.*, vol. 144, pp. 485–496, Oct. 2017, doi: 10.1016/j.polymdegradstab.2017.09.006.

[147] P. Hazelton, M. Ye, and X. Chen, “Introduction to Conducting Polymers,” in *ACS Symposium Series*, vol. 1438, E. Nazarzadeh Zare and P. Makvandi, Eds., Washington, DC: American Chemical Society, 2023, pp. 1–7. doi: 10.1021/bk-2023-1438.ch001.

[148] M. Giorcelli, P. Savi, A. Khan, and A. Tagliaferro, “Analysis of biochar with different pyrolysis temperatures used as filler in epoxy resin composites,” *Biomass Bioenergy*, vol. 122, pp. 466–471, Mar. 2019, doi: 10.1016/j.biombioe.2019.01.007.

[149] K. Ahmed, M. Hasan, and J. Haider, “Electrical and Mechanical Properties of Sugarcane Bagasse Pyrolyzed Biochar Reinforced Polyvinyl Alcohol Biocomposite Films,” *J. Compos. Sci.*, vol. 5, no. 9, Art. no. 9, Sep. 2021, doi: 10.3390/jcs5090249.

[150] C. Unterweger *et al.*, “Electrically Conductive Biocomposites Based on Poly(3-hydroxybutyrate-co-3-hydroxyvalerate) and Wood-Derived Carbon Fillers,” *J. Compos. Sci.*, vol. 6, no. 8, Art. no. 8, Aug. 2022, doi: 10.3390/jcs6080228.

[151] C. O. Umerah, D. Kodali, S. Head, S. Jeelani, and V. K. Rangari, “Synthesis of carbon from waste coconutshell and their application as filler in bioplast polymer filaments for 3D printing,” *Compos. Part B Eng.*, vol. 202, p. 108428, Dec. 2020, doi: 10.1016/j.compositesb.2020.108428.

[152] S. M. Jasim and N. A. Ali, “Properties characterization of plasticized polylactic acid /Biochar (bio carbon) nano-composites for antistatic packaging,” 2019, doi: DOI:%2010.20723/ijp.17.42.13-26.

[153] J. Xu *et al.*, “Raman spectroscopy of biochar from the pyrolysis of three typical Chinese biomasses: A novel method for rapidly evaluating the biochar property,” *Energy*, vol. 202, p. 117644, Jul. 2020, doi: 10.1016/j.energy.2020.117644.

[154] A. C. Fingolo *et al.*, “Boosting Electrical Conductivity of Sugarcane Cellulose and Lignin Biocarbons through Annealing under Isopropanol Vapor,” *ACS Sustain. Chem. Eng.*, vol. 8, no. 18, pp. 7002–7010, May 2020, doi: 10.1021/acssuschemeng.0c00320.

[155] Z. Husain *et al.*, “Nano-sized mesoporous biochar derived from biomass pyrolysis as electrochemical energy storage supercapacitor,” *Mater. Sci. Energy Technol.*, vol. 5, pp. 99–109, Jan. 2022, doi: 10.1016/j.mset.2021.12.003.

[156] R. S. Gabhi, D. W. Kirk, and C. Q. Jia, “Preliminary investigation of electrical conductivity of monolithic biochar,” *Carbon*, vol. 116, pp. 435–442, May 2017, doi: 10.1016/j.carbon.2017.01.069.

[157] A. Noori, M. Bartoli, A. Frache, E. Piatti, M. Giorcelli, and A. Tagliaferro, “Development of Pressure-Responsive PolyPropylene and Biochar-Based Materials,” *Micromachines*, vol. 11, no. 4, p. 339, Mar. 2020, doi: 10.3390/mi11040339.

[158] L. Li *et al.*, “Waste eggshell membrane-templated synthesis of functional Cu2+–Cu+/biochar for an ultrasensitive electrochemical enzyme-free glucose sensor,” *RSC Adv.*, vol. 11, no. 31, pp. 18994–18999, May 2021, doi: 10.1039/D1RA00303H.

[159] L. Cao *et al.*, “Rapid pyrolysis of Cu2+-polluted eggshell membrane into a functional Cu2+-Cu+/biochar for ultrasensitive electrochemical detection of nitrite in water,” *Sci. Total Environ.*, vol. 723, p. 138008, Jun. 2020, doi: 10.1016/j.scitotenv.2020.138008.

[160] M. Giorcelli *et al.*, “High-Temperature Annealed Biochar as a Conductive Filler for the Production of Piezoresistive Materials for Energy Conversion Application,” *ACS Appl. Electron. Mater.*, vol. 3, no. 2, pp. 838–844, Feb. 2021, doi: 10.1021/acsaelm.0c00971.

[161] W. Sun, S. M. Lipka, C. Swartz, D. Williams, and F. Yang, “Hemp-derived activated carbons for supercapacitors,” *Carbon*, vol. 103, pp. 181–192, Jul. 2016, doi: 10.1016/j.carbon.2016.02.090.

[162] D. Thomas, N. B. Fernandez, M. D. Mullassery, R. Surya, and L. E. Jacob, “Banana stem biochar composite with polyaniline for energy storage applications,” *Results Chem.*, vol. 6, p. 101088, Dec. 2023, doi: 10.1016/j.rechem.2023.101088.

[163] L. W. Endler, F. Wolfart, A. S. Mangrich, M. Vidotti, and L. F. Marchesi, “Facile method to prepare biochar–NiO nanocomposites as a promisor material for electrochemical energy storage devices,” *Chem. Pap.*, vol. 74, no. 5, pp. 1471–1476, May 2020, doi: 10.1007/s11696-019-00987-4.

[164] G. Akgül, D. Iglesias, P. Ocon, and E. Moreno Jiménez, “Valorization of Tea-Waste Biochar for Energy Storage,” *BioEnergy Res.*, vol. 12, no. 4, pp. 1012–1020, Dec. 2019, doi: 10.1007/s12155-019-10025-6.

[165] S. Li, X. Li, Q. Deng, and D. Li, “Three kinds of charcoal powder reinforced ultra-high molecular weight polyethylene composites with excellent mechanical and electrical properties,” *Mater. Des.*, vol. 85, pp. 54–59, Nov. 2015, doi: 10.1016/j.matdes.2015.06.163.

[166] N. Nan, D. B. DeVallance, X. Xie, and J. Wang, “The effect of bio-carbon addition on the electrical, mechanical, and thermal properties of polyvinyl alcohol/biochar composites,” *J. Compos. Mater.*, vol. 50, no. 9, Art. no. 9, Apr. 2016, doi: 10.1177/0021998315589770.

[167] M. Bartoli *et al.*, “Pressure-Responsive Conductive Poly(vinyl alcohol) Composites Containing Waste Cotton Fibers Biochar,” *Micromachines*, vol. 13, no. 1, Art. no. 1, Jan. 2022, doi: 10.3390/mi13010125.

[168] M. Giorcelli and M. Bartoli, “Development of Coffee Biochar Filler for the Production of Electrical Conductive Reinforced Plastic,” *Polymers*, vol. 11, no. 12, p. 1916, Nov. 2019, doi: 10.3390/polym11121916.

[169] “Beech,” FrenchTimber. Accessed: Apr. 07, 2025. [Online]. Available: https://www.frenchtimber.com/en/french-species/beech/

[170] A. V. Miroshnikova *et al.*, “Reductive Fractionation of Flax Shives in Ethanol Medium over RuNi Bimetallic Catalysts,” *Int. J. Mol. Sci.*, vol. 24, no. 14, p. 11337, Jul. 2023, doi: 10.3390/ijms241411337.

[171] “Flax, a Norman treasure |.” Accessed: Apr. 07, 2025. [Online]. Available: https://www.seine-maritime-tourisme.com/en/destination/nature-sensation/flax-a-norman-treasure/

[172] D. Purcell-Meyerink, M. A. Packer, T. T. Wheeler, and M. Hayes, “Aquaculture Production of the Brown Seaweeds Laminaria digitata and Macrocystis pyrifera: Applications in Food and Pharmaceuticals,” *Molecules*, vol. 26, no. 5, Art. no. 5, Jan. 2021, doi: 10.3390/molecules26051306.

[173] M. Fertah, A. Belfkira, E. montassir Dahmane, M. Taourirte, and F. Brouillette, “Extraction and characterization of sodium alginate from Moroccan *Laminaria digitata* brown seaweed,” *Arab. J. Chem.*, vol. 10, pp. S3707–S3714, May 2017, doi: 10.1016/j.arabjc.2014.05.003.

[174] W.-J. Liu, H. Jiang, and H.-Q. Yu, “Development of Biochar-Based Functional Materials: Toward a Sustainable Platform Carbon Material,” *Chem. Rev.*, vol. 115, no. 22, pp. 12251–12285, Nov. 2015, doi: 10.1021/acs.chemrev.5b00195.

[175] C. Wen *et al.*, “Biochar as the effective adsorbent to combustion gaseous pollutants: Preparation, activation, functionalization and the adsorption mechanisms,” *Prog. Energy Combust. Sci.*, vol. 99, p. 101098, Nov. 2023, doi: 10.1016/j.pecs.2023.101098.

[176] S.-H. Jung and J.-S. Kim, “Production of biochars by intermediate pyrolysis and activated carbons from oak by three activation methods using CO2,” *J. Anal. Appl. Pyrolysis*, vol. 107, pp. 116–122, May 2014, doi: 10.1016/j.jaap.2014.02.011.

[177] M. Viana, P. Jouannin, C. Pontier, and D. Chulia, “About pycnometric density measurements,” *Talanta*, vol. 57, no. 3, pp. 583–593, May 2002, doi: 10.1016/S0039-9140(02)00058-9.

[178] S. Columbu, M. Mulas, F. Mundula, and R. Cioni, “Strategies for helium pycnometry density measurements of welded ignimbritic rocks,” *Measurement*, vol. 173, p. 108640, Mar. 2021, doi: 10.1016/j.measurement.2020.108640.

[179] G. E. Decker and E. D. Bloch, “Using Helium Pycnometry to Study the Apparent Densities of Metal–Organic Frameworks,” *ACS Appl. Mater. Interfaces*, vol. 13, no. 44, pp. 51925–51932, Nov. 2021, doi: 10.1021/acsami.1c07304.

[180] A. M. Geddis, “RAPID ESTIMATE OF SOLID VOLUME IN LARGE TUFF CORES USING A GAS PYCNOMETER”.

[181] D18 Committee, *Test Method for Specific Gravity of Soil Solids by Gas Pycnometer*. doi: 10.1520/D5550-14.

[182] M. Thommes *et al.*, "Physisorption of gases, with special reference to the evaluation of surface area and pore size distribution (IUPAC Technical Report)," *Pure Appl. Chem.*, vol. 87, no. 9–10, pp. 1051–1069, Oct. 2015, doi: 10.1515/pac-2014-1117.

[183] L. Ter-Minassian-Saraga, "Reporting experimental pressure-area data with film balances (Recommendations 1984)," *Pure Appl. Chem.*, vol. 57, no. 4, pp. 621–632, 1985, doi: 10.1351/pac198557040621.

[184] P. Parthasarathy, H. R. Mackey, S. Mariyam, S. Zuhara, T. Al-Ansari, and G. McKay, "Char Products From Bamboo Waste Pyrolysis and Acid Activation," *Front. Mater.*, vol. 7, p. 624791, Jan. 2021, doi: 10.3389/fmats.2020.624791.

[185] "Scanning Electron Microscopy | Nanoscience Instruments." Accessed: Apr. 07, 2025. [Online]. Available: https://www.nanoscience.com/techniques/scanning-electron-microscopy/

[186] J. I. Goldstein, D. E. Newbury, J. R. Michael, N. W. M. Ritchie, J. H. J. Scott, and D. C. Joy, *Scanning Electron Microscopy and X-Ray Microanalysis*. Springer, 2017.

[187] "SEM/EDS Analysis | RTI Laboratories." Accessed: Apr. 07, 2025. [Online]. Available: https://rtilab.com/techniques/sem-eds-analysis/

[188] L. M. Ng and R. Simmons, "Infrared Spectroscopy," *Anal. Chem.*, vol. 71, no. 12, pp. 343–350, Jun. 1999, doi: 10.1021/a1999908r.

[189] Y. Ozaki, "Infrared Spectroscopy—Mid-infrared, Near-infrared, and Far-infrared/Terahertz Spectroscopy," *Anal. Sci.*, vol. 37, no. 9, pp. 1193–1212, Sep. 2021, doi: 10.2116/analsci.20R008.

[190] T. Hasegawa, *Quantitative Infrared Spectroscopy for Understanding of a Condensed Matter*. Tokyo: Springer Japan, 2017. doi: 10.1007/978-4-431-56493-5.

[191] N. J. Harrick, "TOTAL INTERNAL REFLECTION AND ITS APPLICATION TO SURFACE STUDIES," *Ann. N. Y. Acad. Sci.*, vol. 101, no. 3, pp. 928–959, Jan. 1963, doi: 10.1111/j.1749-6632.1963.tb54948.x.

[192] H. Tiernan, B. Byrne, and S. G. Kazarian, "ATR-FTIR spectroscopy and spectroscopic imaging for the analysis of biopharmaceuticals," *Spectrochim. Acta. A. Mol. Biomol. Spectrosc.*, vol. 241, p. 118636, Nov. 2020, doi: 10.1016/j.saa.2020.118636.

[193] S. Kumar, L. Prasad, P. P. Bijlwan, and A. Yadav, "Thermogravimetric analysis of lignocellulosic leaf-based fiber-reinforced thermosets polymer composites: an overview," *Biomass Convers. Biorefinery*, vol. 14, no. 12, pp. 12673–12698, Jun. 2024, doi: 10.1007/s13399-022-03332-0.

[194] T. Sebio-Puñal, S. Naya, J. López-Beceiro, J. Tarrío-Saavedra, and R. Artiaga, "Thermogravimetric analysis of wood, holocellulose, and lignin from five wood species," *J. Therm. Anal. Calorim.*, vol. 109, no. 3, pp. 1163–1167, Sep. 2012, doi: 10.1007/s10973-011-2133-1.

[195] P. Gill, T. T. Moghadam, and B. Ranjbar, “Differential Scanning Calorimetry Techniques: Applications in Biology and Nanoscience,” *J. Biomol. Tech. JBT*, vol. 21, no. 4, pp. 167–193, Dec. 2010.

[196] P. J. Haines, M. Reading, and F. W. Wilburn, “Chapter 5 - Differential Thermal Analysis and Differential Scanning Calorimetry,” in *Handbook of Thermal Analysis and Calorimetry*, vol. 1, M. E. Brown, Ed., in Principles and Practice, vol. 1. , Elsevier Science B.V., 1998, pp. 279–361. doi: 10.1016/S1573-4374(98)80008-3.

[197] F. Pawlak, M. Aldas, J. López-Martínez, and M. D. Samper, “Effect of Different Compatibilizers on Injection-Molded Green Fiber-Reinforced Polymers Based on Poly(lactic acid)-Maleinized Linseed Oil System and Sheep Wool,” *Polymers*, vol. 11, no. 9, Art. no. 9, Sep. 2019, doi: 10.3390/polym11091514.

[198] J. M. Ferri, O. Fenollar, A. Jorda-Vilaplana, D. García-Sanoguera, and R. Balart, “Effect of miscibility on mechanical and thermal properties of poly(lactic acid)/ polycaprolactone blends,” *Polym. Int.*, vol. 65, no. 4, pp. 453–463, 2016, doi: 10.1002/pi.5079.

[199] A. W. Hull, “A NEW METHOD OF CHEMICAL ANALYSIS.,” *J. Am. Chem. Soc.*, vol. 41, no. 8, pp. 1168–1175, Aug. 1919, doi: 10.1021/ja02229a003.

[200] T. Alford, L. C. Feldman, and J. W. Mayer, *Fundamentals of nanoscale film analysis*. Springer US, 2007. doi: 10.1007/978-0-387-29261-8.

[201] H. Khan, A. S. Yerramilli, A. D’Oliveira, T. L. Alford, D. C. Boffito, and G. S. Patience, “Experimental methods in chemical engineering: X-ray diffraction spectroscopy—XRD,” *Can. J. Chem. Eng.*, vol. 98, no. 6, pp. 1255–1266, 2020, doi: 10.1002/cjce.23747.

[202] S. Matsuoka, Ed., *Relaxation phenomena in polymers*. in SPE books from Hanser publishers. Munich: Hanser, 1992.

[203] K. Menard, *Dynamic Mechanical Analysis: A Practical Introduction*. CRC Press, 1999. doi: 10.1201/9781420049183.

[204] W. K. Goertzen and M. R. Kessler, “Dynamic mechanical analysis of carbon/epoxy composites for structural pipeline repair,” *Compos. Part B Eng.*, vol. 38, no. 1, pp. 1–9, Jan. 2007, doi: 10.1016/j.compositesb.2006.06.002.

[205] M. A. Ruz-Cruz, P. J. Herrera-Franco, E. A. Flores-Johnson, M. V. Moreno-Chulim, L. M. Galera-Manzano, and A. Valadez-González, “Thermal and mechanical properties of PLA-based multiscale cellulosic biocomposites,” *J. Mater. Res. Technol.*, vol. 18, pp. 485–495, May 2022, doi: 10.1016/j.jmrt.2022.02.072.

[206] N. Besnard, J.-C. Badot, O. Dubrunfaut, S. Franger, and P. Tran-Van, “Étude diélectrique de matériaux composites pour batteries lithium-ion, des basses fréquences aux micro-ondes,” ResearchGate. Accessed: Apr. 08, 2025. [Online]. Available: https://www.researchgate.net/publication/278800864_Etude_dielectrique_de_materiaux_composites_pour_batteries_lithium-ion_des_basses_frequences_aux_micro-ondes

[207] M. Jacob, K. T. Varughese, and S. Thomas, “Dielectric characteristics of sisal–oil palm hybrid biofibre reinforced natural rubber biocomposites,” *J. Mater. Sci.*, vol. 41, no. 17, pp. 5538–5547, Sep. 2006, doi: 10.1007/s10853-006-0298-y.

[208] F. Benabed and T. Seghier, “Dielectric Properties and Relaxation Behavior of High Density Polyethylene (HDPE),” *Appl. Mech. Mater.*, vol. 799–800, pp. 1319–1324, Oct. 2015, doi: 10.4028/www.scientific.net/AMM.799-800.1319.

[209] C. Itu, S. Vlase, M. L. Scutaru, and A. Modrea, “Bending behavior of a high rigidity plate made by a composite panel,” *Procedia Manuf.*, vol. 32, pp. 144–150, Jan. 2019, doi: 10.1016/j.promfg.2019.02.195.

[210] A. E. Romero *et al.*, “Tensile Properties of 3D Printed Polymeric Pieces: Comparison of Several Testing Setups,” *Ing. E Investig.*, vol. 41, no. 1, p. e84467, Mar. 2021, doi: 10.15446/ing.investig.v41n1.84467.

[211] C. E. Brewer *et al.*, “New approaches to measuring biochar density and porosity,” *Biomass Bioenergy*, vol. 66, pp. 176–185, Jul. 2014, doi: 10.1016/j.biombioe.2014.03.059.

[212] A. Tomczyk, Z. Sokołowska, and P. Boguta, “Biochar physicochemical properties: pyrolysis temperature and feedstock kind effects,” *Rev. Environ. Sci. Biotechnol.*, vol. 19, no. 1, pp. 191–215, Mar. 2020, doi: 10.1007/s11157-020-09523-3.

[213] S. Wang *et al.*, “Physicochemical and sorptive properties of biochars derived from woody and herbaceous biomass,” *Chemosphere*, vol. 134, pp. 257–262, Sep. 2015, doi: 10.1016/j.chemosphere.2015.04.062.

[214] M. S. Nitin Thukral, “Microalgae as Future Fuel: Real Opportunities and Challenges,” *J. Thermodyn. Catal.*, vol. 06, no. 01, 2015, doi: 10.4172/2157-7544.1000139.

[215] J. Lehmann and S. Joseph, Eds., *Biochar for environmental management: science and technology*. London ; Sterling, VA: Earthscan, 2009.

[216] H. S. Kambo and A. Dutta, “A comparative review of biochar and hydrochar in terms of production, physico-chemical properties and applications,” *Renew. Sustain. Energy Rev.*, vol. 45, pp. 359–378, May 2015, doi: 10.1016/j.rser.2015.01.050.

[217] D. Chen *et al.*, “Effects of biochar on availability and plant uptake of heavy metals – A meta-analysis,” *J. Environ. Manage.*, vol. 222, pp. 76–85, Sep. 2018, doi: 10.1016/j.jenvman.2018.05.004.

[218] W. Ding, X. Dong, I. M. Ime, B. Gao, and L. Q. Ma, “Pyrolytic temperatures impact lead sorption mechanisms by bagasse biochars,” *Chemosphere*, vol. 105, pp. 68–74, Jun. 2014, doi: 10.1016/j.chemosphere.2013.12.042.

[219] R. Luque *et al.*, “Functionalized interconnected porous materials for heterogeneous catalysis, energy conversion and storage applications: Recent advances and future perspectives,” *Mater. Today*, vol. 73, pp. 105–129, Mar. 2024, doi: 10.1016/j.mattod.2023.05.001.

[220] H. Zhang, C. Chen, E. M. Gray, and S. E. Boyd, “Effect of feedstock and pyrolysis temperature on properties of biochar governing end use efficacy,” *Biomass Bioenergy*, vol. 105, pp. 136–146, Oct. 2017, doi: 10.1016/j.biombioe.2017.06.024.

[221] M. Keiluweit, P. S. Nico, M. G. Johnson, and M. Kleber, “Dynamic Molecular Structure of Plant Biomass-Derived Black Carbon (Biochar),” *Environ. Sci. Technol.*, vol. 44, no. 4, pp. 1247–1253, Feb. 2010, doi: 10.1021/es9031419.

[222] Y. Cuixia, X. Yingming, W. Lin, L. Xuefeng, S. Yuebing, and J. Hongtao, “Effect of different pyrolysis temperatures on physico-chemical characteristics and lead(ii) removal of biochar derived from chicken manure,” *RSC Adv.*, vol. 10, no. 7, pp. 3667–3674, 2020, doi: 10.1039/C9RA08199B.

[223] A. Uroić Štefanko and D. Leszczynska, “Impact of Biomass Source and Pyrolysis Parameters on Physicochemical Properties of Biochar Manufactured for Innovative Applications,” *Front. Energy Res.*, vol. 8, Jul. 2020, doi: 10.3389/fenrg.2020.00138.

[224] S. Rajkovich, A. Enders, K. Hanley, C. Hyland, A. R. Zimmerman, and J. Lehmann, “Corn growth and nitrogen nutrition after additions of biochars with varying properties to a temperate soil,” *Biol. Fertil. Soils*, vol. 48, no. 3, pp. 271–284, Apr. 2012, doi: 10.1007/s00374-011-0624-7.

[225] M. Ahmad *et al.*, “Biochar as a sorbent for contaminant management in soil and water: A review,” *Chemosphere*, vol. 99, pp. 19–33, Mar. 2014, doi: 10.1016/j.chemosphere.2013.10.071.

[226] J. Coates, “Interpretation of Infrared Spectra, A Practical Approach,” in *Encyclopedia of Analytical Chemistry*, 1st ed., R. A. Meyers, Ed., Wiley, 2000. doi: 10.1002/9780470027318.a5606.

[227] B. H. Stuart, *Infrared Spectroscopy: Fundamentals and Applications*, 1st ed. in Analytical Techniques in the Sciences. Wiley, 2004. doi: 10.1002/0470011149.

[228] A. B. D. Nandiyanto, R. Oktiani, and R. Ragadhita, “How to Read and Interpret FTIR Spectroscope of Organic Material,” *Indones. J. Sci. Technol.*, vol. 4, no. 1, p. 97, Mar. 2019, doi: 10.17509/ijost.v4i1.15806.

[229] B. Chen, D. Zhou, and L. Zhu, “Transitional Adsorption and Partition of Nonpolar and Polar Aromatic Contaminants by Biochars of Pine Needles with Different Pyrolytic Temperatures,” *Environ. Sci. Technol.*, vol. 42, no. 14, pp. 5137–5143, Jul. 2008, doi: 10.1021/es8002684.

[230] J. Yu, L. Sun, C. Berrueco, B. Fidalgo, N. Paterson, and M. Millan, “Influence of temperature and particle size on structural characteristics of chars from Beechwood pyrolysis,” *J. Anal. Appl. Pyrolysis*, vol. 130, pp. 127–134, Mar. 2018, doi: 10.1016/j.jaap.2018.01.018.

[231] S. K. Das, G. K. Ghosh, R. Avasthe, and K. Sinha, “Morpho-mineralogical exploration of crop, weed and tree derived biochar,” *J. Hazard. Mater.*, vol. 407, p. 124370, Apr. 2021, doi: 10.1016/j.jhazmat.2020.124370.

[232] M. Keiluweit, P. S. Nico, M. G. Johnson, and M. Kleber, “Dynamic Molecular Structure of Plant Biomass-Derived Black Carbon (Biochar),” *Environ. Sci. Technol.*, vol. 44, no. 4, pp. 1247–1253, Feb. 2010, doi: 10.1021/es9031419.

[233] S. Anto *et al.*, “Activation strategies for biochar to use as an efficient catalyst in various applications,” *Fuel*, vol. 285, p. 119205, Feb. 2021, doi: 10.1016/j.fuel.2020.119205.

[234] M. Aboughaly, A. Babaei-Ghazvini, P. Dhar, R. Patel, and B. Acharya, “Enhancing the Potential of Polymer Composites Using Biochar as a Filler: A Review,” *Polymers*, vol. 15, no. 19, Art. no. 19, Jan. 2023, doi: 10.3390/polym15193981.

[235] C. Yang *et al.*, “Valorization of Biomass-Derived Polymers to Functional Biochar Materials for Supercapacitor Applications via Pyrolysis: Advances and Perspectives,” *Polymers*, vol. 15, no. 12, p. 2741, Jan. 2023, doi: 10.3390/polym15122741.

[236] H. Moustafa, C. Guizani, C. Dupont, V. Martin, M. Jeguirim, and A. Dufresne, “Utilization of Torrefied Coffee Grounds as Reinforcing Agent To Produce High-Quality Biodegradable PBAT Composites for Food Packaging Applications,” *ACS Sustain. Chem. Eng.*, vol. 5, no. 2, pp. 1906–1916, Feb. 2017, doi: 10.1021/acssuschemeng.6b02633.

[237] C. Botta, C. M. Grottola, D. Amato, and M. R. Acocella, “Biochar as Sustainable Filler of Recycled Polylactic Acid (PLA): A New Generation of Processable Biocomposites,” *Polymers*, vol. 16, no. 23, p. 3347, Jan. 2024, doi: 10.3390/polym16233347.

[238] M. Tesfaye, R. Patwa, A. Gupta, M. J. Kashyap, and V. Katiyar, “Recycling of poly (lactic acid)/silk based bionanocomposites films and its influence on thermal stability, crystallization kinetics, solution and melt rheology,” *Int. J. Biol. Macromol.*, vol. 101, pp. 580–594, Aug. 2017, doi: 10.1016/j.ijbiomac.2017.03.085.

[239] K. P. Menard, *Dynamic Mechanical Analysis: A Practical Introduction, Second Edition*, 2nd ed. Boca Raton: CRC Press, 2008. doi: 10.1201/9781420053135.

[240] S. Farah, D. G. Anderson, and R. Langer, “Physical and mechanical properties of PLA, and their functions in widespread applications — A comprehensive review,” *Adv. Drug Deliv. Rev.*, vol. 107, pp. 367–392, Dec. 2016, doi: 10.1016/j.addr.2016.06.012.

[241] K. M. Z. Hossain, A. J. Parsons, C. D. Rudd, I. Ahmed, and W. Thielemans, “Mechanical, crystallisation and moisture absorption properties of melt drawn polylactic acid fibres,” *Eur. Polym. J.*, vol. 53, pp. 270–281, Apr. 2014, doi: 10.1016/j.eurpolymj.2014.02.001.

[242] H. Li and M. A. Huneault, “Effect of nucleation and plasticization on the crystallization of poly(lactic acid),” *Polymer*, vol. 48, no. 23, pp. 6855–6866, Nov. 2007, doi: 10.1016/j.polymer.2007.09.020.

[243] M. R. Snowdon, F. Wu, A. K. Mohanty, and M. Misra, “Comparative study of the extrinsic properties of poly(lactic acid)-based biocomposites filled with talc versus sustainable biocarbon,” *RSC Adv.*, vol. 9, no. 12, pp. 6752–6761, Feb. 2019, doi: 10.1039/C9RA00034H.

[244] P. Roy *et al.*, “Production Cost of Biocarbon and Biocomposite, and Their Prospects in Sustainable Biobased Industries,” *Sustainability*, vol. 16, no. 13, Jun. 2024, doi: 10.3390/su16135633.

[245] V. John *et al.*, “Investigation, Prospects, and Economic Scenarios for the Use of Biochar in Small-Scale Agriculture in Tropical,” *Agriculture*, vol. 15, no. 15, Aug. 2025, doi: 10.3390/agriculture15151700.

[246] R. B. Kalengyo, M. G. Ibrahim, M. Fujii, and M. Nasr, “Utilizing orange peel waste biomass in textile wastewater treatment and its recyclability for dual biogas and biochar production: a techno-economic sustainable approach,” *Biomass Convers. Biorefinery*, vol. 14, no. 16, pp. 19875–19888, Aug. 2024, doi: 10.1007/s13399-023-04111-1.

[247] P. M. Yeletsky, R. N. Maganov, T. S. Ainullov, R. R. Yakupov, A. I. Shamsullin, and V. A. Yakovlev, “High-throughput carbon dioxide sequestration into sustainable solid products by miscanthus cultivation: A review,” *Biofuels Bioprod. Biorefining*, vol. n/a, no. n/a, doi: 10.1002/bbb.70065.

[248] “Subregional Comparison for Forest- to-Product Biomass Supply Chains on the Pacific West Coast, USA”, Accessed: Jan. 05, 2026. [Online]. Available: https://doi.org/10.13031/aea.12526

[249] R. I. Rubel and L. Wei, “Economic Assessment of Biochar-Based Controlled-Release Nitrogen Fertilizer Production at Different Industrial Scales,” *Waste Biomass Valorization*, vol. 16, no. 12, pp. 6833–6849, Dec. 2025, doi: 10.1007/s12649-025-03096-4.

[250] B. Trollip and R. D. Merckel, “Production of a nutrient enriched biochar: a techno-economic feasibility analysis,” *Biofuels Bioprod. Biorefining*, vol. 19, no. 6, pp. 1497–1514, 2025, doi: 10.1002/bbb.2812.

[251] S. Fawzy, A. I. Osman, N. Mehta, D. Moran, A. H. Al-Muhtaseb, and D. W. Rooney, “Atmospheric carbon removal *via* industrial biochar systems: A techno-economic-environmental study,” *J. Clean. Prod.*, vol. 371, p. 133660, Oct. 2022, doi: 10.1016/j.jclepro.2022.133660.

[252] D. Dickinson, L. Balduccio, J. Buysse, F. Ronsse, G. van Huylenbroeck, and W. Prins, “Cost-benefit analysis of using biochar to improve cereals agriculture,” *GCB Bioenergy*, vol. 7, no. 4, pp. 850–864, 2015, doi: 10.1111/gcbb.12180.

[253] N. N. Ahmed, R. Pokharel, J. Miesel, and C. M. Saffron, “Assessing Feedstock Availability and Economic Feasibility of Utilizing Forest Biomass for Biochar Production in Stationary and Portable Systems in Michigan,” *GCB Bioenergy*, vol. 17, no. 5, p. e70030, 2025, doi: 10.1111/gcbb.70030.

[254] A. Kumar, K. Saini, and T. Bhaskar, “Hydochar and biochar: Production, physicochemical properties and techno-economic analysis,” *Bioresour. Technol.*, vol. 310, p. 123442, Aug. 2020, doi: 10.1016/j.biortech.2020.123442.

[255] R. Bergman, K. Sahoo, K. Englund, and S. H. Mousavi-Avval, “Lifecycle Assessment and Techno-Economic Analysis of Biochar Pellet Production from Forest Residues and Field Application,” *Energies*, vol. 15, no. 4, p. 1559, Feb. 2022, doi: 10.3390/en15041559.

[256] S. Shabangu, D. Woolf, E. M. Fisher, L. T. Angenent, and J. Lehmann, “Techno-economic assessment of biomass slow pyrolysis into different biochar and methanol concepts,” *Fuel*, vol. 117, pp. 742–748, Jan. 2014, doi: 10.1016/j.fuel.2013.08.053.

[257] J. M. Bressanin *et al.*, “Techno-economic and environmental assessment of polylactic acid production integrated with the sugarcane value chain,” *Sustain. Prod. Consum.*, vol. 34, pp. 244–256, Nov. 2022, doi: 10.1016/j.spc.2022.09.009.

[258] S. J. H. Bandara, “Exploring the Potential of Biochar in Enhancing U.S. Agriculture,” *Reg. Sci. Environ. Econ.*, vol. 2, no. 3, Aug. 2025, doi: 10.3390/rsee2030023.

[259] “France - Corporate - Taxes on corporate income.” Accessed: Nov. 05, 2025. [Online]. Available: https://taxsummaries.pwc.com/france/corporate/taxes-on-corporate-income

[260] “Polylactic Acid (PLA) Price Index, Chart 2025 and Trend.” Accessed: Nov. 27, 2025. [Online]. Available: https://www.imarcgroup.com/polylactic-acid-pricing-report

[261] “Tasa de inflación en Francia | 1958-2025 Datos | 2026-2027 Expectativa.” Accessed: Nov. 27, 2025. [Online]. Available: https://es.tradingeconomics.com/france/inflation-cpi

ANNEXES

Annexes

Annex 1. Technical data sheet of PLA

NatureWorks

Ingeo™ Biopolymer 2003D Technical Data Sheet

For Fresh Food Packaging and Food Serviceware

Ingeo biopolymer 2003D, a NatureWorks LLC product, is a thermoplastic resin derived from annually renewable resources and is specifically designed for use in fresh food packaging and food serviceware applications. Ingeo biopolymer 2003D is a transparent general purpose extrusion grade that is used naturally or as part of a formulated blend. This is a high molecular weight biopolymer grade that processes easily on conventional extrusion equipment. Extruded roll stock is readily thermoformable. See table at right for properties.

Typical Material & Application Properties (1)

Physical Properties	Ingeo 2003D	ASTM Method
Specific Gravity	1.24	D792
MFR, g/10 min (210°C, 2.16kg)	6	D1238
Clarity	Transparent	
Mechanical Properties		
Tensile Strength @ Break, psi (MPa)	7,700 (53)	D882
Tensile Yield Strength, psi (MPa)	8,700 (60)	D882
Tensile Modulus, kpsi (GPa)	500 (3.5)	D882
Tensile Elongation, %	6.0	D882
Notched Izod Impact, ft-lb/in (J/m)	0.3 (16)	D256
Shrinkage is similar to PET (2)		
Heat Distortion Temperature (°C)	55	E2092

(1) Typical properties; not to be construed as specifications.
(2) Refer to Ingeo biopolymer Sheet Extrusion Processing Guide

Applications

Potential applications for Ingeo biopolymer 2003D include:

- Dairy containers
- Food serviceware
- Transparent food containers
- Hinged-ware
- Cold drink cups

Processing Temperature Profile (1)

Melt Temperature	410°F	210°C
Feed Throat	113°F	45°C
Feed Temperature	355°F	180°C
Compression Section	375°F	190°C
Metering Section	390°F	200°C
Adapter	390°F	200°C
Die	375°F	190°C
Screw Speed	20-100 rpm	

(1) These are starting points and may need to be optimized.

Processing Information

Ingeo biopolymer 2003D is easily processed on conventional extrusion equipment. The material is stable in the molten state, provided that the drying procedures are followed. More detailed recommendations and processing requirements are found in the Ingeo biopolymer sheet extrusion processing guide, the purging technical data sheet, and the drying and crystallizing processing guide, all of which can be found at www.natureworksllc.com.

Machine Configuration

Ingeo biopolymer 2003D will process on conventional extrusion machinery with the following equipment: General purpose screw with L/D ratios from 24:1 to 32:1 and compression ratio of 2.5:1 to 3:1. Smooth barrels are recommended.

Process Details

Startup and Shutdown

Ingeo biopolymer 2003D is not compatible with a wide variety of commodity resins, and special purging sequences should be followed:

1. Clean extruder and bring temperatures to steady state with low viscosity, general purpose polystyrene or polypropylene.
2. Vacuum out hopper system to avoid contamination.
3. Introduce Ingeo biopolymers into the extruder at the operating conditions used in Step 1.
4. Once Ingeo biopolymer has purged, reduce barrel temperatures to desired set points.
5. At shutdown, purge machine with high viscosity polystyrene or polypropylene.

Drying

In-line drying may be required. A moisture content of less than 0.025% (250 ppm) is recommended to prevent viscosity degradation. Typical drying conditions for crystallized granules are 2 hours at 195°F (90°C) or to a dew point of -40°F (-40°C), airflow rate of greater than 0.5 cfm/lbs per hour

of resin throughput. The resin should not be exposed to atmospheric conditions after drying. Keep the package sealed until ready to use and promptly reseal any unused material. Pellets that have been exposed to the atmosphere for extended time periods will require additional drying time. Amorphous regrind must be crystallized prior to drying, to assure efficient and effective drying.

Food Packaging Status

U.S. Status

On January 3, 2002 FCN 000178 submitted by NatureWorks LLC to FDA became effective. This effective notification is part of list currently maintained on FDA's website at

http://www.fda.gov/food/ingredientspackaginglabeling/packagingfcs/notifications/default.htm

This grade of Ingeo biopolymer may therefore be used in food packaging materials and, as such, is a permitted component of such materials pursuant to section 201(s) of the Federal, Drug, and Cosmetic Act, and Parts 182, 184, and 186 of the Food Additive Regulations. All additives and adjuncts contained in the referenced Ingeo biopolymer formulation meet the applicable sections of the Federal Food, Drug, and Cosmetic Act. The finished polymer is approved for all food types and B-H use conditions. We urge all of our customers to perform GMP (Good Manufacturing Procedures) when constructing a package so that it is suitable for the end use.

European Status

This grade of Ingeo biopolymer complies with Plastics Regulation 10/2011 as amended. No SML's for the above referenced grade exist in Plastics Regulation 10/2011 as amended. NatureWorks LLC would like to draw your attention to the fact that the EU- Plastics Regulation 10/2011, which applies to all EU-Member States, includes a limit of 10 mg/dm2 of the overall migration from finished plastic articles into food. In accordance with Plastics Regulation 10/2011 the migration should be measured on finished articles placed into contact with the foodstuff or appropriate food simulants for a period and at a temperature which are chosen by reference to the contact conditions in actual use, according to the rules laid down in Plastics Regulation 10/2011.

Please note that it is the responsibility of both the manufacturers of finished food contact articles as well as the industrial food packers to make sure that these articles in their actual use are in compliance with the imposed specific and overall migration requirements.

This grade as supplied meets European Parliament and Council Directive 94/62/EC of 20 December 1994 on packaging and packaging waste heavy metal content as described in Article 11.

Should you need further clarification, contact NatureWorks LLC.

Bulk Storage Recommendations

The resin silos recommended and used by NatureWorks LLC are designed to maintain dry air in the silo and to be isolated from the outside air. This design would be in contrast to an open, vented to atmosphere system that we understand to be a typical polystyrene resin silo. Key features that are added to a typical (example: polystyrene) resin silo to achieve this objective include a cyclone and rotary valve loading system and some pressure vessel relief valves. The dry air put to the system is sized to the resin flow rate out of the silo. Not too much dry air would be needed and there may be excess instrument air (-30°F dew point) available in the plant to meet the needs for dry air. Our estimate is 10 scfm for a 20,000 lb/hr rate resin usage. Typically, resin manufacturers specify aluminum or stainless steel silos for their own use and avoid epoxy-lined steel.

Safety and Handling Considerations

Safety Data Sheets (SDS) for Ingeo biopolymers are available from NatureWorks. SDS's are provided to help customers satisfy their own handling, safety, and disposal needs, and those that may be required by locally applicable health and safety regulations. SDS's are updated regularly; therefore, please request and review the most current SDS's before handling or using any product.

The following comments apply only to Ingeo biopolymers; additives and processing aids used in fabrication and other materials used in finishing steps have their own safe-use profile and must be investigated separately.

Hazards and Handling Precautions

Ingeo biopolymers have a very low degree of toxicity and, under normal conditions of use, should pose no unusual problems from incidental ingestion or eye and skin contact. However, caution is advised when handling, storing, using, or disposing of these resins, and good housekeeping and controlling of dusts are necessary for safe handling of product. Pellets or beads may present a slipping hazard.

No other precautions other than clean, body-covering clothing should be needed for handling Ingeo biopolymers. Use gloves with insulation for thermal protection when exposure to the melt is localized. Workers should be protected from the possibility of contact with molten resin during fabrication.

Handling and fabrication of resins can result in the generation of vapors and dusts that may cause irritation to eyes and the upper respiratory tract. In dusty atmospheres, use an approved dust respirator.

Good general ventilation of the polymer processing area is recommended. At temperatures exceeding the polymer melt temperature (typically 175°C), polymer can release fumes, which may contain fragments of the polymer, creating a potential to irritate eyes and mucous membranes. Good general ventilation should be sufficient for most conditions. Local exhaust ventilation is recommended for melt operations. Use safety glasses (or goggles) to prevent exposure to particles, which could cause mechanical injury to the eye. If vapor exposure causes eye discomfort, improve localized fume exhausting methods or use a full-face respirator.

The primary thermal decomposition product of PLA is acetaldehyde, a material also produced during the thermal degradation of PET. Thermal decomposition products also include carbon monoxide and hexanal, all of which exist as gases at normal room conditions. These species are highly flammable, easily ignited by spark or flame, and can also auto ignite. For polyesters such as PLA, thermal decomposition producing flammable vapors containing acetaldehyde and carbon monoxide can occur in almost any process equipment maintaining PLA at high temperature over longer residence times than typically experienced in extruders, fiber spinning lines, injection molding machines, accumulators, pipe lines and adapters. As a rough guideline based upon some practical experience, significant decomposition of PLA will occur if polymer residues are held at temperatures above the melting point for prolonged periods, e.g., in excess of 24 hours at 175°C, although this will vary significantly with temperature.

Combustibility

Ingeo biopolymers will burn. Clear to white smoke is produced when product burns. Toxic fumes are released under conditions of incomplete combustion. Do not permit dust to accumulate. Dust layers can be ignited by spontaneous combustion or other ignition sources. When suspended in air, dust can pose an explosion hazard. Firefighters should wear positive-pressure, self-contained breathing apparatuses and full protective equipment. Water or water fog is the preferred extinguishing medium. Foam, alcohol-resistant foam, carbon dioxide or dry chemicals may also be used. Soak thoroughly with water to cool and prevent re-ignition.

Disposal

DO NOT DUMP INTO ANY SEWERS, ON THE GROUND, OR INTO ANY BODY OF WATER. For unused or uncontaminated material, the preferred option is to recycle into the process otherwise, send to an incinerator or other thermal destruction device. For used or contaminated material, the disposal options remain the same, although additional evaluation is required. Disposal must be in compliance with Federal, State/Provincial, and local laws and regulations.

Environmental Concerns

Generally speaking, lost pellets, while undesirable, are benign in terms of their physical environmental impact, but if ingested by wildlife, they may mechanically cause adverse effects. Spills should be minimized, and they should be cleaned up when they happen. Plastics should not be discarded into the environment.

Product Stewardship

NatureWorks has a fundamental duty to all those that use our products, and for the environment in which we live. This duty is the basis for our Product Stewardship philosophy, by which we assess the health and environmental information on our products and their intended use, and then take

appropriate steps to protect the environment and the health of our employees and the public.

Customer Notice

NatureWorks encourages its customers and potential users of its products to review their applications from the standpoint of human health and environmental quality. To help ensure our products are not used in ways for which they were not intended or tested, our personnel will assist customers in dealing with ecological and product safety considerations. Your sales representative can arrange the proper contacts. NatureWorks literature should be consulted prior to the use of the company's products.

NOTICE:
No freedom from infringement of any patent owned by NatureWorks LLC or others is to be inferred. No information in this publication can be considered a suggestion to infringe patents.

The technical information, recommendations and other statements contained in this document are based upon tests or experience that NatureWorks believes are reliable, but the accuracy or completeness of such information is not guaranteed. Many factors beyond NatureWorks control can affect the use and performance of a NatureWorks product in a particular application, including the conditions under which the product is used and the time and environmental conditions in which the product is expected to perform. Since these factors are uniquely within the user's knowledge or control, it is essential that the user evaluate the NatureWorks product to determine whether it is fit for a particular purpose and suitable for the user's method of application. In addition, because use conditions are outside of NatureWorks control and applicable laws may differ from one location to another and may change with time, Customer is solely responsible for determining whether products and the information in this document are appropriate for Customer's use and for ensuring that Customer's workplace, use and disposal practices are in compliance with applicable laws and regulations. NatureWorks LLC assumes no obligation or liability for the information in this document.

NATUREWORKS MAKES NO WARRANTY, EXPRESS OR IMPLIED, REGARDING THE INFORMATION CONTAINED HEREIN OR ITS PRODUCTS, INCLUDING BUT NOT LIMITED TO ANY WARRANTY AS TO ACCURACY OR COMPLETENESS OF INFORMATION, OR ANY IMPLIED WARRANTY OF MERCHANTABILITY OR FITNESS FOR A PARTICULAR PURPOSE.

NOTICE REGARDING PROHIBITED USE RESTRICTIONS: Unless specifically agreed to in writing by NatureWorks, NatureWorks LLC will not knowingly sell or sample any product into any of the following commercial or developmental applications (i) components of or packaging for tobacco products, (ii) components of products intended for human or animal consumption, (iii) any application that is intended for any internal contact with human body fluids or body tissues, (iv) as a critical component in any medical device that supports or sustains human life, (v) in any product that is designed specifically for ingestion or internal use by pregnant women, (vi) in any application designed specifically to promote or interfere with human reproduction, (vii) in microbeads, including those used in personal care/cosmetic applications, or (vii) to manufacture bottles or bottle pre-forms in North America.

For additional information please contact NatureWorks via our website on the tab called FAQ's or by clicking here.

NatureWorks
15305 Minnetonka Blvd., Minnetonka, MN 55345

Annex 2. Comparison of mass degradation in biomass, biochar, and biocomposites.

This appendix shows the mass degradation of the three types of biomass used, as well as the biochar and biocomposites produced from them.

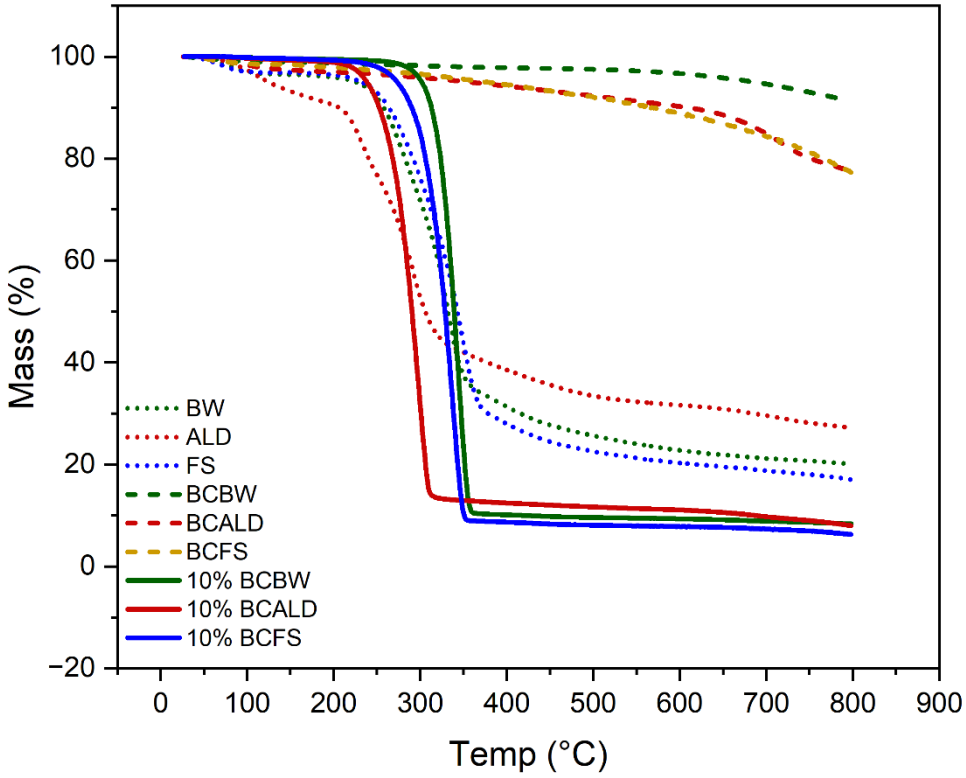

Figure A2: Mass degradation curves with respect to the temperature of biomass, biochar and PLA-biochar compounds (10 wt.%). Heated at a constant rate of 10 °C·min-1 from 25 to 800 °C, under an inert 20 ml·min-1 argon atmosphere.

Thermogravimetric analysis shows a clear difference in thermal stability among the samples, related to their structure and level of carbonization. The biomass samples (BW, ALD, FS) have a typical profile for lignocellulosic materials, with a multistage mass loss. Hemicellulose and cellulose degrade between 210°C and 380°C. In contrast, the biochar (BCBW, BCALD, BCFS) shows better thermal stability up to 800°C and leave behind significant carbon residues (up to 92%). This confirms a condensed aromatic structure after the pyrolysis process. The behaviour of the 10% biocomposites is interesting. Incorporating biochar changes the decomposition rates. The 10% BCALD sample has the lowest onset temperature (T_{onset}) at about 250°C. This suggests that the specific composition of the algae might have a catalytic or destabilizing effect on the matrix. It reduces the thermal processing window compared to the wood or straw versions.

Annex 3. Conversion table of certain monetary values into euros

This appendix shows a table with the conversion to euros of certain monetary values retrieved from the literature, according to the exchange rate on the date of publication of the referenced article. Exchange rate consulted on https://www.x-rates.com/

Table A3: conversion of certain monetary values into euros

Ref.	Concept	Publication date	Original Price	Exchange rate (€)	Final Price (€/kg)	Total Value (M€)
[245]	Biochar cost produced in traditional Small-Scale biochar production	Aug-2025	0.03 USD·kg^{-1}	0.86	0.03	
			0.08 USD·kg^{-1}		0.07	
[246]	Biochar cost produced in Small-Scale / Batch and Prototype mobile	Aug-2024	0.03 USD·kg^{-1}	0.91	0.03	
			2.06 USD·kg^{-1}		1.87	
			0.87 USD·kg^{-1}		0.79	
[247]	Industrial Scale biochar production	Oct-2025	50 USD·ton^{-1}	0.86	0.04	
			150 USD·ton^{-1}		0.13	
			130 USD·ton^{-1}		0.11	
[252]	Biochar production Poland	Feb-2014	30 USD·ton^{-1} CO_2	0.73	0.02 per kg CO_2	
			39 USD·ton^{-1}		0.03	
			85 USD·ton^{-1}		0.06	
[244]	Biochar cost NPV biochar an biocomposite plans. CANADA	Jun-2024	513.1 CAD·kg^{-1}	0.68	0.35	
			42,9 M CAD		-	29.08
			34,0 M CAD			23.05
			34,8 M CAD			23.59
[258]	Biochar market projection	Aug-2025	478, M USD	0.86		410.84

Annex 4. ETIA budget proposal

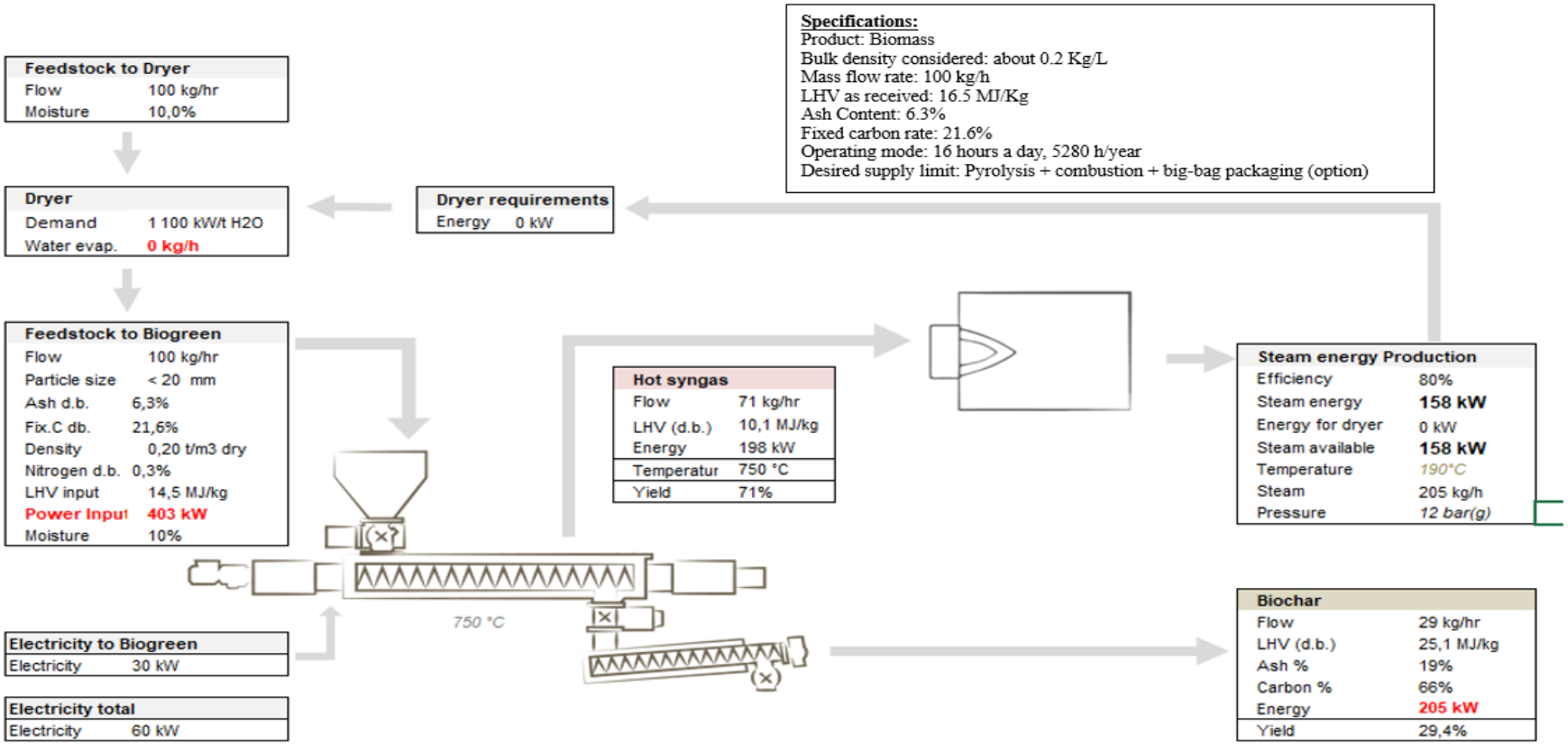

Solution technique:

BIOGREEN 300 with combustion

Composed of:

1. 1 Loading hopper 1 m3, cylindrical flat bottom design with dripper
2. 1 Volumetric dosing screw
3. 1 vertical chute to pyrolype reactor
4. 1 Spirajoule 300L6 pyrolysis reactor (electric heating technology in the absence of oxygen)
5. 1 Current rectifier for Spirajoule power 60 kW and associated power cable
6. 1 Biochar cooling screw (by double cold water jacket)
7. 1 300L biochar recovery hopper with cylindrical flat bottom design with devouring
8. 1 conveyor screw to big-bag
9. Hot gas piping pyrolyser connection to combustion chamber with thermal expansion compensator (short distance less than 1 m)
10. 250 KWt combustion unit (dual fuel natural gas / pyrogas burner, combustion chamber, instrumentation and fans).
11. general control cabinet with PLC and HMI SIEMENS
12. Painted steel support and platform according to ETIA standard
13. Equipment prewiring
14. ETIA standard services (FAT, documentation, remote installation support, commissioning)
15. 1 year warranty

Core process Budget price FCA (+/-10%): 1 300 000 € (Cost of the combustion unit represent 500 000 €).

Big-bag packaging option (16h production autonomy):

Composed of:

1. 1 Distrubution screw with 4 outlets
2. 3 Vanne guillotine
3. 3 big-bag filling station 2 m3

Option Budget price FCA (+/-10%): 95 000 €

Exclusion:

1. Transport and unloading
2. Installation, handling equipment and connection
3. Civil Engineering & HVAC
4. On-site security required
5. Upstream/downstream equipment
6. Flue gas energy recovery and flue gas filtration (To be studied according to heat needs and local emission limit of the project)
7. Cold water for cooling (Requires
8. Fluids and consumables
9. LVB
10. Anything not explicitly mentioned above 6.5 kW of cold at 30°C).

Delivery time:

8-10 Months from order to delivery FCA

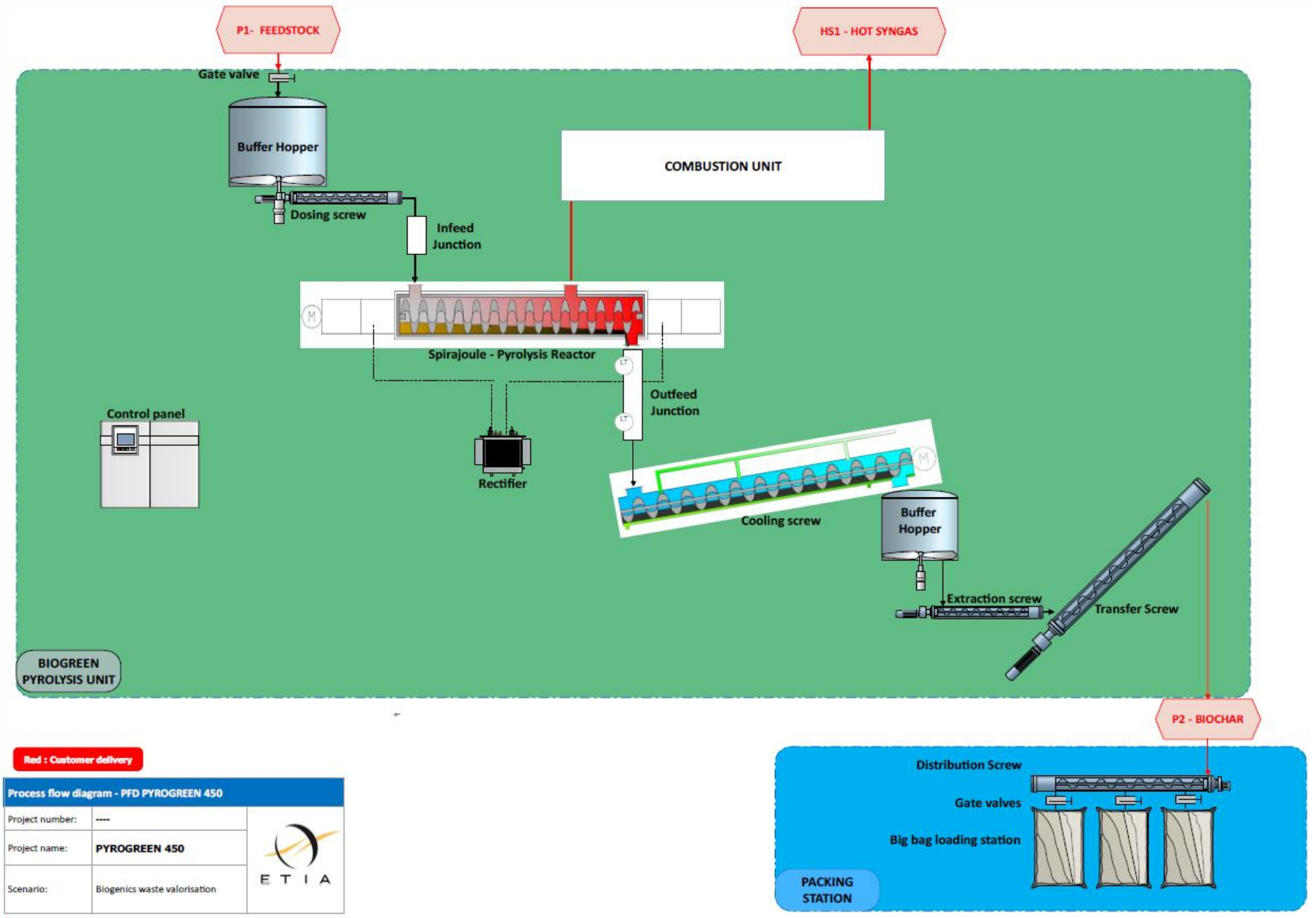
P1- FEEDSTOCK
HS1 - HOT SYNGAS
Gate valve
Buffer Hopper
COMBUSTION UNIT
Dosing screw
Infeed Junction
Spirajoule - Pyrolysis Reactor
Outfeed Junction
Control panel
Rectifier
Cooling screw
Buffer Hopper
Extraction screw
Transfer Screw
BIOGREEN PYROLYSIS UNIT
P2 - BIOCHAR
Red : Customer delivery
Process flow diagram - PFD PYROGREEN 450
Project number: ----
Project name: PYROGREEN 450
Scenario: Biogenics waste valorisation
ETIA
Distribution Screw
Gate valves
Big bag loading station
PACKING STATION

Annex 5. Market prices collection data online

Table A5 was created using data collected online in October 2025. Averaging the prices gives an approximate price of €26 per kg for composite granules, €6 per kg for PLA, €3 per kg for biochar, and €20 per kg for tomato clips.

Table A5: market prices for biochar, PLA, biocomposite pellets, and tomato clips, compiled from various online sources

Company	Product	Type	Price (€/kg)	Notes	Links
3DJake / Spectrum	FGF Pellet PLA Carbon	Composite	33.59	Retail composite pellets	https://www.3djake.fr
Nanovia	PLA Wood	Composite	18.30	Pellets 40% pine	https://nanovia.tech
Eolasprints	PLA Pellets	PLA virgin	6.99	Retail PLA pellets	https://eolasprints.com
Arianeplast	PLA Pellets	PLA virgin	10.00	French PLA supplier	https://www.arianeplast.com
SmartMaterials3D	PELLETSMART PLA	PLA virgin	10.45	Premium PLA	https://www.smartmaterials3d.com
Alibaba (exporters)	PLA pellets bulk	PLA virgin	2.19-2.76	Large-scale sourcing	https://www.alibaba.com
Rezomes / others	Industrial biochar	Biochar	0.53–0.80	Bulk biochar	https://shop.rezomes.com
Agrifournitures	Biochar retail	Biochar	4.60	Agri/garden retail	https://agrifournitures.fr
frenc alibaba	Biochar	Biochar	0.34-1.62	Organic activated carbon	https://french.alibaba.com
AUXINE	Wood biochar	Biochar	5.90	Biochar of wood waste	https://www.auxine-shop.fr
Adorla	Wood biochar	Biochar	1.30	Biochar of wood waste	https://www.adorla.com
ecoforce	Wood biochar	Biochar	9.00	Wood biochar	https://www.leroymerlin.fr
AUXINE	Tomato clips	Bioplastic PLA	49.90	Biodegradable, estimated weight of 1.5g/clip	https://www.auxine-shop.fr
Triangle	Tomato clips	NA	19.30	Biodegradable, estimated weight of 1.5g/clip	https://www.triangle-outillage.fr
Direct-filet	Tomato clips	PP (Polypropylène)	9.30	non-biodegradable, estimated weight of 1.5g/clip	https://www.direct-filet.com
Jardinet	Tomato clips	Corn starch	33.06	Biodegradable, estimated weight of 1.5g/clip	https://www.jardinet.fr

Annex 6. Loan Amortization

Table A6: loan amortization calculations				
Bank loan financing		**5,500,000.00**		
Period		**5 years**		
Annual interest		**5%**		
Year	**Share (€)**	**Interests (€)**	**Amortization (€)**	**Outstanding balance (€)**
1	1,245,501.42	252,447.53		4,506,946.11
2	1,245,501.42	201,641.01	1,043,860.41	3,463,085.70
3	1,245,501.42	148,235.13	1,097,266.29	2,365,819.40
4	1,245,501.42	92,096.90	1,153,404.52	1,212,414.88
5	1,245,501.42	33,086.54	1,212,414.88	€ 0.00

Annex *7*. Cash Flow of scenarios 2-4

Table A7.1: Cash flow scenario 2, 100% sales											
Year	**CAPEX (k€)**	**Income (k€)**	**OPEX (k€)**	**EBITDA (k€)**	**Depreciation**	**EBIT**	**Interests**	**EBT**	**Tax**	**Net profit (k€)**	**Free Cash Flow (k€)**
0	4,336.90										-4,336.90
1		3,195.84	2,023.81	1,172.03	433.69	738.34	252.45	485.90	121.47	364.42	798.11
2		3,243.78	2,054.16	1,189.61	433.69	755.92	201.64	554.28	138.57	415.71	849.40
3		3,292.43	2,084.98	1,207.46	433.69	773.77	148.24	625.53	156.38	469.15	902.84
4		3,341.82	2,116.25	1,225.57	433.69	791.88	92.10	699.78	174.95	524.84	958.53
5		3,391.95	2,147.99	1,243.95	433.69	810.26	33.09	777.18	194.29	582.88	1,016.57
6		3,442.83	2,180.21	1,262.61	433.69	828.92	0.00	828.92	207.23	621.69	1,055.38
7		3,494.47	2,212.92	1,281.55	433.69	847.86	0.00	847.86	211.97	635.90	1,069.59
8		3,546.89	2,246.11	1,300.78	433.69	867.09	0.00	867.09	216.77	650.31	1,084.00
9		3,600.09	2,279.80	1,320.29	433.69	886.60	0.00	886.60	221.65	664.95	1,098.64
10		3,654.09	2,314.00	1,340.09	433.69	906.40	0.00	906.40	226.60	679.80	1,113.49

Table A7.2: Cash flow scenario 3, 100% sales											
Year	**CAPEX (k€)**	**Income (k€)**	**OPEX (k€)**	**EBITDA (k€)**	**Depreciation**	**EBIT**	**Interests**	**EBT**	**Tax**	**Net profit (k€)**	**Free Cash Flow (k€)**
0	4,935.49										-4,935.49
1		3,425.19	2,220.98	1,204.21	493.55	710.66	252.45	458.21	114.55	343.66	837.21
2		3,476.57	2,254.30	1,222.27	493.55	728.72	201.64	527.08	131.77	395.31	888.86
3		3,528.72	2,288.11	1,240.61	493.55	747.06	148.24	598.82	149.71	449.12	942.67
4		3,581.65	2,322.43	1,259.22	493.55	765.67	92.10	673.57	168.39	505.18	998.73
5		3,635.37	2,357.27	1,278.10	493.55	784.55	33.09	751.47	187.87	563.60	1,057.15
6		3,689.90	2,392.63	1,297.28	493.55	803.73	0.00	803.73	200.93	602.79	1,096.34
7		3,745.25	2,428.52	1,316.73	493.55	823.19	0.00	823.19	205.80	617.39	1,110.94
8		3,801.43	2,464.94	1,336.49	493.55	842.94	0.00	842.94	210.73	632.20	1,125.75
9		3,858.45	2,501.92	1,356.53	493.55	862.98	0.00	862.98	215.75	647.24	1,140.79
10		3,916.33	2,539.45	1,376.88	493.55	883.33	0.00	883.33	220.83	662.50	1,156.05

Table A7.3: Cash flow scenario 4, 100% sales											
Year	**CAPEX (k€)**	**Income (k€)**	**OPEX (€)**	**EBITDA (k€)**	**Depreciation**	**EBIT**	**Interests**	**EBT**	**Tax**	**Net profit (k€)**	**Free Cash Flow (k€)**
0	5,475.26										-5,475.26
1		6,601.04	3,300.52	3,300.52	547.53	2,752.99	252.45	2,500.55	625.14	1,875.41	2,422.94
2		6,700.06	3,350.03	3,350.03	547.53	2,802.50	201.64	2,600.86	650.22	1,950.65	2,498.17
3		6,800.56	3,400.28	3,400.28	547.53	2,852.75	148.24	2,704.52	676.13	2,028.39	2,575.91
4		6,902.57	3,451.28	3,451.28	547.53	2,903.76	92.10	2,811.66	702.91	2,108.74	2,656.27
5		7,006.10	3,503.05	3,503.05	547.53	2,955.53	33.09	2,922.44	730.61	2,191.83	2,739.36
6		7,111.20	3,555.60	3,555.60	547.53	3,008.07	0.00	3,008.07	752.02	2,256.05	2,803.58
7		7,217.86	3,608.93	3,608.93	547.53	3,061.41	0.00	3,061.41	765.35	2,296.05	2,843.58
8		7,326.13	3,663.07	3,663.07	547.53	3,115.54	0.00	3,115.54	778.88	2,336.65	2,884.18
9		7,436.02	3,718.01	3,718.01	547.53	3,170.49	0.00	3,170.49	792.62	2,377.86	2,925.39
10		7,547.56	3,773.78	3,773.78	547.53	3,226.26	0.00	3,226.26	806.56	2,419.69	2,967.22